ISSN: 2408-2384 (Online)

Environment and Natural Resources Journal

Volume 21, Number 5, September - October 2023

Environment and Natural Resources Journal (EnNRJ)
Volume 21, Number 5, September - October 2023 ISSN: 2408-2384 (Online)

AIMS AND SCOPE

The Environment and Natural Resources Journal is a peer-reviewed journal, which provides insight scientific knowledge into the diverse dimensions of integrated environmental and natural resource management. The journal aims to provide a platform for exchange and distribution of the knowledge and cutting-edge research in the fields of environmental science and natural resource management to academicians, scientists and researchers. The journal accepts a varied array of manuscripts on all aspects of environmental science and natural resource management. The journal scope covers the integration of multidisciplinary sciences for prevention, control, treatment, environmental clean-up and restoration. The study of the existing or emerging problems of environment and natural resources in the region of Southeast Asia and the creation of novel knowledge and/or recommendations of mitigation measures for sustainable development policies are emphasized.

The subject areas are diverse, but specific topics of interest include:

- Biodiversity
- Climate change
- Detection and monitoring of polluted sources e.g., industry, mining
- Disaster e.g., forest fire, flooding, earthquake, tsunami, or tidal wave
- Ecological/Environmental modelling
- Emerging contaminants/hazardous wastes investigation and remediation
- Environmental dynamics e.g., coastal erosion, sea level rise
- Environmental assessment tools, policy and management e.g., GIS, remote sensing, Environmental Management System (EMS)
- Environmental pollution and other novel solutions to pollution
- Remediation technology of contaminated environments
- Transboundary pollution
- Waste and wastewater treatments and disposal technology

Schedule
Environment and Natural Resources Journal (EnNRJ) is published 6 issues per year in January-February, March-April, May-June, July-August, September-October, and November-December.

Publication Fees
There is no cost of the article-processing and publication.

Ethics in publishing
EnNRJ follows closely a set of guidelines and recommendations published by Committee on Publication Ethics (COPE).

Environment and Natural Resources Journal (EnNRJ)
Volume 21, Number 5, September - October 2023 ISSN: 2408-2384 (Online)

Editorial Office Address
Research Management and Administration Section,
Faculty of Environment and Resource Studies, Mahidol University
999, Phutthamonthon Sai 4 Road, Salaya, Phutthamonthon, Nakhon Pathom, Thailand, 73170
Phone +662 441 5000 ext. 2108 Fax. +662 441 9509-10
Website: https://ph02.tci-thaijo.org/index.php/ennrj/index
E-mail: ennrjournal@gmail.com

Environment and Natural Resources Journal (EnNRJ)
Volume 21, Number 5, September - October 2023 ISSN: 2408-2384 (Online)

CONTENT

REVIEW ARTICLE

Application of Local Species for Sustainable Phytoremediation[#]

Naiyanan Ariyakanon[*]

Department of Environmental Science, Faculty of Science, Chulalongkorn University, Bangkok 10330, Thailand

ARTICLE INFO

Received: 29 May 2023
Received in revised: 2 Aug 2023
Accepted: 11 Aug 2023
Published online: 20 Sep 2023
DOI: 10.32526/ennrj/21/20230125

Keywords:
Local plants/ Sustainable phytoremediation/ Heavy metals/ Thailand

*** Corresponding author:**
E-mail: anaiyanan@yahoo.com

[#] This review article was invited by the Editor-in-Chief.

ABSTRACT

Phytoremediation is green technology based on the application of plants to remediate contaminated media. This paper reviews five species of local plants used for phytoremediation in Thailand: *Pteris vittata* L., *Pityrogramma calomelanos* L., *Chrysopogon zizanioides* L., *Eichhornia crassipes* (Mart.) Solms, and *Pistia stratiotes* L. For each plant, its pollutant removal efficiency and mechanism is reviewed. The main mechanisms of phytoremediation, such as phytoextraction, rhizofiltration, phytostabilization, phytodegradation, rhizodegradation, and phyto-volatilization, are concisely described. Screening local plants for phytoremediation is a cost-effective and easy to manage approach to derive suitable plants that are resistant to harmful environmental conditions. To be suitable, plants should have a fast growth rate, produce a large biomass yield, have a high tolerance to the toxic effects of the pollutants, and have a good capacity for pollutant uptake. Moreover, applying the proper species for each contaminant enhances the removal efficiency and supports sustainable phytoremediation.

1. INTRODUCTION

The rapid global urbanization and the development of industrialization has significantly increased soil and water pollution. These pollutants include various organic and inorganic compounds, such as heavy metals, pesticides, petroleum waste, and radionuclides, that threaten the ecosystem and enhance human health risks (Singh and Pant, 2023). Phytoremediation is one of the most promising technologies for environmental cleanup. It is defined as using green plants to remove, contain, and render environmental toxicants (Hettiarachchi et al., 2019). Both soil and water pollution from various sources are found across Thailand, and phytoremediation is a developing approach within the country and so is reviewed in this manuscript.

Most of the research reviewed in this paper deals with the phytoremediation of soil and water contaminated with heavy metals. Phytoextraction refers to removing metals using a plant's ability to absorb metals from the soil or water into its roots and then translocate most of them to the aboveground biomass. Metal hyperaccumulator plants have developed several regulatory mechanisms to survive in a metal-contaminated environment, including heavy metal absorption, transportation, chelation, and detoxification (Memon et al., 2021). In Thailand, two kinds of ferns, *Pityrogramma calomelanos* L. and *Pteris vittata* L., have been shown to be arsenic (As) hyperaccumulators, while *Chrysopogon zizanioides* L., *Eichhornia crassipes* (Mart.) Solms, and *Pistia stratiotes* L. are candidate plant species for removing heavy metals from water. These five kinds of plants are common in Thailand, grow fast, and suit the climate.

Sustainable remediation projects are evaluated based upon their social, economic, and positive vs. negative environmental impacts (EnvironWiki, 2023). Sustainable phytoremediation is a promising technique for mitigating human environmental impacts and limiting adverse socio-economic impacts. However, to increase the efficiency of sustainable phytoremediation, it is necessary to raise the knowledge, risk assessment, public awareness, and acceptance of this technology among scientists, industry, stakeholders, government agencies, and non-governmental organizations (Latif et al., 2023).

Citation: Ariyakanon N. Application of local species for sustainable phytoremediation. Environ. Nat. Resour. J. 2023;21(5):381-389. (https://doi.org/10.32526/ennrj/21/20230125)

2. MECHANISM OF PHYTOREMEDIATION

The phytoremediation process can be separated into the six categories of phytoextraction, rhizofiltration, phytostabilization, phytodegradation, rhizodegradation, and phytovolatilization.

(1) Phytoextraction involves the absorption of toxic metals from the environment (topsoil, surface or ground water) by plant roots and then translocation to shoots and deposition at the vacuole, cell wall, cell membrane, and other inactive parts in the plant tissues (Kafle et al., 2022). Therefore, phytoextraction is an attractive method for the cleanup of heavy metal-contaminated sites by using the potential plants, which in Thailand includes *Chrysopogon zizanioides*, *Spirodela polyrhiza*, *Pistia stratiotes*, *Eichhornia crassipes*, and *Pennisetum purpureum* (Yang et al., 2020).

(2) Rhizofiltration is the adsorption or precipitation of contaminants that are in the solution surrounding the root zone onto plant roots or absorption into the roots. Plant roots excrete specific chemicals in the root environment, creating biogeochemical conditions that precipitate contaminants onto the roots or in the water body (Akhtar et al., 2017).

(3) Phytostabilization can occur through the precipitation of heavy metals or reduction of the metal valency in the rhizosphere, with absorption and sequestration within root tissues, or adsorption onto root cell walls. This process uses metal-tolerant plant species to immobilize heavy metals belowground and so decrease their bioavailability, thereby preventing their migration into the ecosystem and reducing the likelihood of metals entering the food chain (Yan et al., 2020).

(4) Phytodegradation involves the plants' transformation or breakdown of organic contaminants through metabolic processes. The degradation of pollutants occurs inside or outside the plant through enzymes produced by roots, such as dehalogenases, nitroreductases, and peroxidases (Nedjimi, 2021). For example, it was reported that *Vetiveria zizanioides* could clean up 97% of trinitrotoluene from the soil (Das et al., 2010).

(5) Rhizodegradation refers to the breakdown of organic contaminants in rhizospheric soil using microorganisms. Exudates from plant roots, such as sugars, amino acids, and flavonoids, increase the microbial activity in the rhizosphere. The root exudates are a carbon and nitrogen source, providing a nutrient-rich environment for microorganisms and encouraging microbial activity (Latif et al., 2023).

(6) Phytovolatilization is the uptake of pollutants from the soil or water that are then converted into less toxic but volatile forms and are then released into the atmosphere via plant transpiration via the leaves or foliage system. This approach can be applied to the detoxification of organic pollutants and some heavy metals like selenium (Se), mercury (Hg), and As (Mahar et al., 2016).

3. SELECTION OF LOCAL SPECIES FOR PHYTOREMEDIATION

Appropriate selection of the plant species for the contaminants and geochemical site is crucial for effective phytoremediation. Therefore, the use of local species for phytoremediation is considered advantageous (already adapted) and they should possess the following characteristics:

(1) High tolerance to the toxic effects of the respective heavy metals and/or other pollutants.

(2) Good ability to uptake, translocate, or degrade the contaminants.

(3) High growth rate, high biomass production, and an extensive root system.

(3) High resistance to stressful environmental conditions, pests, weeds, and pathogens.

(4) Easy to cultivate and harvest.

(5) Low maintenance cost.

(6) Increase ecological value and support soil resilience.

Other factors, such as the temperature, pH, solar radiation, nutrient availability, and salinity, can greatly influence the phytoremediation potential and growth of the plant (Ali et al., 2020).

4. THE LOCAL PLANTS APPLIED TO CONTAMINATED SITES IN THAILAND

There are five principal plant species being utilized or well-studied for phytoremediation within Thailand, and these are discussed in turn as follows: (1) *Pteris vittata* L. (Chinese brake fern) and (2) *Pityrogramma calomelanos* L. (silverback fern).

The lead (Pb) tolerance and accumulation in ferns, including *Pteris vittata* (Figure 1) and *Pityrogramma calomelanos* (Figure 2), have been studied. The plants were collected from the Bo Ngam lead mine site. In hydroponic and pot experiments, *P. calomelanos* accumulated the highest concentration of Pb (root 14,161.1 mg/kg and frond 402.7 mg/kg) compared to *P. vittata*. The ferns were found to have a translocation factor of less than 1. When *P. vittata* and *P. calomelanos* were grown in contaminated mine soil

for six months, *P. vittata* tolerated a higher soil Pb level (94,584-101,405 mg/kg) and accumulated more Pb in its frond (4,829.6 mg/kg) than *P. calomelanos* (3,605.1 mg/kg) (Soongsombat et al., 2009).

In Thailand, *P. vittata* and *P. calomelanos* were found in As contaminated land, such as the Ron Phibun District (Nakorn Si Thammarat Province) and Bannang Sata District (Yala Province) (Visoottiviseth et al., 2002). These areas in the Ron Phibun District to Ronna-Suangchan Mountain were part of a former tin mining area that resulted in As-contaminated soil in southern Thailand. The As concentrations in the topsoil ranged from 21 to 14,000 mg/g in Ron Phibun and from 540 to 16,000 mg/g in Bannang Sata. The researchers selected the plants based on the following criteria: high As tolerance, high bioaccumulation factor, short life cycle, high propagation rate, wide distribution, and large shoot biomass. The results indicated that the highest As concentrations in leaves of *P. calomelanos* and *P. vittata* were 8,350 and 6,030 mg/g, respectively, (Visoottiviseth et al., 2002).

The As uptake in most plants rarely exceeds 1 mg/kg. The WHO limits As in plants because plants do not readily translocate As from the roots to the shoots (Santra et al., 2013). Therefore, *P. calomelanos* and *P. vittata* are considered as As hyperaccumulators. With respect to the translocation and distribution of As in *P. vittata*, the As is believed to be taken up from the soil by the phosphate uptake system as As (V). However, within the root exudates and xylem sap of *P. vittata*, As was found in different forms of As, including As (III), As (V), mono-methyl arsenic acid, and dimethylarsinic acid. The reduction of As (V) to As (III) occurs in the frond of the fern (Fayiga and Saha, 2016). The presence of As (V) and As (III) induces plant antioxidant production higher antioxidant activity and results in a higher superoxide dismutase, catalase, and ascorbate peroxidase (APX), in *P. vittata* than in two non-hyperaccumulators, indicating the ability of *P. vittata* to get rid of reactive oxygen species and free radicals (Srivastava et al., 2005).

Moreover, increased ascorbate and glutathione (GSH) levels significantly increased the level of As uptake and translocation in *P. vittata* (Wei et al., 2010). Note that GSH is a precursor to phytochelatins that are involved in detoxifying As in *P. vittata* (Rosen, 2002). The other mechanism of As detoxification in *P. vittata* is the chelation of arsenite by ligands and binding with thiol groups, followed by sequestration away from the sites of metabolism in the cytoplasm, probably into the vacuole or cell wall (Pandey et al., 2015).

Figure 1. *P. vittata* (Photo courtesy of Assistant Professor Dr. Rossarin Pollawatn)

Figure 2. *P. calomelanos* (Photo courtesy of Emeritus Professor Dr. Thaweesakdi Boonkerd)

The effects of phosphorus fertilizer and rhizosphere microbe amendments on As accumulation by *P. calomelanos* were investigated in greenhouse and field experiments (Jankong et al., 2007). The greenhouse experiments used contaminated soils from Ron Phibun District of Nakhon Si Thammarat Province in Thailand with As concentrations of 136-269 mg/kg. The addition of phosphorus fertilizer significantly increased the plant biomass, rhizosphere microbes, and As accumulation in *P. calomelanos*. The enhanced phosphorus and level of rhizosphere bacteria increased the As phytoextraction, while rhizofungi significantly reduced the total As concentration in plants but increased the plant biomass (Upatham et al., 2014).

(3) *Chrysopogon zizanioides* L. (vetiver grass)

Vetiver grass (*Vetiveria zizanioides* has recently been reclassified as *Chrysopogon zizanioides*) is a tall, fast-growing perennial grass with a massive deep-penetrating root system (Figure 3) that originated from India. However, it is widely cultivated in tropical regions and in Thailand its cultivation was promoted for soil and water conservation in 1991 and then for slope stabilization, erosion control, and environmental improvement (Roongtanakiat, 2006). There are many ecotypes of vetiver grass due to ecological variation, and they show different tolerances/adaptations to different habitats. Nowadays, these cultivars of *C. zizanioides* are commonly found in all regions of Thailand.

Figure 3. Sapling of *C. zizanioides*

Chrysopogon zizanioides has an excellent potential to remediate contaminated water and soil because this plant can tolerate high levels of heavy metals and pollutants. Moreover, its unique morphological and physiological characteristics include a high growth rate, adaptability to extreme environmental conditions, and a long root system. It can grow in soil across a very broad pH range of 3.3-12.5 and temperature range from 15-55^{o}C. Moreover, it has a finely structured and vigorous root structure that can grow 3-4 m deep within the first year (Wikipedia, 2023a).

Various studies have demonstrated the successful application of this species as a remedy for removing pollutants and heavy metals in Thailand's contaminated or intoxicated soil and water (Roongtanakiat et al., 2007; Rotkittikhun et al., 2007). Therefore, the ability of *C. zizanioides* to uptake heavy metals from industrial wastewater has been investigated. Three vetiver ecotypes, Kamphaeng Phet-2, Sri Lanka, and Surat Thani, were cultured in four types of industrial wastewater sampling from a milk factory, a battery manufacturing plant, an electric lamp plant, and an ink manufacturing facility. The plants cultured in wastewater from a milk factory showed the highest plant growth and had the highest manganese (Mn), iron (Fe), zinc (Zn), and Pb removal efficiencies of 33.72%, 27.63%, 52.73%, and 8.94%, respectively. The *C. zizanioides* grown in wastewater from an ink manufacturing facility showed the highest copper (Cu) removal capacity of up to 87.5%, although the root growth was retarded as a Cu toxicity symptom (Roongtanakiat et al., 2007).

The Pb accumulation in the shoots and roots of four ecotypes of *C. zizanioides*; three from Thailand (Surat Thani, Songkhla, and Kamphaeng Phet) and one from Sri Lanka, was found to be similar in all four ecotypes. Plants accumulated higher Pb concentrations in the roots (4,100-5,900 mg/kg) than in the shoots (248-422 mg/kg). However, the application of 20% (w/w) pig manure was the most effective treatment (compared to inorganic fertilizer) to improve the biomass of vetiver grown in Pb-contaminated soils, which was due to the pig manure's increased electrical conductivity and reduced diethylenetriamine pentaacetate-extractable Pb concentration in the soils (Rotkittikhun et al., 2007).

Investigation of the mechanism of heavy metal uptake from sulphuric acid discharge in *C. zizanioides* and their subsequent metabolism revealed that the vetiver shoot displayed increased levels of amino acid

metabolism, glutathione metabolism, TCA, and the urea cycle. The roots showed accumulated ornithine and oxaloacetate levels and downregulated phosphor-lipid, phosphorylated metabolites, cellular respiration, glyoxylate, and amino acid metabolism. Organic acids and glutathione were secreted from the roots for rhizospheric metal chelation (Kiiskila et al., 2020).

The role of arbuscular mycorrhizal fungi (AMF) associated with *C. zizanioides* grown in heavy metal-contaminated soils in phytoremediation greenhouse studies has been evaluated in several studies. The inoculation of AMF (*Rhizophagus intraradices* and *Glomus versiforme*) into Pb-contaminated soil increased the shoot and root dry weight of the *C. zizanioides* and increased both the Pb levels in the shoot and the root uptake levels (Bahraminia et al., 2016). Likewise, inoculation of a $HgCl_2$-contaminated soil with AMF (MykovamTM and *Glomus* sp.) increased the overall *C. zizanioides* weight more than the plants grown in the uninoculated soil for all tested $HgCl_2$ concentrations (Bretaña et al., 2019). The AMF improved the mineral uptake of the plants, reduced the contaminant toxicity, and increased the plant's tolerance to environmental stress in the associated hosts. The metals were absorbed through the fungal hyphae and then transported to the plant. Moreover, the presence of the AMF contributed to metal immobilization in the soil (Sahraoui et al., 2022).

(4) Eichhornia crassipes (Mart.) Solms (water hyacinth)

Eichhornia crassipes is a fast-growing free-floating macrophyte with a fibrous root system (Figure 4). This plant was first introduced to Thailand in 1901 by King Chulalongkorn the Great (Rama V), who brought it back from a visit to Indonesia and was grown in Sa Pathum Palace, a royal residence. However, due to its high growth rate and ease of dispersal, some water hyacinths colonized nearby canals, including Khlong Samsen, Klong Prem Prachakorn, and Khlong Phadung Krung Kasem (Ariyakanon, 2018), and then spread further. Nowadays, *E. crassipes* is widespread across the surface water in Thailand (Plant pest in Thailand, 2023). The optimum growth temperature of *E. crassipes* is 25-30°C with a maximum temperature of 33-35°C and its pH tolerance is estimated at pH 5.0-7.5. However, *E. crassipes* does not grow once the average salinity is greater than 15% (Wikipedia, 2023b).

Eichhornia crassipes has been studied for phytoremediation because of its rapid proliferation rate and high biomass production without showing many toxic symptoms (Malar et al., 2015). This plant is considered a multipurpose phytoremediator because it decontaminates inorganic nutrients, toxic metals, and persistent organic pollutants (Mishra and Maiti, 2017). It has been reported that *E. crassipes* is a promising plant species for the remediation of natural waterbodies/wastewater polluted with low levels of Zinc (Zn), chromium (Cr), copper (Cu), cadmium (Cd), Lead (Pb), silver (Ag), and nickel (Ni) (Priyanka et al., 2017). Evaluation of the heavy metal removal by *E. crassipes* in the Bueng Makkasan Pond (Central Thailand) revealed the accumulation of heavy metals (Zn, Mn, Cu, Cd, Pb, and Ni) in the roots of *E. crassipes* was significantly higher than in the shoots. This plant also absorbed nutrients (N, P, K, Ca, and Mg) from the wastewater (Chunkao et al., 2012). The high tolerance and affinity of *E. crassipes* for heavy metal accumulation are due to the high cellulose content and its functional groups, including amino ($-NH_2$), carboxyl (-COOH), hydroxyl (-OH), and sulfhydryl (-SH) groups (Patel, 2012).

The application of *E. crassipes* for wastewater treatment on a laboratory scale was evaluated using residential and surimi wastewater at 10-50% (v/v). The water parameters, including total Kjeldahl nitrogen (TKN) and total phosphorus (TP), biological oxygen demand (BOD), chemical oxygen demand (COD), and total suspended solids (TSS), in each wastewater were analyzed before and after phytoremediation. The removal efficiency of TKN, TP, BOD, COD, and TSS in 10% (v/v) residential wastewater ranged from 61.4 to 90.1%, while for 10% (v/v) surimi wastewater it was in the range of 62.3 to 90.6%, respectively, (Wattanapanich et al., 2020).

Three mechanisms have been described for the heavy metal removal from water by *E. crassipes*: root absorption, foliar absorption, and adsorption (Zhang et al., 2015). The root absorption uses carboxyl groups in the root systems that cause cation exchange inside the cell membrane and stimulate the movement of the heavy metals in the roots by an active absorption process. Foliar absorption occurs when contaminants are passively absorbed by stoma cells and cracks in the cuticle. A comparatively low amount of contaminant absorption takes place by foliar absorption. Finally, the adsorption process occurs at the rhizosphere of the plant, where *E. crassipes* has dense fibrous roots that help to trap suspended solids and bacteria. This offers proper attachment sites for the growth of fungus and bacteria; hence the contaminants get absorbed easily because of the ionic imbalance throughout the cell membrane (Aqdas and Hashmi, 2023).

Figure 4. *E. crassipes*

(5) *Pistia stratiotes* L. (water lettuce)

Pistia stratiotes is a free-floating and perennial aquatic macrophyte (Figure 5). It was first discovered from the Nile near Lake Victoria in Africa, but is now widely distributed in tropical and subtropical fresh waterways, especially in slow-moving rivers, lakes, and ponds, including across Thailand. The optimal growth temperature of this species is 22-30°C, but it can endure extreme temperatures of up to 35°C. The optimal pH of this is plant is slightly acidic water (pH 6.5-7.2) (Wikipedia, 2023c).

Currently, *P. stratiotes* is distributed in every part of Thailand and is commonly found in standing surface water, including lakes and ponds (BGO Plant Databases, 2023). It can remove several heavy metals from water due to its extensive root systems (Farnese et al., 2014). The advantages of *P. stratiotes* are that it is fast-growing with a large biomass, can cover large water surfaces, and requires an uncomplicated harvesting process (Pang et al., 2023).

Thirteen species of aquatic plants collected from unpolluted water around Bangkok, Thailand, including *Lemna minor*, *Typha angustifolia*, and *P. stratiotes*, were tested for their heavy metal accumulation in the laboratory. The results showed that *P. stratiotes* did not tolerate a high concentration of Cd (10 mg/L). However, at low Cd concentrations (0.1 and 1.0 mg/L), it accumulated 182.09 and 2,554.52 mg/kg DW, respectively, (Bunluesin et al., 2004). The removal capacity of chlorpyrifos from the water by the two aquatic plants, *P. stratiotes* and *L. minor*, collected from the ponds at Kasetsart University, Bangkok, Thailand, was investigated in the laboratory. An initial chlorpyrifos concentration of 0.1 mg/L was reduced to an undetectable level from 4 and 5 days after culturing with *L. minor* and *P. stratiotes*, respectively, and to 82.0±1.7% and 87.0±2.1%, respectively, at an initial chlorpyrifos concentration of 0.5 mg/L (Prasertsup and Ariyakanon, 2011).

Both *E. crassipes* and *P. stratiotes* could decolorize and detoxify five different textile dyes: CI Direct Blue 201, Cibacron Blue, Cibanone Gold Yellow, Vat Green, and Moxilon Blue. The decolorization mechanisms of Direct Blue 201 dye by *E. crassipes* and *P. stratiotes* were based on biosorption and intracellular enzyme activities (Ekanayake et al., 2021). In addition, phyto-remediation of industrial sewage sludge with wetland plants on a pilot scale revealed *E. crassipes*, *Salvinia molesta*, and *P. stratiotes* as promising candidates for the removal of Cu, Cr, Cd, Ni, and Zn (Kodituwakku and Yatawara, 2020).

Plant tolerance to heavy metal stress is a complex process that includes a series of metabolic adjustments. These include the activation of detoxification and antioxidant defence systems and related protective metabolic pathways, the transformation of metabolic pathways in the plant, and the content change of many substances to reconstruct metabolic balance. The metabolic changes in *P. stratiotes* to alleviate the phytotoxicity effect of a Zn and Cd combination at different concentrations was evaluated in the laboratory. The results revealed that *P. stratiotes* increased heat dissipation in the leaf photosynthetic apparatus to reduce the damage caused by excess excitation energy to the photosystem II (PS II) reaction center and safeguard the balance between absorption and utilization of light energy. The plant also increased the APX activity and the oxidized

ascorbic acid (i.e., dehydroascorbic acid) content in the leaves to enhance the antioxidant capacity of the ascorbate-glutathione (AsA-GSH) cycle and maintain the stability of the reduced glutathione (GSH) and oxidized glutathione (GSSG) contents. Finally, the plant increased the levels of carnosol, and substances related to lipid metabolism (including the cutin, suberine, and wax biosynthesis pathway), to maintain cell stability and increase resistance to the combined stress of Zn and Cd (Li et al., 2022).

Figure 5. *P. stratiotes*

5. FUTURE PERSPECTIVES FOR PHYTO-REMEDIATION

Phytoremediation is an eco-friendly technology with great potential to decontaminate soil and water. To date, some mechanisms of the plant's ability to uptake heavy metals or organic pollutants have been explicitly studied at the cellular level. However, clarification of the mechanism related to specific genes and enzymes in plants is missing yet is essential to increase our knowledge and phytoremediation efficiency.

- Many successful cases of phytoremediation have been reported. However, most of these studies are at the greenhouse or small pilot scale. Actual real-world application studies, such as in wastewater treatment systems in factories, municipalities, and canteens, are lacking yet are critical for achieving a better environment for the next generation.
- The interaction between microorganisms in the rhizosphere and plants is complex, but poorly resolved. Therefore, it is necessary to understand it in more detail to improve metal uptake. Moreover, it will be related to discovering new metabolites and mechanisms for optimizing the degradation of organic pollutants.
- Current research has established that the use of nanotechnology and transgenic plants can enhance the phytoremediation efficiency. However, if these technologies are to be implemented in the environment, their potential adverse environmental impact and suitable and comprehensive regulatory systems must also be developed.
- After the phytoremediation process, the appropriate management of harvested plants should be carefully applied. The correct disposal of harvested plants needs to be clarified to avoid subsequent environmental (human health and ecological) risks.
- The contribution and coordination of scientists, local communities, industrial sectors, and government authorities through educational programs is required to enact long-term sustainable phytoremediation in Thailand.

6. CONCLUSION

The pollutant removal efficiency of five local plant species in Thailand and their uptake mechanism was reviewed. Two kinds of fern, *P. vittata* and *P. calomelanos*, were found in As-contaminated soil and found to be As hyperaccumulators. *C. zizanioides is* generally found in all regions of Thailand and is tolerant to extreme environmental conditions (pH and temperature) and has a long root system. It can be applied for heavy metal removal from soil and wastewater. *E. crassipes* is widespread in the surface water across Thailand and has a suitable optimum growth temperature of 25-30 °C and pH tolerance at

5.0-7.5. It can be applied to remove some heavy metals and nutrients from water. *P. stratiotes* is mostly found in standing surface water, including lakes and ponds, in every part of Thailand. It can be applied to remove heavy metals, chlorpyrifos, and textile dyes from contaminated water. Because these five plant species can uptake high concentration of pollutants, proper management of the plants after harvesting should be carefully applied. This process could then lead to sustainable phytoremediation.

ACKNOWLEDGEMENTS

Photos of *P. calomelanos* and *P. vittata* were supported by Emeritus Professor Dr. Thaweesakdi Boonkerd and Assistant Prof. Dr. Rossarin Pollawatn, Plants of Thailand Research Unit, Department of Botany, Faculty of science, Chulalongkorn University. The author expresses appreciation for their kind assistance. The author thanks Dr. Robert Butcher for editing the grammar of this final manuscript.

REFERENCES

Akhtar ABT, Yasar A, Rabia Ali R, Irfan R. Phytoremediation using aquatic Macrophytes. In: Ansari AA, Gill SS, Gill R, Lanza GR, Newman L, editors. Phytoremediation: Management of Environmental Contaminants. Springer International Publishing; 2017. p. 259-76.

Ali S, Abbas Z, Rizwan M, Zaheer IE, Yavas I, Unay A, et al. Application of foating aquatic plants in phytoremediation of heavy metals polluted water: A review. Sustainability 2020;12(5):Article No. 1927.

Aqdas A, Hashmi I. Role of water hyacinth *(Eichhornia crassipes)* in integrated constructed wetlands: A review on its phytoremediation potential. International Journal of Environmental Science and Technology 2023;20:2259-66.

Ariyakanon A. Water hyacinth and wastewater treatment. Environmental Journal 2018;22:49-55 (in Thai).

Bahraminia M, Zarei M, Ronaghi A, Ghasemi-Fasaei R. Effectiveness of arbuscular mycorrhizal fungi in phytoremediation of lead-contaminated soil by vetiver grass. International Journal of Phytoremediation 2016;18:730-7.

BGO Plant Databases. *Pistia stratiotes.* The Botanical Garden Organization [internet]. 2023 [cited 2023 Jul 24]. Available from: http://www.qsbg.org/Database/BOTANIC_Book%20full%20option/search_detail.asp?botanic_id=1625.

Bretaña BL, Salcedo S, Casim L, Manceras R. Growth performance and inorganic mercury uptake of Vetiver (*Chrysopogon zizanoides* Nash) inoculated with arbuscular mycorrhiza fungi (AMF): Its implication to phytoremediation. Journal of Agricultural Research, Development, Extension and Technology 2019;25(1):39-47.

Bunluesin S, Kruatrachue M, Pokethitiyook P, Lanza GR, Upatham ES, Soonthornsarathool V. Plant screening and comparison of *Ceratophyllum demersum* and *Hydrilla verticillata* for cadmium accumulation. Bulletin of Environmental Contamination and Toxicology 2004;73:591-8.

Chunkao K, Nimpee C, Duangmal K. The King's initiatives using water hyacinth to remove heavy metals and plant nutrients from wastewater through Bueng Makkasan in Bangkok, Thailand. Ecological Engineering 2012;39:40-52.

Das P, Datta R, Makris KC, Sarkar D. Vetiver grass is capable of removing TNT from soil in the presence of urea. Environmetal Pollution 2010;158:1980-3.

Ekanayake MS, Udayanga D, Wijesekara I, Manage P. Phytoremediation of synthetic textile dyes: Biosorption and enzymatic degradation involved in efficient dye decolorization by *Eichhornia crassipes* (Mart.) Solms and *Pistia stratiotes* L. Environmental Science and Pollution Research 2021;28: 20476-86.

EnvironWiki. Sustainable remediation [internet]. 2023 [cited 2023 Apr 22]. Available from: http://www.enviro.wiki/index.php?title=Sustainable_Remediation.

Farnese FS, Oliveira JA, Gusman GS, Leao GA, Silveira NM, Silva PM, et al. Effects of adding nitroprusside on arsenic stressed response of *Pistia stratiotes* L. under hydroponic conditions. International Journal of Phytoremediation 2014; 16(2):123-37.

Fayiga AO, Saha UK. Arsenic hyperaccumulating fern: Implications for remediation of arsenic contaminated soils. Geoderma 2016;284:132-43.

Hettiarachchi E, Paul S, Cadol D, Frey B, Rubasinghege G. Mineralogy controlled dissolution of uranium from airborne dust in simulated lung fluids (SLFs) and possible health implications. Environmental Science and Technology Letters 2019;6(2):62-7.

Jankong P, Visoottiviseth P, Khokiattiwong S. Enhanced phytoremediation of arsenic contaminated land. Chemosphere 2007;68:1906-12.

Kafle A, Timilsina A, Gautam A, Adhikari K, Bhattarai A, Aryal N. Phytoremediation: Mechanisms, plant selection and enhancement by natural and synthetic agents. Environmental Advances 2022;8:Article No. 100203.

Kiiskila JD, Li K, Sarkar D, Datta R. Metabolic response of vetiver grass (*Chrysopogon zizanioides*) to acid mine drainage. Chemosphere 2020;240:Article No. 124961.

Kodituwakku K, Yatawara M. Phytoremediation of industrial sewage sludge with *Eichhornia crassipes*, *Salvinia molesta*, and *Pistia stratiotes* in batch fed free water flow constructed wetlands. Bulletin of Environmental Contamination and Toxicology 2020;104:627-33.

Latif A, Abbas A, Iqbal J, Azeem M, Asghar W, Ullah R, et al. Remediation of environmental contaminants through phytotechnology. Water, Air, and Soil Pollution 2023; 234:Article No. 139.

Li Y, Xin J, Tian R. Physiological defense and metabolic strategy of *Pistia stratiotes* in response to zinc-cadmium co-pollution. Plant Physiology and Biochemistry 2022;178:1-11.

Mahar A, Wang P, Ali A, Awasthi MK, Lahori AH, Wang Q, et al. Challenges and opportunities in the phytoremediation of heavy metals contaminated soils: A review. Ecotoxicology and Environmental Safety 2016;126:111-21.

Malar S, Sahi SV, Favas PJC, Venkatachalam P. Mercury heavy-metal-induced physiochemical changes and genotoxic alterations in water hyacinths (*Eichhornia crassipes* Mart.). Environmental Science and Pollution Research 2015;22: 4597-608.

Memon A, Kusur F, Memon M. Metal Hyperaccumulator plants and their role in phytoremediation. In: Prasad R, editor.

Phytoremediation for Environmental Sustainability. Springer Nature; 2021. p. 1-24.

Mishra S, Maiti A. The efficiency of *Eichhornia crassipes* in the removal of organic and inorganic pollutants from wastewater: A review. Environmental Science and Pollution Research 2017;24:7921-37.

Nedjimi B. Phytoremediation: A sustainable environmental technology for heavy metals decontamination. SN Applied Sciences 2021;3:Article No. 286.

Pandey S, Rai R, Rai LC. Biochemical and molecular basis of As toxicity and tolerance in microbes and plants. In: Flora SJS, editor. Handbook of Arsenic Toxicology. Academic Press; 2015. p. 627-74.

Pang YL, Quek YY, Lim S, Shuit SH. Review on phytoremediation potential of floating aquatic plants for heavy metals: A promising approach. Sustainability 2023;15:1-23.

Patel S. Threats, management and envisaged utilizations of aquatic weed *Eichhornia crassipes*: An overview. Reviews in Environmental Science and Bio/Technology 2012;11:249-59.

Plant Pest in Thailand. *Eichhornia crassipes* (Mart.) Solms [internet]. 2023 [cited 2023 Jul 24]. Available from: http://ippc.acfs.go.th/pest/G001/T010/WEED030.

Prasertsup P, Ariyakanon N. Removal of chlorpyrifos by water lettuce (*Pistia stratiotes* L.) and duckweed (*Lemna minor* L.). International Journal of Phytoremediation 2011;13:383-95.

Priyanka S, Shinde O, Sarkar S. Phytoremediation of industrial mines wastewater using water hyacinth. International Journal of Phytoremediation 2017;19:87-96.

Rosen BP. Biochemistry of arsenic detoxification. FEBS Letters 2002;529(1):86-92.

Roongtanakiat N. Vetiver in Thailand: General aspects and basic studies. KU Science Journal 2006;24:13-9.

Roongtanakiat N, Tangruangkiat S, Meesat R. Utilization of vetiver grass (V*etiveria zizanioides*) for removal of heavy metals from industrial wastewaters. ScienceAsia 2007;33: 397-403.

Rotkittikhun P, Chaiyarat R, Kruatrachue M, Pokethitiyook P, Baker AJM. Growth and lead accumulation by the grasses *Vetiveria zizanioides* and *Thysanolaena maxima* in lead-contaminated soil amended with pig manure and fertilizer: A glasshouse study. Chemosphere 2007;66:45-53.

Sahraoui ALH, Calonne-Salmon M, Labidi S, Meglouli H, Fontaine J. Arbuscular mycorrhizal fungi-assisted phytoremediation: Concepts, challenges, and future perspectives. Assisted Phytoremediation 2022;3:49-99.

Santra SC, Samal AC, Bharttacharya P, Banerjee S, Biswas A, Majumdar J. Arsenic in food chain and community health risk: A study in Gangetic West Bengal. Procedia Environmental Sciences 2013;18:2-13.

Singh H, Pant G. Phytoremediation: Low input-based ecological approach for sustainable environment. Applied Water Science 2023;13:Article No. 85.

Soongsombat P, Kruatrachue M, Chaiyarat R, Pokethitiyook P, Ngernsansaruay C. Lead tolerance in *Pteris vittata* and *Pityrogramma calomelanos* and their potential for phytoremediation of lead-contaminated soil. International Journal of Phytoremediation 2009;11:396-412.

Srivastava M, Ma LQ, Singh N, Singh S. Antioxidant responses of hyperaccumulator and sensitive fern species to arsenic. Journal of Experimental Botany 2005;56:1335-42.

Upatham ES, Pokethitiyook P, Panich-Pat T, Lanza GR. Phytoremediation in Thailand: A summary of selected research and case histories. In: Ansari AA, Gill SS, Gill R, Lanza GR, Newman L. editors. Phytoremediation: Management of Environmental Contaminants. Switzerland: Springer International Publishing; 2014. p. 333-48.

Visoottiviseth P, Francesconi K, Sridokchan W. The potential of Thai indigenous plant species for the phytoremediation of arsenic contaminated land. Environmental Pollution 2002;118 453-61.

Wattanapanich C, Durongpongtorn N, Ariyakanon N. Performance of water hyacinth (*Eichhornia crassipes*) in the treatment of residential and surimi wastewater. Environment Asia 2020;13(2):124-37.

Wei S, Ma LQ, Saha U, Mathews S, Sundaram S, Rathinasabapathi B, et al. Sulfate and glutathione enhanced arsenic accumulation by arsenic hyperaccumulator *Pteris vittata L.* Environmental Pollution 2010;158:1530-5.

Wikipedia. *Chrysopogon zizanioides* [internet]. 2023a [cited 2023 Apr 9]. Available from: https://en.wikipedia.org/wiki/ Chrysopogon_zizanioides.

Wikipedia. *Pistia stratiotes* [internet]. 2023c [cited 2023 Jul 24]. Available from: https://en.wikipedia.org/wiki/Pistia.

Wikipedia. *Pontederia crassipes* [internet]. 2023b [cited 2023 Jul 24]. Available from: https://en.wikipedia.org/wiki/Pontederia _crassipes.

Yan A, Wang Y, Tan SN, Yusof MLM, Ghosh S, Chen Z. Phytoremediation: A promising approach for revegetation of heavy metal-polluted soil. Frontiers of Plant Science 2020;11:Article No. 359.

Yang W, Gu J, Zhou H, Huang F, Yuan T, Zhang J, et al. Efect of three napier grass varieties on phytoextraction of Cd- and Zn-contaminated cultivated soil under mowing and their safe utilization. Environmental Science and Pollution Research 2020;27:16134-44.

Zhang F, Wang X, Yin D, Peng B, Tan C, Liu Y, et al. Efficiency and mechanisms of Cd removal from aqueous solution by biochar derived from water hyacinth (*Eichhornia crassipes*). Journal of Environmental Management 2015;153:68-73.

Assessing Social Vulnerability to Climate Change in a Fishery-Dependent Village in South Central Vietnam

Olumide Samuel Olowe[1], Harliqueen S. Jacinto[2*], Jomel S. Limbago[2], Ewumi Azeez Folorunso[3], Isaac Sarfo[4], and Christopher Brown[1]

[1]Graduate School of World Fisheries University, Pukyong National University, Busan, Korea
[2]Fisheries and Aquatic Sciences Department, Cavite State University Naic, Bucana Malaki, Naic, Cavite, Philippines
[3]Faculty of Fisheries and Protection of Waters, South Bohemian Research Center of Aquaculture and Biodiversity of Hydrocenoses, Institute of Aquaculture and Protection of Waters, University of South Bohemia in Ceske Budejovice, České Budějovice 370 05, Czech Republic
[4]Research Institute for History of Science and Technology, Nanjing University of Information Science and Technology, 210044 Nanjing-Jiangsu, China

ARTICLE INFO

Received: 30 Jan 2023
Received in revised: 13 Jun 2022
Accepted: 15 Jun 2023
Published online: 23 Aug 2023
DOI: 10.32526/ennrj/21/20230027

Keywords:
Vietnam/ Social vulnerability/ Fisheries/ Aquaculture/ Climate change/ Resources-dependent livelihoods

*** Corresponding author:**
E-mail: harliqueen.jacinto@cvsu-naic.edu.ph

ABSTRACT

Fishery-dependent communities are highly susceptible to the impacts of climate change due to their proximity to vulnerable coastal areas and reliance on ecosystem services for their livelihoods. The study assessed the effects of climate change on the socioeconomic livelihoods and adaptive capacity of Xuan Tu, a community located in South Central Vietnam. The assessment employed the social vulnerability index (SVI) and adaptive capacity index (ACI). A hybrid data collection approach was utilized to gather information from households, and a composite method was employed to aggregate the data, enabling an assessment of community vulnerability. The findings indicated exposure, sensitivity, and adaptive capacity index values of 0.16, 0.34, and 0.26, respectively. The community exhibited a moderate vulnerability to climate change, with a social vulnerability index of 0.43. Notably, economic sufficiency, access to social groups, and level of education emerged as significant factors in reducing social vulnerability. To adapt to climate change, the community modified their fish feeding practices, fish culture methods, increased technology usage, and diversified their sources of income. However, the study identified a lack of institutional support as a significant obstacle to the community's autonomous adaptation. Based on these results, the study recommends livelihood diversification and the implementation of planned adaptation strategies to enhance preparedness for climate emergencies in South Central Vietnam.

1. INTRODUCTION

Countries in Southeast Asia are among the most vulnerable to climate change owing to socioeconomic factors and high climate risk exposure (Kay et al., 2023). Due to their proximity to high-risk areas, rural households and communities below the poverty line in Southeast Asia face the dual challenge of climate change impacts and unsustainable urbanization (Arfanuzzaman and Dahiya, 2019; Marotzke et al., 2020). Moreover, the dependency of these communities on natural resources for their livelihoods makes them more vulnerable to short-term and long-term climate change impacts (Asfaw et al., 2021).

Vietnam, a Southeast Asian country, is significantly impacted by extreme climatic events caused by rising temperatures, sea level rise, salinity intrusion, and increased typhoon intensity (Schmidt-Thome et al., 2015; Trinh, 2018; Nguyen et al., 2019). These changes have devastated key sectors contributing to the country's economic growth, such as the fishery sector (Do et al., 2021). The fishery sector, which experiences an average annual growth rate of 7.9%, employs 10% of the population and contributes 4-5% to the GDP, making it one of Vietnam's most promising economic sectors (Nguyen et al., 2017b).

Citation: Olowe OS, Jacinto HS, Limbago JS, Folorunso A, Sarfo I, Brown C. Assessing social vulnerability to climate change in a fishery-dependent village in South Central Vietnam. Environ. Nat. Resour. J. 2023;21(5):390-401. (https://doi.org/10.32526/ennrj/21/20230027)

Vietnam's coastal communities rely heavily on the fishery sector for their livelihoods, making them particularly susceptible to climate stressors and disturbances (Nguyen et al., 2019). The south-central coast of Vietnam, in particular, has witnessed a rise in heavy rainfall and temperatures, rendering it more vulnerable to tropical cyclones (Ngo-Duc, 2014; Ho, 2018). In recent years, Khanh Hoa province in Southeast Asia has experienced a series of tropical cyclone events (Mau et al., 2019; Tran-Quang et al., 2020). Notably, the province has faced the destructive impact of record-breaking typhoons, such as Mirinae and Damrey, which have caused severe damage to aquaculture cages, fishing crafts, and shelters (DiGregorio, 2013).

Vulnerability assessment of coastal communities to climate change offers information on the impact of changes on their livelihood and ability to cope at the household level (Otto et al., 2017). Vulnerability assessment is multidisciplinary, with no generally accepted assessment method (Murphy et al., 2015). It may focus on the risk-hazard approach relying on biophysical and top-down information using climate projections or socioeconomic conditions relying on bottom-up information at the household level (Hammill et al., 2013). A concept used in assessing human ability or inability to cope with negative externalities in their livelihood is termed social vulnerability (Kelly and Adger, 2000). Social vulnerability determines the localized sensitivity of a community to climate change and the community's ability to cope with extreme events (Khan, 2012; Nguyen et al., 2019). Assessment at the household level is core to social vulnerability assessment as it directly targets vulnerable groups for effective risk management (Mason et al., 2021). It uses indices selected from deductive and inductive approaches. The former creates a social vulnerability index based on prior knowledge from the existing literature, while the latter uses variables that influence social vulnerability (Yoon, 2012). Studies on social vulnerability have also been undertaken in Vietnam (Adger, 1999; Rubin, 2014; Avelino et al., 2018; Huynh and Stringer, 2018; Huong et al., 2019). These studies focused on agriculture and natural resources, mainly in the Red River Delta and the Mekong Delta in the south.

To date, there are limited climate vulnerability studies in the south-central region of Vietnam, especially in Khanh Hoa Province. Despite being significant producer of spiny lobster with a 1,506 MT contribution to the country's total lobster production in 2020 (Hai and Speelman, 2020; Du et al., 2022; Phu et al., 2022), there is a lack of studies investigating climate vulnerability in the region. Specifically, there is no current study on the vulnerability of Xuan Tu Village, located in Khanh Hoa Province, where lobster farming originated. Moreover, Xuan Tu Lagoon is home to seagrass beds that support various aquatic fauna and flora, although the seagrass population has declined over the years due to the impact of extensive aquaculture and climate change (Nguyen et al., 2022). Given the significance of Xuan Tu Village for aquaculture and aquatic biodiversity in Vietnam, it is imperative to investigate the impact of climate change on this village to develop effective adaptation and resilience measures. Hence, this study targets this research gap by assessing social vulnerability at household scales in a coastal community in south-central Vietnam, building on existing social vulnerability assessment approaches. As there is no definitive index or approach to defining social vulnerability, a bottom-up approach was used based on the researchers' understanding of vulnerability (Khan, 2012). The study identified the socioeconomic vulnerability of the village at the household level and evaluated the factors influencing adaptation strategies and adaptive capacity. This work will enable government agencies to prioritize local adaptation strategies to climate change vulnerability.

2. METHODOLOGY

2.1 Description of the study area

Xuan Tu is a coastal village in Van Hung commune in Khanh Hoa, a South-Central Province in Vietnam (Figure 1). Xuan Tu Village covers 80 ha, with a total population of 2,735 people belonging to 553 households (Hue, 2010). With a bay area of 472 ha, 75% of the household are engaged in fishery activities (aquaculture and capture fishing), with a fish culture area of 118 ha, establishing the village as a prominent center for lobster aquaculture in Khanh Hoa (Tuan, 2004; Hue, 2010). Fishing activities have been banned near the co-managed Trao Reef Marine Reserve (Nguyen, 2010). The village lacks a medical facility but is accessible with good road networks and basic amenities such as the internet, telecommunications, and electricity. The village's proximity to the sea means it is affected by increased tropical cyclones, among other large-scale climate events in the Khanh Hoa Province.

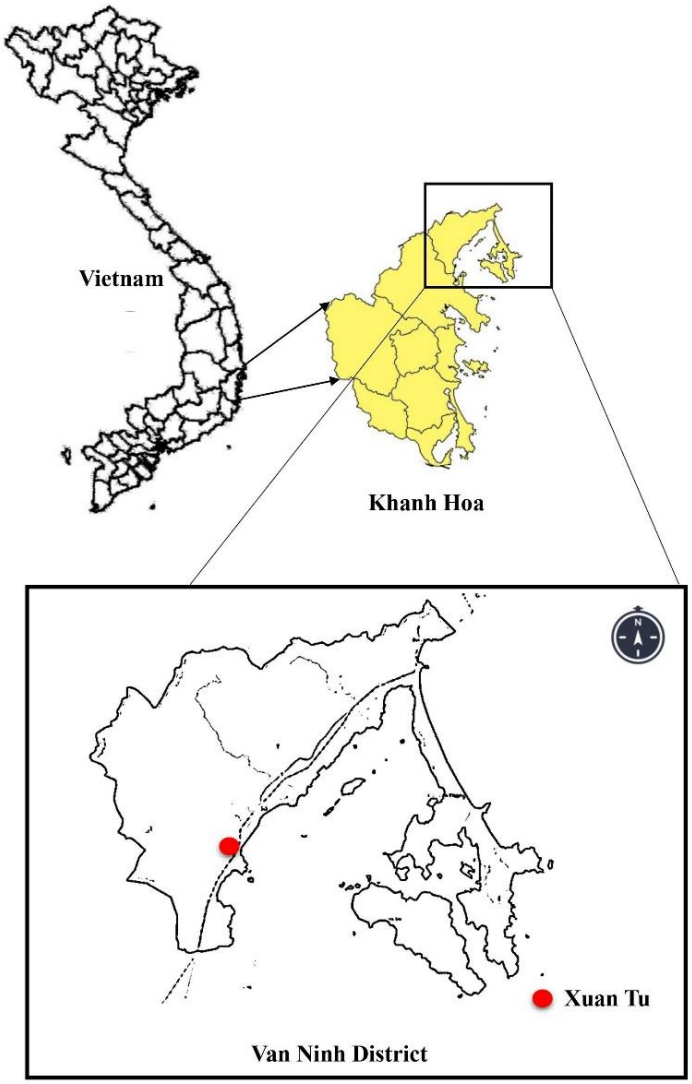

Figure 1. Map of Xuan Tu, a coastal village in South Central Vietnam

2.2 Data collection

This study employed a mixed-method approach using questionnaires and key informant interviews. A semi-structured questionnaire was administered to 61 heads of households (male and female). This method to ensure equal representation of households is based on a previously described method (Yamane, 1967). The mathematical representation of the sample size calculation is as follows:

$$n = \frac{N}{1 + N(e)^2} = \frac{553}{1 + 553(10\%)^2} = 84$$

Where; n represents the sample size, N denotes the total number of households, and e represents the assumed margin of error (10%). A higher margin error was used to balance between precision and practicality due to practical constraints such as time, resources, and responsiveness which may limit the ability to obtain a larger sample. However, some of the households were unresponsive.

Before implementation, a qualified translator from Nha Trang University translated the questionnaire into Vietnamese. Additionally, a qualified independent translator checked for accuracy to ensure translated accuracy and appropriateness, and the discrepancies were resolved through collaborative discussions. The interviews were conducted by a trained Vietnamese scientific interpreter familiar with the subject matter. The survey was designed with four sections: demographic characteristics, perception, livelihood, and adaptation measures. Four individuals in the community: a government official (village head), a manager of the Trao reef, an NGO official, and a spiritual leader, were interviewed to enrich the data collected. These interviewees were selected based on contacts made during the preliminary survey and

consultation with a researcher from Nha Trang University in Khanh Hoa Province, Vietnam, who was familiar with the area. Data collection was carried out from November 2017 to February 2018. It began with a preliminary survey and pilot testing of the questionnaire with 10 households in the community. This provided an overview of the general conditions of the community and facilitated the selection of indicators used in this study. The indicators were based on reviews of past disasters as reflected in previous studies (Wu et al., 2002; Zahran et al., 2008; Hou et al., 2016). Additional inputs were considered from community experts along with the household questionnaires administered. However, this may be subjective because the approach is characterized by expert knowledge and with lesser indicators (Vincent, 2004). The indicators were sub-subdivided to fit in with the IPCC's determinants of climate change: exposure, sensitivity, and adaptive capacity (IPCC, 2014). The Vietnam government statistical office supplied meteorological data on annual temperature, mean annual rainfall, data on storms, and coastal erosion, which form the exposure to climate change. These were selected based on consultation with the community leader and the Trao Reef Protected Area Officer. The data collected were used to develop a social vulnerability index and adaptive capacity index for climate change.

2.3 Indicator's functional relationship

Vulnerability indicators should be selected based on theoretical linkages between drivers of social vulnerability and socioeconomic conditions (Adger and Vincent, 2005). The criteria for selecting indicators were based on objective observation from the community and communication with the key informants, which were then linked to existing literature. There is no established standardized indicator or framework for quantifying vulnerability to hazards (Cutter et al., 2010). The IPCC determinant of vulnerability is exposure, sensitivity, and adaptive capacity (Table 1). According to IPCC (2001), exposure refers to the nature and degree to which a system is exposed to significant climatic variations. Indicators of exposure include mean annual temperature (Mendoza et al., 2014), mean annual precipitation, percentage of storms (Žurovec et al., 2017), and flood occurrences (Mendoza et al., 2014). Meanwhile, the level of sensitivity refers to how much risk exposure impacts the system. Indicators of sensitivity are; lack of income diversification (Eakin and Bojórquez-Tapia, 2008), percentage of fishers above 60 years (Wu et al., 2002), percentage of households without hazard-resistant shelter, and percentage of female-headed households (Jepson and Colburn, 2013). Exposure and sensitivity affect communities by increasing their susceptibility, hence their positive (+) relationship with vulnerability. Adaptive capacity describes the ability of a system to cope and create opportunities in a climate-related event. Adaptive capacity to climate change is dependent on access to loans, level of literacy (Deressa et al., 2008), access to information (Lo and Emmanuel, 2013), social group (Egyir et al., 2015), and poverty level (Adger, 1999). Adaptive capacity reduces vulnerability to climate change as it aids coping and development of adaptation strategies; therefore, it negatively (-) influences vulnerability. Table 2 shows the indicators of adaptive capacity identified from previous studies (Tan et al., 2018; Salik et al., 2015; Tan et al., 2018; Umamaheswari et al., 2021) and subjectively by the authors based on communication with experts in the community.

Table 1. Dimensions and indicators of vulnerability

Dimensions of vulnerability	Indicators	Explanation	References
Exposure	Mean annual temperature (+)	To understand climate pattern	Mendoza et al. (2014)
	Mean annual precipitation (+)	To understand climate pattern	Žurovec et al. (2017)
	Percentage of storms (+)	To detect the frequency of disasters	
	Percentage of flood occurrence (+)	To detect the frequency of disasters	Mendoza et al. (2014)
Sensitivity	Lack of income diversification (+)	To identify the livelihood status of the households	Eakin and Bojórquez-Tapia (2008)
	Percentage of fishers above 60 years (+)	Identify age-related sensitivity	Wu et al. (2002)
	Percentage of households without hazard resistant shelter (+)	To identify the preparedness of the households	Wu et al. (2002)

Table 1. Dimensions and indicators of vulnerability (cont.)

Dimensions of vulnerability	Indicators	Explanation	References
Sensitivity	Percentage of female-headed households (+)	To figure out if the gender of households affects coping	Jepson and Colburn (2013)
Adaptive capacity	Access to loan (-)	To identify whether they have access to credit	Ahsan and Warner (2014)
	Percentage of people with secondary school education (-)	To identify the level of literacy	Deressa et al. (2008)
	Percentage of people with access to information (-)	To identify their knowledge of climate change	Lo and Emmanuel (2013)
	Access to at least one social group (-)	To understand whether they have social supports	Egyir et al. (2015)
	Percentage of people above the poverty line (-)	To understand if income affects their copy mechanism	Adger (1999)

Table 2. Indicators of adaptive capacity

Component	Indicators	Explanation	References
Social support	Access to at least one social group	-	Tan et al. (2018)
	Percentage of people with secondary education	Education level of the household head	Salik et al. (2015)
	Percentage of people with quality shelter	The infrastructure is critical in determining a vulnerable population's ability to adapt.	Salik et al. (2015)
	Access to at least one information service	Access to technical information on the climatic occurrence	Tan et al. (2018)
Economic sufficiency	Access to loan	To determine whether households have access to credit	Tan et al. (2018)
	Percentage of people with diversified income	To understand whether households generate income from alternate livelihood activities	Umamaheswari et al. (2021)
	Improved technology	Access to improve fishing gear and cages	
	Per capita income	Higher-income might improve coping ability	
Institutions/ governance	Early warning from the district officer	Communication and early warning about impending climatic extremes	Umamaheswari et al. (2021)
	External support for adaptation		
	Climate education		
	Financial support from institutions		

2.4 Data analyses

The data were analyzed quantitatively to assess social vulnerability and adaptive capacity. Indicators of exposure and adaptive capacity were measured using different scales and units. For comparison, the indicators used were normalized. Indicator values were normalized between 0 and 1 based on the United Nations Development Program (UNDP, 1990) parameters for measuring the Human Development Index (HDI). The functional relationships of the indicators were used to determine the normalization equation. For positive correlation, the equation is as follows:

$$Xij = \frac{Xi - Min.\ Xj}{Max.\ Xj - Min.Xj}$$

And for negative correlation, the equation:

$$Xij = \frac{Max.\ Xj - Xi}{Max.\ Xj - Min.\ Xj}$$

Where; X_{ij} is the value of the normalized indicator (j) to study area (i), X_i is the actual value of the indicator to (i), and Min. X_j and Max X_j are the minimum and maximum values of the indicators, respectively. After normalization, the indicators were summarized into simple averages to form composite

indices using an equal weight method. This method assumes that all indicator variables carry the same weight and was chosen for simplicity and transparency. Interestingly, there is no consensus or justification for ranking the indicators into ranges of importance or priority (Cutter et al., 2010). Weighted averages introduce an element of arbitrary choice, and regression-based weight is only visible when there is an objective measure of vulnerability outcome (Heltberg and Bonch-Osmolovskiy, 2011). The normalized indicators were integrated into the composite subindices per their dimensions. The arithmetic mean of the indicators makes up this subindex. Therefore, the final value of the vulnerability index is obtained by the arithmetic sum of sub-indices (O'Brien et al., 2004; Žurovec et al., 2017). Quantification of social vulnerability must be mathematically expressed to show the relationship between the components (Nguyen et al., 2017a). Therefore, the mathematical expression, adapted from a previously described formula (Ahsan and Warner, 2014) for the social vulnerability index, is as follows:

$$\mathrm{SVI} = \sum \frac{1}{\mathrm{n}} \mathrm{E}, \mathrm{S}, \mathrm{AC} \quad (3)$$

Where; SVI is the social vulnerability index; E is exposure; S is sensitivity; AC is the Adaptive Capacity, and n is 3, representing E, S, and AC. An inverse value (1 minus indicator score) for adaptive capacity was used for the index calculation due to its inverse relationship with vulnerability (Ahsan and Warner, 2014). The index was scaled from 0 (low vulnerability) to 1 (high vulnerability) based on a previously described composite indicator framework (Ahsan and Warner, 2014). Descriptive statistics, including frequencies and percentages, were used to summarize data from the semi-structured questionnaire on fisher's demographic characteristics.

3. RESULTS

3.1 Characteristics and livelihood of the respondents

As shown in Figure 2, 51% of the population's livelihood strategy is linked to aquaculture, which is closely followed by fishing (31%). Fishmongers comprised 7% of the respondents, while people involved in other livelihood activities, such as net knitters and boat engineers, constituted 11% of the respondents. The dominance of aquaculture is reflected in the income it generates, as shown in Figure 3. The income generated from aquaculture exceeds that from fishing and other occupations.

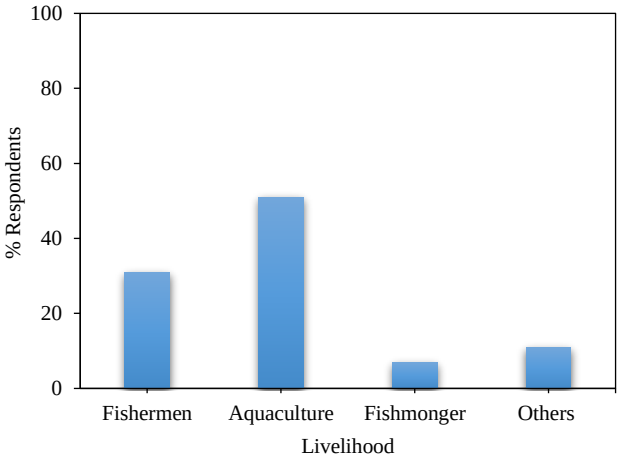

Figure 2. Livelihood of households in Xuan Tu Village, South Central Vietnam

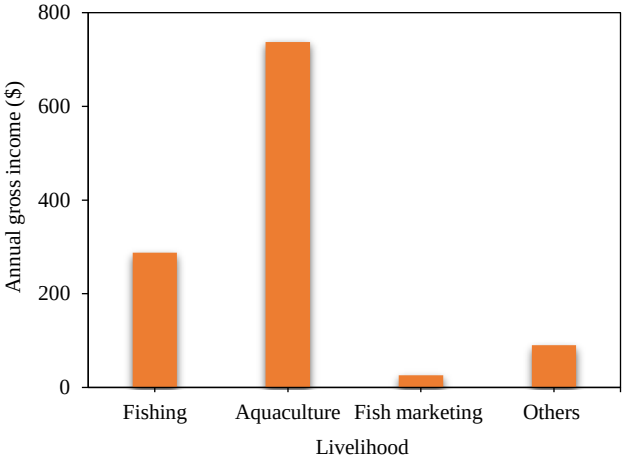

Figure 3. Annual income per livelihood in dollars (1$=22,769 Vietnamese dong)

3.2 Social vulnerability index (SVI) of the village of Xuan Tu

The sub-index of social vulnerability was calculated from vulnerability dimensions and analyzed using Microsoft Excel 2016. The findings from the analysis show that the index values of exposure, sensitivity, and adaptive capacity were 0.16, 0.34, and 0.26, respectively (Figure 4). Social vulnerability was determined by calculating the arithmetic mean of the sub-indices to give 0.43 a social vulnerability index. From the results, the social vulnerability of Xuan Tu Village is medium.

3.3 Adaptive capacity index

Based on the standard deviation of the indicators, the adaptive capacity sub-indices were ranked as follows: social capital ranked highest at 55%, economic sufficiency at 44%, and institutional support ranked lowest at 1%. The economic

sufficiency of the community is aided by access to loans and moderate-income generation, as illustrated in Figure 5. Apart from the early warning support from institutions, the findings illustrated in Figure 6 show that there is little support from institutions on climate education and financial support. Figure 7 shows that, socially, the community was better off due to the higher level of education, access to social groups, and access to information from various sources. However, they do not have access to shelters capable of withstanding extreme weather events.

3.4 Adaptation strategies

The findings revealed that the farmers changed the feeding regime and the type of fish cultured in response to climate change (Figure 8). Furthermore, there was an increase in the use of technology, and a few diversified their livelihood. However, a larger percentage of the respondents do not have adaptation strategies.

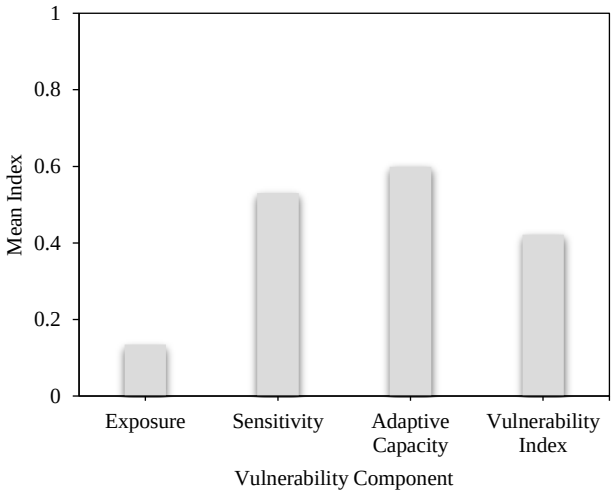

Figure 4. Social vulnerability index of Xuan Tu Village, South Central Vietnam

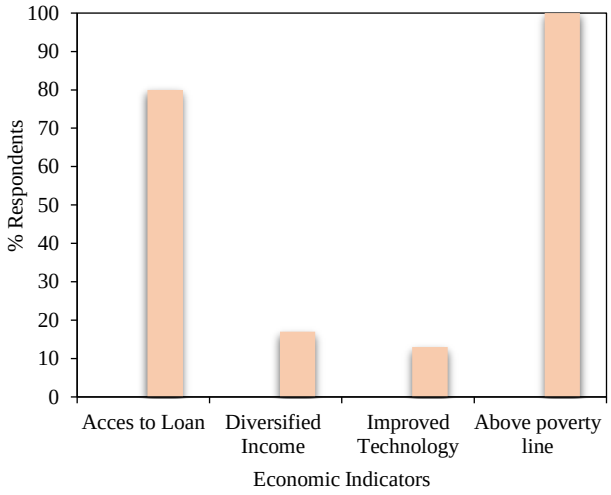

Figure 5. Economic indicators of adaptive capacity

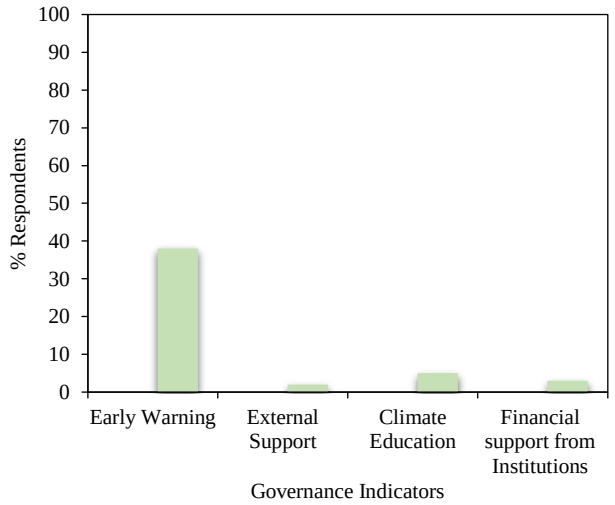

Figure 6. Governance Indicators of adaptive capacity

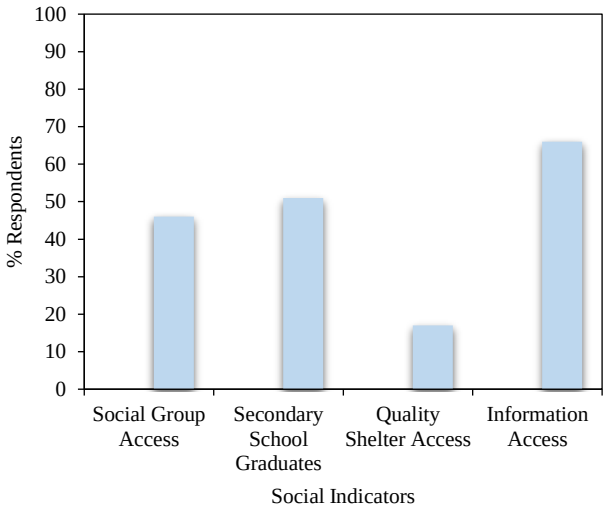

Figure 7. Social indicators of adaptive capacity

4. DISCUSSION

4.1 Social vulnerability and livelihoods

A community's vulnerability is site-specific; it can be determined by the communities' geographical location, exposure, and sensitivity (Adger et al., 2003; Ahsan and Warner, 2014). Our findings revealed that Xuan Tu is moderately vulnerable. Social vulnerability of a community describes the effects of social, economic and institutional factors that made them susceptible to climate change (Tate, 2012). We infer that the village's proximity to the sea, which dictated their livelihood, exposed them to the direct impact of climate hazards. This finding corroborates other researchers' assertion that communities in southern

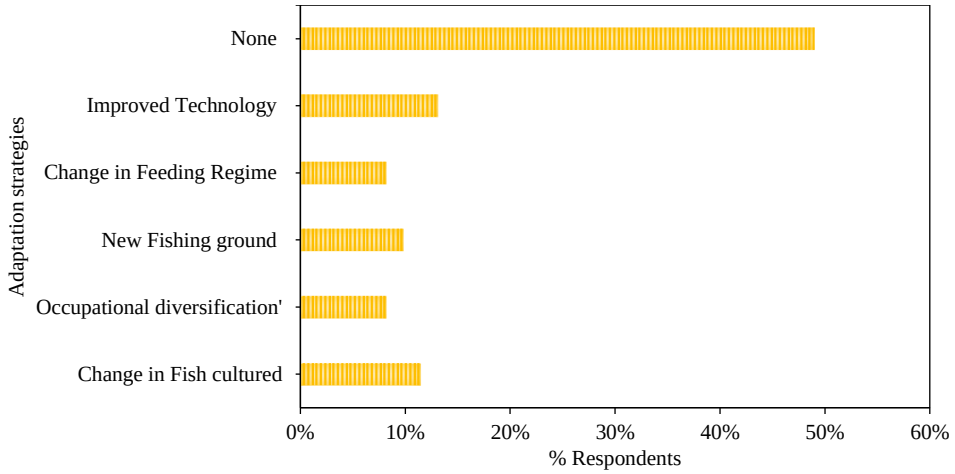

Figure 8. Adaptation strategies initiated by fish farmers in Xuan Tu Village

Vietnam are vulnerable due to their proximity to the body of water and aquaculture activities (Huynh et al., 2019; Truong et al., 2022). This study's higher sensitivity and medium vulnerability agreed with a previous study (Badjeck et al., 2010). Natural resource-dependent households, especially in fish-based communities, are sensitive to climate variability. This sensitivity within these communities can be attributed to climate-sensitive natural resources; therefore, their services are highly prone to extreme stressors or changes (Füssel, 2012; Okpara et al., 2017; Huynh and Stringer, 2018). For example, the agriculture-dependent households in Danang, Vietnam, were more vulnerable to climate change than those with diversified income sources (Huynh and Stringer, 2018). With 49% of households not diversifying their livelihoods, there would be a further increase in individual household susceptibility levels in the future, as the current single-livelihood approach is not sustainable. A sustainable livelihood approach is dynamic and ecologically coherent to achieve sustainability (Hussein and Nelson, 1998; Natarajan et al., 2022). Meanwhile, livelihoods which rely solely on agriculture and lack diversification are unsustainable (Barrett et al., 2001; Beltrán-Tolosa et al., 2022). With the inability to diversify into alternative income-generating activities, there is a tendency to increase sensitivity. Within a fishing-based livelihood, higher sensitivity and lower adaptive capacity where all households are exposed to the same stressor result in greater vulnerability, thus reducing a communities' ability to cope during climatic events. In addition to the low percentage of income diversification, it was found that most households in the area do not have access to quality shelters. Climate-resilient housing infrastructure helps mitigate the risk of climate-related vulnerability (Hernández, 2022). Lack of access to quality shelter could exacerbate climate change's impact and lead to displacement and loss of livelihoods. Fishermen face risks due to shifts in climate patterns caused by the overall increase in global temperatures and fluctuations in precipitation (Vincent-Akpu and Annor-Frempong, 2017). The ability of their households to adapt livelihood strategies will be influenced by governance processes, policies, and institutional capabilities (Huynh and Stringer, 2018). However, institutional discrimination exists in Vietnam, and impoverished individuals are inherently more at risk of natural disasters due to limited access to state resources (Adger, 1999). In the case of Xuan Tu, there is a clear indication of the requirement for detailed policies to reduce vulnerability to climate-related disasters at a local level.

Social vulnerability, defined as individuals' inability to cope with the consequences of hazards effectively, reflects the societal dynamics and its foundational social, economic, and political circumstances (Rubin, 2014). Recognizing the social vulnerability of Xuan Tu is influenced by various socioeconomic factors and institutional lapses is to provide evidence for decision-makers to provide adequate social improvements to tackle climate change. However, our choice of indicators and the selection criteria might have created a bias that could affect the result's credibility. Social vulnerability assessment is subjective and future considerations should focus on a more robust method of analysis that would reduce redundancy and uncertainty.

4.2 Adaptive capacity

A positive correlation exists between access to a social group, literacy level, economic welfare, and adaptive capacity. People with higher levels of education, income, and access to social gatherings have a greater propensity to adapt/cope with climate change, thus improving their resilience (Adger et al., 2003; Abdul-Razak and Kruse, 2017; Sarfo et al., 2019; Tran et al., 2020). The findings show that households in Xuan Tu are economically capable due to their higher-than-average income, surpassing the national average of $129 (General Statistics Office of Vietnam, 2021). A previous study observed similar findings for Southern coastal zones (Nguyen et al., 2019). Furthermore, higher income improved the adaptive capacity of agriculture-dependent communities in the Nikachu watershed, Bhutan (Choden et al., 2020). The income generated could have reduced their vulnerability because the access to capital will make it easier to adapt or restart after climate shock (Nor Diana et al., 2022). The higher education rate among respondents will positively correlate with or influence adaptive capacity within the community, and this is consistent with the findings of agrarian households in Bhutan and farmers in Nicaragua (Choden et al., 2020; Quiroga et al., 2020). Vulnerability is socially constructed and influenced by varying institutions and economics (Adger et al., 2003). Consequently, higher income and medium support from groups could improve the ability to withstand extreme climate hazards. In our study, the access to a social group in the households may have influenced their adaptive capacity. Similar findings were observed when assessing climate change in the Northern Mountainous Region of Vietnam (Ho and Kingsbury, 2019). Collective actions of society can improve their resilience in the face of threats posed by extreme climate events (Adger et al., 2003; Sarfo et al., 2019).

Higher education and access to social groups could have allowed them access to information. Information on climate change or early warnings can improve readiness to cope or adapt, improving adaptive capacity. This implies that respondents with access to information have a higher adaptive capacity than farmers with less access (Abdul-Razak and Kruse, 2017). Marine Conservation and Community Development (MCD), an NGO working in the community, asserted the Khanh Hoa People's Party Committee had a climate action plan between 2010 and 2015. MCD is important in creating adaptive livelihood through establishing an Eco-café, and support for the Local reef-protected area since 2008, coupled with training on the snout otter clam culture model. However, education on climate change is low in the community, and government efforts in the committee should focus on early warning systems prior to climate-induced events and should provide financial support to vulnerable social groups. The participation of citizens and stakeholders is an important aspect of climate governance (Sarfo et al., 2019). Hence, considerable efforts should be directed at 'social learning and institutional reflexivity' for efficient participation. The medium value of the adaptive capacity signifies that a community has a good capacity to cope with adverse situations, consistent with a previous study (Vincent-Akpu and Annor-Frempong, 2017).

4.3 Adaptation strategy and its barriers

Local communities rely on local knowledge, which is relevant in building resilience over climate change (Klein et al., 2014). In the case of Xuan Tu, the adaptation strategies were based on prevailing conditions which may not be a response to climate change. In response to the reduction in the catch, fishermen changed their fishing grounds by moving further into the South China Sea - a key informant attributed this change to migration and aquaculture. The cage density of lobster aquaculture and the conflict between water users is a problem in this community; this may have led to the change in the fishing ground (Tuan, 2004). These adaptation strategies are consistent with the findings of (Huynh et al., 2021) in two coastal communities in central Vietnam. Eight percent of households diversified into aquaculture, thus increasing their monthly earnings. Similarly, fishermen adapt their livelihood by diversifying into agriculture and other means in Trung Làng (Leithäuser and Holzhacker, 2020). However, these are autonomous adaptations, which are spontaneous responses to the impacts of climate change (IPCC, 2001). Barriers to these adaptations arise from the lack of financial assistance for affected individuals or units, hindering growth. The top-down government structure, which is non-participatory in ecological management, is also a significant challenge (Gverdtsiteli, 2023). Policies and governance processes play a role in determining property allocation and household livelihood strategies. Inadequate financial support, such as credit facilities and incentives, significantly affects unplanned

strategies (Avelino et al., 2018). This is in contrast to urban areas where adaptation plans are crucial for the development and sustainability of cities (Huynh and Stringer, 2018).

5. CONCLUSION

In conclusion, Xuan Tu Village is moderately vulnerable to climate change due to its exposure to environmental changes and the sensitivity of their livelihood. The study highlights that the village's economic and social capacities have strengthened its ability to adapt to climate change. Insufficient government assistance has hindered the community's efforts to adapt to climate change, highlighting the need for additional support from governmental or non-governmental organizations. There is a clear indication for renewed detailed policies to reduce vulnerability to climate-related disasters at the local level and a shift in priorities away from the government's current emphasis on national-level climate change adaptation initiatives to policies for disaster risk reduction. These policies should focus on building stronger community networks, improving access to information and resources, and involving the community in decision-making processes related to climate change. Additionally, efforts should be made to enhance the community's economic and social capacities by creating new livelihood opportunities or improving existing ones.

ACKNOWLEDGEMENTS

We thank the staff and students of the Center for Foreign Languages, Nha Trang University, and the Centre for Marine Life Conservation and Community Development of Marine Life (MCD), Vietnam, for their support during the study.

REFERENCES

Abdul-Razak M, Kruse S. The adaptive capacity of smallholder farmers to climate change in the Northern Region of Ghana. Climate Risk Management 2017;17:104-22.

Adger WN. Social Vulnerability to climate change and extremes in coastal Vietnam. World Development 1999;27(2):249-69.

Adger WN, Huq S, Brown K, Conway D, Hulme M. Adaptation to climate change in the developing world. Progress in Development Studies 2003;3(3):179-95.

Adger WN, Vincent K. Uncertainty in adaptive capacity. Comptes Rendus Geoscience 2005;337(4):399-410.

Ahsan MdN, Warner J. The socioeconomic vulnerability index: A pragmatic approach for assessing climate change led risks: A case study in the south-western coastal Bangladesh. International Journal of Disaster Risk Reduction 2014;8: 32-49.

Arfanuzzaman Md, Dahiya B. Sustainable urbanization in Southeast Asia and beyond: Challenges of population growth, land use change, and environmental health. Growth and Change 2019;50(2):725-44.

Asfaw A, Bantider A, Simane B, Hassen A. Smallholder farmers' livelihood vulnerability to climate change-induced hazards: Agroecology-based comparative analysis in Northcentral Ethiopia (*Woleka* Sub-basin). Heliyon 2021;7(4):1-14.

Avelino JE, Crichton RN, Valenzuela VP, Odara MGN, Padilla MAT, Kiet N, et al. Survey tool for rapid assessment of socio-economic vulnerability of fishing communities in Vietnam to climate change. Geosciences 2018;8:1-16.

Badjeck MC, Allison EH, Halls AS, Dulvy NK. Impacts of climate variability and change on fishery-based livelihoods. Marine Policy 2010;34(3):375-83.

Barrett CB, Reardon T, Webb P. Nonfarm income diversification and household livelihood strategies in rural Africa: Concepts, dynamics, and policy implications. Food Policy 2001; 26(4):315-31.

Beltrán-Tolosa LM, Cruz-Garcia GS, Ocampo J, Pradhan P, Quintero M. Rural livelihood diversification is associated with lower vulnerability to climate change in the Andean-Amazon foothills. PLOS Climate 2022;1(11):1-26.

Choden K, Keenan RJ, Nitschke CR. An approach for assessing adaptive capacity to climate change in resource dependent communities in the Nikachu watershed, Bhutan. Ecological Indicators 2020;114:1-13.

Cutter LS, Christopher, Burton G, Emrich CT. Disaster resilience indicators for benchmarking baseline conditions. Journal of Homeland Security and Emergency Management 2010; 7(1):1-24.

Deressa T, Hassan R, Ringler C. Measuring Ethiopian Farmers' Vulnerability to Climate Change Across Regional States (Discussion Paper No. 806), IFPRI Discussion Paper. Washington DC: International Food Policy Research Institute (IFPRI); 2008.

DiGregorio M. Learning from Typhoon Mirinae: Urbanization and Climate Change in Quy Nhon City, Vietnam. Hanoi, Vietnam: Institute for Social and Environmental Transition-Vietnam; 2013. p. 1-64.

Do VQ, Phung ML, Truong DT, Pham TTT, Dang VT, Nguyen TK. The impact of extreme events and climate change on agricultural and fishery enterprises in Central Vietnam. Sustainability 2021;13:1-17.

Du HT, Hieu NM, Kunzmann A. Negative effects of fish cages on coral reefs through nutrient enrichment and eutrophication in Nha Trang Bay, Viet Nam. Regional Studies in Marine Science 2022;55:1-7.

Eakin H, Bojórquez-Tapia LA. Insights into the composition of household vulnerability from multicriteria decision analysis. Global Environmental Change 2008;18(1):112-27.

Egyir I, Ofori K, Antwi G, Ntiamoa-Baidu Y. Adaptive capacity and coping strategies in the face of climate change: A comparative study of communities around two protected areas in the coastal savanna and transitional zones of Ghana. Journal of Sustainable Development 2015;8(1):1-15.

Füssel HM. Vulnerability to climate change and poverty. In: Edenhofer O, Wallacher J, Lotze-Campen H, Reder M, Knopf B, Müller J, editors. Climate Change, Justice and Sustainability: Linking Climate and Development Policy. Dordrecht: Springer Netherlands; 2012. p. 9-17.

General Statistics Office of Vietnam. Statistical data [Internet]. 2021 [cited 2021 Oct 26]. Available from: https://www.gso.gov.vn/en/statistical-data/.

Gverdtsiteli G. Authoritarian environmentalism in Vietnam: The construction of climate change as a security threat. Environmental Science and Policy 2023;140:163-70.

Hai ATN, Speelman S. Economic-environmental trade-offs in marine aquaculture: The case of lobster farming in Vietnam. Aquaculture 2020;516:1-45.

Hammill A, Bizikova L, Dekens J, McCandless M. Comparative Analysis of Climate Change Vulnerability Assessments: Lessons from Tunisia and Indonesia. Bonn and Eschborn, Germany: Deutsche Gesellschaft für Internationale Zusammenarbeit (GIZ) GmbH; 2013.

Heltberg R, Bonch-Osmolovskiy M. Mapping Vulnerability to Climate Change. Policy Research Working Paper 5554. Washington DC, USA: World Bank Publications; 2011.

Hernández D. Climate justice starts at home: Building resilient housing to reduce disparate impacts from climate change in residential settings. American Journal of Public Health 2022;112(1):66-8.

Ho S, Kingsbury A. Community adaptation and climate change in the Northern Mountainous Region of Vietnam: A case study of ethnic minority people in Bac Kan Province. Asian Geographer 2019;37:1-19.

Ho C. The climate change in Vietnam and its impact on agricultural sector in Vietnam. Proceedings of the Conference in the School of Environmental Science and Management-University of the Philippines Los Baños; Nov 18th, 2018; Los Baños, Laguna: Philippines; 2018.

Hou J, Lv J, Chen X, Yu S. China's regional social vulnerability to geological disasters: Evaluation and spatial characteristics analysis. Natural Hazards 2016;84(1):97-111.

Hue NT. Socioeconomic monitoring for coastal resource management projects in Vietnam and Cambodia: final report [Internet]. 2010 [cited 2019 Feb 17]. Available from: https://repository.library.noaa.gov/view/noaa/803.

Huong NTL, Yao S, Fahad S. Assessing household livelihood vulnerability to climate change: The case of Northwest Vietnam. Human and Ecological Risk Assessment: An International Journal 2019;25(5):1157-75.

Hussein K, Nelson J. Sustainable Livelihoods and Livelihood Diversification. IDS Working Paper 69. Brighton, United Kingdom: Institute of Development Studies; 1998. p. 1-32.

Huynh HLT, Do AT, Dao TM. Climate change vulnerability assessment for Can Tho City by a set of indicators. International Journal of Climate Change Strategies and Management 2019;12(1):147-58.

Huynh LTM, Stringer LC. Multi-scale assessment of social vulnerability to climate change: An empirical study in coastal Vietnam. Climate Risk Management 2018;20:165-80.

Huynh PTA, Le ND, Le STH, Tran TN. Adaptive livelihood strategies among small-scale fishing households to climate change-related stressors in Central Coast Vietnam. International Journal of Climate Change Strategies and Management 2021;13:492-510.

Intergovernmental Panel on Climate Change (IPCC). Climate Change 2001: The Scientific Basis. Contribution of Working Group I to The Third Assessment Report of the IPCC. Cambridge, United Kingdom: Cambridge University Press; 2001.

Intergovernmental Panel on Climate Change (IPCC). Summary for policymakers. In: Field CB, Barros VR, Dokken DJ, Mach KJ, Mastrandrea MD, Bilir TE, editors. Climate Change 2014: Impacts, Adaptation and Vulnerability. Cambridge, United Kingdom: Cambridge University Press; 2014. p. 1-32.

Jepson M, Colburn LL. Development of Social Indicators of Fishing Community Vulnerability and Resilience in the U.S. Southeast and Northeast Regions. U.S. Department of Commerce: NOAA Technical Memorandum NMFS-F/SPO-129; 2013.

Kay S, Avillanosa AL, Cheung VV, Dao HN, Gonzales BJ, Palla HP, et al. Projected effects of climate change on marine ecosystems in Southeast Asian seas. Frontiers in Marine Science 2023;10:1-17.

Kelly PM, Adger WN. Theory and practice in assessing vulnerability to climate change and facilitating adaptation. Climatic Change 2000;47(4):325-52.

Khan S. Vulnerability assessments and their planning implications: A case study of the Hutt Valley, New Zealand. Natural Hazards 2012;64(2):1587-607.

Klein JA, Hopping KA, Yeh ET, Nyima Y, Boone RB, Galvin KA. Unexpected climate impacts on the Tibetan Plateau: Local and scientific knowledge in findings of delayed summer. Global Environmental Change 2014;28:141-52.

Leithäuser H, Holzhacker RL. Local experience, knowledge, and community adaptations to environmental change: The case of a fishing village in central Vietnam. Regional Environmental Change 2020;20(4):1-11.

Lo H, Emmanuel T. The Influence of US Development Assistance on the Adaptive Capacity to Climate Change: Insights from Senegal. Oxfam America Research Backgrounder Series; 2013.

Marotzke J, Semmann D, Milinski M. The economic interaction between climate change mitigation, climate migration and poverty. Nature Climate Change 2020;10(6):518-25.

Mason K, Lindberg K, Haenfling C, Schori A, Marsters H, Read D, et al. Social vulnerability indicators for flooding in Aotearoa New Zealand. International Journal of Environmental Research and Public Health 2021;18(8):1-31.

Mendoza ME, The BD, Naret H, Ballaran JV, Arias JK. Assessing vulnerability to climate change impacts in Cambodia, the Philippines and Vietnam: An analysis at the commune and household level. Journal of Environmental Science and Management 2014;17(2):78-91.

Murphy DJ, Wyborn C, Yung L, Williams DR. Key Concepts and Methods in Social Vulnerability and Adaptive Capacity. General Technical Report RMRS-GTR-328. Fort Collins, CO: U.S. Department of Agriculture, Forest Service, Rocky Mountain Research Station; 2015.

Mau LD, Dung NTT, Hoan PS, Tuan NV, Cong NC, Bac PT, et al. Activity features of tropical cyclone in Truong Sa archipelago region, Khanh Hoa Province. Vietnam Journal of Marine Science and Technology 2019;19:35-41.

Natarajan N, Newsham A, Rigg J, Suhardiman D. A sustainable livelihoods framework for the 21st century. World Development 2022;155(4):1-16.

Ngo-Duc T. Climate change in the coastal regions of Vietnam. In: Thao ND, Takagi H, Esteban M, editors. Coastal Disasters and Climate Change in Vietnam. Oxford: Elsevier; 2014. p. 175-98.

Nguyen CV, Horne R, Fien J, Cheong F. Assessment of social vulnerability to climate change at the local scale: Development

and application of a Social Vulnerability Index. Climatic Change 2017a;143:355-70.

Nguyen KA, Liou YA, Terry JP. Vulnerability of Vietnam to typhoons: A spatial assessment based on hazards, exposure and adaptive capacity. Science of the Total Environment 2019;682:31-46.

Nguyen TKH, Hien PTT, Thu TTN, Lebailly P. Vietnam's fisheries and aquaculture development's policy: Are exports performance targets sustainable? Oceanography and Fisheries Open Access Journal 2017b;5(4):1-10.

Nguyen THH. Co-Management in Trao Reef Marine Reserve, Vietnam: A Transaction Costs Approach [dissertation]. Vietnam: The Norwegian College of Fishery Science University of Tromso, Norway and Nha Trang University; 2010.

Nguyen XV, Nguyen-Nhat NT, Nguyen XT, Dao VH, McDermid KJ, Papenbrock J. Microsatellite-based analysis of the genetic diversity and population structure of the seagrass species *Thalassia hemprichii* from southern Viet Nam. Aquatic Botany 2022;178:1-8.

Nor Diana MI, Zulkepli NA, Siwar C, Zainol MR. Farmers' adaptation strategies to climate change in Southeast Asia: A systematic literature review. Sustainability 2022;14(6):1-15.

O'Brien K, Leichenko R, Kelkar U, Venema H, Aandahl G, Tompkins H, et al. Mapping vulnerability to multiple stressors: Climate change and globalization in India. Global Environmental Change 2004;14(4):303-13.

Okpara UT, Stringer LC, Dougill AJ. Using a novel climate-water conflict vulnerability index to capture double exposures in Lake Chad. Regional Environmental Change 2017;17(2):351-66.

Otto IM, Reckien D, Reyer CPO, Marcus R, Le Masson V, Jones L, et al. Social vulnerability to climate change: A review of concepts and evidence. Regional Environmental Change 2017;17(6):1651-62.

Phu LH, Kim-Hong PT, Chung TV, Binh TV, Dung LT, Ngoc PH, et al. Environmental concerns for sustainable mariculture in coastal waters of South-Central Vietnam. Sustainability 2022;14(13):1-16.

Quiroga S, Suárez C, Diego Solís J, Martinez-Juarez P. Framing vulnerability and coffee farmers' behaviour in the context of climate change adaptation in Nicaragua. World Development 2020;126:1-13.

Rubin O. Social vulnerability to climate-induced natural disasters: Cross-provincial evidence from Vietnam. Asia Pacific Viewpoint 2014;55(1):67-80.

Salik KM, Jahangir S, Zahdi Wul Z, Hasson Sul. Climate change vulnerability and adaptation options for the coastal communities of Pakistan. Ocean and Coastal Management 2015;112:61-73.

Sarfo I, Otchwemah HB, Kumara PBTP. Effectiveness of adaptation strategies among coastal communities in Ghana: The case of dansoman in the Greater Accra Region. Current Journal of Applied Science and Technology 2019;35:1-12.

Schmidt-Thome P, Nguyen TH, Pham TL, Jarva J, Nuottimäki K. Climate change in Vietnam. In: Schmidt-Thomé P, Nguyen TH, Pham TL, Jarva J, Nuottimäki K, editors. Climate Change Adaptation Measures in Vietnam. Edinburgh: Springer International Publishing; 2015. p. 7-15.

Tan S, Li T, Huntsinger L. Analyzing herder adaptive capacity to climate change: A case study from an Ecologically Fragile Area in Inner Mongolia, People's Republic of China. Human Ecology 2018;46(3):399-409.

Tate E. Social vulnerability indices: A comparative assessment using uncertainty and sensitivity analysis. Natural Hazards 2012;63(2):325-47.

Tran TA, Tran TQ, Tran NT, Nguyen HT. The role of education in the livelihood of households in the Northwest region, Vietnam. Educational Research for Policy Practice 2020; 19(1):63-88.

Tran-Quang D, Pham-Thanh H, Vu TA, Kieu C, Phan-Van T. Climatic shift of the tropical cyclone activity affecting Vietnam's Coastal Region. Journal of Applied Meteorology and Climatology 2020;59(10):1755-68

Trinh TA. The impact of climate change on agriculture: findings from Households in Vietnam. Environmental and Resource Economics 2018;71(4):897-921.

Truong DD, Dat TT, Hang ND, Huan LH. Vulnerability assessment of climate change in Vietnam: A case study of Binh Chanh District, Ho Chi Minh City. Frontiers in Environmental Science 2022;10:1-11.

Tuan LA. Case Study of Spiny Lobster Cage Culture, Xuan Tu Lagoon, Van Ninh District, Central Vietnam (No. Tropeca Case Study 4). Vietnam: UK Department for International Development Aquaculture and Fish Genetics Research Programme; 2004. p. 1-12.

Umamaheswari T, Sugumar G, Krishnan P, Ananthan PS, Anand A, Jeevamani JJJ, et al. Vulnerability assessment of coastal fishing communities for building resilience and adaptation: Evidences from Tamil Nadu, India. Environmental Science and Policy 2021;123:114-30.

United Nations Development Programme (UNDP). Human Development Report 1990: Concept and Measurement of Human Development. UN Plaza New York: Oxford University Press; 1990.

Vincent-Akpu IF, Annor-Frempong F. Social vulnerability of small scale coastal fisher's livelihood to climate change. International Journal of Human Capital in Urban Management 2017;2(3):171-80.

Vincent K. Creating an Index of Social Vulnerability to Climate Change for Africa: Tyndall Centre Working Paper No. 56. Tyndall Centre for Climate Change Research; 2004. p. 1-41.

Wu SY, Yarnal B, Fisher A. Vulnerability of coastal communities to sea-level rise: A case study of Cape May County, New Jersey, USA. Climate Research 2002;22(3):255-70.

Yamane T. Statistics: An Introductory Analysis. 2nd ed. New York: Harper and Row; 1967.

Yoon DK. Assessment of social vulnerability to natural disasters: A comparative study. Natural Hazards 2012;63(2):823-43.

Zahran S, Brody SD, Peacock WG, Vedlitz A, Grover H. Social vulnerability and the natural and built environment: A model of flood casualties in Texas. Disasters 2008;32(4):537-60.

Žurovec O, Čadro S, Sitaula BK. Quantitative assessment of vulnerability to climate change in rural municipalities of Bosnia and Herzegovina. Sustainability 2017;9(7):1-18.

Carbon Storage of Leyte Sab-A Basin Peatland, Philippines

Pearl Aphrodite Bobon-Carnice[1*], Jeffrey P. Chanton[2], Veronica P. Migo[3,4], and Decibel V. Faustino-Eslava[3]

[1]Department of Natural Sciences, Eastern Visayas State University, Leyte, Philippines
[2]Department of Earth, Ocean, and Atmospheric Science, Florida State University, Tallahassee, Florida, USA
[3]School of Environmental Science and Management, University of the Philippines Los Baños, Philippines
[4]Department of Chemical Engineering, University of the Philippines Los Baños, Philippines

ARTICLE INFO

Received: 13 Jan 2023
Received in revised: 9 Jun 2023
Accepted: 19 Jun 2023
Published online: 11 Sep 2023
DOI: 10.32526/ennrj/21/20230015

Keywords:
Aboveground carbon stocks/ Belowground carbon stocks/ Carbon sequestration/ Land-use change/ Marshland/ Tropical peat swamp forest

*** Corresponding author:**
E-mail:
pearl.carnice@evsu.edu.ph

ABSTRACT

Leyte Sab-A Basin peatland (LSBP) is the second largest peatland in the Philippines and comprises 3,088 ha (31 km^2). The study estimated the C storage and carbon sequestration capacity of the peatland's four (4) ecotypes, namely, swamp forest (SF), marshland (ML), agroforestry (AF), and agricultural land (AL) using allometric equations. SF rendered the highest downed wood C-stocks followed by AL and AF. For the litter C-stocks, AF rendered the highest, followed by SF, ML, and AL. SF rendered the highest root C-stocks and CO_2 sequestered, followed by AL and AF. C% is highest in ML with values ranging from 32-43 C% across the soil peat depth, while SF ranges from 29-34 C%, and AL and AF both with 19-37 C%. The LSBP stores 36.6 Tg of C and 134.5 Tg of CO_2 sequestered. This C storage amount can represent 0.04% of tropical peat carbon.

1. INTRODUCTION

Peatlands have been widely accepted to store a massive amount of carbon. Although peatlands account for only 3% of the world's land surface, they are one of the major reservoirs of global soil carbon (C), which is currently estimated to be over 600 Gt carbon (Page et al., 2011; Yu et al., 2010; Yu et al., 2011). Tropical peatlands covering 440,000 km^2 represent about 11% of the world's peatland areas, with the Leyte Sab-A Basin representing 31 km^2 (0.007%) of that area. Page et al. (2011) estimate that 77% of the tropical peat C storage is in Southeast Asia. The tropical peat reservoir is estimated to be 88.6 (81.7-91.0) Gt (Pg) C or 15-19% of the global peat carbon pool.

Aside from sequestering carbon, peat swamp forests provide numerous ecosystem services, including the provision of forest products, hydrological regulation (Dommain et al., 2016), nutrient cycling, and habitat for many endangered and rare species of animals with high biodiversity indices (Nowak, 2013; Cheyne and Macdonald, 2011; Posa et al., 2011). Despite these values, Southeast Asian peatlands are being disturbed by anthropogenic activities such as draining, deforestation, and intensive burning, primarily for agricultural and tree plantation purposes (Margono et al., 2014; Miettinen et al., 2012).

Intense economic and social pressures for timber, land for food crops, and oil palm plantations contribute to Southeast Asia's rapid degradation of peatlands. As a result, massive amounts of carbon gas are transmitted to the atmosphere through the loss of biomass and peat oxidation and burning. One good example is the 1997 widespread wildfires in forested peatlands of Indonesia following a severe El Niño. Extrapolations showed an estimate of 0.81 to 2.57 Gt of carbon were discharged into the atmosphere in 1997 because of burning peat and vegetation in Indonesia - an amount that is equal to 13-40% of the mean yearly worldwide carbon emissions from non-sustainable power sources (Page et al., 2010; Page et al., 2011).

Considering the potential impacts of peatlands degradation at both the regional and global scale, failure to account for these vulnerable C pools can cause biogeochemical and climate models to

Citation: Bobon-Carnice PA, Chanton JP, Migo VP, Faustino-Eslava DV. Carbon storage of Leyte Sab-A Basin Peatland, Philippines. Environ. Nat. Resour. J. 2023;21(5):402-416. (https://doi.org/10.32526/ennrj/21/20230015)

underestimate the future increases in CO_2, which could further enhance anthropogenic-driven climate change. Tragically, the protection of peatlands as a forest isn't under any Kyoto Protocol (KP) Mechanisms or its adaptability systems, for example, Joint Implementation (JI) Program and the Clean Development Mechanism (CDM). In contrast, the C stocks in peatlands are excluded from the United Nations Framework Convention on Climate Change (UNFCC). It could be one of the principal reasons peatlands have been adequately exposed to survival transformation and waste in recent years since strategy-making bodies are not straightforwardly tending to peatland assurance. However, the KP mechanisms and UNFCC are now considering peatlands. The first commitment period was from 2008 to 2012 (Barthelmes et al., 2015; FAO, 2020).

Agusan Marsh and Leyte Sab-A Basin are where important peatland areas were identified in the Philippines. However, there is a lack of targeted research on peatlands in Agusan Marsh despite it being declared a protected wetland under Presidential Proclamation No. 913. Meanwhile, the Protected Areas and Wildlife Bureau (PAWB-DENR, 2009; PAWB-DENR, 2013) nominated the Leyte Sab-A Basin as a Peat Site Profile in Southeast Asia. However, this recognition from the ASEAN is still in process. Aside from this, no other exhaustive scientific study has been conducted on the site. Still, it holds a series of swamps as Leyte's most significant water catchment, which supports wildlife and local communities.

Leyte Sab-A Peatland Basin in the Philippines is categorized as a tropical peatland of Southeast Asia similar to Malaysia (Peninsular; Sabah), Brunei, Thailand, Papua New Guinea, Vietnam, and Indonesia. Leyte Sab-A Basin is the second largest peatland in the Philippines and comprises 3,088 ha. It is an elongated basin from NW to SE on the Philippine Island of Leyte (ADB, 2000). The basin comprises four main ecotypes: swamp forest (SF), marshland (ML), agroforestry (AF), and agricultural land (AL). Massive efforts of the government to convert peatland to agricultural land have not been experienced in the Philippines as it has been in many of these other countries. The conversion of many hectares of peatland in Central Kalimantan, Indonesia, has suffered consequential losses through its Mega Rice Project (Nuthammachot et al., 2019). There are many abandoned lands in Leyte Sab-A Peatland, although a governing body was established (and consequently abolished) to manage it. In contrast to the increased fire incidents in Malaysian and Indonesian peatlands (Tonks et al., 2017; Miettinen et al., 2012), Leyte Sab-A Peatland has experienced subsidence and abandonment of land due to consistently low productivity in agriculture. The remaining untouched grounds of the Leyte Sab-A Peatland Basin have become more vulnerable to conversion as the local people explore more ways to use it since the majority of the land of the community belongs to this resource.

This study characterizes carbon storage in the Leyte Sab-A Peatland Basin's four dominant ecotypes. By doing so, the organic matter allocated to standing trees, downed wood, litter, roots, and soil peat will be described as influencing the aboveground and belowground carbon pool. In addition, abundant species, the presence of water, and the accessibility of the ecotype will also shed light on the existing management and development of the peatland. Lastly, the total carbon content and carbon dioxide sequestered are computed, which will highlight the importance of the Leyte Sab-A Peatland on the extent, distribution, and regional carbon budget of tropical peatlands in Southeast Asia. The study's main objective was to estimate the current C storage of the Leyte Sab-A Basin peatland. Specifically, it determined that the aboveground C storage of the peatland are in the following pools: aboveground carbon comprised of standing trees, downed wood, and litter, and belowground carbon stored in root biomass and the peat soil at different soil depth.

2. METHODOLOGY

2.1 Study sites

The peatland site was identified as Leyte Sab-A Basin Peatland (LSBP), which traverses three municipalities: Santa Fe, Alang-Alang, and San Miguel, Leyte. The peatland is a freshwater-type palustrine wetland system consisting of shallow, slow-moving, and stagnant water. It has a mixture of closed or shaded forest swamps where tall emergent macrophytes grow thick and shade the water from the wind and direct sunlight and an open or unshaded swamp where water lilies and submerged macrophytes dominate. The watershed area is about 18,508 ha (ADB, 2000). Figure 1 shows the location of the LSBP in Leyte Island, Philippines, and the different transects for sampling in the peatland. Figure 2 shows the different ecotypes identified in the peatland with its corresponding vegetation.

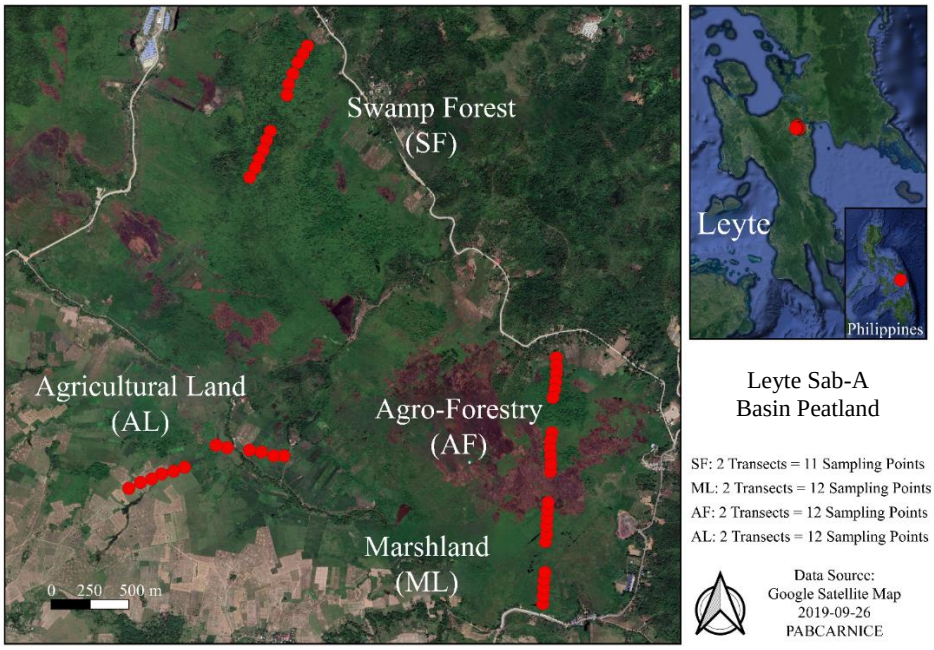

Figure 1. Location of all representative 47 core sampling points in LSBP, Leyte, Philippines

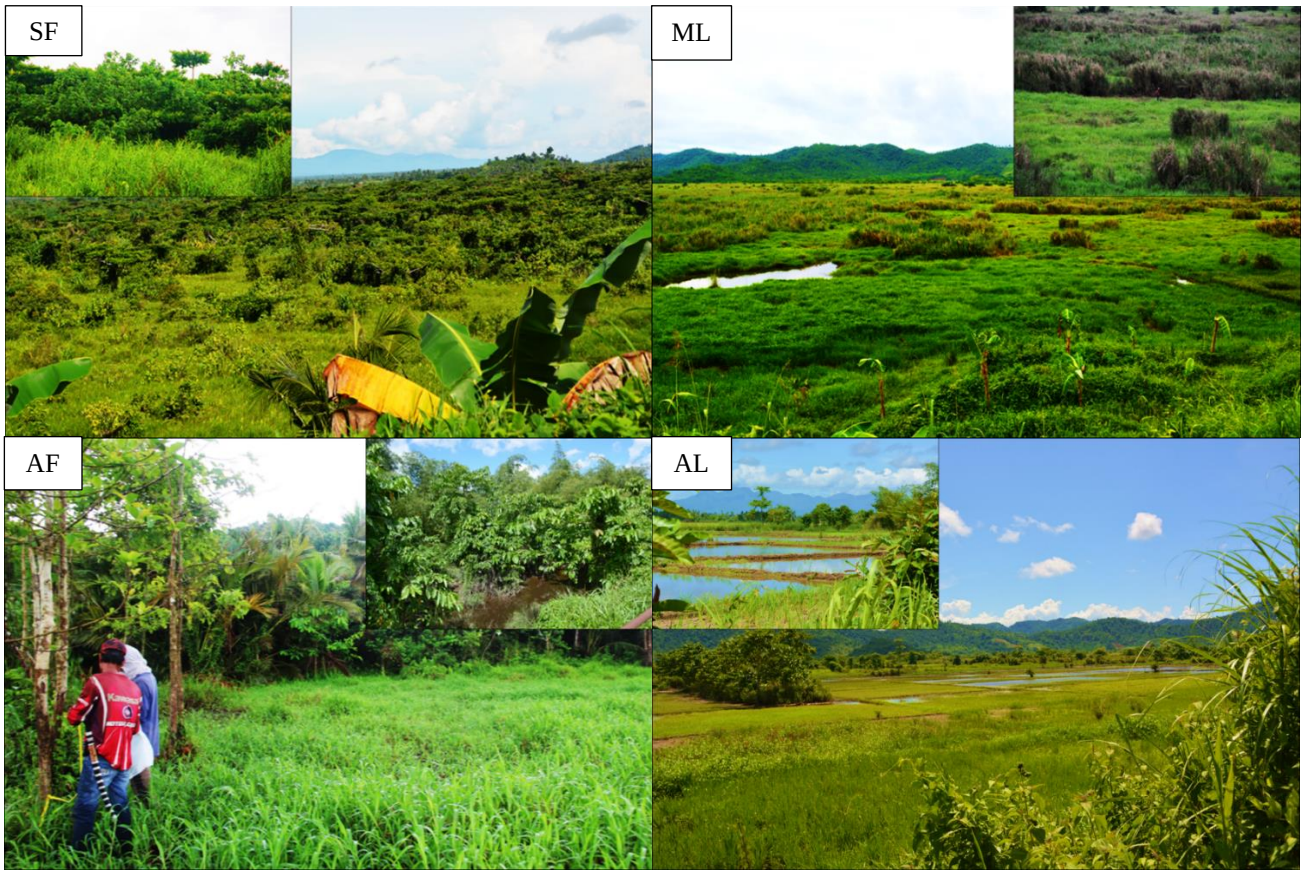

Figure 2. The SF, ML, AF, and AL ecotypes and their vegetation of Leyte Sab-A Basin Peatland

Further, Figure 3 shows the details of the carbon stock assessment scheme in different pools. The standing trees, downed wood, and litter were measured for aboveground C. The root biomass and peat soil at specific depths represent belowground carbon. Downed wood refers to dead or fallen tree branches and woody debris no longer standing and resting on the ground. It includes fallen tree trunks, branches, and woody materials.

2.2 Biomass sampling plots

The study is guided by the protocol used in the ecosystem carbon stocks assessment of tropical peatland forests of Indonesia and Micronesia (Kauffman et al., 2011; Kauffman and Donato, 2012; Kauffman et al., 2016). Figure 4 illustrates the general plot layout to quantify ecosystem C pools following the general carbon assessment scheme in Figure 3. Six plots were established in every ecotype stand along a 250 m transect.

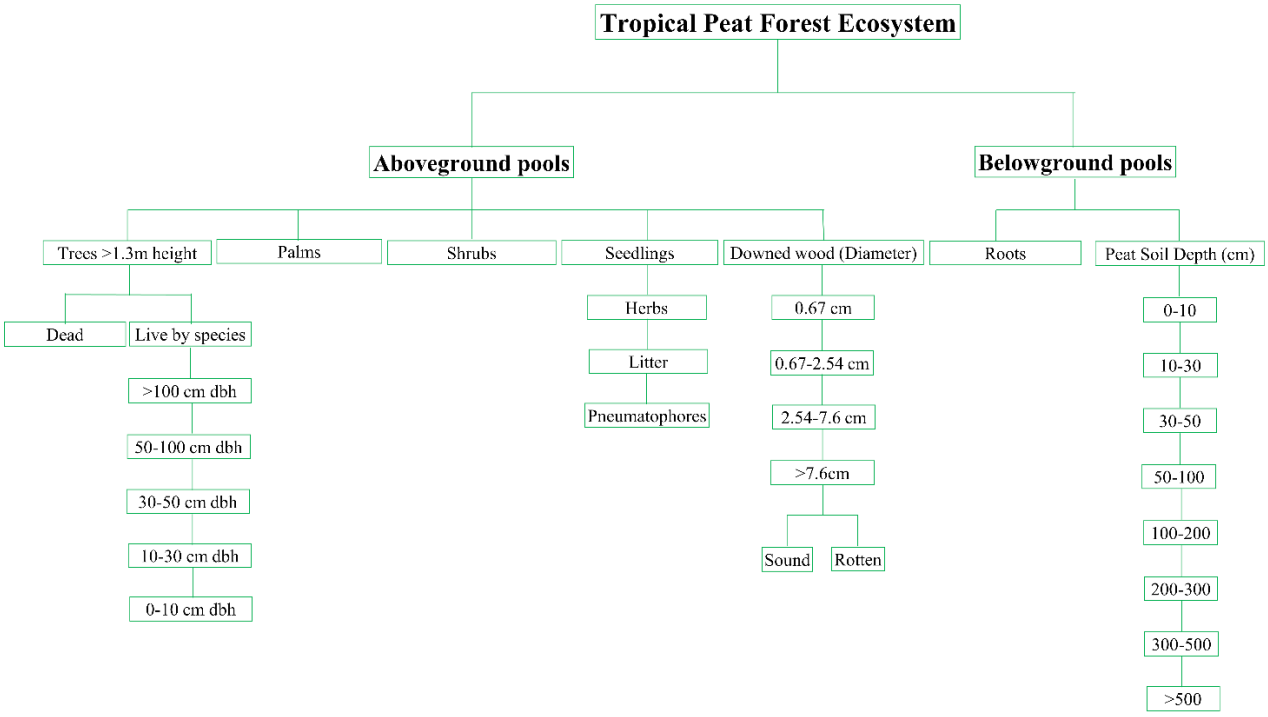

Figure 3. Carbon stock assessment scheme in LSBP

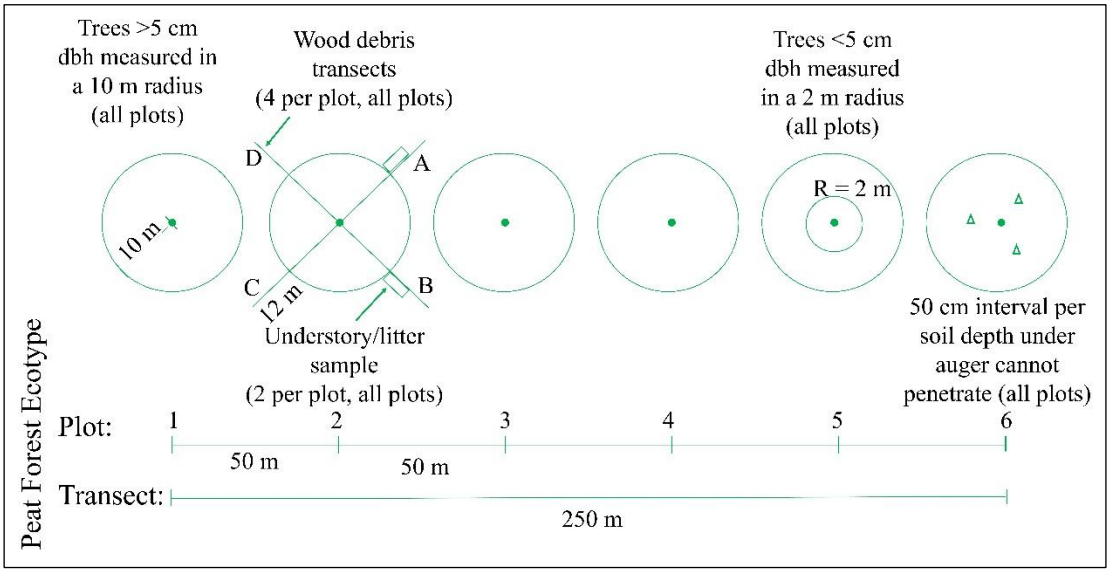

Figure 4. General plot layout to quantify ecosystem C pools of LSBP

2.3 Measuring aboveground carbon pools

2.3.1 Tree biomass: All trees that are >5 cm in diameter were measured in the 10 m radius plot. The smaller trees having <5 cm in diameter were measured in a 2 m radius nested plot.

The biomass equation formula (Bobon-Carnice and Lina, 2017; Bobon-Carnice and Lina, 2021) is as follows:

$$AGB = 21.297 - 6.953 \times (dbh) + 0.740 \times (dbh)^2$$

Where; AGB=aboveground dry matter, kg/tree; and dbh=diameter at breast height, cm.

The total tree biomass multiplied by the average C content of wood (standard value of 45%) is the equivalent value of C stock.

2.3.2 Downed wood: Downed wood was measured using the planar intercept technique (Dibble and Rees, 2005). In each plot, four (4) transects were measured to determine the downed wood mass, which totals 24 transects in each plot.

The equation for calculating the volume of medium to fine (<7.6 cm diameter) downed wood is:

$$\text{Volume } (m^3/ha) = \pi^2 \times (Ni \times \frac{QMDi^2}{8} \times L)$$

Where; Ni=the count of intersecting woody debris pieces in size class i; QMDi=the quadratic mean diameter of size class i (cm); QMD=quadratic mean diameter; and L=transect length (m).

The equation for calculating the volume of large (>7.6 cm diameter) downed wood is:

$$\text{Volume } (m^3/ha) = \pi^2 \times (\frac{d1^2 + d2^2 + d3^2 + \cdots dn^2}{8} \times L)$$

Where; d_1, ...d_n=diameters of intersecting pieces of large deadwood (cm); and L=the length of the transect line for large size class (m).

Downed wood mass is calculated as the volume multiplied by its mean specific gravity and converted to Mg/ha.

2.3.3 Litter: In each plot, litter sampling was done in 2 micro-plots (50 × 50 cm). Three values were determined based on litter: the fresh weight of the litter sample (FW), the fresh weight of a litter subsample (FWs), and the dry weight of the litter subsample (DWs). In addition, a moisture correction factor (M) was calculated based on the water lost (H_2O, g) from the dried litter subsample. From the formula:

$$\frac{DWs}{FWs} \times FW = DW$$

C stock is estimated as C_{litter}=DW × 0.45 (Bobon-Carnice and Lina, 2017; Bobon-Carnice and Lina, 2021). Litter C stock was then scaled to the standard unit Mg/ha by converting the area of the sampling frame to a hectare and the weight of the sample to Mg.

2.4 Measuring belowground carbon pools

2.4.1 Peat soil: A fabricated Russian peat auger was used in collecting peat samples. Six (6) sub-sampling core points on each transect (2 transects per ecotype) were collected uniformly with a depth interval of 50 cm from the surface (0-50, 50-100 cm) until the auger could not penetrate anymore. All peat soil samples inside the auger core were collected, placed in adequately labeled plastic bags, and brought immediately to the screen house. Each sample was weighed, prepared for initial air drying, and then freeze-dried.

Organic C and N concentrations were analyzed by combustion to CO_2 and N_2 at 1,020°C in an automated CHN elemental analyzer coupled with a Thermo Finnigan Delta XP isotope ratio mass spectrometer for C ($\delta^{13}C$) and N ($\delta^{15}N$) determination, which was done at the National High Magnetic Field Laboratory at Florida State University. Bulk density (Db) will be determined using the core sampling method. Peat C stock was calculated using the equation (Neufeldt, 2005; Donato et al., 2011; Howard et al., 2014):

$$\text{Peat C stocks (Mg C/ha)} = \frac{\%SOC}{100} \times \text{soil depth (m)} \times \text{bulk density } \left(\frac{Mg}{m^3}\right) \times \frac{10{,}000\ m^2}{ha}$$

2.4.2 Root biomass: Belowground biomass for the roots present was also estimated using allometric equations following Cairns et al. (1997):

$$Y = \exp\ [-1.0587 + 0.8836 \times \ln (AGB)]$$

Where; Y=root biomass in Mg/ha of dry matter; ln=natural logarithm; exp="e to the power of"; and ABD=aboveground biomass in Mg/ha of dry matter.

2.5 Data analysis and calculations

All data were subjected to descriptive analysis first and then analyzed using analysis of variance at $p<0.05$. Factor(s) causing a significant difference between means based on the test statistics values (F-computed) was then subjected to Scheffé's Test at $p<0.05$. Finally, total carbon density was predicted by testing for the significant interaction between soil depth and ecotype using the Analysis of Covariance (ANCOVA). All statistical analysis was done using SPSS (Student Version 2019, SPSS Inc.,).

3. RESULTS AND DISCUSSION

3.1 Aboveground pools

3.1.1 Standing trees: The different ecotypes are a significant factor in C-stocks' difference (P-value=2.05E-06) for standing trees. SF rendered the highest mean of C-stocks of (mean±SE) 14.0±1.7 Mg C/ha, followed by AL with 4.7±1.0 Mg C/ha and AF with 2.2±0.5 Mg C/ha (Figure 5(a)). Pairwise comparison through Scheffé's Method test showed that SF had significantly higher C-stocks than AL and AF. On the other hand, C-stocks of AL and AF are found to be not significantly different from each other. Therefore, untouched ecotypes such as an SF have significantly higher C-stocks for standing trees than ecotypes with frequent human activities.

The exact sequence of results was also observed in CO_2 sequestered by the standing trees of the SF. SF ecotype is superior with 51.4±6.4 Mg CO_2/ha, followed by AL (17.2±3.8 Mg CO_2/ha) and AF (8.0±1.7 Mg CO_2/ha) (Figure 5(f)). Such results are due to the diameter at breast height (dbh) values and the number of trees in each ecotype. SF's standing trees C-stock results are comparable to the intermediate forest (IF) standing tree C-stocks of Caimpugan Peatland in Agusan Marsh, Philippines, with 14.42 Mg C/ha (Alibo and Lasco, 2012). The C stock of standing trees of SF is lower than the live standing trees in the Peruvian cloud montane peat forest (69.3±13.4 Mg C/ha) (Román-Cuesta et al., 2011), but much higher than an open peatland mosaic live vegetation (1.9±0.2 Mg C/ha) in Minnesota, USA (Weishampel et al., 2009).

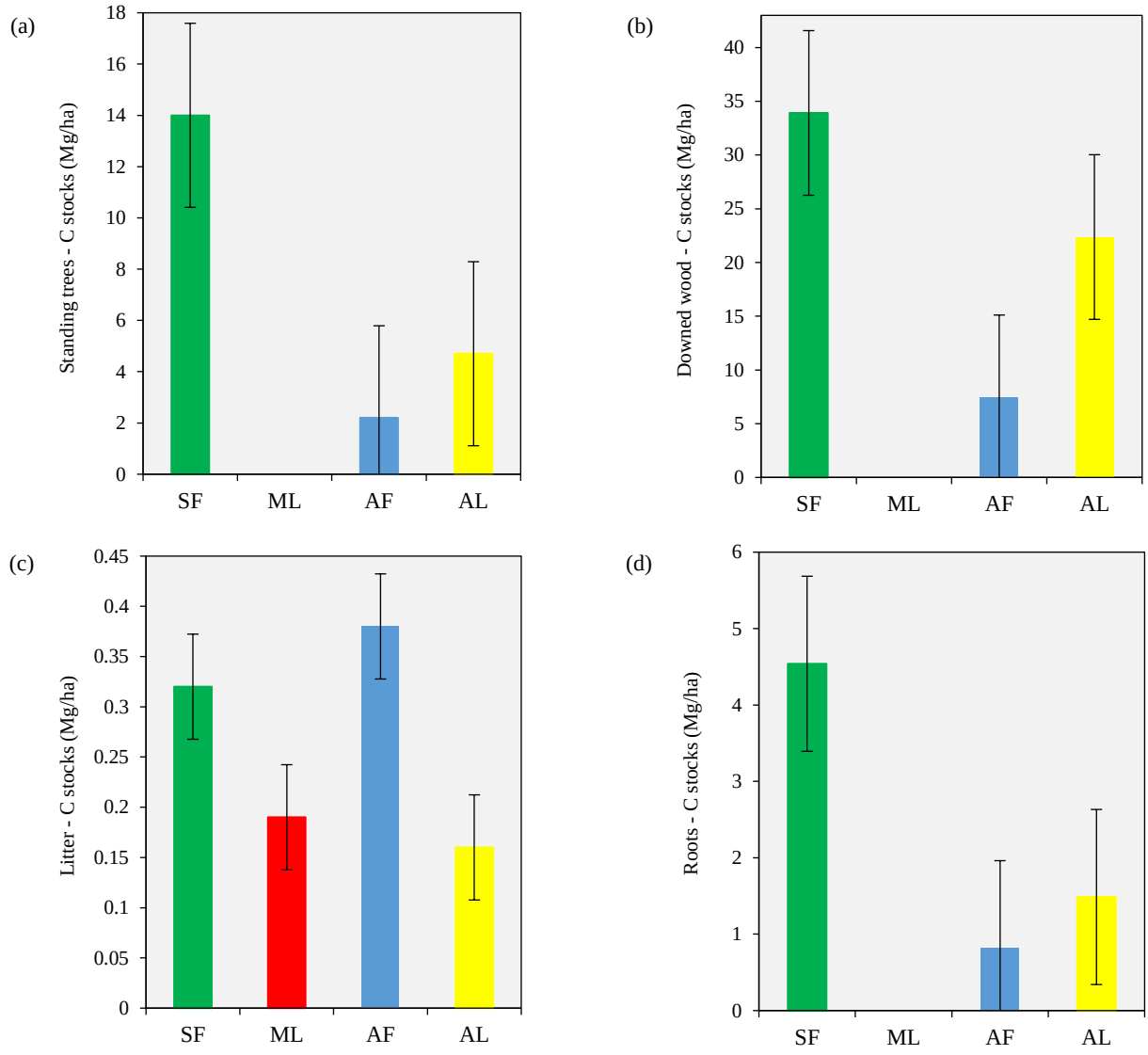

Figure 5. Mean C-stocks (a to e) and CO_2 sequestered (f to j) of standing trees, downed wood, litter, roots, and peat soil C-stocks across all four ecotypes

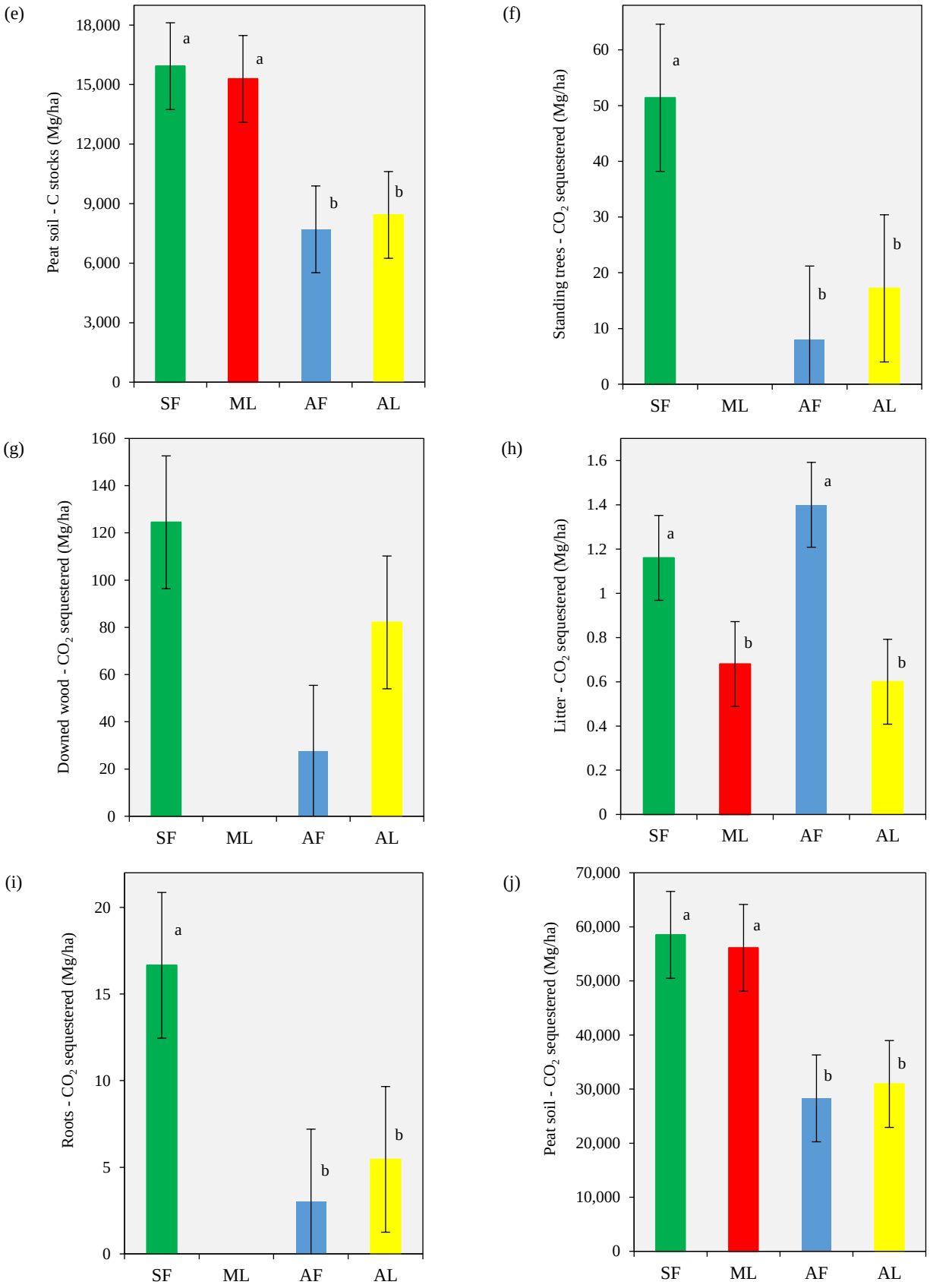

Figure 5. Mean C-stocks (a to e) and CO_2 sequestered (f to j) of standing trees, downed wood, litter, roots, and peat soil C-stocks across all four ecotypes (cont.)

3.1.2 Downed wood: Results showed that C-stocks from downed wood were significantly different across ecotypes (P-value=0.029). SF rendered the highest downed wood C-stocks (33.92±5.38 Mg C/ha), followed by AL (22.37±7.34 Mg C/ha), and AF as the least (7.45±3.63 Mg C/ha) (Figure 5(b)). Such results are higher than the fallen deadwood in Andean cloud peat montane forest with only 6.7±3.2 Mg C/ha (Román-Cuesta et al., 2011), and in the peat swamp wetlands of Chiapas, Mexico, with 12.5±2.8 Mg C/ha (Adame et al., 2015).

For the amount of CO_2 sequestered in downed wood, the value reached 124.5±19.7 Mg C/ha in the SL ecotype, followed by AL (82.10±13.33 Mg C/ha) and AF (27.3±13.3 Mg C/ha) as depicted in Figure 5(g). Also, it must be noted that no standing trees were found inside the representative sampling plots of the ML ecotype because grasses and sedges dominate it.

3.1.3 Litter: Results show in LSBP that the mean litter C-stocks between ecotypes are significantly different from each other (P-value=6.7571E-09). AF rendered the highest litter C stock (0.39±0.02 Mg C/ha), which is not statistically different from SF C stock (0.32±0.03 Mg C/ha). On the other hand, carbon stocks of ML (0.19±0.01 Mg C/ha) and AL (0.16±0.02 Mg C/ha) are not significantly different (Figure 5(c)), and the C stocks of AF and SF are significantly higher than them. Consequently, the same pattern can be observed in the CO_2 sequestered across all ecotypes (Figure 5(h)).

Although there are avenues where litter can store more C, the computed values are low compared to the litter C stock of the three vegetation zones in Caimpugan Peatland in Agusan Marsh, Philippines, which ranged from 4.16 ton/ha to 34.49 ton/ha (Alibo and Lasco, 2012). The characteristic basin topography of LSBP, with the lowest registered elevation of 11.5 above sea level, mainly contributes to the water level in the peatland such that water is almost always present in all parts of the land. Therefore, it can influence the lower density of standing trees that can tolerate persistent waterlogged conditions leading to less litterfall across all ecotypes.

3.1.4 Total aboveground C-stocks and CO_2 sequestered

SF had the highest total aboveground C stock (48.24 Mg C/ha), followed by AL (27.23 Mg C/ha), AF (10.03 Mg C/ha), and lastly, ML (0.19 Mg C/ha) with a mean total aboveground C of 21.42 Mg C/ha (Figure 6). LSBP has lower calculated aboveground C-stocks than the 150-250 ton/ha estimated average aboveground C stock of tropical peatlands (Rieley and Page, 2008). However, it is comparable to the intermediate forest (31.16-43.40 ton/ha) and pygmy forest (8.45-16.56 ton/ha) mean aboveground C-stocks of Caimpugan Peatland, Philippines (Alibo and Lasco, 2012). Consequently, aboveground C stocks in the Philippines, both LSBP and Caimpugan Peatland, are quite low compared to the primary and secondary forest in Central Kalimantan, Indonesia, with 204±32 and 172±17 Mg C/ha but at par with its oil palm plantation with 29±0.3 Mg C/ha (Novita et al., 2021). It further implies that LSBP vegetation is quite degraded. Nonetheless, downed wood contributed most to the aboveground C storage across all ecotypes, followed by standing trees and litter.

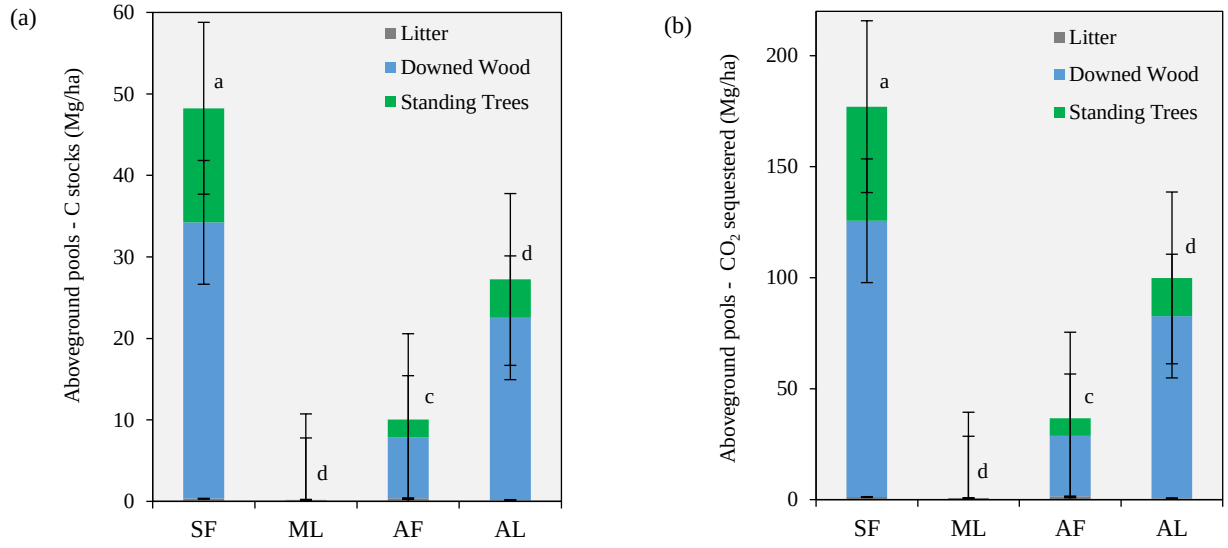

Figure 6. Total C-stocks and CO_2 sequestered of aboveground (a, b) and belowground biomass (c, d)

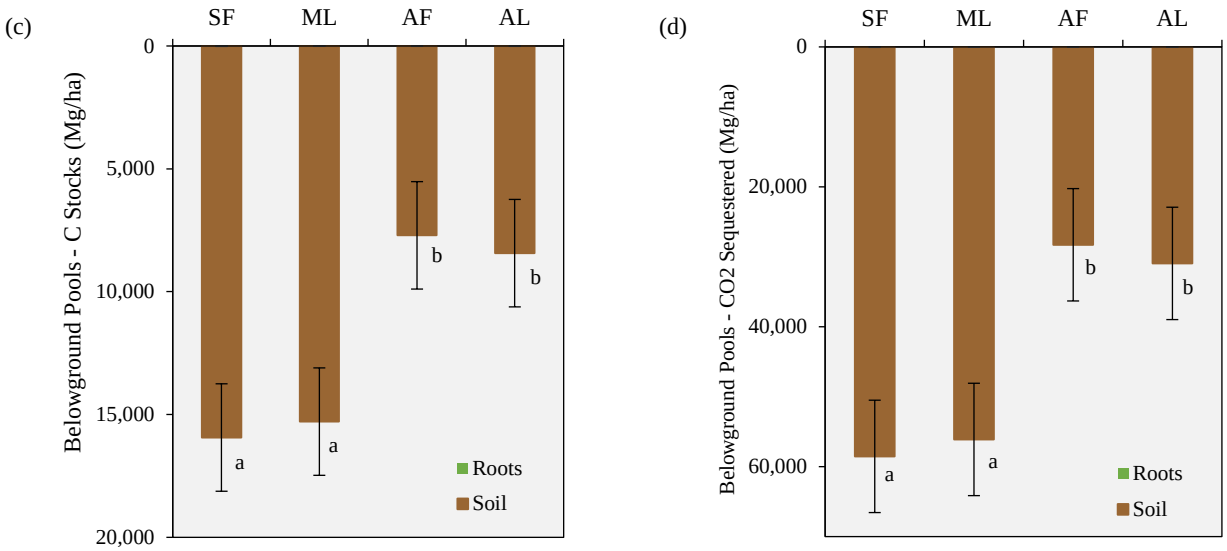

Figure 6. Total C-stocks and CO_2 sequestered of aboveground (a, b) and belowground biomass (c, d) (cont.)

Estimating aboveground C-stocks is critical in each ecotype so that it is easy to determine which pools should be prioritized in terms of protection, preservation, and increasing C storage. It must be noted that compared with the belowground counterpart, aboveground C pools are more susceptible to anthropogenic disturbances. AF and AL are the ecotypes frequently visited by the residents at the study site. Each total is lower than that of the lesser disturbed SF. Even for the specifics of an aboveground pool (standing trees, downed wood, litter), AF and AL tend to behave similarly, with values of C-stocks not significantly different from one another but consistently lower than SF.

3.2 Belowground pools

3.2.1 Root biomass: SF rendered the highest root C-stocks (4.54±0.59 Mg C/ha) and CO_2 sequestered (16.66±2.16 Mg/ha), which are both significantly different from AL (1.49±0.31 Mg C/ha; 5.46±1.12 Mg/ha CO_2 sequestered) and AF (0.82±0.16 Mg C/ha; 3.00±0.58 Mg/ha CO_2 sequestered), but AL and AF are not significantly different from each other (Figure 5(d) and Figure 5(i)). However, root biomass C-stocks are meager compared to the other C pools. It could be due to the type of roots and varying root concentration as it goes down into soil layers.

3.2.2 Soil peat and bulk density: The highest mean bulk density across all depths is 0.074 g/cm^3 (AF), and mean values across ecotypes are statistically significant with each other except SF (0.062 g/cm^3), which is quite similar to AL (0.066 g/cm^3) and ML (0.059 g/cm^3) values. All ecotypes tend to have a similar range of bulk density of 0.055-0.064 g/cm^3 at the topsoil (0-50 cm) and entirely stayed in that range, but AL increased at 100-150 cm to 0.088 g/cm^3, as well as AF at 150-200 cm to 0.104 g/cm^3 (Figure 8(a)). Very high bulk density (0.088-0.99 g/cm^3 range for SF, ML, and AF) was recorded at the last soil depth penetrated by the peat sampler, suggesting the layer is compacted.

The mean values for dry bulk density across all ecotypes are low (SF=0.062 g/cm^3; ML=0.059 g/cm^3; AF=0.074 g/cm^3; AL=0.066 g/cm^3) compared with the 0.09 g/cm^3 peat bulk density of sites across Southeast Asia (Page et al., 2010). The results are closer to Northern Island's mean bulk density (0.069 g/cm^3) of non-forested raised bogs (Tomlinson and Davidson, 2000). AF mean bulk density is significantly higher than its ecotype counterparts, suggesting that this land use is more compacted than the rest. It can be observed in the field that AF is more accessible to the people and lies closer to the local trails, which have many activities that can lead to compaction.

3.2.3 Soil peat and C%: Figure 7(b) shows that C% is highest in ML with values ranging from 31.8-43.3 C% across the soil peat depth while SF ranges from 29.2-34.0 C%, AL with 19.1-37.4 C% and AF with 19.1-37.4 C%. ML and AL have close values of 41.9 C% and 41.4 C%, respectively, at the peat's top 0-50 cm layer. However, the value decreased for AL in the 100-150 cm layer.

The mean value of ML (40.5 C%) is higher than the other three ecotypes and is significantly different

from other means. This value is unsurprising because of the many vital grasses and sedges dominating the ML. In the field, it can be observed that grasses have piled up over the years that can be used as a walking trail to access the innermost portion of the peatland basin while maintaining buoyancy over the standing water below. C% in ML has only substantially decreased from the mean when it reached the 650-700 cm soil depth, which is already impenetrable in AL and AF ecotypes. Notably, this ML value of 35.7 C% is close to the 33.0 C% in SF at the same depth. Hence, it implies the influence of water presence on the carbon content and even the impenetrability of that layer.

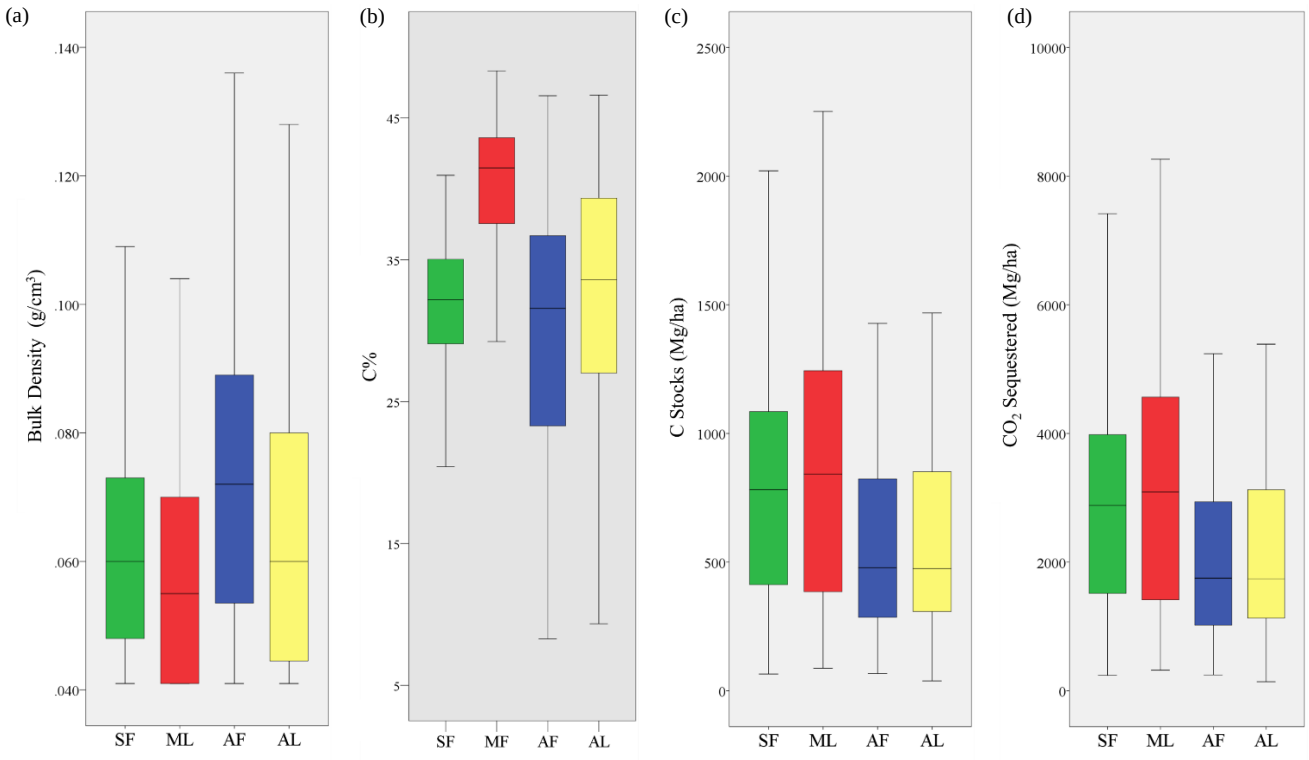

Figure 7. Box plot of (a) means bulk density (g/cm^3), (b) C%, (c) C-stocks (Mg/ha), and (d) CO_2 sequestered (Mg/ha) across four ecotypes

It also explains why the 0-50 cm upper layer of ML and AL have values close to each other (41.9 C% and 41.39 C%, respectively). However, the mean of AL (32.6 C%) has become significantly different and lower than that of ML because of the many years of cultivating the peatland for planting rice and some root crops. When the soil is opened, it is exposed to various transformations of its organic matter. It is subjected to a series of plowing and harrowing and other activities that lower its C content through time. At the same time, many C has been removed as harvestable plant parts leaving or returning only a fraction into the soil.

Peat soil organic C-stocks of LSBP contributed significantly to the belowground C-stocks of the whole peatland. SF rendered the highest peat soil C-stocks with 15,932±1,247 Mg C/ha and 58,515±4,586 Mg CO_2/ha sequestered, followed by ML with 15,288±1,013 Mg C/ha and 56,110±3,718 Mg CO_2/ha sequestered, which are not significantly different with each other; however, they are both significantly different from AL with 8,431±908 Mg C/ha, and 30,941±3,335 Mg CO_2/ha sequestered and AF with 7,706±582 Mg C/ha, and 28,282±2,136 Mg CO_2/ha sequestered (Figure 5(e) and Figure 5(j)). Such results are attributed to the soil profile depth in each ecotype where SF and ML reached 900 cm and 850 cm, respectively, while AL is down to 650 cm and AF to 600 cm.

Figure 7 and Figure 8 also show that C%, C-stocks, and CO_2 sequestered significantly increase as depth increases. The C-stocks in the SF peat soil of LSBP are higher than the 6,838 Mg/ha C-stocks of combined swamp forests in a vast dome-shaped Changuinola peatland in San San Pond Sak wetland complex in Panama (Upton et al., 2018). Sjögersten et al. (2018) described the Changuinola peatland as consistent with a surface water pool of 18.2 cm (highest) in the hardwood forest type and the lowest,

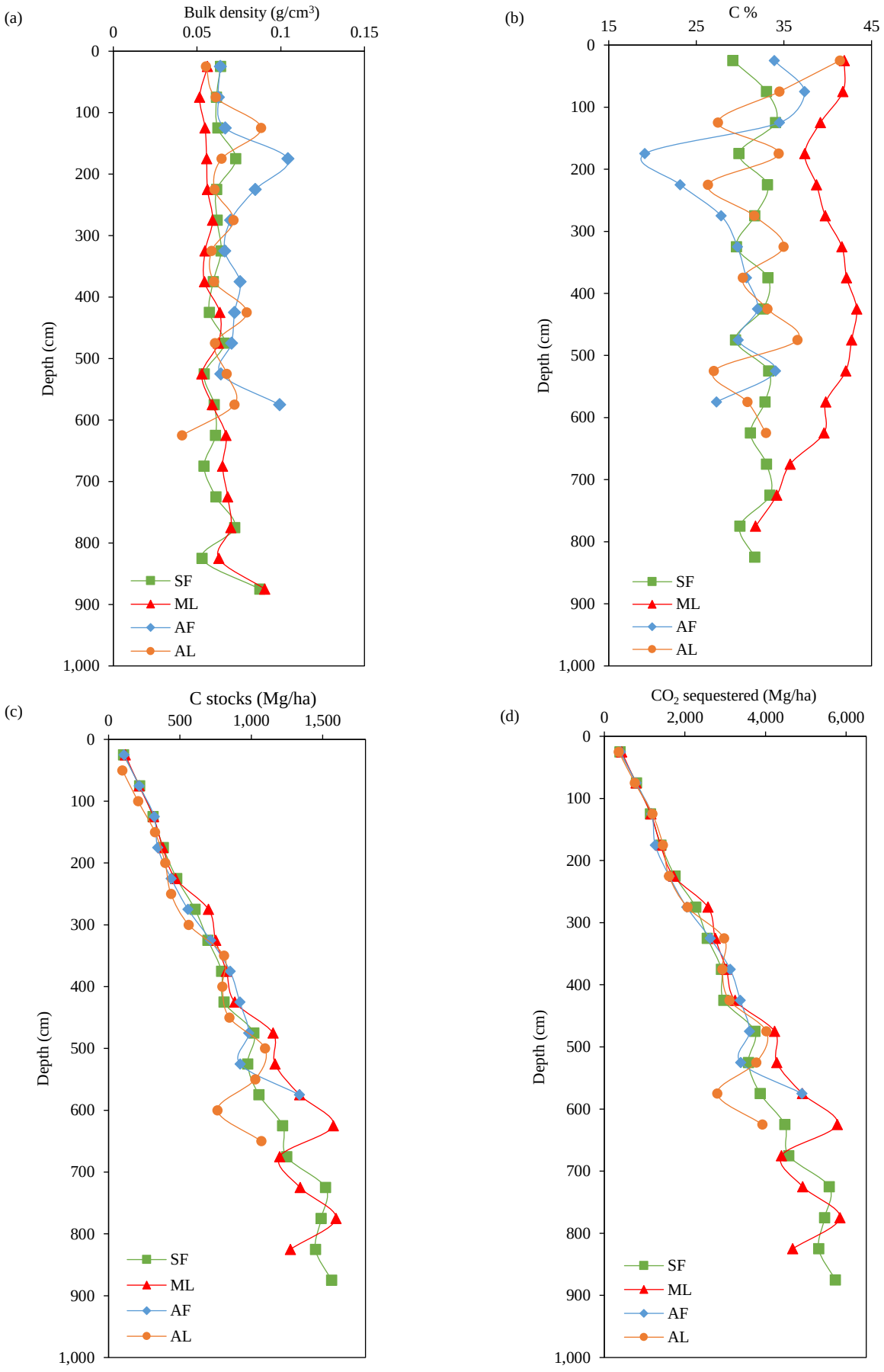

Figure 8. Depth function of (a) mean bulk density (g/cm^3), (b) C%, (c) C-stocks (Mg/ha), and (d) CO_2 sequestered (Mg/ha) across four ecotypes

8.1 cm in the stunted forest. In LSBP, water is almost always present in the ML, which registered higher C-stocks owing to the deeper extent of its soil peat (8.5 m) in contrast to the shallower Changuinola peatland (2.2-4.0 m depth range for the forest types).

3.2.4 Total belowground C-stocks and CO_2 sequestered: SF rendered the highest belowground C-stocks of LSBP with 15,936.59 Mg C/ha, the same results with the aboveground C-stocks (Figure 5(a) to Figure 5(c)). It is attributed to its peat depth that reaches up to 900 cm belowground. Previously, the sampled ML of peatland had the lowest aboveground C stock because of the few amounts of litter, and no standing trees and downed wood found. ML registered a high value of 15,288.94 Mg C/ha for the belowground C stock, second to SF. It is all attributed to the deep layers of soil peat. ML followed SF with 15,288.94 Mg C/ha even without the root biomass, which is not significantly different from each other (Figure 5(c)); but is significantly different from AL 8,432.51 Mg C/ha and AF 7,707.26 Mg C/ha.

The mean values of AF (549.1 Mg C/ha) and AL (569.7 Mg C/ha) C-stocks across all depths are not statistically different from each other but are statistically different with SF (849 Mg C/ha) and ML (778 Mg C/ha). However, such calculations neglect soil depths on each ecotype, and results showed that SF is still superior, followed by ML, AL, and AF. Further, SF and ML could sequester CO_2 (58,515 Mg/ha and 56,110 Mg/ha, respectively, Figure 5(d)) but are not statistically different.

3.3 Total C-stocks and CO_2 sequestered of LSBP

SF rendered the highest total C-stocks among the four ecotypes with 15,984.83 Mg/ha and sequestered 58,709.17 Mg/ha of CO_2 (Figure 9(a) and 9(b)). Such results are not statistically different from ML which rendered 15,289.13 Mg/ha and could sequester 56,111.12 Mg/ha of CO_2. However, AL and AF are statistically different from both ML and SF. AL rendered 8,459.72 Mg/ha C-stocks and sequestered 31,047.19 Mg/ha of CO_2, while AF rendered 7,717.28 Mg/ha C-stocks and 28,322.40 Mg/ha of CO_2 sequestered. The mean C-stocks of the four (4) ecotypes are 11,862.74 Mg/ha, which is comparable to >5,000 Mg C/ha of tropical peatlands (Rieley et al., 2008; Moore et al., 2013), and the whole LSBP with 3,088 ha has 36.63 Tg (0.037 Pg) of C, which could also sequester 134.47 Tg/ha of CO_2.

In the review by Page et al. (2010), the Philippines has a minimum of 60-2,400 km^2 out of 196,404-332,152 km^2 of tropical peatlands. Based on these minimum area values and assumptions of 1-2 m soil peat thickness and using the 60 kg/m^3 volumetric carbon density, estimates for the total C content of South East Asia is 11.8 Gt up to 39.8 Gt (Pg). The lower estimate for the Philippines alone is 0.004 Gt (Pg), while the upper estimate is 0.288 Gt (Pg) C storage. With the findings of the current study on LSBP, its C storage value can shift the carbon budget in the region (Table 1).

Compared to tropical forests, the total C-stocks of the peatland SF is much higher than the 393 Mg C/ha of C from the natural forests of a 20,438-ha watershed inside the Philippine National Oil Company geothermal plant, also in Leyte Island. It is also higher than the 418 Mg/ha C content of the secondary forests in Mt. Makiling Forest Reserve in Laguna, where the biomass contributed 43% C and the soil organic C 40% (Lasco et al., 2004).

Compared to other peatlands, the SF ecotype is higher than the 975±51 Mg/ha C-stocks from the secondary peat swamp forest of North Selangor Peat Swamp Forest situated on the west coast of Peninsular Malaysia (Tonks et al., 2017). In all ecotypes of LSBP, more than 99% of the carbon storage is contributed by peat soil. As per a review of other literature, as seen in Table 1, most peat depths are 300 to 500 cm (Sjögersten et al., 2021; Novita et al., 2021; Anshari et al., 2022; Tonks et al., 2017; Orella et al., 2022). In this study, peat depth reached up to 900 cm, as all peat samples from the surface until the peat auger could not penetrate anymore were sampled and analyzed to get the overall C-stock estimation of the LSBP ecosystem. In contrast with the study of Decena et al. (2022) in the same area, the study only considered the 1 m depth, which could be an underestimation.

Subsequently, the results further emphasize the importance of regulating activities that may impact the natural process in the peat soil and threaten the longer residence time of C in the soil. One significant threat to this was explained by a three-year study by Hirano et al. (2007), who concluded that the lowering of groundwater level because of the drainage disturbance to the tropical peat swamp forest in Central Kalimantan, Indonesia has resulted in the peatland becoming a carbon source and released CO_2 into the atmosphere. As a result, portions of LSBP have also been converted into AF. However, the C-stocks of this converted peatland are still higher than the forest

plantations with a combined value of 315 ton/ha located at the Leyte geothermal field (Lasco et al., 2002), hence, emphasizing the carbon sequestration of a peatland, whether intact or converted. Nevertheless, the conversion of peatland into other land use must be examined thoroughly because of its implications on the amount of carbon that can be held into the peatland ecosystem.

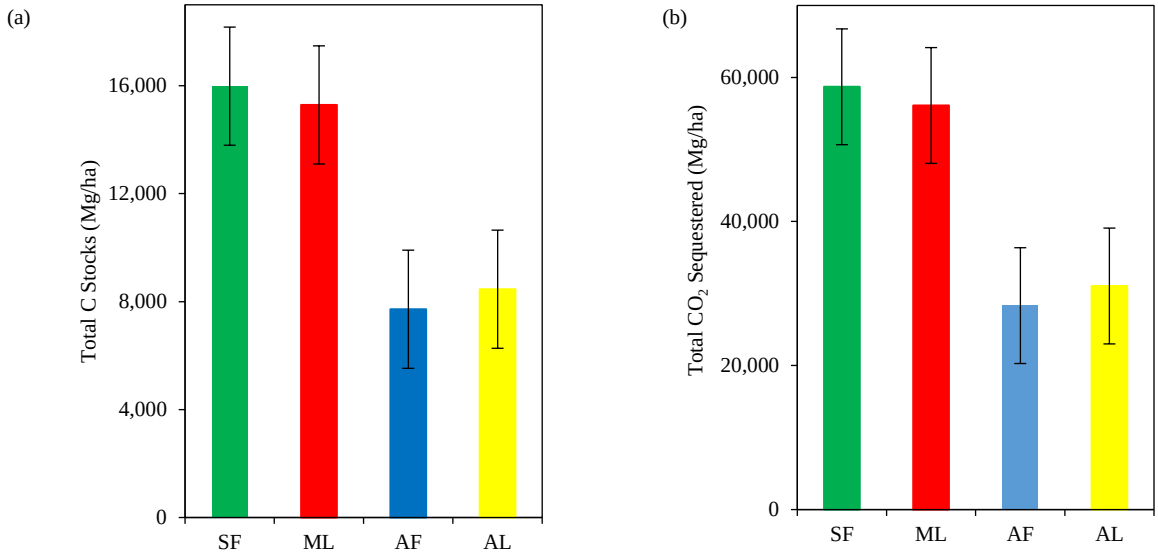

Figure 9. Total C-stocks and CO_2 sequestered (Mg/ha) of LSBP

Table 1. Summary of ecosystem C-stocks of peat swamp forest and natural forest

Location	Peat depth (cm)	Ecotypes	Ecosystem C (Mg C/ha)	Sources
Tropical area	-	Tropical Peatlands	~250 to >5,000	Rieley et al. (2008); Moore et al. (2013)
Campeche and Tabasco, Mexico	350	Peat Swamp Forests	3,130	Sjögersten et al. (2021)
Central Kalimantan, Indonesia	290	Primary Peat Swamp Forest	1,526±316	Novita et al. (2021)
West Kalimantan Province, Indonesia	500	Bush Fern, Secondary Forest, Oil Palm Plantation	1,253	Anshari et al. (2022)
North Selangor, Malaysia	125-273	Secondary Peat Swamp Forest	975±151	Tonks et al. (2017)
Agusan del Sur, Philippines	100	Undisturbed Peat Swamp Forest	750	Orella et al. (2022)
Oriental Mindoro, Philippines	100	Disturbed Peat Swamp Forest	595	Orella et al. (2022)
Makiling Forest Reserve, Philippines	-	Natural Secondary Forest	418	Lasco et al. (2004)
Leyte Geothermal Reserve, Philippines	-	Natural Forest	393	Lasco et al. (2002)
Leyte Sab-A Basin Peatland, Philippines	900	Peat Swamp Forest, Marshland, Agroforestry, and Agricultural Land	11,863	This study

4. CONCLUSION

The study found significant differences in the C storage of different components of the aboveground and belowground C-stocks among the four ecotypes in the peatland. The results indicate that all ecotypes had higher C-stocks in the belowground pool, likely due to the deep soil peat reaching 900 cm. The mean C-stocks of the four ecotypes were 11,862 Mg/ha. Furthermore, the marshland ecotype, dominated by grasses and with lesser biomass on the surface, was similar to the SF ecotype but had higher C-stocks in its soil peat layers. The study's objective of assessing the C-stocks in the peatland was achieved. The whole LSBP, with an area of 3,088 ha, was found to have a computed value of 36.6 Tg of C-stocks. It can sequester 134.5 Tg/ha of CO_2, a staggering amount of C storage. These findings have significant implications for regional C budget projections in Southeast Asia, highlighting the long-term importance of the peatland basin in the face of numerous threats to its function.

ACKNOWLEDGEMENTS

The first author would like to acknowledge the crucial contribution of Dr. Ma. Victoria O. Espaldon and Dr. Nina M. Cadiz in polishing the dissertation. Dr. Jeremy D. Owens and Mr. Burt H. Wolff for assessing all the analyses conducted in National High Magnetic Field Laboratory, Florida State University, Tallahassee, FL, USA. Commission on Higher Education-Faculty Development Program II for giving the first author a Ph.D. graduate scholarship and the Fulbright Scholarship Program for granting a Ph.D. Exchange Scholarship and funding the study.

REFERENCES

Adame MF, Santini NS, Tovilla C, Vázquez-Lule A, Castro L, Guevara M. Carbon stocks and soil sequestration rates of tropical riverine wetlands. Biogeosciences 2015;12:3805-18.

Alibo VLB, Lasco RD. Carbon storage of Caimpugan peatland in Agusan Marsh, Philippines and its role in greenhouse gas mitigation. Journal of Environmental Science and Management 2012;15(2):55-8.

Anshari GZ, Gusmayanti E, Afifudin M, Ruwaimana M, Hendricks L, Gavin DG. Carbon loss from a deforested and drained tropical peatland over four years as assessed from peat stratigraphy. Catena 2022;208:Article No. 105719.

Asian Development Bank (ADB). Environmental Evaluation of Swamps and Marshlands Project, Final Report. Philippines: Environmental Evaluation of Swamps and Marshlands; 2000.

Barthelmes A, Couwenberg J, Risager M, Tegetmeyer C, Joosten H. Peatlands and Climate in a Ramsar Context: A Nordic-Baltic Perspective. Denmark: Nordic Council of Ministers; 2015.

Bobon-Carnıce PA, Lina S. Carbon storage and nutrient stocks distribution of three adjacent land use patterns in Lake Danao National Park, Ormoc, Leyte, Philippines. Journal of Science, Engineering, and Technology 2017;5:1-4.

Bobon-Carnice PA, Lina SB. Changes in carbon and nutrient stocks of secondary forest transformations under Ultisol in Leyte Island, Philippines. Mindanao Journal of Science and Technology 2021;19(1):116-36.

Cairns MA, Brown S, Helmer EH, Baumgardner GA. Root biomass allocation in the world's upland forests. Oecologia 1997;111:1-11.

Cheyne SM, Macdonald DW. Wild felid diversity and activity patterns in Sabangau peat-swamp forest, Indonesian Borneo. Oryx 2011;45(1):119-24.

Decena SC, Villacorta-Parilla S, Arribado AO, Macasait DR, Arguelles MS, Salamia SS, et al. Impact of land use conversion on carbon stocks and selected peat physico-chemical properties in the Leyte Sab-A Basin Peatland, Philippines. Wetlands 2022;42:1-6.

Dibble AC, Rees CA. Does the lack of reference ecosystems limit our science? A case study in non-native invasive plants as forest fuels. Journal of Forestry 2005;103(7):329-38.

Donato DC, Kauffman JB, Murdiyarso D, Kurnianto S, Stidham M, Kanninen M. Mangroves among the most carbon-rich forests in the tropics. Nature Geoscience 2011;4(5):293-7.

Dommain R, Dittrich I, Giesen W, Joosten H, Rais DS, Silvius M, et al. Ecosystem services, degradation and restoration of peat swamps in the Southeast Asian tropics. Peatland Restoration and Ecosystem Services: Science, Policy and Practice 2016;23:253-88.

Food and Agriculture Organization of the United Nations (FAO). Peatlands Mapping and Monitoring - Recommendations and Technical Overview. Rome: FAO; 2020.

Hirano T, Segah H, Harada T, Limin S, June T, Hirata R, et al. Carbon dioxide balance of a tropical peat swamp forest in Kalimantan, Indonesia. Global Change Biology 2007; 13(2):412-25.

Howard J, Hoyt S, Isensee K, Telszewski M, Pidgeon E. Coastal Blue Carbon: Methods for Assessing Carbon Stocks and Emissions Factors in Mangroves, Tidal Salt Marshes, and Seagrasses. Arlington, Virginia, USA: Conservation International, Intergovernmental Oceanographic Commission of UNESCO, International Union for Conservation of Nature; 2014.

Kauffman JB, Heider C, Cole TG, Dwire KA, Donato D. Ecosystem carbon stocks of Micronesian mangrove forests. Wetlands 2011;31:343-52.

Kauffman JB, Donato DC. Protocols for the Measurement, Monitoring, and Reporting of Structure, Biomass and Carbon Stocks in Mangrove Forests. Working Paper 86. Bogor, Indonesia: Center for International Forestry Research; 2012.

Kauffman JB, Arifanti VB, Basuki I, Kurnianto S, Novita N, Murdiyarso D, et al. Protocols for the Measurement, Monitoring, and Reporting of Structure, Biomass, Carbon Stocks and Greenhouse Gas Emissions in Tropical Peat Swamp Forests. Bogor, Indonesia: Center for International Forestry Research; 2016.

Lasco RD, Lales JS, Arnuevo MT, Guillermo IQ, de Jesus AC, Medrano R, et al. Carbon dioxide (CO_2) storage and sequestration of land cover in the Leyte Geothermal Reservation. Renewable Energy 2002;25(2):307-15.

Lasco RD, Guillermo IQ, Cruz RV, Bantayan NC, Pulhin FB. Carbon stocks assessment of a secondary forest in Mount Makiling Forest Reserve, Philippines. Journal of Tropical Forest Science 2004;1:35-45.

Margono BA, Potapov PV, Turubanova S, Stolle F, Hansen MC. Primary forest cover loss in Indonesia over 2000-2012. Nature Climate Change 2014;4(8):730-5.

Miettinen J, Shi C, Liew SC. Two decades of destruction in Southeast Asia's peat swamp forests. Frontiers in Ecology and the Environment 2012;10(3):124-8.

Moore S, Evans CD, Page SE, Garnett MH, Jones TG, Freeman C, et al. Deep instability of deforested tropical peatlands revealed by fluvial organic carbon fluxes. Nature 2013;493(7434):660-3.

Neufeldt H. Carbon stocks and sequestration potentials of agricultural soils in the federal state of Baden-Württemberg, SW Germany. Journal of Plant Nutrition and Soil Science 2005;168(2):202-11.

Novita N, Kauffman JB, Hergoualc'h K, Murdiyarso D, Tryanto DH, Jupesta J. Carbon stocks from peat swamp forest and oil palm plantation in Central Kalimantan, Indonesia. In: Djalante R, Jupesta J, Aldrian E, editors. Climate Change Research, Policy and Actions in Indonesia. Springer Nature Switzerland; 2021. p. 203-27.

Nowak K. Mangrove and peat swamp forests: Refuge habitats for primates and felids. Folia Primatologica 2013;83(3-6):361-76.

Nuthammachot N, Phairuang W, Stratoulias D. Estimation of carbon emission in the ex-mega rice project, Indonesia based

on SAR satellite images. Applied Ecology and Environmental Research 2019;17(2):2489-99.

Orella J, Africa DR, Bustillo CH, Pascua N, Marquez C, Adornado H, et al. Above-and-belowground carbon stocks in two contrasting peatlands in the Philippines. Forests 2022;13(2): Article No. 303.

Page S, Wust R, Banks C. Past and present carbon accumulation and loss in Southeast Asian peatlands. Pages News 2010; 18(1):25-7.

Page SE, Rieley JO, Banks CJ. Global and regional importance of the tropical peatland carbon pool. Global Change Biology 2011;17(2):798-818.

Posa MR, Wijedasa LS, Corlett RT. Biodiversity and conservation of tropical peat swamp forests. BioScience 2011;61(1):49-57.

Protected Areas and Wildlife Bureau, Department of Natural Resources (PAWB-DENR). National Action Plan Sustainable Use and Protection of Philippine Peatlands. Philippines: Department of Environment and Natural Resources and Protected Areas and Wildlife Bureau; 2009.

Protected Areas and Wildlife Bureau Department of Natural Resources (PAWB-DENR). The National Wetlands Action Plan for the Philippines 2011-2016. Philippines: National Wetlands Action Plan for the Philippines (NWAPP); 2013.

Rieley JO, Page SE. Carbon budgets under different land uses on tropical peatland. Proceedings of the 13th International Peat Congress; 2008 Jun 8; Tullamore, Ireland; 2008.

Román-Cuesta RM, Salinas N, Asbjornsen H, Oliveras I, Huaman V, Gutiérrez Y, et al. Implications of fires on carbon budgets in Andean cloud montane forest: The importance of peat soils and tree resprouting. Forest Ecology and Management 2011;261(11):1987-97.

Sjögersten S, Aplin P, Gauci V, Peacock M, Siegenthaler A, Turner BL. Temperature response of ex-situ greenhouse gas emissions from tropical peatlands: Interactions between forest type and peat moisture conditions. Geoderma 2018;324:47-55.

Sjögersten S, De La Barreda-Bautista B, vBrown C, Boyd D, Lopez-Rosas H, Hernández E, et al. Coastal wetland ecosystems deliver large carbon stocks in tropical Mexico. Geoderma 2021;403:Article No. 115173.

Tomlinson RW, Davidson L. Estimates of carbon stores in four Northern Irish lowland raised bogs. Suo 2000;51(3):169-79.

Tonks AJ, Aplin P, Beriro DJ, Cooper H, Evers S, Vane CH, et al. Impacts of conversion of tropical peat swamp forest to oil palm plantation on peat organic chemistry, physical properties and carbon stocks. Geoderma 2017;289:36-45.

Upton A, Vane CH, Girkin N, Turner BL, Sjögersten S. Does litter input determine carbon storage and peat organic chemistry in tropical peatlands? Geoderma 2018;326:76-87.

Weishampel P, Kolka R, King JY. Carbon pools and productivity in a 1-km^2 heterogeneous forest and peatland mosaic in Minnesota, USA. Forest Ecology and Management 2009; 257(2):747-54.

Yu Z, Loisel J, Brosseau DP, Beilman DW, Hunt SJ. Global peatland dynamics since the Last Glacial Maximum. Geophysical Research Letters 2010;37:Article No. 13.

Yu Z, Beilman DW, Frolking S, MacDonald GM, Roulet NT, Camill P, et al. Peatlands and their role in the global carbon cycle. Eos, Transactions American Geophysical Union 2011;92(12):97-8.

Soil Carbon Stock and Soil Properties under Different Land Use Types of Agriculture

Utain Chanlabut[1] and Benchawan Nahok[2*]

[1]*Department of General Science, Faculty of Science and Technology, Muban Chombueng Rajabhat University, Ratchaburi, Thailand*
[2]*Department of General Science, Faculty of Education, Chaiyaphum Rajabhat University, Chaiyaphum, Thailand*

ARTICLE INFO

Received: 8 Mar 2023
Received in revised: 20 Jun 2023
Accepted: 22 Jun 2023
Published online: 5 Sep 2023
DOI: 10.32526/ennrj/21/20230056

Keywords:
Soil carbon storage/ Soil organic carbon/ Agriculture/ Ratchaburi Province/ Land use/ Soil properties

*** Corresponding author:**
E-mail: nahok.b@gmail.com

ABSTRACT

Agriculture soils play a crucial role in carbon storage and food security. However, uncertainty remains about soil carbon stocks due to spatial variability. This study estimated soil carbon stocks in agricultural land and examined the impact of land use and soil properties on soil organic carbon in Ratchaburi Province, Thailand. Soil samples were collected at three depths (0-10, 10-20, and 20-30 cm) within five different land use types: cassava, coconut, paddy fields, pineapple, and sugarcane. The results revealed that soil organic carbon decreased with increasing depth. Significant differences in soil carbon and soil properties were observed among land uses. The carbon stocks at 0-30 cm depth were as follows: coconut (35.87 mg C/ha), paddy fields (31.17 mg C/ha), sugarcane (28.02 mg C/ha), pineapple (21.79 mg C/ha), and cassava (16.12 mg C/ha). The carbon stocks were significantly correlated with sand, density, clay, silt, and pH. This study highlights the impact of land use types on carbon stocks in agricultural soils and emphasizes the role of soil properties, particularly soil texture, in influencing carbon storage variability. Furthermore, the study highlights the carbon storage potential in agricultural areas, which could guide the formulation of policies to utilize agricultural land to offset CO_2 emissions from other sectors.

1. INTRODUCTION

Soils provide many ecosystem services (Rodrigues et al., 2021). Specifically, they serve as the largest carbon reservoir in terrestrial ecosystems, storing significant amounts of carbon (Lal, 2004; Stockmann et al., 2015; Stockmann et al., 2013). Within the top meter of soil, organic carbon stock is estimated at 1,325-1,408 Pg, which is four times greater than biotic reservoirs and three times greater than atmospheric reservoirs (Batjes, 2016; Lorenz and Lal, 2018; Scharlemann et al., 2014). Given that soil acts as both a source and sink of atmospheric CO_2, particularly in agriculture, soil organic carbon reservoirs have become a critical and challenging subject on a global scale (Amelung et al., 2020; Jobbágy and Jackson, 2000; Todd-Brown et al., 2014).

Recently, the potential of agricultural soil to mitigate climate change and enhance food security has become a critical topic on various political agendas. The 4 per 1,000 initiative was introduced during the 21st Conference of Parties (COP21) to the United Nations Framework Convention on Climate Change (UNFCCC). The core concept of this initiative proposed that an annual increase of 0.4% in soil organic carbon stock in the upper 30 to 40 cm of soil could offset CO_2 emissions resulting from fossil fuel combustion (Minasny et al., 2017). Moreover, an increased soil organic carbon can improve soil quality and contribute to food security (Arunrat et al., 2020a; Pan et al., 2009). For instance, increasing the SOC content by 1 g/kg can lead to a rice yield boost of 302 kg/ha (Arunrat et al., 2020a). Consequently, agricultural soils are increasingly being utilized as a survival door to mitigate and adapt to the effects of climate change and ensure food security (Minasny et al., 2017).

Agriculture accounts for almost half of Thailand's area. Ratchaburi Province is a prominent cultivation hub within the country, covering half the area of the province, or around 263,366 ha (Land Development Department, 2022a). Agricultural lands in the province consist of various land uses such as

Citation: Chanlabut U, Nahok B. Soil carbon stock and soil properties under different land use types of agriculture. Environ. Nat. Resour. J. 2023;21(5):417-427. (https://doi.org/10.32526/ennrj/21/20230056)

coconut, pineapple, paddy fields, cassava, and sugarcane (Land Development Department, 2022a). Agricultural soils can act as either carbon sources or sinks (Freibauer et al., 2004) due to the significant impact of agricultural practices on soil carbon storage, including tillage, fertilizer use, and land-use changes (Dignac et al., 2017). As a substantial portion of this province is dedicated to agriculture, any alterations in the soil carbon could result in significant environmental consequences, particularly concerning greenhouse gas emissions. However, predicting their effects may be challenging without disclosing the amount of carbon stored in the soil and the factors that influence it.

Soil carbon storage in agriculture is varied depending on many environmental factors, particularly in different land use types (Tan et al., 2004). Previous studies demonstrated variations in soil carbon stocks across various agricultural sites in the country. For instance, paddy fields in Chiang Mai Province exhibited SOC stocks ranging from 21.61 to 21.84 mg C/ha (Arunrat et al., 2022), while the range was 14.9 to 21.3 mg C/ha in Kalasin Province (Bridhikitti, 2017). A corn field in Nakhon Ratchasima Province had a soil carbon storage of 57 mg C/ha (Lichaikul et al., 2006), and diverse agricultural types in Nan Province had a storage of 42.08 mg C/ha (Pibumrung et al., 2008). However, the specific soil carbon storage for land use types in Ratchaburi Province remains poorly understood. Estimation of soil carbon storage is crucial for agricultural soils, particularly in the topsoil layer that significantly influences crop yield (Sun et al., 2010) and is susceptible to land use change (Veldkamp et al., 2003).

Therefore, the objectives of the study were (1) to evaluate and compare soil carbon stocks among different agricultural land use types and (2) to investigate the relationship between SOC and soil properties. This research aimed to provide valuable insights into soil carbon storage in agricultural soils and the influence of land use types on carbon storage. Furthermore, the study offers vital information for policymakers and land managers, enabling them to make informed decisions regarding soil management strategies for climate change mitigation.

2. METHODOLOGY

2.1 Study areas

The study was carried out in Ratchaburi Province, covering an area of over 5,196 km^2, situated between 13°32'21" N and 99°49'11" E. Of the total area, approximately 50.71% is dedicated to agriculture encompassing several land use types. These include paddy field (10.07%), sugarcane (9.45%), cassava (3.42%), coconut (4.81%), and pineapple (4.22%) (Land Development Department, 2022a). The chosen study area represents these agricultural types across ten districts within the province. Figure 1 displays the sampling sites for the five-land uses and provides examples of the study areas.

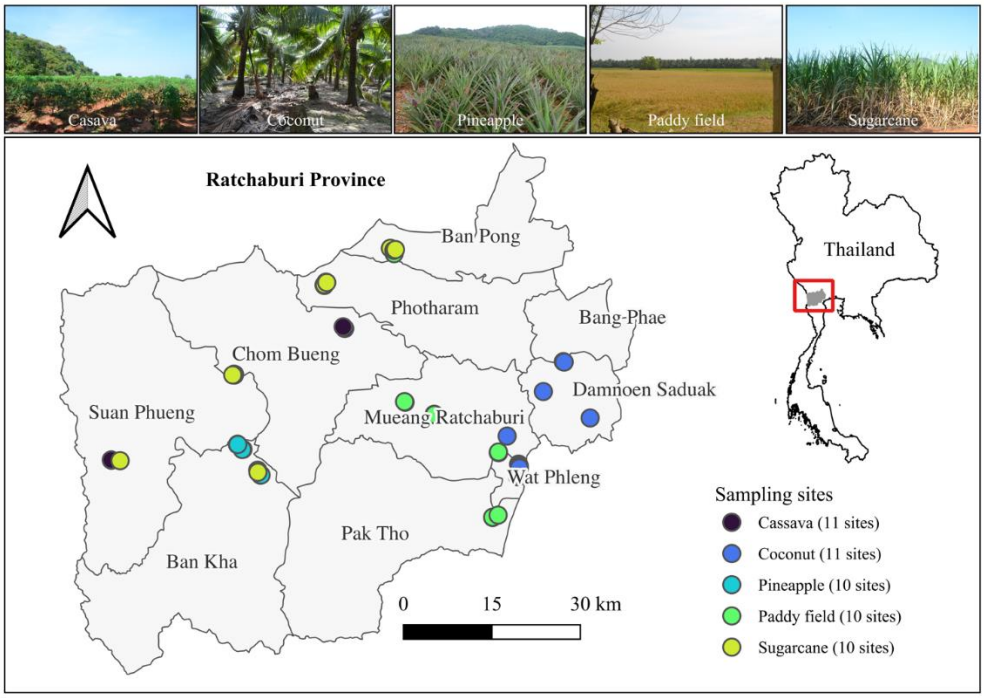

Figure 1. Examples of land use types and locations of sampling sites

In the study sites, 15 different soil series were identified by georeferencing the coordinates of the study sites on the soil series map (Land Development Department, 2022b). These soil series were Tha Yang (Kanhaplic Haplustults), Bangkok (Vertic Endoaquepts), Chan Tuk (Typic Ustipsamments), Alluvial Complex (Fluventic Endoaquepts (Haplustepts)), Thonburi (Vertic Endoaquepts), Lat Ya (Kanhaplic Haplustults), Khao Luang (Typic (Kandic) Paleustults), Khao Phlong (Kanhaplic Haplustults), Damnoen Saduak (Typic Haplaquolls), Chom Bueng (Arenic (Grossarenic) Haplustalfs), Bang Phae (Typic Endoaquolls), Pak Tho (Plinthic Palequults), Tap Salao (Ultic (Typic) Haplustalfs), Bang Khen (Vertic Endoaquepts), and Takhli (Entic Haplustolls). Each land use in this study consisted of multiple soil series as well as land histories and farmer practices (Table 1).

Table 1. Soil series with land history and farmer practices under the agricultural land uses

Land use types	Soil series with land history and farmer practices
Cassava	• Soil series: Tap Salao (18%), Chan Tuk (18%), Chom Bueng (18%), Alluvial Complex (18%), Tha Yang (9%), Khao Luang (9%), Khao Phlong (9%) • Land history: continuous cultivation for over 5 years • Farmer practices: - Heavy tractor soil preparation - plowing, harrowing, and ridge creation - Plant residue practice: removal of residues after harvest - Application of chemical fertilizers
Coconut	• Soil series: Thonburi (36%), Damnoen Saduak (27%), Bang Phae (18%), Bang Khen (9%), Bangkok (9%) • Land history: - Multi-generational coconut cultivation - Age range of coconut trees: 4-10 years • Farmer practices: - Furrow creation between coconut tree rows - Furrow irrigation: Standing water in furrows between tree rows - Plant residue practice: Residue retention in the backyard - Fertilizer use: Utilization of mud from furrows for tree fertilization and weed control
Pineapple	• Soil series: Tha Yang (60%), Chan Tuk (30%), Lat Ya (10%) • Land history: - Cultivated since approximately 2014 or earlier - Located in the foothills and connected to a forested area • Farmer practices: - Heavy tractor soil preparation for planting: o Once every 4 years in Tha Yang and Lat Ya, as pineapples have a lifespan of 4 years o Every year in Chan Tuk, as pineapples have a lifespan of only 1 year - Non-removal of plant residues after harvest - Manual weed control practices involving pulling and digging - Application of chemical fertilizers and plant hormones during the reproductive season
Paddy fields	• Soil series: Bangkok (50%), Pak Tho (20%), Khao Phlong (20%), Alluvial Complex (10%) • Land history: Long-term rice cultivation • Farmer practices: - Rice cultivation twice a year - Long-term presence of standing water during the cultivation period - Two rounds of plowing: one for soil preparation and another before planting - Utilization of chemical fertilizers - Harvesting using a combine harvester - Absence of burning stubble
Sugarcane	• Soil series: Khao Luang (30%), Lat Ya (30%), Alluvial Complex (10%), Tha Yang (10%), Khao Phlong (10%), Takhli (10%) • Land history: Over ten years cultivation • Farmer practices: - Heavy tractor for soil preparation and management - Utilization of chemical fertilizers and sugar factory by-products - Sugarcane burning practiced in some areas before harvesting

Remark: The percentages shown in parentheses for each soil series indicate their proportion, which was calculated by dividing the number of sampling points where the soil series was found by the total number of sampling points within each agricultural area.

2.2 Soil sampling and analysis

Sample collection was taken during June-July 2022. Soil samples were obtained from a total of 52 locations representing five different agricultural land use types: cassava (11 sites), coconut (11 sites), pineapple (10 sites), and paddy field (10 sites) (Figure 1). At each site, three soil pits were arranged in a triangular pattern to reduce soil heterogeneity and create composite samples. Soil samples were collected from three consecutive depths (0-10, 10-20, 20-30 cm) using stainless steel corers. Three replicate samples were combined for composite samples for each depth. A core was hammered at the center of triangular plot to obtain an undisturbed sample used in soil bulk density analysis. Then, soil samples were conveyed to a laboratory for preparation and analysis.

The composited samples were air dried at room temperature and were subsequently sieved through a 2-mm mesh before conducting analyses for organic carbon, soil pH, and soil texture. Soil bulk density was determined by assessing the dry weight per unit volume of the soil core after it had been dried at 105°C in a hot oven for 24 h (Blake and Hartage, 1986). Soil texture was analyzed using the hydrometer method (Bouyoucos, 1962). Soil pH was determined by preparing a 1:1 soil-to-water mixture and utilized a pH meter according to the procedure described by Thomas (1996). The wet oxidation method was employed for the analysis of soil organic carbon (Walkley and Black, 1934).

2.3 Estimation of total carbon stocks.

The total carbon stock was determined by calculating the product of SOC content and soil bulk density up to a specified depth. The equation used to calculate the total carbon stock is provided below (Ellert et al., 2007).

$$C_{stock} = \sum_{1}^{N} D \times C \times T \times 0.1 \quad (1)$$

The term C_{stock} denotes the total carbon stock (mg C/ha), where D refers to soil bulk density (g/cm³), and C represents SOC content (g C/kg) determined using the wet oxidation method developed by Walkley and Black. T represents the thickness of the soil layers (cm), while N represents the number of soil depths, which includes three consecutive depths (0-10, 10-20, and 20-30 cm).

2.4 Statistical analysis

Normal distribution assumption was tested using the Shapiro-Wilk method. Data analysis was performed using R Studio (RStudio Team, 2020). A two-way ANOVA was conducted to examine the effects of land-use type and soil depth on carbon stock, SOC, and soil properties. To determine significant mean differences of soil parameters among land use types and soil depths, the Tukey HSD test was employed. Pearson's correlation was utilized to investigate the relationship between soil properties.

3. RESULTS AND DISCUSSION

3.1 Soil characteristics

The soil properties under five agricultural land uses were examined. The means and standard error for the soil parameters are presented in Table 2.

Table 2. Physicochemical soil characteristics under five agricultural land use

Soil properties	Land use types				
	Cassava	Coconut	Pineapple	Paddy field	Sugarcane
pH (ranges)					
0-10 cm	5.10-7.00	5.90-7.70	4.40-7.20	4.20-7.60	5.00-7.00
10-20 cm	4.80-6.90	5.90-7.70	4.50-7.30	5.20-7.60	4.90-7.10
20-30 cm	5.30-7.00	6.20-7.80	4.50-7.40	5.00-7.80	4.90-7.30
Density (g/cm^3)					
0-10 cm	1.47±0.03^{ab}	1.29±0.07^{b}	1.45±0.04^{ab}	1.34±0.07^{ab}	1.42±0.04^{ab}
10-20 cm	1.51±0.04^{ab}	1.27±0.04^{b}	1.57±0.04^{a}	1.47±0.07^{ab}	1.51±0.07^{ab}
20-30 cm	1.51±0.06^{ab}	1.26±0.05^{b}	1.62±0.05^{a}	1.45±0.09^{ab}	1.50±0.06^{ab}
Sand (%)					
0-10 cm	71.81±2.92^{a}	24.09±2.73^{c}	61.84±4.32^{ab}	48.35±5.32^{b}	58.71±2.46^{ab}
10-20 cm	71.63±2.71^{a}	21.71±2.16^{c}	61.03±4.38^{a}	43.55±5.57^{b}	57.72±2.31^{ab}
20-30 cm	70.15±2.89^{a}	22.44±2.46^{c}	60.43±4.75^{a}	40.35±6.07^{b}	57.72±2.45^{a}

Table 2. Physicochemical soil characteristics under five agricultural land use (cont.)

Soil properties	Land use types				
	Cassava	Coconut	Pineapple	Paddy field	Sugarcane
Silt (%)					
0-10 cm	8.20±1.27^{c}	42.95±5.28^{a}	12.00±2.13^{bc}	23.67±4.58^{b}	14.57±2.48^{bc}
10-20 cm	8.92±1.46^{c}	44.75±4.31^{a}	12.62±2.08^{c}	28.07±3.87^{b}	16.98±2.53^{bc}
20-30 cm	9.81±1.76^{c}	45.29±4.29^{a}	13.42±2.31^{c}	31.87±4.21^{b}	17.13±2.68^{c}
Clay (%)					
0-10 cm	19.99±1.89^{b}	32.96±3.29^{a}	26.16±2.52^{ab}	27.99±2.93^{ab}	26.72±1.71^{ab}
10-20 cm	19.44±1.57^{b}	33.55±3.40^{a}	26.35±2.56^{ab}	28.39±3.87^{ab}	25.30±1.64^{ab}
20-30 cm	20.04±1.32^{b}	32.28±3.53^{a}	26.15±2.67^{ab}	27.79±3.65^{ab}	25.15±1.99^{ab}

Remarks: The soil parameters are presented as Mean±SE, except for soil pH, which is shown as ranges. The different letters indicated significant mean differences within each soil property ($p<0.05$).

3.1.1 Soil reaction (pH)

The soil pH varied across the different agricultural land uses, ranging from 4.20 to 7.80, which encompassed a wide pH range from extremely acidic to slightly alkaline. The pH values were influenced by land use types. For cassava, the pH ranged from very strongly acidic to neutral (4.8-7.0), while coconut exhibited a range from moderately acidic to slightly alkaline (5.90-7.80). Pineapple showed a pH range from extremely acidic to slightly alkaline (4.40-7.40), and paddy fields exhibited a similar range from extremely acidic to slightly alkaline (4.20-7.80). Sugarcane displayed a pH range from very strongly acid to neutral (4.90-7.30). Overall, these findings indicate high variability in soil pH within agricultural soils, influenced by factors such as land use type and soil depth.

3.1.2 Soil bulk density

Soil bulk density exhibited variations among different land use types and depths. In the 0-10 cm depth, 10-20 cm depth, and 20-30 cm depth, the soil bulk density ranged from 1.29 to 1.47 g/cm^3, 1.27 to 1.57 g/cm^3, and 1.26 to 1.62 g/cm^3, respectively (Table 2). Significant differences in soil bulk densities were observed among the land use types ($p<0.05$), while no significant differences were found among the soil depths ($p>0.05$) (Table 2).

At 0-10 cm depth, coconut exhibited the lowest soil density (1.29±0.07 g/cm^3), while cassava had the highest density (1.47±0.03 g/cm^3). Additionally, pineapple and sugarcane also showed high soil density in this depth range (Table 2). At 10-20 cm depth, coconut displayed the lowest bulk density (1.27±0.04 g/cm^3), whereas pineapple showed the highest bulk density (1.57±0.04 g/cm^3). Pineapple exhibited the highest bulk density at 20-30 cm depth (1.62±0.05 g/cm^3), whereas coconut had the lowest bulk density (1.26±0.06 g/cm^3).

Land used for pineapple, sugarcane, and cassava exhibited higher soil bulk density compared to paddy fields and coconut plantations. Wang et al. (2022) suggested that tillage practices involving the use of large tractor equipment contribute to soil compaction. This finding aligned with our observations, as we found that large tractors are commonly employed in the three land uses in this study.

Alternatively, the lower bulk density of coconut and paddy fields may be attributed to their higher organic matter content. A previous study of Islam et al. (2014) had shown a negative correlation between soil bulk density and SOC content, supporting this explanation.

In addition, soil texture could affect soil bulk density (Díaz-Zorita and Grosso, 2000). Our observations indicated that land use areas characterized by high soil density tend to have a higher sand content. Conversely, land uses with low density exhibit lower sand content.

3.1.3 Soil texture and particle distribution

Sand particle in the top layer (0-10 cm) was highest in cassava (71.81±2.92), followed by pineapple (61.84±4.32), sugarcane (58.71±2.46), paddy fields (48.35±5.32), and coconut (24.09±2.73). The trend was similar at deeper depths (10-20 cm and 20-30 cm), with the lowest sand content in coconut and the highest sand content in cassava.

For silt particles, coconut had the highest silt content in the topsoil (42.95±5.28), followed by paddy fields (23.67±4.58), sugarcane (14.57±2.48), pineapple (12.00±2.13), and cassava (8.20±1.27), respectively. Coconut still had the highest silt content at deeper depths, while cassava had the lowest.

For clay particles, coconut had the highest clay content in the topsoil (32.96±3.29), followed by paddy fields (27.99±2.93), sugarcane (26.72±1.71), pineapple (26.16±2.52), and cassava (19.99±1.89). The trend was similar at the deeper depths, with the highest clay content in coconut and the lowest clay content in cassava (Table 2).

Across land uses and soil depths, cassava exhibited the highest sand content, followed by pineapple, sugarcane, paddy fields, and coconut, respectively. Both coconut and paddy fields displayed higher silt content compared to the other land uses, while cassava and pineapple showed lower soil bulk density. Coconut had the highest clay content, whereas cassava had the lowest. Overall, these results suggested that soil particle composition varied among land use types. The soils in coconut and paddy fields contained higher silt and clay content but lower sand content compared to the soils in pineapple, cassava, and sugarcane.

The soil textures studied here were primarily categorized as sandy loam, clay, loamy sand, clay loam, loam, sandy clay loam, silty clay loam, sand, and silt loam. Soil with a higher proportion of coarse particles may limit the accumulation of SOC (Arunrat et al., 2020a). However, soil with a higher proportion of fine particles have a greater capacity to store carbon as silt and clay particles influence the maximum carbon storage level in soils (Matus, 2021).

3.2 Soil organic carbon content

A two-way ANOVA was conducted to analyze the impact of land use type and soil depth on soil organic carbon (SOC) content levels in agricultural soils. The results indicated that land use type and soil depth contributed to statistical differences in the mean of the SOC content ($p<0.05$). The means and standard error of the SOC contents are presented in Figure 2 and Table S1.

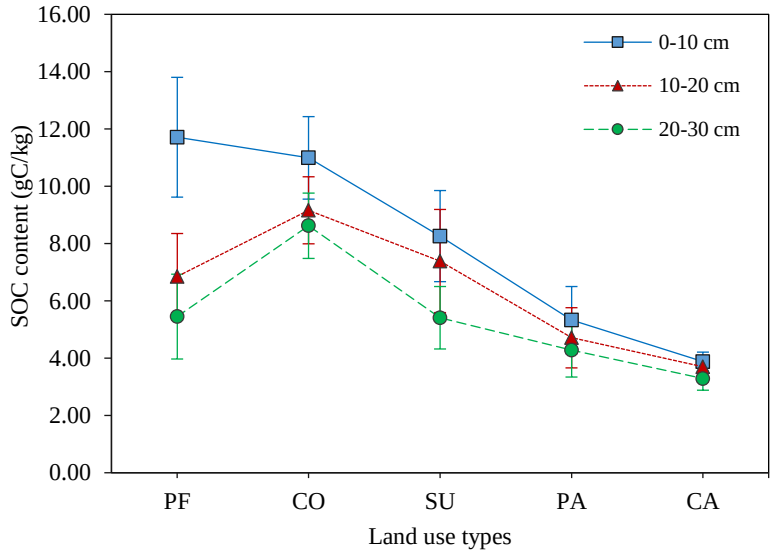

Figure 2. Soil organic carbon content among soil depth and land use types including CA=cassava, CO=coconut, PA=pineapple, PF=paddy fields, and SU=sugarcane

The SOC content was highest at the 0-10 cm depth and lowest at the 20-30 cm depth. Remarkably, the SOC content varied significantly among land use types at each soil depth (Figure 2). The mean SOC ranges were as follows: 3.88±0.33 to 11.71±2.09 g C/kg (0-10 cm), 3.70±0.39 to 9.16±1.17 g C/kg (10-20 cm), and 3.29±0.41 to 8.62±1.14 g C/kg (20-30 cm) (Table S1). Specifically, paddy fields exhibited the highest SOC at the 0-10 cm depth (Figure 2), while cassava had the lowest content. In contrast, coconut plantations displayed the highest SOC levels at both the 10-20 cm and 20-30 cm depths, while cassava plantations consistently demonstrated the lowest SOC content (Figure 2).

The findings supported the objective to investigate the impact of land use type and soil depth on SOC content in agricultural soils. The results clearly demonstrated a significant impact of both land use type and soil depth on SOC levels. In the present study, findings demonstrated a consistent decrease in SOC content with increasing soil depth across agricultural land use types, highlighting the significant impact of soil depth on SOC levels. Previous studies have also reported higher SOC levels in the topsoil of

agricultural lands, indicating a greater deposition of organic matter in the topsoil (Pibumrung et al., 2008). This effect was particularly pronounced in paddy soil, where organic matter tended to accumulate more compared to other areas. Our observation revealed that stubbles were commonly left in the paddy fields, resulting in a high amount of organic matter after decomposition. This practice might explain the significant accumulation of organic carbon.

Although the topsoil had higher SOC content, there were no significant differences in mean SOC across the 0-20 cm depth in both cassava and sugarcane (Table S1), indicating similar SOC content throughout the soil profile. Frequent tillage using large tractors with large blades disrupted the soil layers up to 20 cm deep, likely contributing to the absence of carbon variations between the 0-10 cm and 10-20 cm soil layers. Tillage reduced soil structure stability and led to soil erosion, diminishing organic matter retention (Berhe et al., 2018; Nunes et al., 2020). Soil erosion and deep tillage could result in lower SOC levels, especially in cassava soil with prevalent leaching marks in the topsoil.

3.3 Relationship between SOC and soil properties

The correlation pattern between total carbon stock (SOC stocks) and SOC content with soil properties was similar. Significant positive correlations were observed with silt, clay, and soil pH, while negative correlations were found with sand and soil bulk density (Table 3). In addition, the analysis unveiled significant relationships among soil properties, including positive correlations between soil density and sand, negative correlations with silt, clay, and soil pH, a positive association between soil pH and silt (Table 3).

Table 3. Coefficient value of Pearson's correlation

	SOC stock	SOC content	Density	pH	Sand	Silt	Clay
SOC stock	1						
SOC content	0.959**	1					
Density	-0.232**	-0.455**	1				
pH	0.260**	0.314**	-0.296**	1			
Sand	-0.508**	-0.590**	0.520**	-0.470**	1		
Silt	0.382**	0.509**	-0.572**	0.567**	-0.897**	1	
Clay	0.446**	0.402**	-0.134	0.033	-0.620**	0.209**	1

**Correlation is significant at the 0.01 level (2-tailed).

The coefficients indicated significant correlation between SOC and silt, clay, soil pH, sand, and density, supporting the hypothesis that soil properties influence soil organic carbon (Wiesmeier et al., 2019). The positive correlations indicated that soil pH, silt, and clay content could contribute to higher soil organic carbon in agricultural systems. Tu et al. (2018) suggested that soil pH played a dominant role in determining SOC levels. Similarly, Fujisaki et al. (2018) reported that fine particles (silt and clay) were crucial in increasing the maximum saturation of organic carbon.

However, significant negative correlations indicated that both sand and soil bulk density could contribute to lower soil organic carbon in agricultural systems. In particular, sand was found to have a stronger relationship with both SOC and SOC stock compared to other soil parameters, indicating its greater influence on soil carbon in agricultural systems. Arunrat et al. (2020a) suggested that soils with dominant coarse particles or sandy soils had low fertility and poor soil aggregation, leading to a low potential for carbon storage. Other studies also demonstrated a negative relationship between soil density and SOC (Islam et al., 2014). The ability of SOC to accumulate was likely limited by the increase in soil bulk density caused by a reduction in porosity (Arunrat et al., 2020a).

3.4 Total carbon stocks

The results of the ANOVA tests indicated a significant differences in total carbon stocks among the five land use types (Figure 3). Soil carbon stock across three depths also revealed a trend similar to the SOC content (Table S2). Total carbon stock at a depth of 30 cm for all agricultural land use types was 26.54±2.11 mg C/ha, with a range of 16.12 to 35.87 mg C/ha (Figure 3). Among these types, coconut exhibited the highest total carbon stock (35.87±4.25 mg C/ha), followed by paddy fields (31.17±4.93 mg

C/ha), sugarcane (28.02±5.72 mg C/ha), pineapple (21.79±4.77 mg C/ha), and cassava (16.12±1.54 mg C/ha), respectively.

The findings support the hypotheses that land use types might have a significant difference of total carbon stocks. Theoretically, soil carbon storage is determined by many factors, such as clay mineralogy, specific surface area, aggregation, texture, soil type, natural vegetation, land use and management, topography, parent material, and climate (Wiesmeier et al., 2019). In addition to the effect of land use examined in this study, other factors were also considered. The variation in total carbon stock between land use types could be attributed to the distinct soil series with varying soil textures and compositions of soil particles, as well as their management practices.

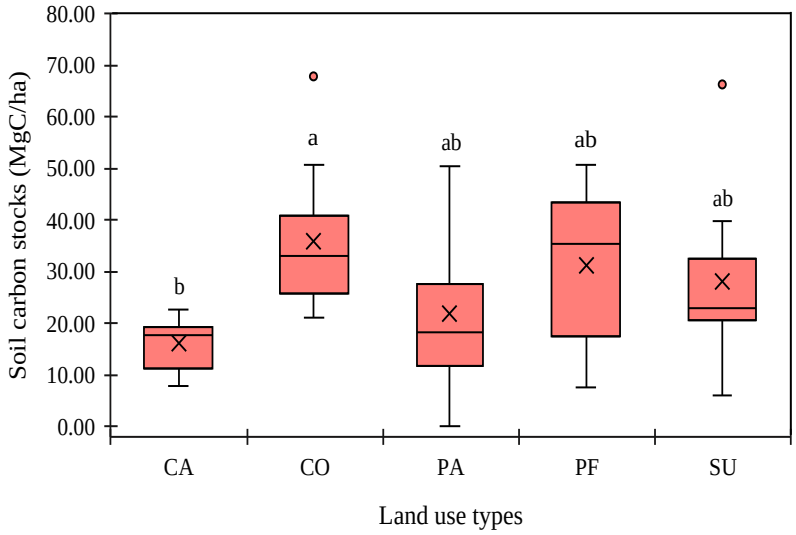

Figure 3. Total carbon stocks at depths of 0-30 cm under five agricultural land-use types: CA=cassava, CO=coconut, PA=pineapple, PF=paddy fields, and SU=sugarcane. The cross inside each box represents the mean value of total carbon stocks. Different letters on the whiskers indicate significant mean differences ($p<0.05$).

The highest total carbon stock in coconut was likely associated with soil series such as Bang Khen, Bang Phae, Bangkok, Damnoen Saduak, and Thonburi, which are characterized by the highest clay content, supported by the results presented in Table 2. The correlation analyses further revealed a positive relationship between soil organic carbon and fine particles (silt and clay), while a negative relationship was observed between soil organic carbon and sand particles (Table 3). Consequently, the significantly higher proportion of fine particles in coconut plantations may account for their greater carbon stock potential. This finding aligned with previous research, which demonstrated that an increased presence of fine particles in aggregated soil can enhance carbon protection, retention, and sequestration (Arunrat et al., 2020b; Conforti et al., 2016).

Paddy fields showed the second highest carbon. The land use consisted of various soil series, including Alluvial Complex, Khao Phlong, Pak Tho, and Bangkok, with different soil textures such as sandy loam, loamy sand, and clay. Although the soil texture could have some influence on soil carbon stocks, the management practices in this land use were likely to have a greater impact on carbon stocks than soil properties alone. A presence of anaerobic conditions during the wet season can reduce decomposition and promote carbon accumulation in paddy soils (Sahrawat, 2005). Additionally, the rich organic matter sediment could settle into the topsoil during the late harvest season (Sahrawat, 2003). The rice straw could provide higher levels of soil organic matter (Kunlanit et al., 2020), while residues from cassava and sugarcane were typically removed after harvest. This phenomenon explains the greater total carbon stock observed in paddy soils.

The total carbon stocks in sugarcane and pineapple were similar (Figure 3). Both land use types showed comparable soil series composition. Pineapple soils primarily consisted of Chan Thuk, Tha Yang, and Lat Ya soil series, which were predominantly sandy loam or loamy sand. Similarly, sugarcane fields included Khao Luang, Lat Ya, Alluvial Complex, Tha Yang, Khao Phlong, and Takhli soil series, mostly sandy loam, or loamy sand, except for Thakhi, characterized by a clay loam or silty clay texture. The

similarity in soil series and their properties may explain the comparable potential of soil carbon stocks between these land use types.

The lowest carbon stock in cassava soils was likely due to the characteristics of the sandy loam and sandy loam soil series used for cassava cultivation (Table 2). The soils with predominant sand particles tended to be low in carbon storage capacity (Arunrat et al., 2020a). Additionally, a higher proportion of sand particle in cassava soils (Table 2) were also consistent with the previous study. The management practices in cassava, such as frequent soil tillage, could further contribute to the lower carbon content. Previous studies suggested that tillage alters and depletes soil carbon (Mehra et al., 2018), which is common in cassava cultivation,. Therefore, the combination of natural soil properties and continuous soil disturbance were key factors affecting the limited carbon sequestration potential of cassava soils.

4. CONCLUSION

The present study investigated soil carbon in agricultural systems within Ratchaburi Province. Each type of agricultural land exhibited distinct carbon storages, with coconut plantations showing the highest potential, followed by paddy fields, sugarcane, pineapples, and cassava. The correlations between soil carbon and soil properties indicated that these soil properties might influence soil carbon within agricultural soils. The discussion revealed the contribution of soil series and management practices to the differences in carbon storage across different land use types. Therefore, the type of land use alone is not the sole factor that results in differences in carbon storage potential. Other factors, including soil series, soil properties, and management practices, also made significant contributions.

Based on the research findings, the following recommendations are advised regarding climate change mitigation and planning policy contribution: Coconut plantations appeared to show high potential for carbon storage in Ratchaburi Province. The plantations are unique to the region, covering almost 5% of the province's land area. As perennial vegetation, they can absorb greenhouse gases similar to forest ecosystems. In the long term, coconut plantations could have a greater potential for carbon storage compared to other agricultural systems in this study. This was primarily due to their management practices, which involve minimizing soil disturbance compared to tillage-based agriculture. This study mainly focused on assessing the potential of soil carbon storage. Conducting further research on carbon sequestration and the carbon footprint within coconut plantations, as well as other agricultural systems, would contribute to a more comprehensive understanding of their role in the regional carbon cycle. Given Ratchaburi Province a model agricultural area in Thailand under the Bio-Circular-Green Economy (BCG) model, coconut plantations could have significant potential for carbon absorption. The plantation might contribute to offsetting carbon emissions from other sectors, supporting the achievement of carbon neutrality in line with the Sustainable Development Goals (SDGs).

ACKNOWLEDGEMENTS

This research was supported by the Fundamental Fund 2022 of Muban Chombueng Rajabhat University (Grant No: 164080). We would like to express our gratitude to all landowners for allowing us access to their fields for the collection of soil samples. We are also thankful for the assistance provided by students in the General Science Education Program at Muban Chombueng Rajabhat University during the field sampling process.

REFERENCES

Amelung W, Bossio D, de Vries W, Kögel-Knabner I, Lehmann J, Amundson R, et al. Towards a global-scale soil climate mitigation strategy. Nature Communications 2020;11:Article No. 5427.

Arunrat N, Kongsurakan P, Sereenonchai S, Hatano R. Soil organic carbon in sandy paddy fields of Northeast Thailand: A review. Agronomy 2020a;10:Article No. 1061.

Arunrat N, Pumijumnong N, Sereenonchai S, Chareonwong U. Factors controlling soil organic carbon sequestration of highland agricultural areas in the Mae Chaem Basin, Northern Thailand. Agronomy 2020b;10:Article No. 305.

Arunrat N, Sereenonchai S, Kongsurakan P, Hatano R. Assessing soil organic carbon, soil nutrients and soil erodibility under terraced paddy fields and upland rice in Northern Thailand. Agronomy 2022;12:Article No. 537.

Batjes NH. Harmonized soil property values for broad-scale modelling (WISE30sec) with estimates of global soil carbon stocks. Geoderma 2016;269:61-8.

Berhe AA, Barnes RT, Six J, Marín-Spiotta E. Role of soil erosion in biogeochemical cycling of essential elements: Carbon, nitrogen, and phosphorus. Annual Review of Earth and Planetary Sciences 2018;46:521-48.

Blake GR, Hartage KH. Bulk density. In: Klute A, editor. Methods of Soil Analysis Part 1. Physical and Mineralogical Methods. Madison: American Society of Agronomy-Soil Science Society of America; 1986. p. 363-75.

Bouyoucos GJ. Hydrometer method improved for making particle size analyses of soils. Agronomy Journal 1962;54:464-5.

Bridhikitti A. Soil and biomass carbon stocks in forest and agricultural lands in tropical climates. Songklanakarin Journal of Science and Technology 2017;39:697-707.

Conforti M, Lucà F, Scarciglia F, Matteucci G, Buttafuoco G. Soil carbon stock in relation to soil properties and landscape position in a forest ecosystem of Southern Italy (Calabria region). Catena 2016;144:23-33.

Dignac M-F, Derrien D, Barré P, Barot S, Cécillon L, Chenu C, et al. Increasing soil carbon storage: Mechanisms, effects of agricultural practices and proxies. A review. Agronomy for Sustainable Development 2017;37(2):Article No. 14.

Díaz-Zorita M, Grosso GA. Effect of soil texture, organic carbon and water retention on the compactability of soils from the Argentinean pampas. Soil and Tillage Research 2000;54: 121-6.

Ellert BH, Janzen H, Vandenbygaart B, Bremer E. Measuring change in soil organic carbon storage. In: Carter M, Gregorich E, editors. Soil Sampling and Methods of Analysis. Boca Raton: CRC Press; 2007. p. 25-38.

Freibauer A, Rounsevell MDA, Smith P, Verhagen J. Carbon sequestration in the agricultural soils of Europe. Geoderma 2004;122:1-23.

Fujisaki K, Chapuis-Lardy L, Albrecht A, Razafimbelo T, Chotte JL, Chevallier T. Data synthesis of carbon distribution in particle size fractions of tropical soils: Implications for soil carbon storage potential in croplands. Geoderma 2018;313: 41-51.

Islam KK, Anusontpornperm S, Kheoruenromne I, Thanachit S. Relationship between carbon sequestration and physico-chemical properties of soils in salt-affected areas, Northeast Thailand. Agriculture and Natural Resources 2014;48:560-76.

Jobbágy EG, Jackson RB. The vertical distribution of soil organic carbon and its relation to climate and vegetation. Ecological Applications 2000;10:423-36.

Kunlanit B, Khwanchum L, Vityakon P. Land use changes affecting soil organic matter accumulation in topsoil and subsoil in Northeast Thailand. Applied and Environmental Soil Science 2020;2020:Article No. 8241739.

Lal R. Soil carbon sequestration to mitigate climate change. Geoderma 2004;123:1-22.

Land Development Department. Report on the state of land-use for the year 2021 [Internet]. 2022a [cited 2023 Jan 28]. Available from: https://webapp.ldd.go.th/lpd/LandUseInfor.php (in Thai).

Land Development Department. Soil series dataset [Internet]. 2022b [cited 2023 May 27]. Available from: https://tswc.ldd.go.th/DownloadGIS/Index_Soil.html (in Thai).

Lichaikul N, Chidthaisong A, Havey NW, Wachrinrat C. Carbon stock and net CO_2 emission in tropical upland soils under different land use. Kasetsart Journal 2006;40:382-94.

Lorenz K, Lal R. Carbon Sequestration in Agricultural Ecosystems. Cham, Switzerland: Springer International Publishing; 2018.

Matus FJ. Fine silt and clay content is the main factor defining maximal C and N accumulations in soils: A meta-analysis. Scientific Reports 2021;11:Article No. 6438.

Mehra P, Baker J, Sojka RE, Bolan N, Desbiolles J, Kirkham MB, et al. Chapter five: A review of tillage practices and their potential to impact the soil carbon dynamics. In: Sparks DL, editor. Advances in Agronomy. Delaware, USA: Academic Press; 2018. p. 185-230.

Minasny B, Malone BP, McBratney AB, Angers DA, Arrouays D, Chambers A, et al. Soil carbon 4 per mille. Geoderma 2017;292:59-86.

Nunes MR, Karlen DL, Moorman TB. Tillage intensity effects on soil structure indicators: A US meta-analysis. Sustainability 2020;12:Article No. 2071.

Pan G, Smith P, Pan W. The role of soil organic matter in maintaining the productivity and yield stability of cereals in China. Agriculture, Ecosystems and Environment 2009; 129:344-8.

Pibumrung P, Gajaseni N, Popan A. Profiles of carbon stocks in forest, reforestation and agricultural land, Northern Thailand. Journal of Forestry Research 2008;19:11-8.

Rodrigues AF, Latawiec AE, Reid BJ, Solórzano A, Schuler AE, Lacerda C, et al. Systematic review of soil ecosystem services in tropical regions. Royal Society Open Science 2021;8:Article No. 201584.

RStudio Team. RStudio: Integrated Development Environment for R [Internet]. 2020 [cited 2023 Jan 28]. Available from: https://posit.co.

Sahrawat KL. Organic matter accumulation in submerged soils. In: Sparks DL, editor. Advances in Agronomy. Delaware, USA: Academic Press; 2003. p. 169-201.

Sahrawat KL. Fertility and organic matter in submerged rice soils. Current Science 2005;88:735-9.

Scharlemann JPW, Tanner EVJ, Hiederer R, Kapos V. Global soil carbon: Understanding and managing the largest terrestrial carbon pool. Carbon Management 2014;5:81-91.

Stockmann U, Adams MA, Crawford JW, Field DJ, Henakaarchchi N, Jenkins M, et al. The knowns, known unknowns and unknowns of sequestration of soil organic carbon. Agriculture, Ecosystems and Environment 2013;164:80-99.

Stockmann U, Padarian J, McBratney A, Minasny B, de Brogniez D, Montanarella L, et al. Global soil organic carbon assessment. Global Food Security 2015;6:9-16.

Sun W, Huang Y, Zhang W, Yu Y. Carbon sequestration and its potential in agricultural soils of China: SOC sequestration and potential in China. Global Biogeochemical Cycles 2010; 24:Article No. GB3001.

Tan ZX, Lal R, Smeck NE, Calhoun FG. Relationships between surface soil organic carbon pool and site variables. Geoderma 2004;121:187-95.

Thomas GW. Soil pH and soil acidity. In: Sparks DL, Page AL, Helmke PA, Loeppert RH, Soltanpour PN, Tabatabai MA, et al, editors. Methods of Soil Analysis: Part 3 Chemical Methods. Madison: American Society of Agronomy-Soil Science Society of America; 1996. p. 475-90.

Todd-Brown KEO, Randerson JT, Hopkins F, Arora V, Hajima T, Jones C, et al. Changes in soil organic carbon storage predicted by earth system models during the 21st century. Biogeosciences 2014;11:2341-56.

Tu C, He T, Lu X, Luo Y, Smith P. Extent to which pH and topographic factors control soil organic carbon level in dry farming cropland soils of the mountainous region of Southwest China. Catena 2018;163:204-9.

Veldkamp E, Becker A, Schwendenmann L, Clark DA, Schulte-Bisping H. Substantial labile carbon stocks and microbial activity in deeply weathered soils below a tropical wet forest: Carbon in deep soils below tropical wet forest. Global Change Biology 2003;9:1171-84.

Walkley A, Black IA. An examination of the Degtjareff Method for determining soil organic matter, and proposed modification of the chromic acid titration method. Soil Science 1934;37:29-38.

Wang X, He J, Bai M, Liu L, Gao S, Chen K, et al. The impact of traffic-induced compaction on soil bulk density, soil stress distribution and key growth indicators of Maize in North China Plain. Agriculture 2022;12:Article No. 1220.

Wiesmeier M, Urbanski L, Hobley E, Lang B, Von Lützow M, Marin-Spiotta E, et al. Soil organic carbon storage as a key function of soils: A review of drivers and indicators at various scales. Geoderma 2019;333:149-62.

Monitoring and Modeling of Spatio-Temporal Urban Expansion and Land Use/Land-Cover Change in Mountain Landscape: A Case Study of Dalat City, Vietnam

Cuong Huu Nguyen, Cuong Van Nguyen, and Tien My Ngoc Nguyen*

Faculty of Land Administration, Ho Chi Minh City University of Natural Resources and Environment, Ho Chi Minh City 72107, Vietnam

ARTICLE INFO

Received: 12 Apr 2023
Received in revised: 3 Jul 2023
Accepted: 6 Jul 2023
Published online: 21 Sep 2023
DOI: 10.32526/ennrj/21/20230086

Keywords:
Land-use/ Land-cover change/ Urbanization/ Logistic regression/ Dalat City/ Markov chain/ Landsat

*** Corresponding author:**
E-mail: tiennnm@hcmunre.edu.vn

ABSTRACT

The lack of ability to control human activities led to changes of land use/land cover (LULC) in Dalat City where rapid urbanization and the demand to expand agricultural land have resulted in dramatic forest reductions. This study assessed the rate and extent of LULC changes over the past 12 years and simulated future scenarios in Dalat City, Lam Dong Province, Vietnam by using an integrated model of Markov chain and logistics regression. Three land-use maps used to analyze land-use change were extracted from satellite images in 2010, 2016, and 2022 by classification approach. The outcome of this process indicates a significant increase in agricultural and built-up land of 48.22 km^2 and 9.36 km^2, respectively; a decrease in forest land of 55.61 km^2, and a minor change in water bodies and bare land in the 2010-2022 period. Prediction maps of land-use change in 2028 and 2034 are generated after the model is validated by comparing the actual map with the prediction map of LULC in 2022 using Kappa statistics. Transition of forest area to other land use types, especially land for expansion of built-up and agricultural land is the crucial trend of land-use change in the future according to the forecast model. Compared to 2022, forest area in 2034 will decrease by 60.65 km^2 while built-up and agricultural land will increase by 14.07 km^2 and 43.61 km^2, respectively. The research results provide valuable information as a foundation for land-use policy planning and local urban development to ensure sustainable development objectives.

1. INTRODUCTION

Urbanization has been taking place across many places throughout the world. Cities have expanded rapidly due to population growth and economic development (Xie et al., 2005; Al-Darwish et al., 2018). The urbanization ratio is an indicator of the development of a country, a region or locality (WB, 2011). The urbanization process of each country can occur fast or slowly depending on conditions and degrees of socioeconomic development.

Urbanization contributes to accelerating economic growth, shifting the economic-labor structure, and changing population distribution. Cities and towns create jobs and incomes for workers, consume a wide range of commodities, and employ a higher-skilled labor force together with modern infrastructure techniques (Fan et al., 2019). However, the urbanization process without scientific planning can cause challenges and risks for sustainable development. Rapid urbanization has socio-economic and environmental negative influences (Lambin et al., 2001), such as loss of agricultural land (Azadi et al., 2011; Mauro, 2020) and flooding (Huong and Pathirana, 2013).

Major cities in Vietnam such as Hanoi, Ho Chi Minh City, and Da Nang have been rapidly urbanizing for the past 10 years. In Vietnam, the urbanization rate increased from 19.6% in 629 cities in 2009 to 39.3% in 833 cities in 2020 (MC, 2022) and the proportion of urban population accounted for 35.0% of the total

Citation: Nguyen CH, Nguyen CV, Nguyen TMN. Monitoring and modeling of spatio-temporal urban expansion and land use/land-cover change in mountain landscape: A case study of Dalat City, Vietnam. Environ. Nat. Resour. J. 2021;21(5):428-442. (https://doi.org/10.32526/ennrj/21/20230086)

population. This rate is forecast to rise to 50.0% in 2030 and 64.8% in 2069 (GSO, 2020). On the one hand, this process brings positive effects on motivating urbanization rapidly across the country. The infrastructure of existing cities has been improved and refurbished, while a lot of new cities have been established. On the other hand, a large area of agricultural land and natural forest are converted to non-agricultural land due to urbanization process. Nearly all suburban farmers who lose their arable land are forced to change their careers. Vietnam has lost 73,000 hectares of annual arable land due to urbanization, affecting the livelihoods of 2.5 million farmers. Six percent of the rice production area decreased due to high-speed industrialization and urbanization (MF, 2009).

Urbanization is a growing challenge for city planners and policymakers who are continuously focusing on computer-based statistical models, and machine learning for a sustainable and livable city (Mustak et al., 2022). Some models of land use and urban expansion have been studied and used to allocate land-use changes explicitly on maps by using the prediction method over the past two decades. Their results are displayed as a land-use map which is a set of grid cells with each plot displaying the land use at a specific position (Verburg et al., 2002). Future urban growth scenario-analysis is crucial for planners to make effective decisions in spatial planning (Wang et al., 2021a). Therefore, developing efficient prediction models to anticipate future land-use changes and urban growth can better serve the work of planners (Ai et al., 2022; Sohl and Claggett, 2013).

A few researchers have used various theoretical and experimental modeling techniques, such as regression modeling, to model, simulate, and predict urban expansion, and land-use change (Alsharif and Pradhan, 2014; Nong and Du, 2011), CA (Cellular Automata) (Falah et al., 2020; Yeh et al., 2021), MC (Markov chain) (Arsanjani et al., 2011; Fathizad et al., 2015), CA-Markov intergrated models (Wang et al., 2021b; Ebrahimipour et al., 2016; Aburas et al., 2021), CA-logistic regression (Azizi et al., 2022; Wang et al., 2019), and machine learning algorithms (Tsagkis et al., 2023; Devendran and Gnanappazham, 2019). Each model has its limitations and has been discussed in many kinds of literature (Mas et al., 2014; Olmedo et al., 2015). The logistic regression analysis has been one of the most frequently utilized approaches for modeling land-use change over the past two decades. Logistics regression in urban expansion models helps to understand the urbanization process and provides an explicit picture of the weights of the independent variables and their related functions (Hu and Lo, 2007; Huang et al., 2009; Arsanjani et al., 2013).

In Vietnam, there haven't been many studies on land use change and urban development. Most research focuses on assessing land-use changes in the past by interpreting and analyzing remote-sensing images over time but not predicting land-use changes for the future. Urbanization studies have only concentrated on two large cities, Hanoi (Pham et al., 2015; Pham and Yamaguchi, 2011; Nguyen et al., 2019) and Ho Chi Minh City (Son et al., 2012).

Vietnam's terrain is very diversified, with hills and mountains occupying a quarter of the area (MARD, 2015). Dalat City, located in the Central Highlands, is one of Vietnam's most famous historical-tourist cities. The cool climate, gorgeous scenery, and historical architectures attract many tourists to this city. Over the past decade, this city has been rapidly developed but not strictly controlled. Urban expansion negatively affects natural resources such as forest land, agricultural land, and tourism landscapes. Dalat City is chosen to study future urban expansion in this research due to the importance of its historical, agricultural, and tourism environment. This research aims to analyze and anticipate urban expansion in Dalat City through land-use changes by interpreting remote-sensing images and applying the Markov chain-logistic regression integrated model. This model helps to better understand urban expansion, examine quantitatively the relationship between land-use change and driving factors, and predict various scenarios for Dalat City's future urban expansion.

2. METHODOLOGY

Figure 1 depicts the process of predicting land-use change using remote sensing images and the Markov chain-logistic regression integrated model. The land-use prediction in 2022 is conducted after analyzing land-use change in the 2010-2016 period. The model accuracy is measured by comparing the prediction map of land-use and the actual map of land-use in 2022 based on the Kappa coefficient. Then, this model is used to forecast land-use change for future periods in 2028 and 2034 (6-year periods).

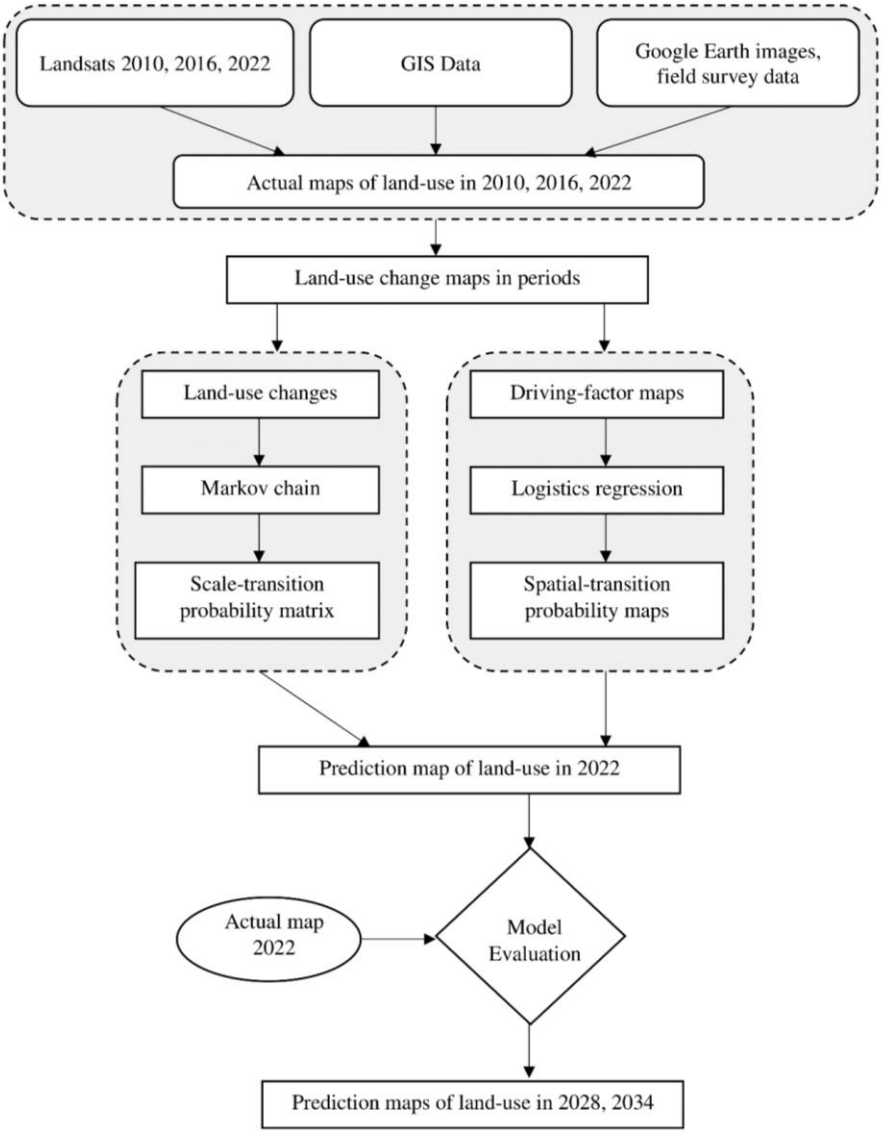

Figure 1. General methodology of the research

2.1 Study area

The research is conducted in Dalat, a city in the Central Highland, located on the Lam Vien Plateau, Lam Dong Province at an altitude of about 1,500 m (4,900 ft) above sea level (Latitude: 11°48′36″-12°01′07″ N; Longitude: 108°19′23″-108°36′27″ S) (Figure 2). With a population of 240,000 people, Dalat is the second most popular mountainous city in Vietnam (LDSO, 2023). It is a unique urban area in Vietnam which has been perfectly planned with famous constructions and exquisite villas from the very beginning. Therefore, it is considered as a museum of Western architecture in the early 20th century (Tranh, 2001).

The terrain of Dalat City is divided into two types: mountain and plain in mountain. It has a mild and cool mountainous climate all year round due to its elevation of 1,500 meters and surrounding mountain ranges and forest flora, particularly pine forests. This city has two distinct seasons: rainy and dry (Tro, 1993). It has favorable soil and climate conditions for the development of temperate plants. Its main arable land area has been allocated to vegetables. Tea and coffee plants are also crucial products in the city's processing industry.

2.2 Data acquisition and processing

The satellite images of Dalat City in three periods of 2010 (Landsat TM), 2016, and 2022 (Landsat OLI/TIR) shown in Table 1 were downloaded from https://earthexplorer.usgs.gov/. They were adjusted to the local coordinate system (VN-2000 with 6° projection zone, 48th zone in the Northern hemisphere, an axis meridian of 105° of East longtitude).

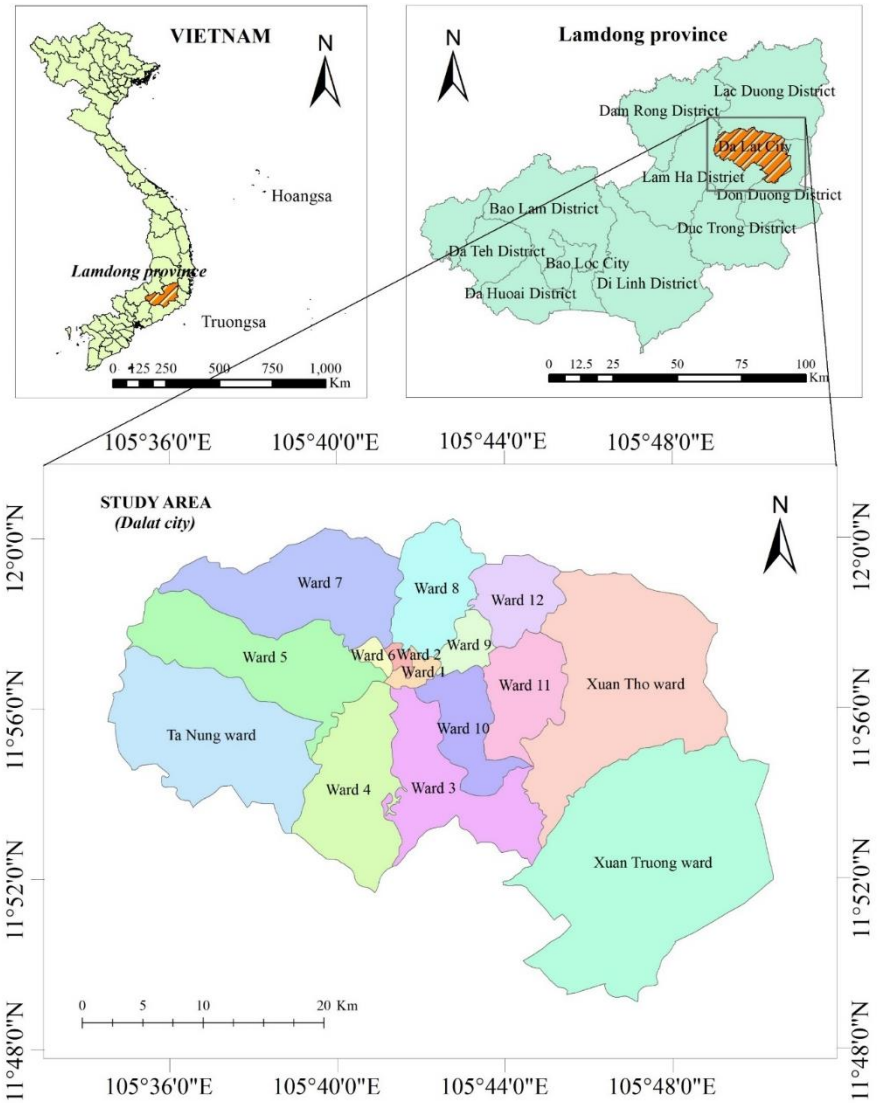

Figure 2. Map of the study area (Dalat City)

Table 1. Characteristics of collected data

Sensor	Month/day/year	Resolution	Path/row
Landsat TM 2010	04/02/2010	30 m × 30 m	124/052
Landsat OLI/TIR 2016	08/03/2016	30 m × 30 m	124/052
Landsat OLI/TIR 2022	20/01/2022	30 m × 30 m	124/052

Furthermore, this study uses GIS data gathered from the People's Committee of Dalat and the Department of Natural Resources and Environment of Lam Dong Province as a reference to support in image interpretation and the generation of driving factor maps. These materials include: (1) a land-use actual map of 2010, 2015, and 2020 at a scale of 1:10000 to assist with image interpretation and mapping of impact factors; (2) a topographic map of Lam Dong Province at a scale of 1:50000 to build slope maps and elevation maps; (3) a high-resolution satellite image data from google earth to assist in satellite image; and (4) the administrative boundary map of Dalat City to determine the study area for the landsat image.

The study used the method of supervised image classification with the Maximum likelihood classifier (Perumal and Bhaskaran, 2010; Richards, 2022). This method works on the principle of using sample data to determine the probability distribution density function, which defines land use types to be classified for each pixel. Then, each land use type is determined according to the LULC having the prior probability.

This interpretation result is evaluated by the Kappa statistical index and the overall accuracy. The

Kappa coefficient is a measure of overall agreement of a matrix (Richards, 2022) with formula (1). The evaluation results show that the accuracy of image interpretation through the Kappa index is very good (Richards, 2022) from 0.9457 to 0.9876. In addition, the overall accuracy of the interpretation results ranges from 95.94% to 99.08% (Table 2).

$$K = \frac{P_0 - P_e}{1 - P_e} \quad (1)$$

The accuracy of observed agreement (P_0) is determined according to the following formula:

$$P_0 = \frac{\sum X_{ii}}{N} \quad (2)$$

The estimate of chance agreement (P_e) is determined according to the following formula:

$$P_e = \frac{\sum X_{i+} X_{+i}}{N^2} \quad (3)$$

Where; N: total number of observations; X_{ii}: observation in row i and column i; Xi+: marginal total of row i; X+i: marginal total of column i.

Table 2. Accuracy of remote-sensing image interpretation

Years	Overall accuracy (%)	Kappa coefficient
2010	98.23	0.9765
2016	99.08	0.9876
2022	95.94	0.9457

The LULC map of land-use in three periods was successfully interpreted (Figure 3). The interpretation of LULC types on the actual map of land use consists of built-up land (residential area, industrial zones, and traffic infrastructure), water bodies (rivers, streams, ponds, and lakes), agricultural land (crops, industrial plants, fruit trees, etc.), and bare land. The manipulated process of image interpretation included the six following steps on Envi 5.3 software (RSI, 2001): (1) geometric correction of satellite images matching to the VN-2000 coordinate system; (2) enhance image quality; (3) crop the image according to the boundary of the study area; (4) set up the image decoding key; (5) classification of remote sensing images; (6) evaluation of classification results (Table 2).

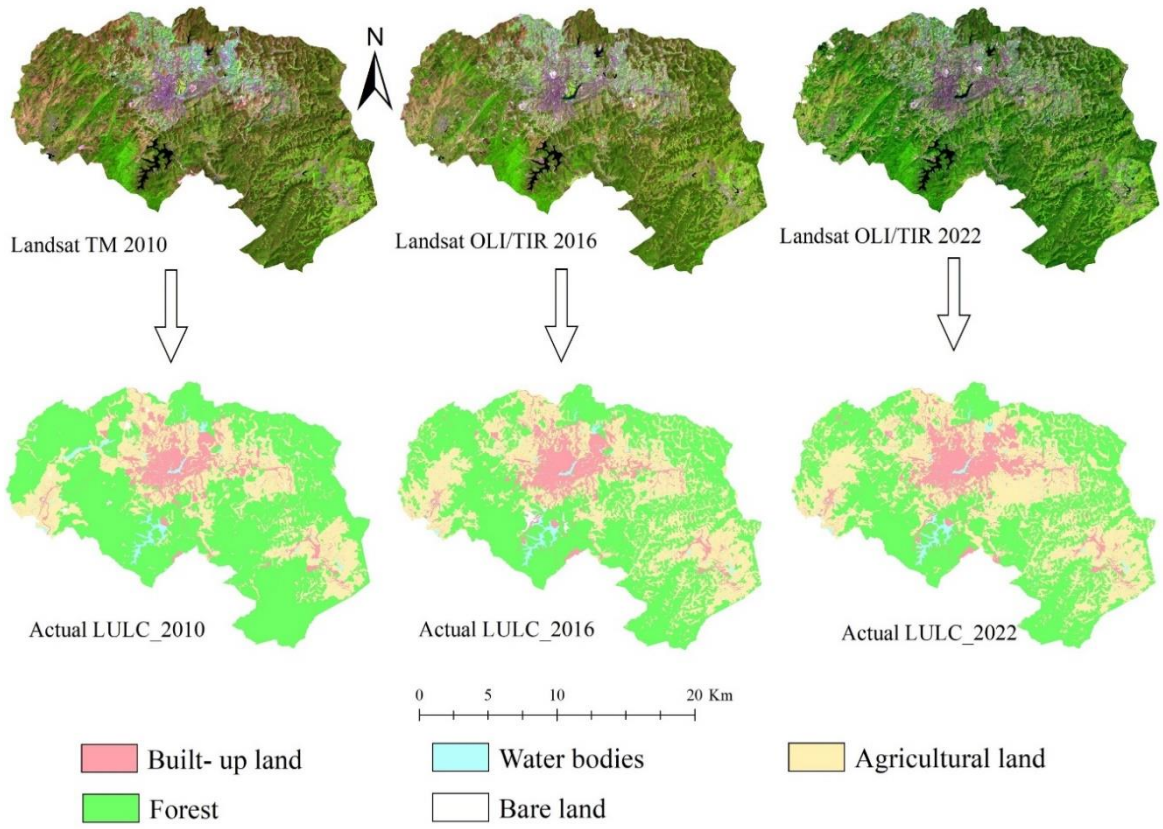

Figure 3. Extracted land use maps of Dalat City in 2010, 2016, and 2022

As an empirical estimation model, logistics regression is a data-driven rather than knowledge-based approach to the choice of predictor variables (Hu and Lo, 2007). Previous studies identified the significant factors that determine the potential for urban expansion and land-use changes (Park et al., 2011; Arsanjani et al., 2013; Musa et al., 2017; Aburas et al., 2017; Shafizadeh-Moghadam et al., 2017; Hassan and Elhassan, 2020; Cheng et al., 2022). This study used 12 factors driving the land-use change process and the data generated as Euclidean Distance maps in the ArcGIS environment (Figure 4).

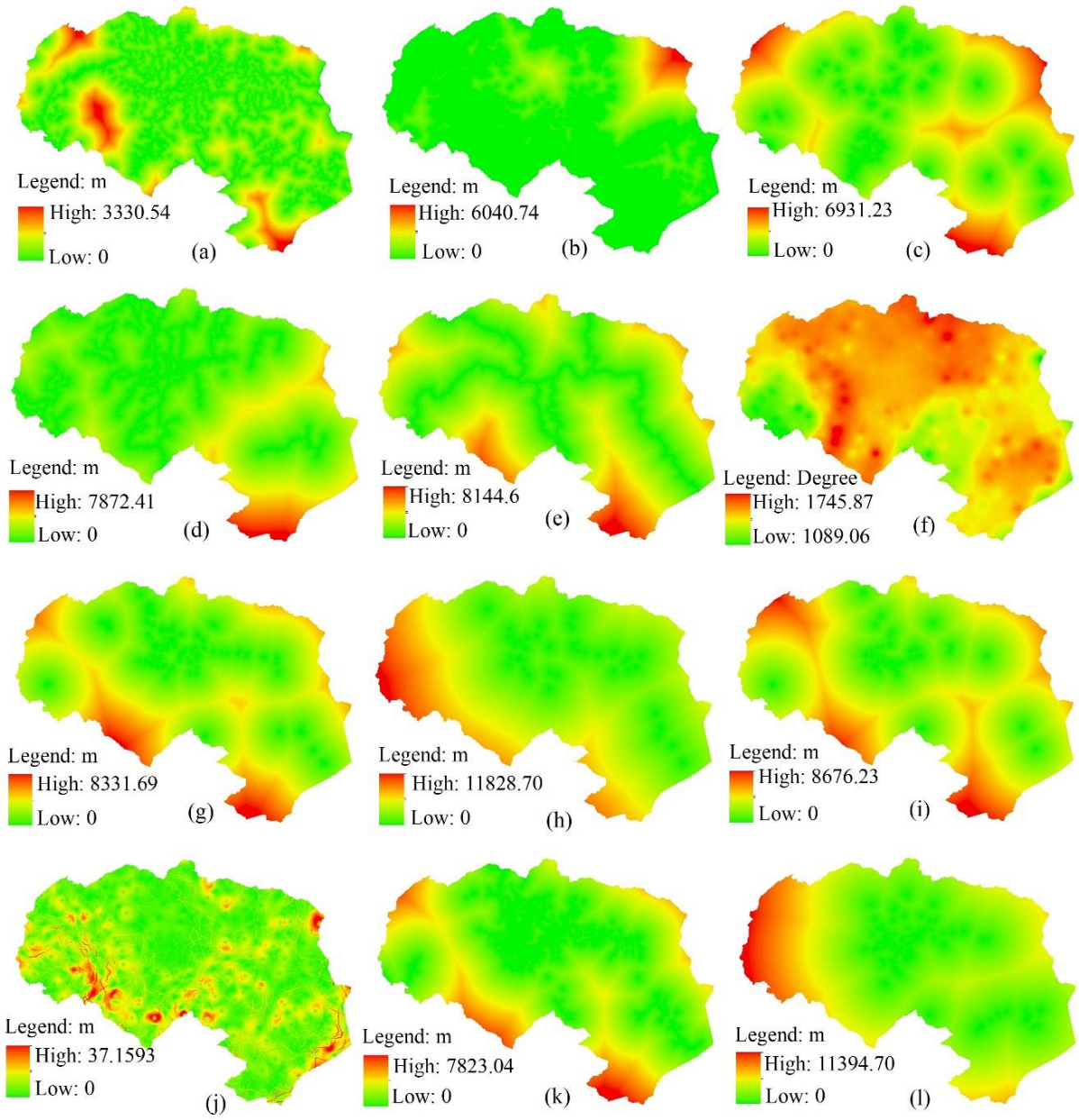

Figure 4. Driving variables associated with the simulation of land use and land cover in Dalat City: (a) distance to water source, (b) distance to nature reserve, (c) distance to tourist area, (d) distance to secondary traffic, (e) distance to main roads, (f) altitude/elevation, (g) distance to educational institutions, (h) distance to religious places, (i) distance to administrative office, (j) slope, (k) distance to residential area, (l) distance to commercial area

2.3 Intergrated model of Markov chain and logistic regression for the future LULC change prediction

The combination of Markov chain and logistics regression has been the most popular integrated model used for modeling spatio-temporal changes. Markov chain analysis, which is a stochastic modeling, has been widely used for land cover variation modeling (Fathizad et al., 2015). It is assumed that the

probability of a system at an initial time and condition can be determined if the change rate observed during the calibration interval (t_1 to t_2) remains the same over the simulation period (t_2 to t_3). Markov chain analysis determines how much land-cover change will occur at a specific time in the future through land cover cross-tabulation (Kamusoko et al., 2009). The Markov chain is applied to determine the future land-use demand for each type of land use according to the following formula (Sang et al., 2011):

$$S_{(t+1)} = P_{ij} \times S_{(t)} \quad (4)$$

Where; $S_{(t)}$ and $S_{(t+1)}$ are the states of the system at an initial time t and t + 1. P_{ij} is the matrix of the transition probability in a specific state and is calculated as follows:

$$P_{ij} = \begin{bmatrix} P_{11} & P_{12} & \cdots & P_{1n} \\ P_{21} & P_{22} & \cdots & P_{2n} \\ \vdots & \vdots & & \vdots \\ P_{n1} & P_{n2} & \cdots & P_{nn} \end{bmatrix} \quad (5)$$

Where; $0 \leq P_{ij} \leq 1$ and $\sum_{j=1}^{n} P_{ij} = 1$.

The Markov chain model is not able to allocate the estimated amount of change and must be integrated with other geospatial models (Arsanjani et al., 2013). Therefore, the Markov chain model integrates with logistics regression spatially to solve this problem.

Logistics regression is used to model and explain the relationship of several independent variables (X) with a binary dependent variable (Y), representing the occurrence or non-occurrence of an event. Logistics regression is applied to determine the probability of the existence or non-existence of each land-use type at all locations and quantify the interaction between different land-use types and transition driving factors (Lin et al., 2011). Spatial land-use change is the dependent variable represented in a raster-binary map. A value of 1 on the generated probability map indicates the presence of a change, and a value of 0 indicates no change. The change probability for each pixel in the raster map is generated based on the following logistic regression equation:

$$P\,(Y = 1|X_1, X_2, \ldots, X_k) = 1/(1 + e^{-(\alpha + \sum \beta_i X_i)}) \quad (6)$$

Where: X_i, which is the independent variable representing driving factors of the land-use change process, can be a continuous or categorical variable; α is the coefficient of the model formula; P (Y=1|X_1, X_2, ..., X_k) is the probability of the dependent variable Y, means that the probability of a pixel changed in land use; and β_i is the coefficient of the variable X_i. The regression coefficient (β_i) reflects the function of the independent explanatory variables. Logistics regression creates the land transition probability map through the regression analysis of driving factors. The land-use prediction map is generated by allocating the number of pixels in the order of spatial transition probability defined by the Markov chain.

3. RESULTS AND DISCUSSION

3.1 Description of land-use change in 2010-2022 period

The land-use change from 2010 to 2022 was determined to quantify the extent and location of the changes. Table 3 and Figure 5 illustrated the changes. The analysis of LULC change was carried out by using land cover data over a 12-year period (2010-2022), with two 6-year sub-periods: 2010-2016 and 2016-2022.

Table 3. Statistical distribution of LULCs from 2010 to 2022

LULC types	2010		2016		2022		2010-2016	2016-2022	2010-2022
	Area (km^2)	Area (%)	Area (km^2)	Area (%)	Area (km^2)	Area (%)	Δ (km^2)	Δ(km^2)	Δ (km^2)
Built-up	33.79	8.57	38.59	9.78	43.15	10.94	4.80	4.56	9.36
Water bodies	8.32	2.11	7.79	1.98	7.78	1.97	-0.53	-0.01	-0.54
Agriculture	104.61	26.52	136.41	34.59	152.83	38.75	31.80	16.42	48.22
Forest	245.39	62.22	209.89	53.22	189.78	48.12	-35.50	-20.11	-55.61
Bare land	2.29	0.58	1.72	0.44	0.86	0.22	-0.57	-0.86	-1.43

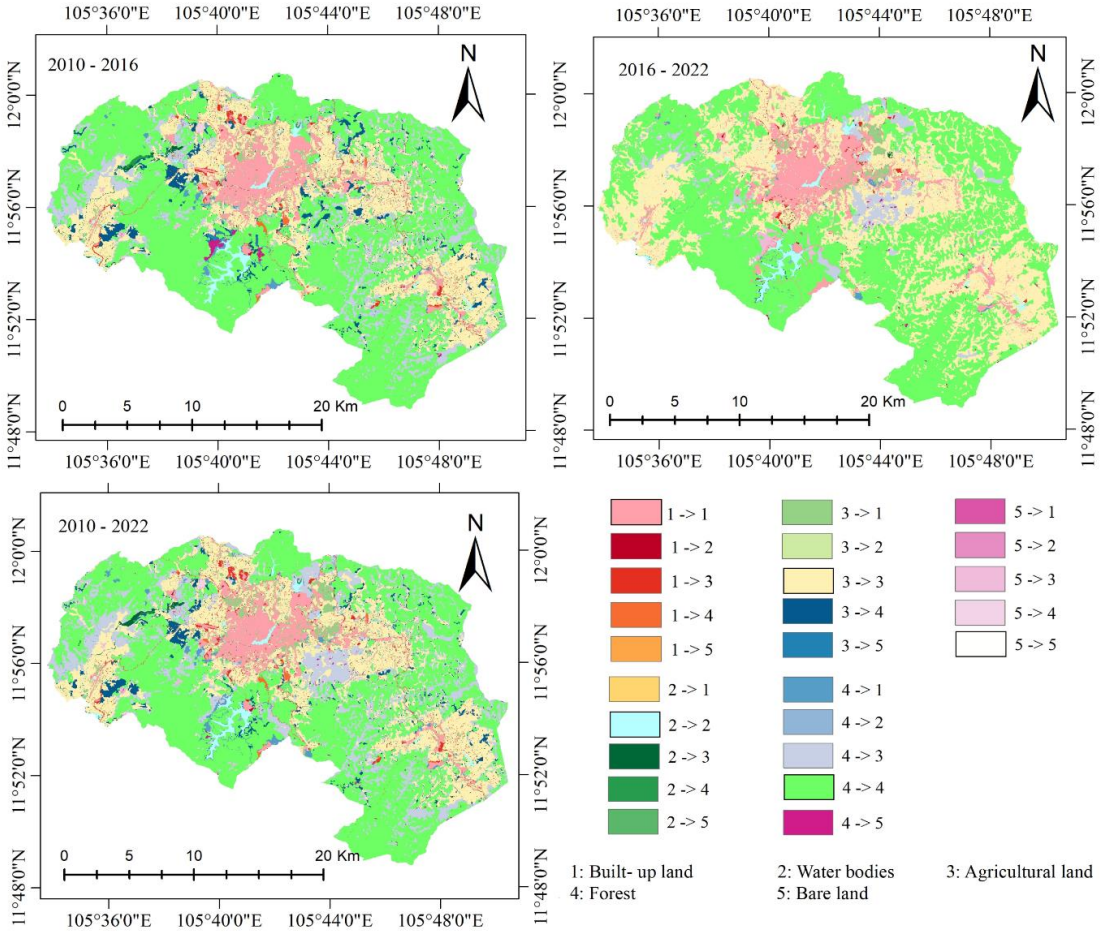

Figure 5. Maps of land use changes in Dalat City

From 2010 to 2022, the land-use types in Dalat City changed dramatically. Specifically, agricultural and built-up land expanded rapidly, while forest land sharply declined. In 2010, forest land covered the most land area, followed by agricultural land, built-up land, water bodies, and bare land. The majority of built-up land was in the city center, with the remainder in the Southeast and West along main roads. Agricultural land was located near residential areas while the forest was in remote areas with complex topography. Over a 12-year period, agriculture land area increased from 104.61 km^2 (26.52% of total land area) to 152.83 km^2 (38.75% of total land area), especially in 2010-2016; the built-up land area expanded steadily in 2010-2022 from 33.79 km^2 (8.57% of total land area) to 43.15 km^2 (10.94% of total land area). However, the forest land area sharply diminished by 55.61 km^2 (from 62.22% to 48.12%). Water bodies and bare land area decreased by 0.54 km^2 and 1.43 km^2, respectively. Built-up land was likely to spread northward from existing residential areas in the central area. Furthermore, a portion of built-up land could be seen expanding along the main road. In addition to expanding from existing areas, agricultural land was also found in forested areas. To better understand the transitions among land use types for the 2010-2022 period, a transition matrix table was created by analyzing in the ArcGIS environment (Table 4). The table data demonstrates the forest area decreased as a result of agricultural growth and built-up land expansion. During the research period, 67.68 km^2 of forest land was lost due to changing to 4.38 km^2 of built-up land and 61.93 km^2 of agricultural land. In addition, 21.39 km^2 of agricultural land decreased due to the transition of 10.78 km^2 to built-up land and 9.14 km^2 to forest land. Currently, the greenhouse area in Dalat City accounts for approximately 57% of the total greenhouse area in Lam Dong Province. (Lam Dong online, 2023). Greenhouses built without planning have disrupted the landscape and urban aesthetic, increased local greenhouse effect and limited biodiversity. Therefore, to reduce greenhouse area during this period, the local goverment made efforts to demolish many greenhouses built for agricultural production, which resulted in a noticeable transition from built-up land to agricultural and forest land.

Table 4. Transition area matrix of land-use types from 2010 to 2022

	LULC types	2022 (km^2)					
		Built-up	Water bodies	Agriculture	Forest	Bare land	Total
2010 (km^2)	Built-up	27.49	0.25	4.34	1.69	0.02	33.79
	Water bodies	0.36	5.43	2.18	0.33	0.02	8.32
	Agriculture	10.78	1.19	83.22	9.15	0.27	104.61
	Forest	4.38	0.87	61.93	177.71	0.50	245.39
	Bare land	0.14	0.04	1.16	0.90	0.05	2.29
	Total	43.15	7.78	152.83	189.78	0.86	

The reduction of forest area and its causes are typical characteristics of localities in the Central Highlands of Vietnam. Due to the suitability of the local soil and climate, vegetable-producing activities thrive. Population increase is also a major source of forest loss in the region, since it leads to the expansion of urban centers, residential areas, industrial production regions, and infrastructure (Müller and Zeller, 2002; Pham et al., 2019). The reduction of forests and vegetation leads to severe degradation of ecosystems, loss of biodiversity, reduction of water holding capacity leading to depletion of water resources, and extreme events such as landslides and erosion (Lambin et al., 2001). The analysis results of land use change from 2010 to 2022 build the foundation for future forecasts.

3.2 Prediction results

3.2.1 Quantification of land change and transition probability maps

In this study, the 2010 LULC map of Dalat City is the first image (t_1), the 2016 LULC map is the second image (t_2), and the 2022 LULC map is the reference image to compare to evaluate the model. The Markov sequence analysis built into the module of TerrSet software to generate a transition probability matrix representing the total area is varied from one LULC layer to another in a given time unit. The Markov series assumed that the policies and development conditions in future scenarios would be the same as in the past. Table 5 show the prediction probability matrix for transition among land types from 2022 to 2034. Figure 6 illustrates the transition probability maps in 2028 and 2034. Forest land with the probability of not changing will be 79.06%, with the remainder continuing to decrease, namely, converting 18.84% to agricultural land, and 1.43% to built-up land. Meanwhile, built-up land is forecast to expand, in addition to converting from forest land to agricultural land at the rate of 6.59%.

An input of logistics regression is driving factor maps combining 2010 and 2016 LULC maps to generate a spatial transition probability map, showing the probability that each pixel changes to another layer or remains constant. Visually, it is possible to see the pixels distributed in the vicinity of existing residential areas and along the roads with the highest transition probability. These results are the basis for forming prediction maps and forecasting future land use changes.

Table 5. Transition probability matrix for 2022-2028 and 2028-2034 periods

	LULC types	Built-up	Water bodies	Agriculture	Forest	Bare land
Probability value 2028	Built-up	0.9025	0.0037	0.0621	0.0314	0.0002
	Water bodies	0.0159	0.8107	0.1208	0.0508	0.0018
	Agriculture	0.0386	0.0074	0.8802	0.0669	0.0069
	Forest	0.0043	0.0008	0.1134	0.8778	0.0037
	Bare land	0.0412	0.0168	0.4531	0.4777	0.0111
Probability value 2034	Built-up	0.8219	0.0066	0.1109	0.0598	0.0007
	Water bodies	0.0327	0.6756	0.1971	0.0922	0.0024
	Agriculture	0.0659	0.0119	0.8006	0.1152	0.0065
	Forest	0.0143	0.0027	0.1884	0.7906	0.0040
	Bare land	0.0570	0.0177	0.4595	0.4575	0.0083

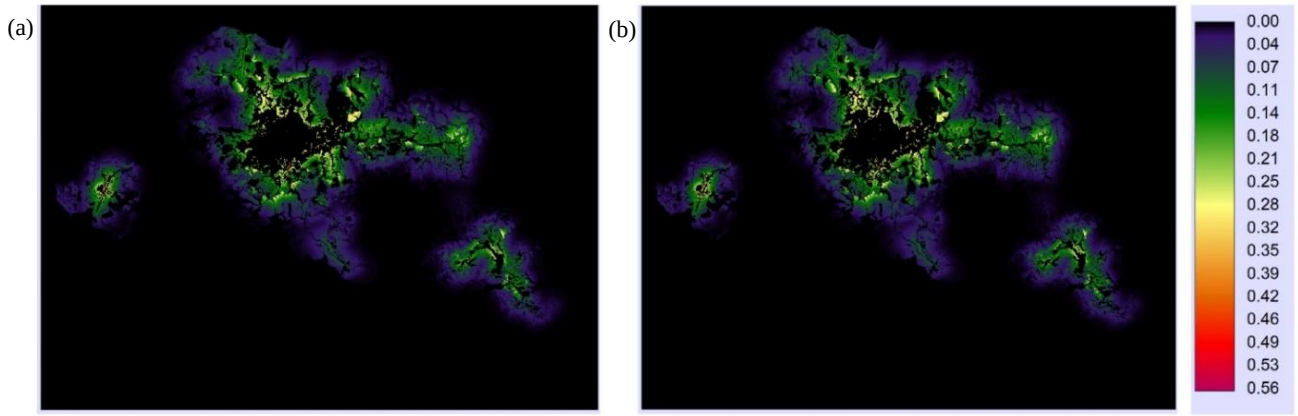

Figure 6. Spatial-transition probability maps in 2028 (a) and 2034 (b)

3.2.2 Validation

Before creating the LULC forecast maps in 2028 and 2034, it is necessary to validate the model output. The validation is performed by matching the LULC actual map with the LULC prediction map in 2022 (Figure 7) using the VALIDATE module in IDRISI software. The accuracy of prediction results is evaluated based on comparing each pair of pixels, expressed by the Kappa statistical index system, including Kappa for locationStrata ($K_{locationStrata}$), location ($K_{location}$), no information (K_{no}), and Kappa standard ($K_{standard}$) (Pontius, 2002; Pontius, 2000). The Kappa values for these variants range from 0 to 1 (0% and 100%); The closer to 100% the value reaches, the higher the agreement accuracy (Christensen and Arsanjani, 2020). Overall, there was a significant level of agreement between the prediction and actual LULC maps (Table 6). The overall Kappa statistical variations of K_{no}=0.8987, $K_{location}$=0.9112, $K_{locationStrata}$=0.9112, $K_{standard}$=0.8743 were achieved. These values are accepted when they are related to the reliability of the model validation for further use (Pontius and Millones, 2011).

Table 6. Land-use prediction map Kappa coefficient in 2022

Kappa coefficient	Value
K_{no}	0.8987
$K_{location}$	0.9112
$K_{locationStrata}$	0.9112
$K_{standard}$	0.8743

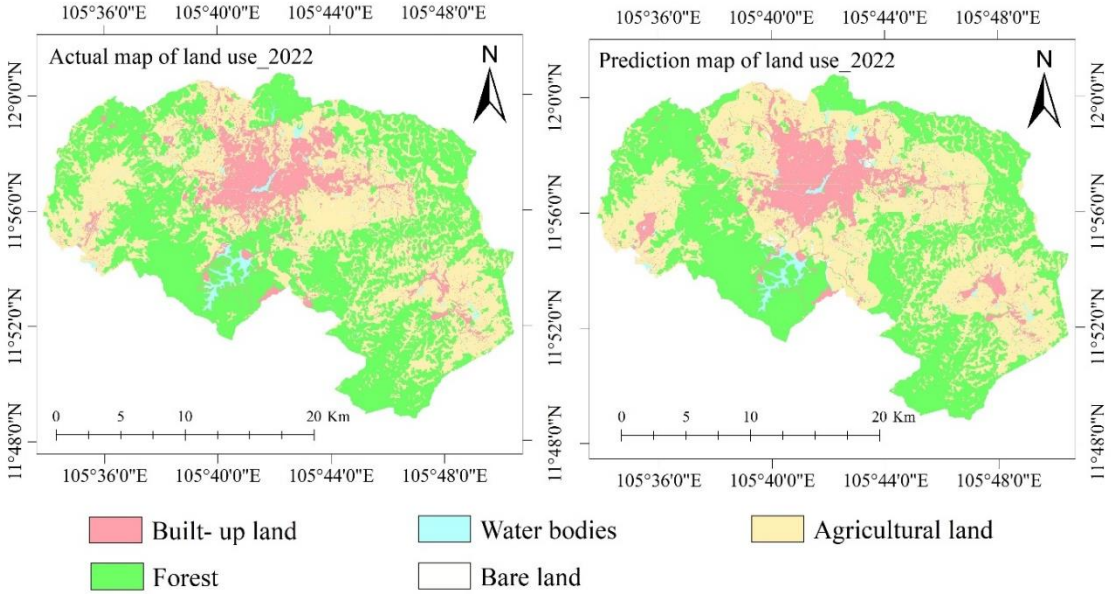

Figure 7. Land use maps in Lam Dong Province in 2022

3.2.3 Land use change prediction results

The results of the LULC forecast for 2028 and 2034 using the integrated model of Markov chain-logistic regression are illustrated in Table 7 and Figure 8. Compared to 2022, the forecast data for 2034 shows that forest land use continues to decrease from 48.12% to 32.74% (from 189.78 km^2 to 129.13 km^2). The agricultural and built-up land areas are forecast to increase by 43.61 km^2 and 14.07 km^2, respectively, accounting for 49.81% and 14.51% of the natural area by 2034.

Figure 8 shows that the spatial destruction of forest area in LULCs is predicted for 2034. Forest cover is fragmented into small and narrow patches by agricultural areas, especially in the Western part of the city. A vast degradation of forest areas can have a negative influence on the local ecological environment.

Table 7. Area statistics of land-use prediction in 2028 and 2034

LULC types	Simulated area (in km^2)		Change detection (in km^2)	
	2028	2034	2028-2022	2034-2022
Built-up	53.30	57.22	10.15	14.07
Water bodies	9.12	9.88	1.34	2.10
Agriculture	185.84	196.44	33.01	43.61
Forest	144.46	129.13	-45.32	-60.65
Bare land	1.68	1.73	0.82	0.87

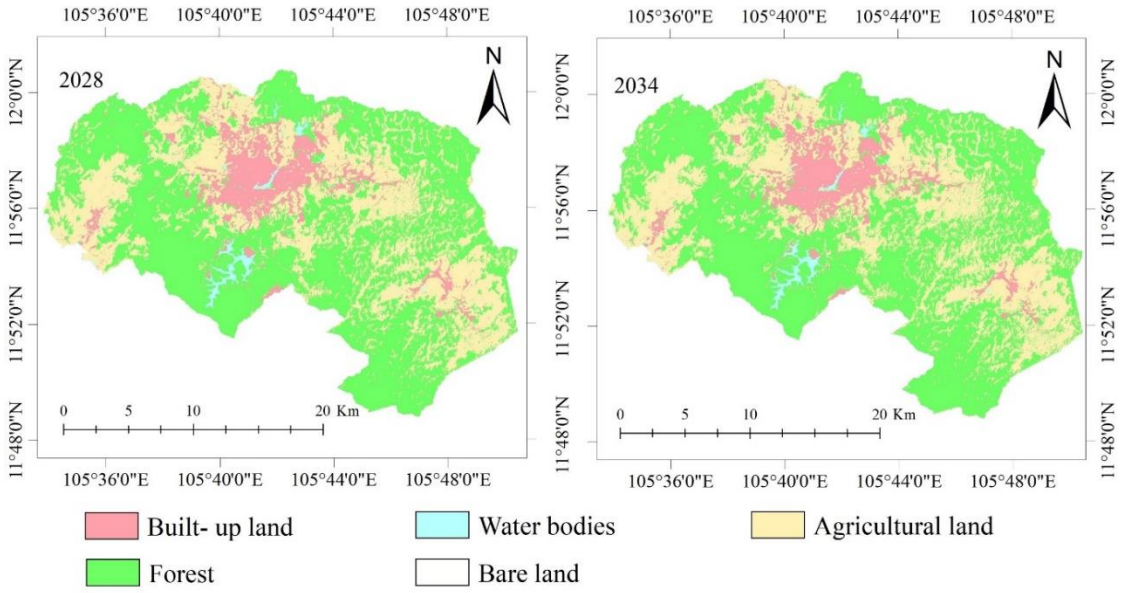

Figure 8. Prediction maps of land-use in Dalat City

Figure 9 shows the development forecast of built-up land area over time and space. According to the simulated output of the Markov chain model, the built-up land area will increase by 53.30 km^2 in 2028 and 57.22 km^2 in 2034. The prediction maps and transition matrix show that agricultural and forest land are converted into built-up land in the study area. Built-up land is forecast to expand in the central urban area, existing residential areas, and across roads. Small and narrow arable land areas are scattered throughout the city. The study results on urban expansion trends occupying other important land types such as forest and agricultural land are similar to other research in developing countries (Ntakirutimana and Vansarochana, 2021; Wang et al., 2021b). The results of the study reinforce the results of previous studies on land use change in mountainous areas. The Central Highlands of Vietnam have experienced a decline in forest land, particularly from 2000 to the present (Müller and Zeller, 2002; Castella and Verburg, 2007; Stephen, 2009). The following factors are the direct causes of deforestation and forest degradation in the area: (i) unsustainable logging, both legal and illegal; (ii) transition of forest land to agricultural land,

including high-value perennial crops and other crops; (iii) transition of forest land to infrastructure construction, particularly hydroelectric power plants; and (iv) population growth, primarily due to free migration (Pham et al., 2019).

Logistics regression used in the study has the advantage of quantitatively determining the relationships between land use change and driving factors such as natural, economic, and social factors. However, the model that incorporates Markov chain - logistic regression also has drawbacks. The spatial-transition probability map generated by the logistic model depends on the quantity and accuracy of the driving factors. Difficulties in data collection and the integration of multiple factors, including demographics and development policy, can reduce the model's accuracy. The Markov chain forecasts future land-use changes based on an analysis of historical land-use changes, assuming the same factors affecting land use over time.

The Markov chain illustrates that changes between land-use types in the future will take place over and over based on historical principles. However, it is a fact that a few phenomena and principles that happened in the past are unlikely to happen again.

However, no specific research method can fully explain all of the processes affecting land use. Hence, to obtain a more comprehensive view, a synthesis of results from various methods is required.

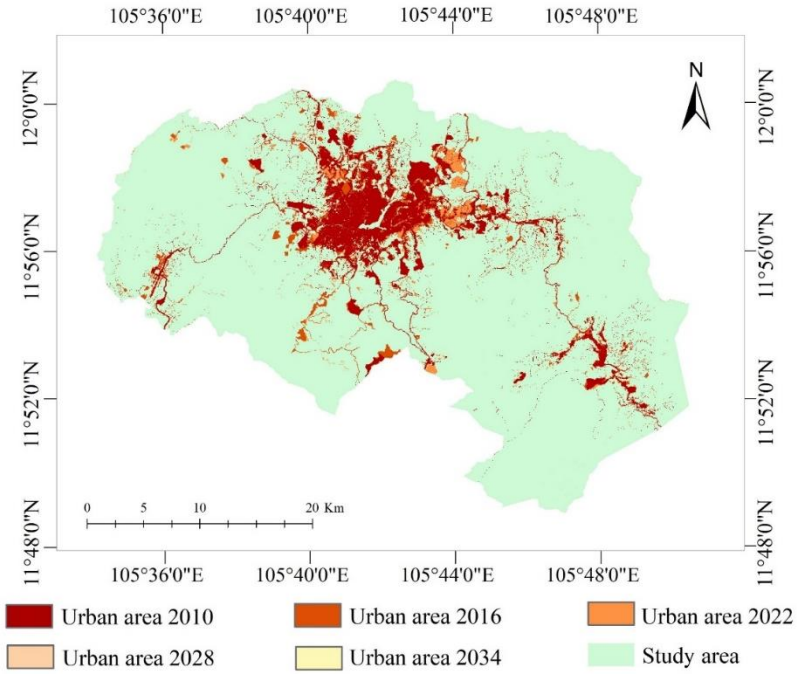

Figure 9. Change in built-up land from 2010 to 2034

4. CONCLUSION

Understanding changes in the spatial pattern of land cover and the urban growth dynamics of any area over time is critical for effective land management and sustainable urban planning. This study used the integrated model of the Markov chain-logistic regression to simulate and forecast land-use changes and urban expansion in Dalat City, especially, applying GIS to create the spatial analysis of land-use changes, building a scale-transition probability matrix among land-use types by the Markov chain, and creating a probability surface of land-use change by logistic regression. This integrated model provides an understanding of the quantity and location of spatial transition probabilities. Twelve driving-factor maps are established from GIS data, and five land-use types are extracted from remote sensing images in 2010, 2016, and 2022 by using supervised classification for analysis.

In the 2010-2022 period, there has been a dramatic shifting trend of LULC categories from agricultural and built-up land to forest land, but water bodies and bare land changed insignificantly. The total area of urban areas was 33.79 km^2 in 2010, increasing by 38.59 km^2 in 2016, and 43.15 km^2 in 2022 at a fairly even rate. A higher rate of urbanization has mainly occurred on formerly agricultural land near existing urban areas, road networks, and easily accessible

zones. The high-speed expansion of agricultural and built-up land converted from forest land can have serious ecological consequences. Therefore, the priority is that policies to boost agricultural production and urban development are obligated to be built in a balanced way to ensure sustainable development for the locality with two objectives: (1) economic development and (2) environmental protection. Through the research results, the integrated model of Markov chain-logistic regression is proposed as an effective tool for further research on the complicated characteristics of urban areas and LULCs.

ACKNOWLEDGEMENTS

The authors would like to thank the People's Committee of Dalat City, the Department of Natural Resources and Environment of Lam Dong Province, and the Enterprise of Image and Geomatics Engineering, Ho Chi Minh City, Vietnam for supporting materials and providing cartographic data for this study. We thank anonymous reviewers and editors for their constructive comments and suggestions.

REFERENCES

Aburas MM, Ho YM, Pradhan B, Salleh AH, Alazaiza MY. Spatio-temporal simulation of future urban growth trends using an integrated CA-Markov model. Arabian Journal of Geosciences 2021;14(2):Article No. 131.

Aburas MM, Ho YM, Ramli MF, Ash'aari ZH. Improving the capability of an integrated CA-Markov model to simulate spatio-temporal urban growth trends using an Analytical Hierarchy Process and Frequency Ratio. International Journal of Applied Earth Observation and Geoinformation 2017; 59:65-78.

Ai B, Xie D, Ma S, Jiang H. An EasyCA model with few steady variables and clone stamp strategy for simulation of urban growth in metropolitan areas. Ecological Modelling 2022;468: Article No.109950.

Al-Darwish Y, Ayad H, Taha D, Saadallah D. Predicting the future urban growth and it's impacts on the surrounding environment using urban simulation models: Case study of Ibb City-Yemen. Alexandria Engineering Journal 2018;57(4):2887-95.

Alsharif AA, Pradhan B. Urban sprawl analysis of Tripoli Metropolitan City (Libya) using remote sensing data and multivariate logistic regression model. Journal of the Indian Society of Remote Sensing 2014;42:149-63.

Arsanjani JJ, Helbich M, Kainz W, Boloorani AD. Integration of logistic regression, Markov chain and cellular automata models to simulate urban expansion. International Journal of Applied Earth Observation and Geoinformation 2013; 21:265-75.

Arsanjani JJ, Kainz W, Mousivand AJ. Tracking dynamic land-use change using spatially explicit Markov Chain based on cellular automata: The case of Tehran. International Journal of Image and Data Fusion 2011;2(4):329-45.

Azadi H, Ho P, Hasfiati L. Agricultural land conversion drivers: A comparison between less developed, developing and developed countries. Land Degradation and Development 2011;22(6):596-604.

Azizi P, Soltani A, Bagheri F, Sharifi S, Mikaeili M. An integrated modelling approach to urban growth and land use/cover change. Land 2022;11(10):Article No. 1715.

Castella JC, Verburg PH. Combination of process-oriented and pattern-oriented models of land-use change in a mountain area of Vietnam. Ecological Modelling 2007;202(3-4):410-20.

Cheng LL, Tian C, Yin TT. Identifying driving factors of urban land expansion using Google Earth Engine and machine-learning approaches in Mentougou District, China. Scientific Reports 2022;12(1):Article No. 16248.

Christensen M, Arsanjani JJ. Stimulating implementation of sustainable development goals and conservation action: Predicting future land use/cover change in Virunga National Park, Congo. Sustainability 2020;12(4):Article No. 1570.

Devendran AA, Gnanappazham L. Comparison of urban growth modeling using deep belief and neural network based cellular automata model: A case study of Chennai metropolitan area, Tamil Nadu, India. Journal of Geographic Information System 2019;11(1):1-6.

Ebrahimipour A, Saadat M, Farshchin A. Prediction of urban growth through cellular automata-Markov chain. Bulletin de la Société Royale des Sciences de Liège 2016;85:824-39.

Falah N, Karimi A, Harandi AT. Urban growth modeling using cellular automata model and AHP (Case study: Qazvin City). Modeling Earth Systems and Environment 2020;6:235-48.

Fan P, Ouyang Z, Nguyen DD, Nguyen TT, Park H, Chen J. Urbanization, economic development, environmental and social changes in transitional economies: Vietnam after Doimoi. Landscape and Urban Planning 2019;187:145-55.

Fathizad H, Rostami N, Faramarzi M. Detection and prediction of land cover changes using Markov chain model in semi-arid rangeland in western Iran. Environmental Monitoring and Assessment 2015;187:Article No. 629.

General Statistics Office (GSO). Completed results of the 2019 Viet Nam population and housing census [Internet]. 2020 [cited 2023 Mar 5]. Available from: https://www.gso.gov.vn/en/data-and-statistics/2020/11/completed-results-of-the-2019-viet-nam-population-and-housing-census/ (in Vietnamese).

Hassan MI, Elhassan SM. Modelling of urban growth and planning: A critical review. Journal of Building Construction and Planning Research 2020;8(4):245-62.

Hu Z, Lo CP. Modeling urban growth in Atlanta using logistic regression. Computers, Environment and Urban Systems 2007;31(6):667-88.

Huang B, Zhang L, Wu B. Spatiotemporal analysis of rural-urban land conversion. International Journal of Geographical Information Science 2009;23(3):379-98.

Huong HT, Pathirana A. Urbanization and climate change impacts on future urban flooding in Can Tho City, Vietnam. Hydrology and Earth System Sciences 2013;17(1):379-94.

Kamusoko C, Aniya M, Adi B, Manjoro M. Rural sustainability under threat in Zimbabwe-simulation of future land use/cover changes in the Bindura District based on the Markov-cellular automata model. Applied Geography 2009;29(3):435-47.

Lam Dong online. How to move the greenhouses out of Da Lat's downtown? [Internet]. 2023 [cited 2023 Jun 15]. Available from: http://baolamdong.vn/toa-soan-ban-doc/202301/giai-

phap-nao-dua-nha-kinh-ra-khoi-noi-o-da-lat-bb05c14/ (in Vietnamese).

Lam Dong Statistics Office (LDSO). Lam Dong Statistical Yearbook 2022. Ha Noi, Viet Nam: Statistical Publishing; 2023 (in Vietnamese).

Lambin EF, Turner BL, Geist HJ, Agbola SB, Angelsen A, Bruce JW, et al. The causes of land-use and land-cover change: Moving beyond the myths. Global Environmental Change 2001;11(4):261-9.

Lin YP, Chu HJ, Wu CF, Verburg PH. Predictive ability of logistic regression, auto-logistic regression and neural network models in empirical land-use change modeling-a case study. International Journal of Geographical Information Science 2011;25(1):65-87.

Mas JF, Kolb M, Paegelow M, Olmedo MT, Houet T. Modelling Land use/cover changes: A comparison of conceptual approaches and softwares. Environmental Modelling and Software 2014;51:94-111.

Mauro G. Rural-urban transition of Hanoi (Vietnam): Using Landsat imagery to map its recent peri-urbanization. ISPRS International Journal of Geo-Information 2020;9(11):Article No. 669.

Ministry of Agriculture and Rural Development of Vietnam (MARD). Agricultural Land-use Manual, Vol. 3. Land Resources in Vietnam: Land-use Current Status and Potential. Ha Noi, Vietnam: Scientific and Technical Publishing; 2015 (in Vietnamese).

Ministry of Construction (MC). Urban development in Vietnam - problems in the next period [Internet]. 2022 [cited 2023 Mar 6]. Available from: https://moc.gov.vn/tl/tin-tuc/74077/phat-trien-do-thi-viet-nam-nhung-van-de-dat-ra-trong-giai-doan-toi.aspx (in Vietnamese).

Ministry of Finance (MF). Agricultural land use and food security [Internet]. 2009 [cited 2023 Mar 6]. Available from: https://mof.gov.vn/webcenter/portal/btcvn/pages_r/l/tin-bo-tai-chinh?dDocName=BTC340505 (in Vietnamese).

Müller D, Zeller M. Land use dynamics in the central highlands of Vietnam: A spatial model combining village survey data with satellite imagery interpretation. Agricultural Economics 2002;27(3):333-54.

Musa SI, Hashim M, Reba MN. A review of geospatial-based urban growth models and modelling initiatives. Geocarto International 2017;32(8):813-33.

Mustak S, Baghmar NK, Singh SK, Srivastava PK. Multi-scenario based urban growth modeling and prediction using earth observation datasets towards urban policy improvement. Geocarto International 2022;37(27):18275-303.

Nguyen TM, Lin TH, Chan HP. The environmental effects of urban development in Hanoi, Vietnam from satellite and meteorological observations from 1999-2016. Sustainability 2019;11(6):Article No. 1768.

Nong Y, Du Q. Urban growth pattern modeling using logistic regression. Geo-Spatial Information Science 2011;14(1):62-7.

Ntakirutimana A, Vansarochana C. Asessment and prediction of land use/land cover change in the National Capital of Burundi using multi-temporary landsat data and cellular automata-Markov chain model. Environment and Natural Resources Journal 2021;19(5):413-26.

Olmedo MT, Pontius Jr RG, Paegelow M, Mas JF. Comparison of simulation models in terms of quantity and allocation of land change. Environmental Modelling and Software 2015;69:214-21.

Park S, Jeon S, Kim S, Choi C. Prediction and comparison of urban growth by land suitability index mapping using GIS and RS in South Korea. Landscape and Urban Planning 2011;99(2):104-14.

Perumal K, Bhaskaran R. Supervised classification performance of multispectral images. Journal of Computing 2010;2(2):124-9.

Pham HM, Yamaguchi Y. Urban growth and change analysis using remote sensing and spatial metrics from 1975 to 2003 for Hanoi, Vietnam. International Journal of Remote Sensing 2011;32(7):1901-15.

Pham TT, Hoang TL, Nguyen DT, Dao TL, Ngo HC, Pham VH. The Context of REDD+ in Vietnam: Drivers, Agents and Institutions. Bogor, Indonesia: Center for International Forestry Research; 2019.

Pham VC, Pham TT, Tong TH, Nguyen TT, Pham NH. The conversion of agricultural land in the peri-urban areas of Hanoi (Vietnam): Patterns in space and time. Journal of Land Use Science 2015;10(2):224-42.

Pontius Jr RG, Millones M. Death to Kappa: Birth of quantity disagreement and allocation disagreement for accuracy assessment. International Journal of Remote Sensing 2011;32(15):4407-29.

Pontius RG. Quantification error versus location error in comparison of categorical maps. Photogrammetric Engineering and Remote Sensing 2000;66(8):1011-6.

Pontius RG. Statistical methods to partition effects of quantity and location during comparison of categorical maps at multiple resolutions. Photogrammetric Engineering and Remote Sensing 2002;68(10):Article No. 1041.

Research Systems, Inc., (RSI). ENVI Tutorials. Portland, USA: StoneTablet; 2001.

Richards JA. Supervised classification techniques. In: Richards JA editor. Remote Sensing Digital Image Analysis. Switzerland: Springer; 2022. p. 263-367.

Sang L, Zhang C, Yang J, Zhu D, Yun W. Simulation of land use spatial pattern of towns and villages based on CA-Markov model. Mathematical and Computer Modelling 2011;54(3-4):938-43.

Shafizadeh-Moghadam H, Tayyebi A, Ahmadlou M, Delavar MR, Hasanlou M. Integration of genetic algorithm and multiple kernel support vector regression for modeling urban growth. Computers, Environment and Urban Systems 2017;65:28-40.

Sohl TL, Claggett PR. Clarity versus complexity: Land-use modeling as a practical tool for decision-makers. Journal of Environmental Management 2013;129:235-43.

Son NT, Chen CF, Chen CR, Chang LY, Thanh BX. Urban growth mapping from Landsat data using linear mixture model in Ho Chi Minh City, Vietnam. Journal of Applied Remote Sensing 2012;6(1):Article No. 063543.

Stephen JL. Dynamics of land cover and land use changes in the upper Ca river basin of Nghe An, Vietnam. Japanese Journal of Southeast Asian Studies 2009;47(3):287-308.

Tranh NH. Ancient Dalat. Ho Chi Minh City, Vietnam: HCMC General Publishing; 2001 (in Vietnamese).

Tro T. Dalat: Highland City. Ho Chi Minh City, Vietnam: HCMC General Publishing; 1993 (in Vietnamese).

Tsagkis P, Bakogiannis E, Nikitas A. Analysing urban growth using machine learning and open data: An artificial neural network modelled case study of five Greek cities. Sustainable Cities and Society 2023;89:Article No. 104337.

Verburg PH, Soepboer W, Veldkamp A, Limpiada R, Espaldon V, Mastura SS. Modeling the spatial dynamics of regional land

use: The CLUE-S model. Environmental Management 2002; 30:391-405.

Wang M, Cai L, Xu H, Zhao S. Predicting land use changes in northern China using logistic regression, cellular automata, and a Markov model. Arabian Journal of Geosciences 2019;12:1-2.

Wang R, Murayama Y, Morimoto T. Scenario simulation studies of urban development using remote sensing and GIS. Remote Sensing Applications: Society and Environment 2021a;22: Article No. 100474.

Wang SW, Munkhnasan L, Lee WK. Land use and land cover change detection and prediction in Bhutan's high altitude city of Thimphu, using cellular automata and Markov chain. Environmental Challenges 2021b;2:Article No. 100017.

World Bank (WB). Vietnam urbanization review: Technical assistance report [Internet]. 2011 [cited 2023 Mar 8]. Available from: https://openknowledge.worldbank.org/handle /10986/2826.

Xie C, Huang B, Claramunt C, Chandramouli C. Spatial logistic regression and GIS to model rural-urban land conversion. Proceedings of the PROCESSUS 2nd International Colloquium on the Behavioural Foundations of Integrated Land-use and Transportation Models: Frameworks, Models and Applications; 2005 Jun 12; University of Toronto: Canada; 2005.

Yeh AGO, Li X, Xia C. Cellular automata modeling for urban and regional planning. In: Shi W, Goodchild MF, Batty M, Kwan MP, Zhang A, editors. Urban Informatics. The Urban Book Series. Singapore: Springer; 2021. p. 865-83.

Forest Restoration in an Abandoned Seasonally Dry Tropical Forest in the Mae Klong Watershed, Western Thailand

Ritthikai Saikhammoon[1], Sarawood Sungkaew[1], Sathid Thinkampaeng[2], Wongsatorn Phumphuang[3], Torlarp Kamyo[4], and Dokrak Marod[1,2*]

[1]Department of Forest Biology, Faculty of Forestry, Kasetsart University, Bangkok 10900, Thailand
[2]Cooperation Centre of Thai Forest Ecological Research Network, Kasetsart University, Bangkok 10900, Thailand
[3]Department of National Parks, Wildlife and Plant Conservation, Bangkok 10900, Thailand
[4]Department of Agroforestry, Maejo University, Phrae 54140, Thailand

ARTICLE INFO

Received: 25 May 2023
Received in revised: 8 Jul 2023
Accepted: 11 Jul 2023
Published online: 8 Sep 2023
DOI: 10.32526/ennrj/21/20230121

Keywords:
Abandoned land/ Canonical correspondence analysis/ Species composition/ Tree distribution

*** Corresponding author:**
E-mail: dokrak.m@ku.ac.th

ABSTRACT

Deforestation for the development of agricultural land is a critical driver of biodiversity loss. We examined the relationships between tree species and environments after the abandonment of a plot of land at the Mae Klong Watershed Research Station, Western Thailand. Vegetation monitoring was conducted every two years on a 16-ha permanent plot established in 2011 until 2019. All trees with diameter at breast height (DBH)≤1 cm were measured. Canonical correspondence analysis (CCA) was performed to investigate the relationships between tree species and environments. We found a total of 199 tree species in the plot, which comprised both pioneer and climax species. The high tree density and low basal area were 1,280 stem/ha and 7.30 m^2/ha, respectively. During 2011-2019, the species richness and total tree density were decreased by nine species (from 206 to 197 species) and 83 stem/ha (from 1,120 to 1,037 stem/ha). In contrast, the total basal area increased from 6.41 to 7.26 stem/ha. According to the measured environmental variables, mixed deciduous species such as *Pterocarpus macrocarpus* and *Xylia xylocarpa* var. *kerrii* preferred higher elevations and drier sites compared to dry evergreen species such as *Dipterocarpus alatus*. Early colonizing species such as *Trema orientalis* and *Ficus* species exhibited rapid population decreases, whereas climax species such as *Lagerstroemia tomentosa* exhibited highly successful regeneration under natural conditions. Artificial reforestation efforts may be required in areas with large disturbance, including the planting of mixed tree species to promote natural regeneration and reduce the recovery period.

1. INTRODUCTION

Compared to other forest types worldwide, tropical forests have high biodiversity and carbon density (Sullivan et al., 2017), which play important roles in ecosystem services such as climate regulation, carbon and water cycles, and food resource production (Good et al., 2015; Lewis et al., 2015; Hansen and DeFries, 2004). However, the rates of deforestation and land use change are increasing rapidly, with losses of over 80 million ha of primary tropical forest since 1990 (FAO and UNEP, 2020). Across the tropics, primary forest is mainly lost through agricultural development, including the promotion of large-scale crop production and commercial tree plantation (Curtis et al., 2018; Klemick, 2011), which are accompanied by biodiversity loss and forest degradation (Chazdon, 2014; Laurance, 2007; Geist and Lambin, 2002). Many such crop areas have been abandoned due to unsustainable practices, leading to the creation of post-disturbance vegetation communities (Van Hall et al., 2017) that vary according to habitat conditions. The impacts of abandonment on biodiversity and ecosystem services also vary greatly, depending on disturbance intensity and frequency (Chazdon, 2003; Collins et al., 2001). Despite the importance of tropical forests, there is relatively little information on succession or recovery in these forests (Poorter et al., 2021).

Citation: Saikhammoon R, Sungkaew S, Thinkampaeng S, Phumphuang W, Kamyo T, Marod D. Forest restoration in an abandoned seasonally dry tropical forest in the Mae Klong Watershed, Western Thailand. Environ. Nat. Resour. J. 2023;21(5):443-457. (https://doi.org/10.32526/ennrj/21/20230121)

Degraded or abandoned cropland is typically characterized by canopy openness, with high sunlight intensity reaching the soil surface and affecting air and soil temperature and humidity near the ground. In tropical forests, plants are categorized into two functional groups based on light requirements: light-demanding (i.e., pioneer) and shade-tolerant (i.e., late successional) species (Matsuo et al., 2021). Generally, pioneer plant species are more abundant along forest edges or in open areas than shade-tolerant species (Marod et al., 2004), due to germination stimulated by light exposure (Aide et al., 2000), whereas late successional species establish later and co-exist with recruited pioneer or early successional species according to environmental gradients (Gustafsson et al., 2016; Swinfield et al., 2016). In seasonally dry tropical forests, degraded sites undergoing natural recovery are susceptible to recurrent disturbances such as fire (Marod et al., 2004), and may experience slower colonization due to large distances from the intact forest edge (Marod et al., 2012). Compared with humid tropical regions, vegetation recovery occurs slowly in the dry tropics, where combustion is easily initiated (Scheper et al., 2021), particularly under the influence of anthropogenic factors (Quesada and Stoner, 2004; Miles et al., 2006; Mabry and Fraterrigo, 2009). Colonization by grasses, bamboos, lianas, and shrubs can also inhibit the survival and regeneration of climax tree species and delay forest restoration (Rother et al., 2015). Various environmental factors can also affect the ability of plants to acquire resources, leading to differences in regeneration rates, forest structure, and species composition among different successional sites (Wang et al., 2019; Mondoni et al., 2020). Early successional species modify light availability within the canopy by providing shade, which also influences the thermal and moisture microclimates to shape the species diversity, composition, and productivity of shade-tolerant species (Gravel et al., 2010). Therefore, an understanding of natural succession processes is important for developing forest conservation strategies for recovering degraded or abandoned areas (Wright, 2005; Sanchez-Azofeifa et al., 2005). Forest restoration programs based on planting suitable species for a given ecological niche should be developed at both regional and national levels to reduce the time required to reach successional climax, which would support ecosystem restoration and mitigate damage related to climate change.

In Thailand, seasonally dry tropical forests are classified into three categories: mixed deciduous forest (MDF) on zonal soils; deciduous dipterocarp forest on poor, leached soils and laterites; and savanna forest on fertile soils (Takahashi et al.; 2012; Marod et al., 2002). The dominant species of MDF include many commercial tree species in the upper canopy such as teak (*Tectona grandis*), *Pterocarpus macrocarpus*, *Xylia xylocarpa* var. *kerrii*, and *Afzelia xylocarpa* and bamboos mainly occupy the middle layer (Marod et al., 2004). Teak generally has the highest commercial value for logging, although it may be absent from MDFs (Thein et al., 2007).

The Mae Klong watershed of western Thailand is predominated by MDF, followed by deciduous dipterocarp forest on mountain ridges and dry evergreen forest along creeks (Marod et al., 1999). Forest degradation in the watershed has mainly been caused by logging and conversion into agricultural areas for upland rice production. Natural disturbance is frequent during the dry season due to forest fires and drought (Marod et al., 2002). These disturbed areas were abandoned after a logging ban in 1989, and natural reforestation was allowed. High recovery rates from non-forest to forested areas were detected in satellite images, especially during the initial phase (1992-1996) (Kamyo, 2016). The early successional stage (1989-1994) was initiated by colonization by short-lived pioneer species including herbaceous species and shrubs such as *Eupatorium odoratum*, *Musa acuminata*, *Saccharum spontaneum*, *Trema orientalis*, *Bauhinia viridescens*, and *Sterculia macrophylla* (Marod, 1995; Takahashi et al., 1995). However, few studies have examined successional processes in seasonally dry tropical forests using large permanent plots. Therefore, the objectives of this study were to examine secondary forest structure and species composition and their influential environmental factors in an abandoned agricultural area undergoing forest recovery, in the Mae Klong Watershed, Kanchanaburi Province, Thailand.

2. METHODOLOGY

2.1 Study area

The study was conducted in a mixed deciduous forest (MDF) on abandoned (post-agricultural) land at the Mae Klong Watershed Research Station (14°35′N, 98°52′E), Thong Pha Phum District, Kanchanaburi Province, western Thailand (Figure 1), covering an area of approximately 109 km^2 and elevation range of 100-950 m.a.s.l. The climate is subtropical, with a long wet

season followed by a short, cool and dry season. Annual rainfall normally exceeds 1,650 mm, and is concentrated from late April to October. The mean monthly temperature is ca. 27.5°C, with a maximum of 39.1°C in April and minimum of 14.6°C in December (Marod et al., 1999). The soil was weathered from alluvial parent material containing sandstone, limestone and quartzite (Suksawang, 1993).

The study area can be classified into four main forest types: MDF with bamboos, deciduous dipterocarp forest (on mountain ridges), dry evergreen forest, and disturbed forest (Kutintara et al., 1995). MDF is mostly scattered the whole areas with deciduous dipterocarp forest on some mountain ridges. The dominant tree species are *Xylia xylocarpa* var. *kerrii*, *Vitex peduncularis*, *Schleichera oleosa*, and *Pterocarpus macrocarpus*. Bamboos are dominant in the understory, including *Bambusa tulda*, *Cephalostachyum pergracile*, *Gigantochloa albociliata*, and *Gigantochloa hasskarliana* (Marod et al., 1999). Signs of forest disturbance from burning and cultivation are observed on the gentler slopes, where the dominant vegetation consists of wild banana (*Musa acuminata*), bamboos, lianas and pioneer tree species such as *Trema orientalis*, *Bauhinia viridescens*, and *Sterculia macrophylla* (Marod, 1995).

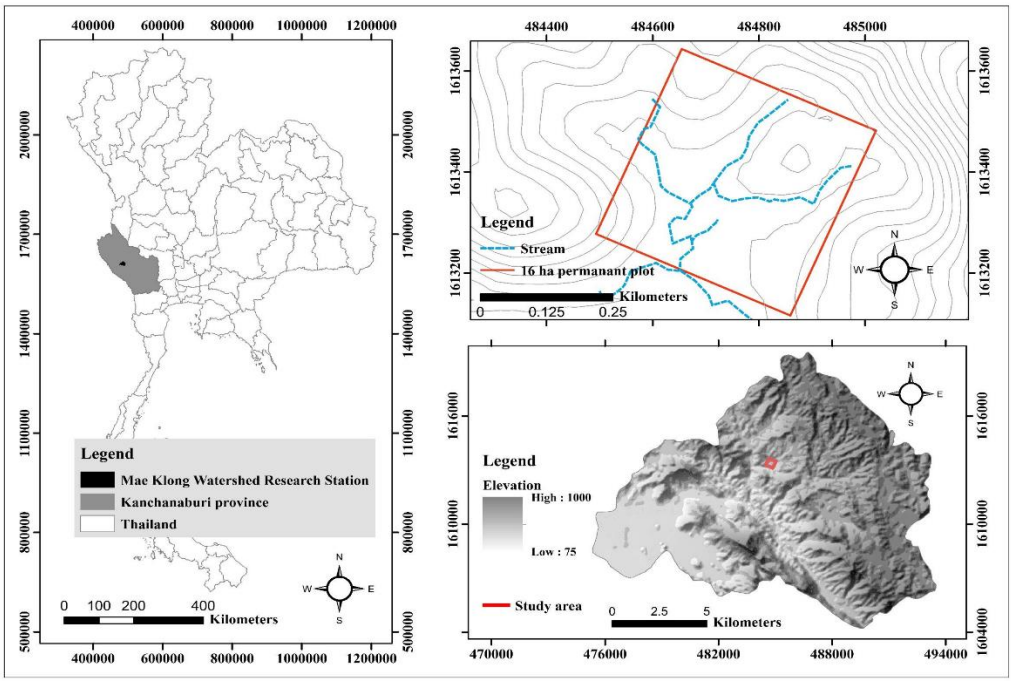

Figure 1. The location of the study area and 16 ha permanent plot in abandoned area of MDF at MKWRS, Kanchanaburi Province

2.2 Plot establishment and tree species investigation

In 2011, a 16-ha permanent plot (400 m × 400 m) was established in an abandoned area where MDF was devastated by cultivation and recovered based on natural succession (Kamyo et al., 2013). The plot was divided into 1,600 subplots (10 m × 10 m) and all trees with diameter at breast height (DBH) ≥2 cm were tagged, identified, and their DBH and positions were recorded every 2 years until 2019. As of 2019, all trees with DBH ≥1 cm were included in the survey. Samples of unidentified species were collected and identified by comparison with specimens at the Forest Herbarium, Department of National Parks, Wildlife and Plant Conservation. Species nomenclature follows Smitinand (2014).

2.3 Environmental data collection

2.3.1 Topographic factors

For each 50 m × 50 m subplot, topographic variables included the mean elevation of the four plot corners, the average slope, and the distance from the nearest stream. These variables were analyzed using the *fgeo* package (Lepore et al., 2019) in the R v3.6.1 software (R Core Team, 2017).

2.3.2 Soil properties

To collect soil samples, the 16-ha plot was divided into 64 subplots, each with 50 m × 50 m, followed the method of Delgado-Baquerizo et al. (2020). In each subplot, five soil samples (center and four corners) were collected from the topsoil (depth, 0-15 cm) and combined into a composite soil sample.

Soil physical and chemical properties were analyzed. The percentages of sand, silt and clay were determined using a hydrometer, according to a modified protocol (Soil Science Division Staff, 2017). Soil pH was determined using a pH meter in a 1:1 soil:water mixture (Beck, 1999). Organic matter was measured using the wet oxidation method (Allison, 1965). Available P was calculated using the Bray II method (Bray and Kurtz, 1945) and exchangeable cations (K^+, Ca^{2+}, and Mg^{2+}) were analyzed using an atomic absorption spectrophotometer with 1 N ammonium acetate (NH_4Oac) (Chapman, 1965). All soil samples were analyzed at the Laboratory of Soil Science, Faculty of Agriculture, Kasetsart University.

2.4 Data analysis

2.4.1 Plant ecological indices

To evaluate the forest structure and species composition, plant ecological indices were constructed based on structural parameters (tree density and basal area) and taxon richness (at species, genus and family levels) (Mohandass et al., 2016). The dominant species and importance value index (IVI) were calculated based on the summation of relative density, dominance and frequency (Krebs, 1994). The Shannon-Wiener index (H') was analyzed following Shannon and Weaver (1949).

2.4.2 Tree species regeneration

A DBH class-distribution based on trees in the 16-ha plot with at least 30 stems was utilized for estimating tree regeneration. We divided the diameter of the stems into classes with 5 cm intervals for each species of tree. We estimated the total stem counts for each diameter class for each tree species to determine the DBH distribution form. Following Shumi et al. (2019), we then visually categorized the DBH distribution form by grouping forms with similar shapes.

2.4.3 Relationships between plant community occurrence and environmental variables

To investigate the influence of environmental factors on plant community establishment, we performed canonical correspondence analysis (CCA). CCA ordination was conducted at the subplot scale (50 m × 50 m) using the cca function in the *vegan* package in R v3.6.1. Tree species classification was performed separately for trees (DBH ≥ 4.5 cm) and saplings (1 ≤ DBH < 4.5 cm) for inclusion in the first matrix, constructed based on IVI values for each subplot. The environmental variables including soil properties (i.e., sand, silt, clay and organic matter content and pH) and topographic factors (i.e., elevation, slope) were used to construct the second matrix.

2.4.4 Statistical analyses

Correlations between species and environmental variables were evaluated using Monte Carlo simulations, with 999 permutations. Correlations between environmental variables were evaluated using Pearson correlation coefficient (R). The significance threshold was $p<0.05$.

3. RESULTS AND DISCUSSION

3.1 Forest structure and species composition

In the 16-ha plot, a total of 20,478 individuals were identified with DBH ≥ 1 cm. These comprised of 199 species, 129 genera and 49 families, the tree density and basal area (BA) were 1,280 stems/ha and 7.30 m^2/ha, respectively. Tree species diversity based on the Shannon-Wiener index was high (H'=4.28). In addition, the forest structure (species composition, tree density and BA) based on trees with DBH ≥ 2 cm varied between the first census (2011) and the last monitor (2019). Across the forest recovery, the decreased trend in density and species number was detected, with 83 stems and 9 species disappearing. Most of these were pioneer species such as *Mallotus paniculatus*, *Bauhinia malabarica*, and *Gmelina asiatica*. While the overall BA had increased from 6.41 to 7.26 m^2/ha.

Among tree species with DBH ≥ 4.5 cm, the tree density was 605 stems/ha and the basal area was 6.91 m^2/ha; these included 176 species, 121 genera and 47 families (Table S1). The species with the highest tree density was *Lagerstroemia tomentosa* (42 stems/ha) followed by *Callerya atropurpurea* (32 stems/ha), *Markhamia stipulata* (29 stems/ha), *Garuga pinnata* (21 stems/ha), *Toona ciliata* (20 stems/ha), *Stereospermum neuranthum* (20 stems/ha), *Croton persimilis* (18 stems/ha), *Albizia lucidior* (18 stems/ha), *Mitragyna rotundifolia* (17 stems/ha), and *Artocarpus lacucha* (13 stems/ha). The 10 most dominant tree species based on relative basal area (%) accounted for 40% of the total basal area; these were *Duabanga grandiflora* (7.92%), followed by *Litsea grandis* (4.61%), *Dipterocarpus alatus* (4.33%), *Lagerstroemia tomentosa* (4.05%), *Albizia lucidior* (3.85%), *Garuga pinnata* (3.44%), *Gmelina arborea* (3.22%), *Toona ciliata* (3.15%), *Callerya atropurpurea* (2.83%), and *Ficus racemosa* (2.53%).The dominant species based

on IVI (%) was *Lagerstroemia tomentosa* (16.77%) followed by *Markhamia stipulata* var. *stipulata* (11.91%), *Callerya atropurpurea* (11.77%), *Garuga pinnata* (10.35%), *Duabanga grandiflora* (9.62%), *Albizia lucidior* (9.59%), *Toona ciliata* (9.31%), *Stereospermum neuranthum* (8.31%), *Litsea grandis* (8.18%), and *Mitragyna rotundifolia* (6.70%).

In family level, Fabaceae, Moraceae, Malvaceae, Phyllantaceae, Lythraceae, and Lamiaceae families had the most species in the permanent plot (21, 15, 13, 11, 8, and 7, respectively). Species of the Fabaceae had the highest tree density, with 88 stems/ha followed by Moraceae (74 stems/ha), Lythraceae (58 stems/ha), Bignoniaceae (57 stems/ha), and Phyllantaceae (35 stems/ha). Species of the Fabaceae also had the highest basal area, with 1.03 m^2/ha, followed by the Lythraceae (0.90 m^2/ha), Moraceae (0.88 m^2/ha), Lauraceae (0.49 m^2/ha), and Bignonaceae (0.45 m^2/ha) (Figure 2).

After 30 years of abandonment (1989-2019), herbaceous species such as *Eupatorium odoratum*, *Musa acuminata*, and *Saccharum spontaneum* were drastically depleted and replaced by woody species at high tree density (605 stems/ha) and low basal area (6.91 m^2/ha), which were lower than many reported values from natural MDF, with tree density and basal area values ranging from 170 to 450 stems/ha and from 17 to 37 m^2/ha, respectively (Marod et al., 1999; Chaiyo et al., 2012). High species diversity (87.94±10.38 species/ha) was observed and a similar trend as previously reported. Kamyo et al. (2013) studied at the same study site with different areas (4-ha permanent plot) and reported tree species diversity increased during 18 years (1992 to 2010) after abandonment from 32 species into 147 species, respectively. In addition, it is also higher than in some selective cutting in MDF permanent plots in this watershed which only 49 species/ha were reported (Yarwudhi et al., 2000). It was high due to the coexisted species between pioneer and late succession species, which is a common phenomenon during forest recovery (Phumphuang et al., 2018; Chen et al., 2020). Likewise, the regeneration of this area was primarily explained by the decline of some pioneer species and the development of some late successional species from 2011-2019. This was consistent with the forest on Barro Colorado Island in Panama, where the abundance of species with heavy wood increased throughout succession (Chave et al., 2008). Thus, the recovery process is still ongoing, as shown by the variation of composition and structure of the forest, especially in a large number of small trees (Sann et al., 2016).

Furthermore, the influences of disturbed factors such as drought, forest fire and undergrowth may be prohibited forest recovery during the successional stages (Lacerda and Kellermann, 2019; Marod et al., 2002). The deep shade of bamboo had a high impact on forest floor light intensity, while a large amount of bamboo litter may have an impact on seedling recruitment by interfering with seedling emergence and preventing newly distributed seeds from reaching an appropriate soil substrate (Larpkern et al., 2011). The intensity of forest fires that can be killed small trees that can also be influenced by the quantity of bamboo litter on the ground (Keeley and Bond, 1999). Forest fires frequently occurred in the study area during the first ten-year period (1990-2000). It not only burnt the herbaceous species but also some pioneer species such as *Trema orientalis* (Kamyo et al., 2013). However, some tree species received a significant vacant area from the forest fire (Marod et al., 1999). Thus, such an environment and natural disturbances significantly contributed to this forest's fluctuation, especially in terms of species composition. The most abundant pioneer species were *Ficus* trees of family Moraceae, including *Ficus hispida*, *Ficus racemosa*, *Ficus auriculata*, *Ficus chartacea*, *Ficus variegata*, *Ficus callosa*, and *Ficus semicordata*. Other pioneer species included *Croton persimilis* (Euphorbiaceae), *Trema orientalis* (Cannabaceae), *Rhus Javanica* (Anacardiaceae), *Litsea grandis* (Lauraceae), *Litsea glutinosa* (Lauraceae), *Microcos paniculata* (Malvaceae), *Colona flagrocarpa* (Malvaceae), *Berrya mollis* (Malvaceae), *Sterculia pexa* (Malvaceae), *Sterculia foetida* (Malvaceae), *Albizia odoratissima* (Fabaceae), *Wrightia arborea* (Apocynaceae), *Morus macroura* (Moraceae), *Erythrina subumbrans* (Fabaceae), *Senna timoriensis* (Fabaceae), *Oroxylum indicum* (Bignoniaceae), and *Bridelia ovata* (Phyllanthaceae). Many of these species facilitate the establishment of late successional species and supply food resources for wildlife (Rueangket et al., 2019). The climax species in this MDF (Marod et al., 1999; Khamyong et al., 2018) have already colonized the area and some species became dominance, such as *Lagerstroemia tomentosa*, *Garuga pinnata*, *Xylia xylocarpa* var. *kerrii*, *Pterocarpus macrocarpus*, *Anogeissus acuminata*, *Schleichera oleosa*, and *Vitex peduncularis*. Some remnant species from the dry evergreen forest, such as *Dipterocarpus alatus*,

Aphanamixis polystachya, and *Toona ciliata*, which mainly occupy riverbanks with high moisture, have performed well in co-establishing with other species. Presently, the forest is recovering, with degraded and non-forest areas have been becoming forested as previously described by Kamyo et al. (2016).

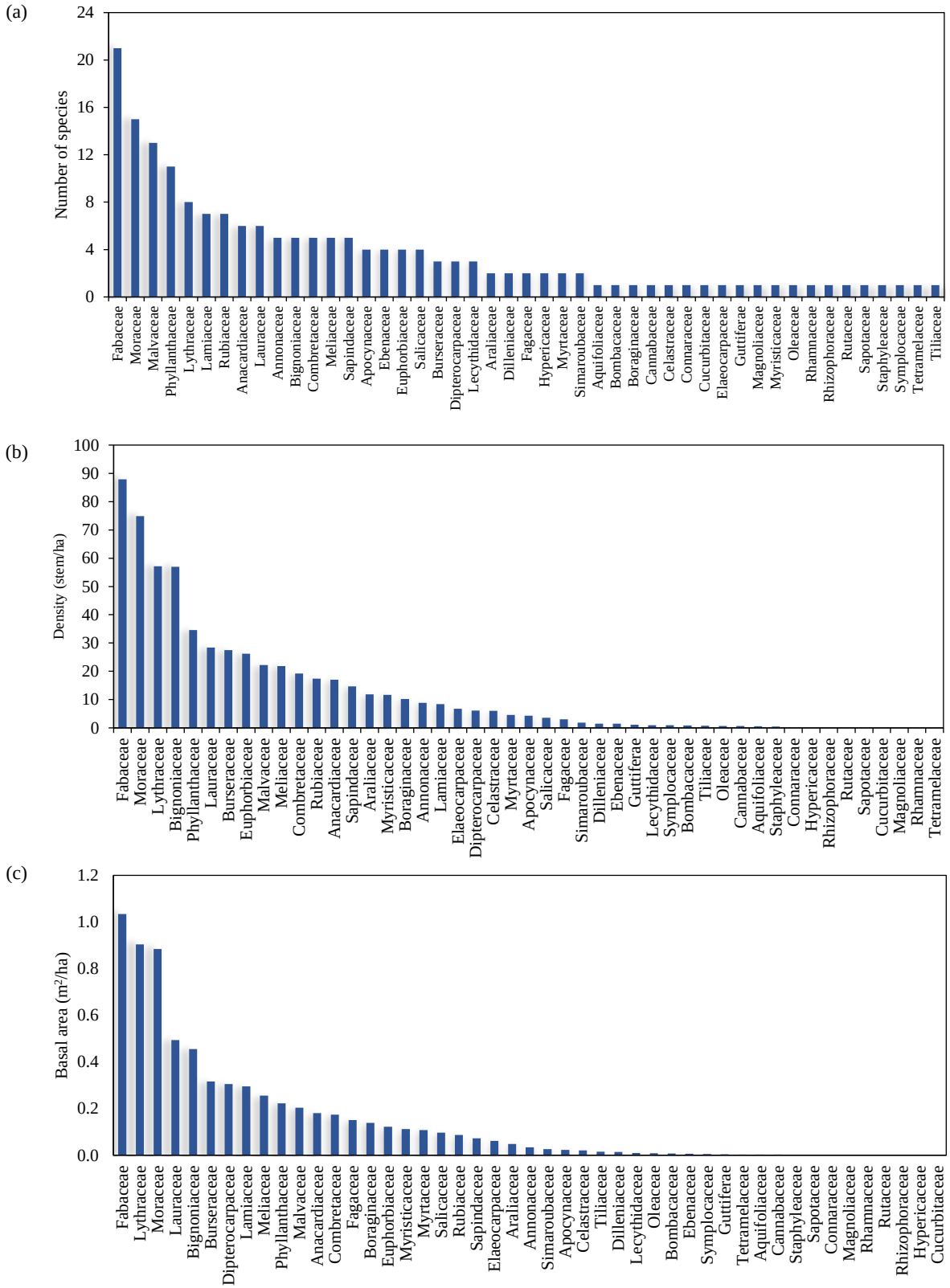

Figure 2. (a) Number of species, (b) tree density, and (c) basal area of families in the permanent plot. Only trees with diameter at breast height (DBH) ≥4.5 cm are included.

3.2 Tree species regeneration

Our analysis of the regenerating tree populations according to DBH class distributions included a total of 94 tree species with populations of ≥ 30 stems. The results showed two types of DBH class distribution: inverted J-shaped (30 species) and irregular (64 species). In both distributions, most stems occur in the lowest DBH classes, with progressively fewer stems in larger DBH classes (Table S1). Considering the dominance of MDF species, only some species in the upper canopy followed an inverted J-shaped distribution, such as *Terminalia triptera*, *Terminalia calamansanai*, and *Artocarpus rigidus* (Figure 3(a-c)). Most shrubby trees in the middle layer also followed an inverted J-shaped distribution, such as *Lepisanthes rubiginosa*, *Millettia leucantha*, and *Millettia brandisiana* (Figure 3(d-f)). These results indicate that these recovering species have a high capacity to maintain a stable population structure because small trees will grow into larger size classes and replace larger trees as they die. Notably, these species will be sustained if mortality is higher among small (suppressed) trees and large trees than among medium-sized co-dominants (Marod et al., 2022).

Species exhibiting irregular DBH class distributions included both climax and pioneer species (Table S1). Climax MDF species with discontinuous DBH class distributions included *Lagerstroemia tomentosa* and *Pterocarpus macrocarpus* (Figure 4(a-b)). The irregular distributions were also observed in pioneer species such as *Morus macroura*, *Litsea glutinosa*, and *Erythrina subumbrans* (Figure 4(c-e)); these were found mainly in canopy gaps, which suggests that the high light conditions characteristic of disturbed areas are required for their successful establishment (Sangsupan et al., 2021; Swinfield et al., 2016; Goodale et al., 2012). Some remnant tree species of dry evergreen forests such as *Dipterocarpus alatus* showed good regeneration performance, with increasing population sizes, despite irregular DBH class distributions (Figure 4(f)). This finding indicates that remnant trees during the early stage after abandonment are important for forest restoration, likely through enhancing seed dispersal and creating suitable environments for plant establishment.

3.3 Environmental factors

The mean±standard deviation (SD) elevation and slope of the study area were 303.05±7.60 m.a.s.l. and 11.97±8.27%, respectively. The soil was slightly acidic (pH 6.32±0.72), with high organic matter content (6.22±0.15%). The soil texture was classified as loam due to the relative content of sand (38.75±0.001%), silt (34.88±4.55%) and clay (26.27±6.11%). Among eight environmental variables including topographic variables (elevation, slope and distance to the nearest stream) and soil properties (soil texture, soil pH and organic matter content), Pearson's correlation analysis showed a strongly positive correlation (R>0.8) only between sand content and pH (R=0.96; Table 1). Among the remaining environmental variables, positive correlations were detected between silt content and pH (R=0.49), sand and silt content (R=0.43), elevation and slope (R=0.63), elevation and distance to the nearest stream (R=0.65), and slope and distance to the nearest stream (R=0.37). By contrast, clay content was negatively correlated with sand content (R=-0.78), silt content (R=-0.78) and soil pH (R=-0.73). Organic matter content was not significantly correlated with any other variable.

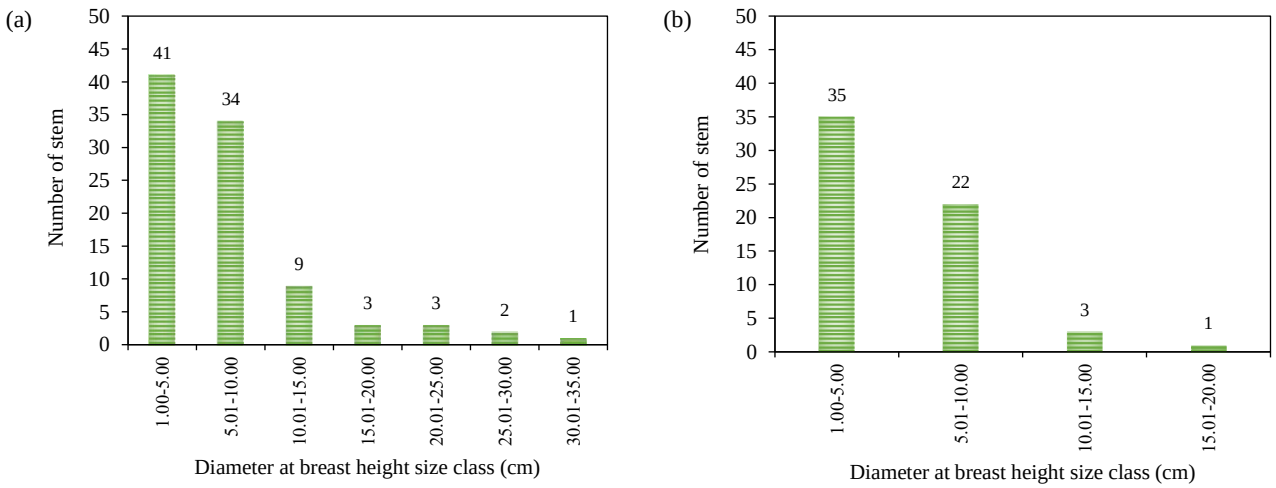

Figure 3. DBH class distributions plotted, showing an inverted J-shaped distributions. (a) *Terminalia triptera*, (b) *Terminalia calamansanai*, (c) *Artocarpus rigidus*, (d) *Lepisanthes rubiginosa*, (e) *Millettia leucantha*, and (f) *Millettia brandisiana*

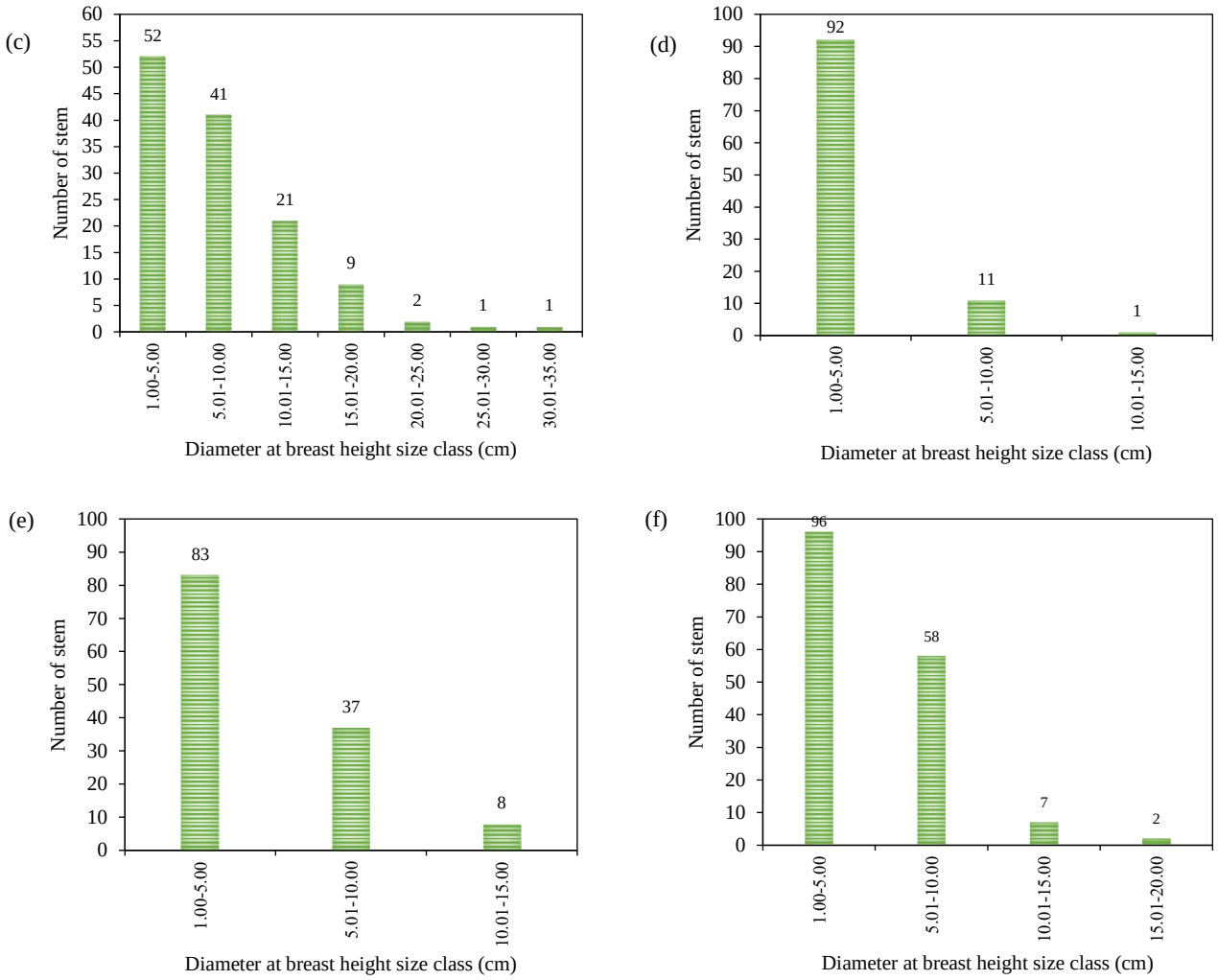

Figure 3. DBH class distributions plotted, showing an inverted J-shaped distributions. (a) *Terminalia triptera*, (b) *Terminalia calamansanai*, (c) *Artocarpus rigidus*, (d) *Lepisanthes rubiginosa*, (e) *Millettia leucantha*, and (f) *Millettia brandisiana* (cont.)

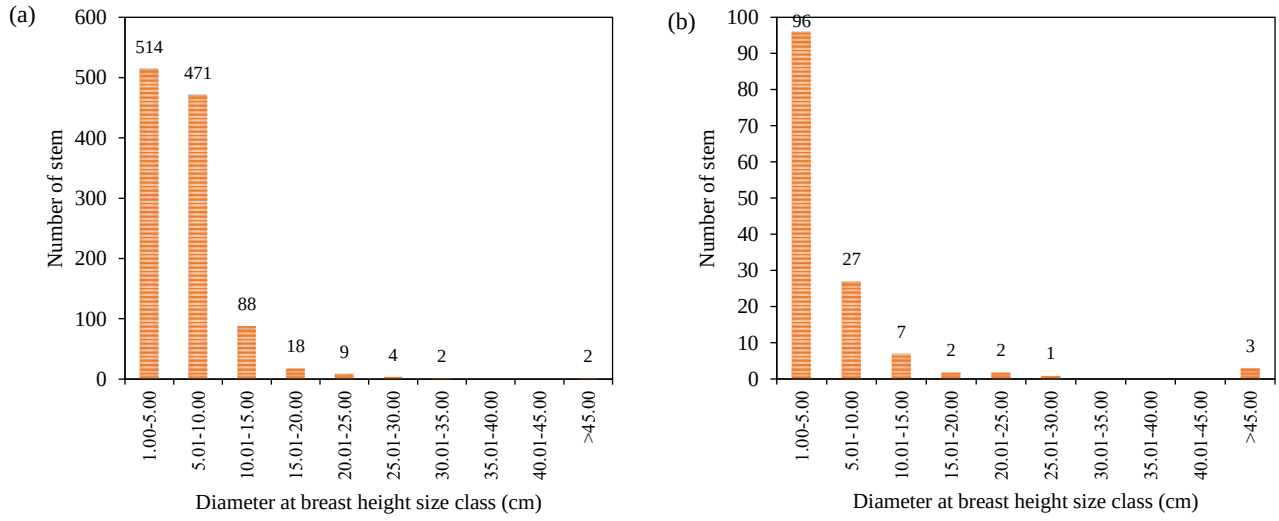

Figure 4. DBH class distributions plotted, showing an irregular distributions: (a) *Lagerstroemia tomentosa*, (b) *Pterocarpus macrocarpus*, (c) *Morus macroura*, (d) *Litsea glutinosa*, (e) *Erythrina subumbrans*, and (f) *Dipterocarpus alatus*

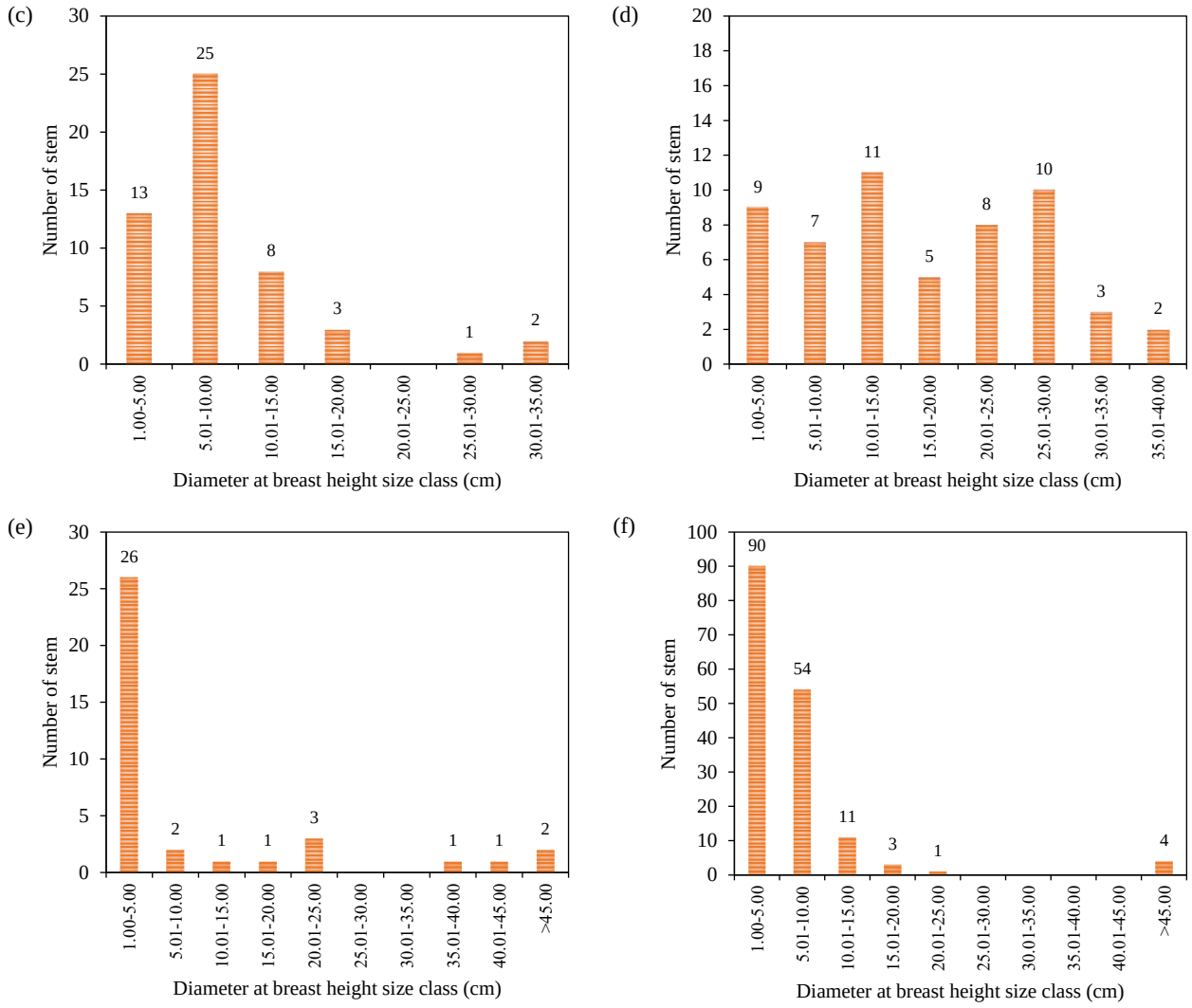

Figure 4. DBH class distributions plotted, showing an irregular distributions: (a) *Lagerstroemia tomentosa*, (b) *Pterocarpus macrocarpus*, (c) *Morus macroura*, (d) *Litsea glutinosa*, (e) *Erythrina subumbrans*, and (f) *Dipterocarpus alatus* (cont.)

Table 1. Pearson's correlation coefficient matrix for environmental factors examined in this study

Factor	Elevation	Slope	Distance to stream	Sand content	Silt content	Clay content	Soil pH	Organic matter content
Elevation	1.00							
Slope	0.631***	1.00						
Distance to stream	0.647***	0.372**	1.00					
Sand content	-0.051	0.012	-0.087	1.00				
Silt content	0.133	-0.023	-0.232	0.427**	1.00			
Clay content	0.037	0.067	0.236	-0.781**	-0.779***	1.00		
pH	-0.016	-0.003	-0.052	0.956***	0.49***	-0.728***	1.00	
Organic matter content	0.172	0.212	0.024	0.02	0.104	0.156	0.043	1.00

Asterisks indicate significant differences (*=p<0.05; **=p<0.01; ***=p<0.001)

During forest succession after abandonment, several environmental factors change rapidly, particularly soil properties. In the early stages of succession, soil is typically poor in nutrients and organic matter. However, as the forest matures, organic matter accumulates and new vegetation growth leads to improved soil quality and nutrient availability (Hooker and Compton, 2003). In the study area, soil in the recovering forest had high organic matter content and was slightly acidic, which is within

the suitable range for plant growth (Marod and Kutintara, 2009). The soil texture was similar to those reported in previous studies for MDF dominated by sandy loam and loam soils (Staelens et al., 2011). Furthermore, environmental factors are complex and interrelated. Topographic factors such as elevation and slope are positively interrelated (Du et al., 2017; Zhang et al., 2013). The elevation range of the permanent plot was 290-360 m.a.s.l., and higher elevation and slope have been associated with increased distance to the nearest stream, which produces a soil moisture gradient (Rong et al., 2017).

3.4 Relationships between tree species occurrence and environmental factors

We performed CCA analyses to evaluate the effects of various environmental factors on species occurrence separately for saplings (DBH<4.5 cm) and trees (DBH ≥4.5 cm). Among trees, the results showed strong correlations between species and all environmental variables, with eigenvalues of 0.31 and 0.20 for the first (CCA1) and second (CCA2) axes, respectively. These high values indicate good predictive performance for species distribution and abundance**.** Pearson correlation analysis showed that the environmental factors were strongly correlated to species occurrence for axis 1 (R=0.860) and axis 2 (R=0.810). The Monte Carlo permutation test confirmed that axis 1 significantly explained the relationship between species occurrence and environmental factors ($p<0.01$). Elevation, slope and distance to the nearest stream strongly influenced the distributions of *Pterocarpus macrocarpus*, *Anogeissus acuminata*, *Terminalia bellirica*, *Markhamia stipulata* var. *stipulata*, and *Gmelina arborea*. These species favored high elevation and longer distances from the nearest river, indicating that they prefer dry conditions for establishment (Phumphuang et al., 2018; Sasunti, 2021). By contrast, dry evergreen forest species such as *Duabanga grandiflora* and *Albizia lucidior* were mainly located in moist sites close to rivers. Some pioneer species were also found in these areas, such as *Ficus auriculata*, *Ficus racemose*, and *Bischofia javanica* (Figure 5). Silt and sand content, as well as soil pH strongly influenced the occurrence of *Horsfieldia amygdalina*, *Pterospermum acerifolium*, *Artocarpus rigidus*, *Protium serratum*, and *Persea declinata*. Clay content, which was negatively correlated with silt and sand content and pH, influenced the distribution of *Xylia xylocarpa* var. *kerrii*, *Dipterocarpus alatus*, and *Artocarpus lacucha*. Many pioneer species such as *Ficus* species and late succession species such as *Duabanga grandiflora* mainly occupied areas with high soil moisture content, as reported previously (Pothasin et al., 2014; Albrecht et al., 2017; Leishangthem and Singh, 2018).

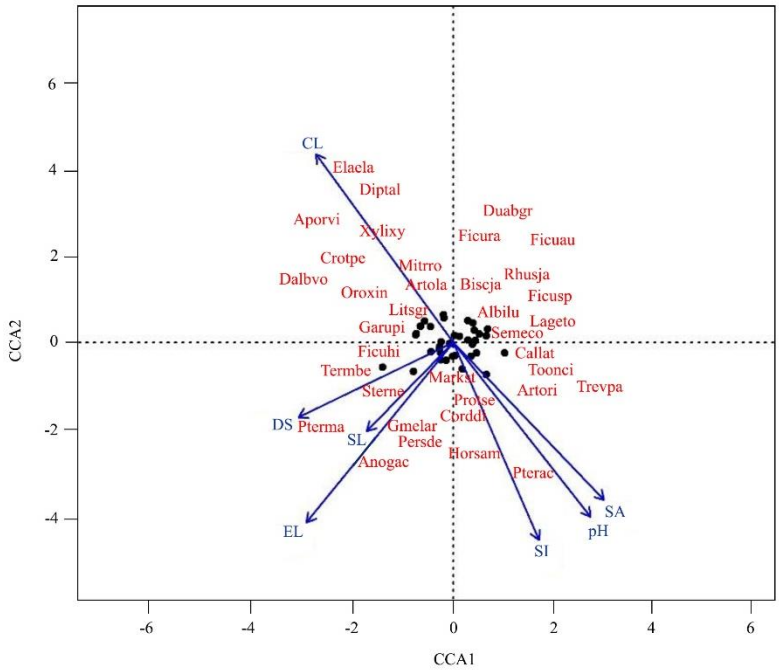

Figure 5. Canonical correspondence analysis ordination diagram for tree species occurrence and environmental factors. Tree species abbreviations are provided in Table S1.

The CCA results for saplings showed eigenvalues of 0.26 and 0.16 for the first (CCA1) and second (CCA2) axes, respectively, and high Pearson's correlation coefficients for both axis 1 (R=0.882) and axis 2 (R=0.872).The Monte Carlo permutation test confirmed that axis 1 significantly explained the tree occurrence variation ($p<0.01$). Silt content, elevation and slope strongly influenced the occurrence of *Monoon viride*, *Siphonodon celastrineus*, *Croton persimilis*, and *Pterospermum acerifolium* (Figure 6). Clay content influenced the regeneration of lowland species such as *Streblus ilicifolius*, *Flacourtia indica*, *Rhus javanica*, *Millettia brandisiana*, and *Baccaurea ramiflora*. Organic matter strongly influenced the occurrence of species including *Dalbergia volubilis*, *Ficus hispida*, and *Terminalia bellirica* but did not influence tree regeneration. These findings indicate that organic matter is more important for providing soil nutrients at the sapling stage than at the mature stage. Previous studies also reported that nutrient availability and soil texture were the major determinants of plant species distribution (Sellan et al., 2019; Marod et al., 2019).

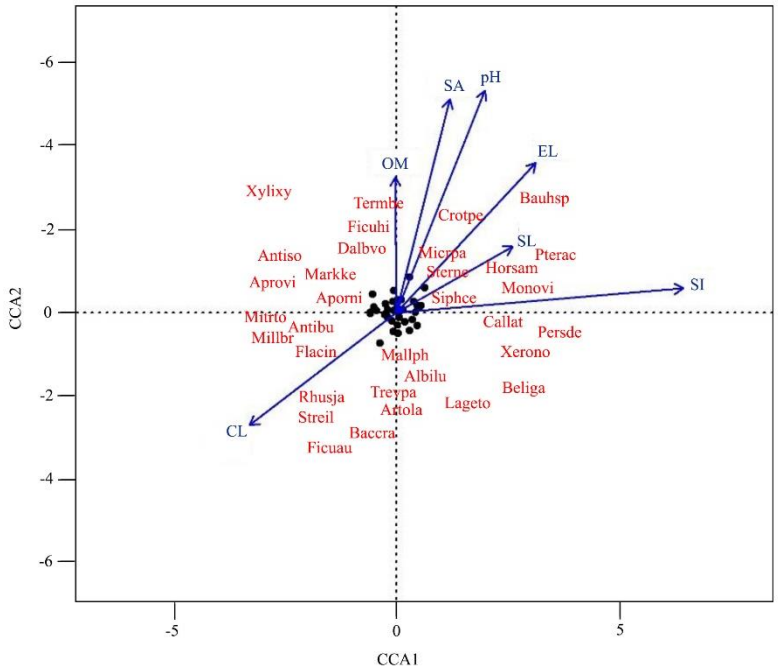

Figure 6. Canonical correspondence analysis ordination diagram for sapling species occurrence and environmental factors. Tree species abbreviations are provided in Table S1.

During the early successional stages, environmental factors significantly influence tree species regeneration, particularly under drought and poor soil conditions (Lebrija-Trejos et al., 2011). Facilitation allows plant species to resist and survive under adverse climate conditions (Bagousse-Pinguet et al., 2014). Thus, pioneer species play a major role in forest restoration in large disturbed areas, by facilitating the establishment of suitable conditions for vegetation restoration, especially soil properties such as increased soil organic matter and nutrients through the accumulation of plant litter (Wang et al., 2016; Zhao et al., 2017). Recently, the cultivation of fast-growing pioneer species (i.e., nurse crops or framework species) has been applied to accelerate natural regeneration (Elliott et al., 2003; Fagundes et al., 2018; Boeschoten et al., 2021). Thus, larger populations of climax species such as *Lagerstroemia tomentosa* in MDF and *Callerya atropurpurea* in dry evergreen forests are establishing throughout the permanent plot, particularly at moist, low-elevation sites (Figure 7(a, b)). By contrast, species such as *Pterocarpus macrocarpus* prefer dry conditions, and are mainly distributed at higher elevations (Figure 7(c)). Some pioneer species persist, such as *Croton persimilis* (Figure 7(d)), whereas species such as *Trema orientalis* was dense on high soil moisture area (180.43 stem/ha) in the early successional stage (Marod, 1995; Takahashi et al., 1995) have almost become depleted (0.625 stem/ha) at present. *Trevesia palmata* was almost exclusively found along river banks (Figure 7(e)), indicating an ecological niche for

this species. These data are important for the selection of suitable pioneer and late successional or climax species for forest restoration programs, to shorten the forest recovery period in degraded areas of Thailand.

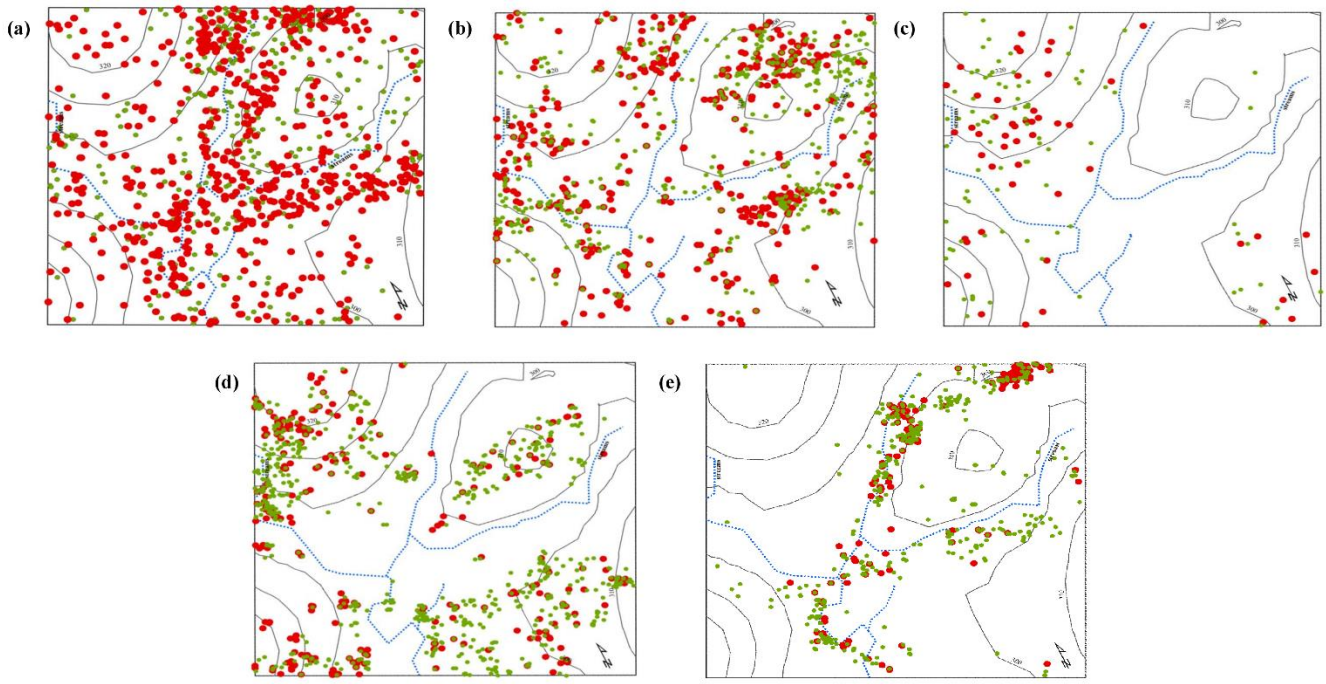

Figure 7. Tree species distribution in the 16-ha permanent plot: (a) *Lagerstroemia tomentosa*, (b) *Callerya atropurpurea*, (c) *Pterocarpus macrocarpus*, (d) *Croton persimilis*, and (e) *Trevesia palmata*. Each dots indicate position of tree (DBH ≥ 4.5, red dots) and sapling (DBH < 4.5, green dots) in the 16 ha permanent plot.

4. CONCLUSION

The natural forest restoration in the 16-ha permanent plot after abandonment about 30 years from shifting cultivation is under well-recovery. The initiated recovery was occupied by herbaceous species, then, drastically depleted and replaced by woody species at high tree density (605 stems/ha) and low basal area (6.91 m^2/ha). Forest fire disturbances were observed, in particular, during the first ten-year recovery period (1990-2000). It not only burnt the herbaceous species but also some pioneer species such as *Trema orientalis*. Then, the coexisted tree species between pioneer and climax species were observed, although, less diversity of pioneer was found. The result from CCA showed that high relationship between tree species and environments for their distribution and coexisting was found. Some species had distinct ecological niches, with dry evergreen forest species preferring moist lowland sites, compared with MDF species. The climax species as *Lagerstroemia tomentosa* showed particularly successful regeneration in the study area which represented by highest IVI, whereas other species recovered more slowly in response to environmental changes. While, pioneer species such as *Musa acuminata*, *Eupatorium odoratum*, *Trema orientalis*, and several *Ficus* species facilitated the formation of a suitable environment for climax species establishment, particularly in terms of increased soil fertility and moisture content. This study was conducted in a watershed with a small area of degraded land (ca. 1 km^2); therefore, the environmental conditions were not so severe as to preclude plant succession, and remnant climax species provided potential seed sources for natural forest regeneration, which can be a key factor in forest recovery.

Therefore, the history of land use changes and the scale and intensity of past disturbances should be considered in designing management strategies to promote natural forest restoration. However, artificial restoration programs should be conducted in regions with large degraded areas and high disturbance intensity. In such regions, we recommend planting both pioneer species such as *Trema orientalis* and *Ficus* trees, and late successional or climax species, *Pterocarpus macrocarpus*, *Terminalia bellirica*, *Lagerstroemia tomentosa*, and *Artocarpus rigidus*, to shorten the recovery period and promote natural regeneration where possible.

ACKNOWLEDGEMENTS

This research was supported in part by a Graduate Program Scholarship from The Graduate School, Kasetsart University, Bangkok, Thailand. We are grateful to the staff of the Mae Klong Watershed Research Station and students from the Thai Forest Ecological Research Network (T-FERN) for their help in the field data collection.

REFERENCES

Aide TM, Zimmerman JK, Pascarella JB, Rivera L, Marcano-Vega H. Forest regeneration in a chronosequence of tropical abandoned pastures: Implications for restoration ecology. Restoration Ecology 2000;8(4):328-38.

Albrecht L, Stallard RF, Kalko EK. Land use history and population dynamics of free-standing figs in a maturing forest. PLoS ONE 2017;12(5):e0177060.

Allison L. Organic carbon. In: Black CA, editor. Methods of Soil Analysis: Part 2 Chemical and Microbiological Properties. Wisconsin: American Society of Agronomy; 1965. p. 1367-78.

Bagousse-Pinguet Y, Xiao S, Brooker RW, Gross N, Liancourt P, Straile D, et al. Facilitation displaces hotspots of diversity and allows communities to persist in heavily stressed and disturbed environments. Journal of Vegetation Science 2014;25(1):66-76.

Beck R. Soil Analysis Handbook of Reference Methods. New York, USA: CRC Press; 1999.

Boeschoten LE, van Breugel M, Bailon M, Balbuena J, Nuñez M, Cerezo A, et al. Framework species approach proves robust in restoring forest on fire prone invasive grass: A case study from Panama. Journal of Sustainable Forestry 2021;40(2):197-215.

Bray RH, Kurtz LT. Determination of total, organic, and available forms of phosphorus in soils. Soil Science 1945;59(1):39-46.

Chaiyo U, Garivait S, Wanthongchai K. Structure and carbon storage in aboveground biomass of mixed deciduous forest in western region, Thailand. GMSARN International Journal 2012;6:143-50.

Chapman HD. Cation exchange capacity. In: Black CA, Evans DD, White JL, Ensminger LE, Clark FE, Dinauer DC, editors. Method of Soil Analysis, Part 2: Chemical and Microbiological Properties. Madison (WI): The American Society of Agronomy; 1965. p. 891-913.

Chave J, Condit R, Muller-Landau HC, Thomas SC, Ashton PS, Bunyavejchewin S, et al. Assessing evidence for a pervasive alteration in tropical tree communities. PLoS Biology 2008;6(3):e45.

Chazdon RL. Tropical forest recovery: Legacies of human impact and natural disturbances. Perspectives in Plant Ecology, Evolution and Systematics 2003;6(1-2):51-71.

Chazdon RL. Second Growth. Chicago: University of Chicago Press; 2014.

Chen X, Wang X, Li J, Kang D. Species diversity of primary and secondary forests in Wanglang Nature Reserve. Global Ecology and Conservation 2020;22:e01022.

Collins LM, Schafer JL, Kam CM. A comparison of inclusive and restrictive strategies in modern missing data procedures. Psychological Methods 2001;6(4):Article No. 330.

Curtis PG, Slay CM, Harris NL, Tyukavina A, Hansen MC. Classifying drivers of global forest loss. Science 2018; 361(6407):1108-11.

Delgado-Baquerizo M, Reich PB, Trivedi C, Eldridge DJ, Abades S, Alfaro FD, et al. Multiple elements of soil biodiversity drive ecosystem functions across biomes. Nature Ecology and Evolution 2020;4(2):210-20.

Du H, Hu F, Zeng F, Wang K, Peng W, Zhang H, et al. Spatial distribution of tree species in evergreen-deciduous broadleaf karst forests in Southwest China. Scientific Reports 2017;7(1):1-9.

Elliott S, Navakitbumrung P, Kuarak C, Zangkum S, Anusarnsunthorn V, Blakesley D. Selecting framework tree species for restoring seasonally dry tropical forests in Northern Thailand based on field performance. Forest Ecology and Management 2003;184(1-3):177-91.

Fagundes M, Weisser W, Ganade G. The role of nurse successional stages on species-specific facilitation in drylands: Nurse traits and facilitation skills. Ecology and Evolution 2018;8(10):5173-84.

Food and Agriculture Organization of the United Nation (FAO), United Nation Environment Programme (UNEP). The State of the World's Forests 2020: Forests, Biodiversity and People. Rome, Italy: FAO; 2020.

Geist HJ, Lambin EF. Proximate causes and underlying driving forces of tropical deforestation tropical forests are disappearing as the result of many pressures, both local and regional, acting in various combinations in different geographical locations. BioScience 2002;52(2):143-50.

Good SP, Noone D, Bowen G. Hydrologic connectivity constrains partitioning of global terrestrial water fluxes. Science 2015;349(6244):175-7.

Goodale UM, Ashton MS, Berlyn GP, Gregoire TG, Singhakumara BMP, Tennakoon KU. Disturbance and tropical pioneer species: Patterns of association across life history stages. Forest Ecology and Management 2012;277(1):54-66.

Gravel D, Canham CD, Beaudet M, Messier C. Shade tolerance, canopy gaps and mechanisms of coexistence of forest trees. Oikos 2010;119(3):475-84.

Gustafsson N, Culley S, Ashdown G, Owen DM, Pereira PM, Henriques R. Fast live-cell conventional fluorophore nanoscopy with ImageJ through super-resolution radial fluctuations. Nature Communications 2016;7(1):Article No. 12471.

Hansen MC, DeFries RS. Detecting long-term global forest change using continuous fields of tree-cover maps from 8-km advanced very high resolution radiometer (AVHRR) data for the years 1982-99. Ecosystems 2004;7(7):695-716.

Hooker TD, Compton JE. Forest ecosystem carbon and nitrogen accumulation during the first century after agricultural abandonment. Ecological Applications 2003;13(2):299-313.

Kamyo T. Gep-Informatics Modeling on Tropical Seasonal Forest Dynamics in Mae Klong Watershed Research Station, Kanchanaburi Province [dissertation]. Bangkok, Kasetsart University; 2016.

Kamyo T, Thinkampaeng S, Panuthai S, Tanaka H, Marod D. Natural forest regeneration in abandoned areas in Mae Klong Watershed Research Station Thong PhaPhoom District, Kanchanaburi Province. Proceedings of the 2nd Thai Forest Ecological Research Network Conference; 2013 Jan 24-26; Maejo University, Chiangmai: Thailand; 2013 (in Thai).

Kamyo T, Marod D, Pattanakiat S, Suksawang S, Panuthai S. Land cover changes in tropical seasonal forests at Mae Klong head watershed, Kanchanaburi Province, Thailand. Maejo

International Journal of Science and Technology 2016; 10(3):304-12.

Keeley JE, Bond WJ. Mast flowering and semelparity in bamboos: The bamboo fire cycle hypothesis. The American Naturalist 1999;154(3):383-91.

Khamyong N, Wangpakapattanawong P, Chairuangsri S, Inta A, Tiansawat P. Tree species composition and height-diameter allomery of three forest types in northern Thailand. Chiang Mai University Journal Of Natural Sciences 2018;17(4):289-306.

Klemick H. Shifting cultivation, forest fallow, and externalities in ecosystem services: Evidence from the Eastern Amazon. Journal of Environmental Economics and Management 2011;61(1):95-106.

Krebs CJ. Ecology: The Experimental Analysis of Distribution and Abundance. New York, USA: Harper Collins Publishers; 1994.

Kutintara U, Marod D, Takahashi M, Nakashizuka T. Growth and dynamics of bamboos in a tropical seasonal forest. In: The International Workshop on the Changes of Tropical Forest Ecosystems by El Niño and Others. Bangkok, Thailand: National Research Council; 1995.

Lacerda AEB, Kellermann B. What is the long-term effect of bamboo dominance on adult trees in the Araucaria Forest? A comparative analysis between two successional stages in southern Brazil. Diversity 2019;11(9):Article No. 165.

Larpkern P, Moe SR, Totland Ø. Bamboo dominance reduces tree regeneration in a disturbed tropical forest. Oecologia 2011; 165:161-8.

Laurance WF. Have we overstated the tropical biodiversity crisis? Trends in Ecology and Evolution 2007;22(2):65-70.

Lebrija-Trejos E, Pérez-García EA, Meave JA, Poorter L, Bongers F. Environmental changes during secondary succession in a tropical dry forest in Mexico. Journal of Tropical Ecology 2011;27(5):477-89.

Leishangthem D, Singh MR. Tree diversity, distribution and population structure of a Riparian Forest from certain zones along the Dikhu River in Nagaland, India. Journal of Forest and Environmental Science 2018;34(1):31-45.

Lepore M, Arellano G, Condit R, Davies S, Detto M, Gonzales-Akre E, et al. Fgeo: Analyze forest diversity and dynamics [Internet]. 2019 [cited 2021 May 7]. Available from: https://CRAN.R-project.org/package=fgeo.

Lewis SL, Edwards DP, Galbraith D. Increasing human dominance of tropical forests. Science 2015;349(6250):827-32.

Mabry CM, Fraterrigo JM. Species traits as generalized predictors of forest community response to human disturbance. Forest Ecology and Management 2009;257(2):723-30.

Marod D. Secondary Successional Pattern in Mixed Deciduous Forest of Mae Klong Watershed Research Station Changwat Kanchanavuri [dissertation]. Bangkok, Kasetsart University; 1995 (in Thai).

Marod D, Duengkae P, Sangkaew S, Racharak P, Suksavate W, Uthairatsamee S, et al. Population structure and spatial distribution of tree species in lower Montane Forest, Doi Suthep-Pui National Park, Northern Thailand. Environment and Natural Resources Journal 2022;20(6):644-63.

Marod D, Hermhuk S, Sungkaew S, Thinkampheang S, Kamyo T, Nuipakdee W. Species composition and spatial distribution of dominant trees in the forest ecotone of a mountain ecosystem, northern Thailand. Environment and Natural Resources Journal 2019;17(3):40-9.

Marod D, Kutintara U. Forest Ecology. Bangkok: Department of Forest Biology, Faculty of Forestry; 2009 (in Thai).

Marod D, Kutintara U, Yarwudhi C, Tanaka H, Nakashisuka T. Structural dynamics of a natural mixed deciduous forest in western Thailand. Journal of Vegetation Science 1999; 10(6):777-86.

Marod D, Kutintara U, Tanaka H, Nakashizuka T. The effects of drought and fire on seed and seedling dynamics in a tropical seasonal forest in Thailand. Plant Ecology 2002;161:41-57.

Marod D, Kutintara U, Tanaka H, Nakashizuka T. Effects of drought and fire on seedling survival and growth under contrasting light conditions in a seasonal tropical forest. Journal of Vegetation Science 2004;15(5):691-700.

Marod D, Lamthai A, Duengkae P, Pattanavibool A. Vegetation structure and floristic composition along the edge of Montane Forest and agricultural land in Um Phang Wildlife Santuary, Western Thailand. Agriculture and Natural Resources 2012; 46(2):162-80.

Matsuo T, Martínez-Ramos M, Bongers F, van der Sande MT, Poorter L. Forest structure drives changes in light heterogeneity during tropical secondary forest succession. Journal of Ecology 2021;109(8):2871-84.

Miles L, Newton AC, DeFries RS, Ravilious C, May I, Blyth S, et al. A global overview of the conservation status of tropical dry forest. Journal of Biogeography 2006;33(3):491-505.

Mohandass D, Hughes AC, Mackay B, Davidar P, Chhabra T. Floristic species composition and structure of a mid-elevation tropical montane evergreen forests (sholas) of the western ghats, southern India. Tropical Ecology 2016;57(3):533-43.

Mondoni A, Orsenigo S, Abeli T, Rossi G, Brancaleoni L, Corli A, et al. Plant regeneration above the species elevational leading edge: Trade-off between seedling recruitment and plant production. Frontiers in Ecology and Evolution 2020;8:Article No. 572878.

Phumphuang W, Marod D, Sungkaew S, Thinkampaeng S. Forest dynamics and tree distribution patterns in dry evergreen forest, northeastern, Thailand. Environment and Natural Resources Journal 2018;16(2):58-67.

Poorter L, Rozendaal DM, Bongers F, Almeida DJS, Álvarez FS, Andrade JL, et al. Functional recovery of secondary tropical forests. Proceedings of the National Academy of Sciences 2021;118(49):e2003405118.

Pothasin P, Compton SG, Wangpakapattanawong P. Riparian Ficus tree communities: The distribution and abundance of riparian fig trees in Northern Thailand. PLoS ONE 2014;9(10):e108945.

Quesada M, Stoner KE. Threats to the conservation of the tropical dry forest in Costa Rica. In: Frankie GW, Mata A, Vinson SB, editors. Biodiversity Conservation in Costa Rica: Learning the Lessons in a Seasonal Dry Forest. Berkeley: University of California Press; 2004. p. 266-80.

R Core Team. A language and environment for statistical computing, R Foundation for Statistical Computing [Internet]. 2017 [cited 2020 Jun 15]. Available from: http://www.R-project.org/.

Rong L, Duan X, Feng D, Zhang G. Soil moisture variation in a farmed dry-hot valley catchment evaluated by a redundancy analysis approach. Water 2017;9(2):Article No. 92.

Rother DC, Pizo MA, Siqueira T, Rodrigues RR, Jordano P.

Community-wide spatial and temporal discordances of seed-seedling shadows in a tropical rainforest. PLoS ONE 2015;10(4):e0123346.

Rueangket A, Duengkae P, Thinkhampang S, Marod D. Utilization of fruit by frugivores in lower montane forest at Doi Suthep-Pui National Park, Chiang Mai Province. Agriculture and Natural Resources 2019;53(5):457-64.

Sanchez-Azofeifa GA, Quesada M, Calvo J, Rodriguez JP, Nassar J, Garvin T, et al. Research priorities for tropical secondary dry forests. Biotropica 2005;37:477-85.

Sangsupan HA, Hibbs DE, Withrow-Robinson BA, Elliott S. Effect of microsite light on survival and growth of understory natural regeneration during restoration of seasonally dry tropical forest in upland northern Thailand. Forest Ecology and Management 2021;489:Article No. 119061.

Sann B, Kanzaki M, Ohta S. Vegetation patterns and species-filtering effects of soil in secondary succession in a tropical dry forest in central Myanmar. Journal of Tropical Ecology 2016;32(2):116-24.

Sasunti A, Asanog L. Tree Species Regeneration in Forest Restoration Area by Economic Tree at Nan Watershed, Nan Province [dissertation]. Chiang Mai, Maejo University; 2021.

Scheper AC, Verweij PA, Kuijk VM. Post-fire forest restoration in the humid tropics: A synthesis of available strategies and knowledge gaps for effective restoration. Science of the Total Environment 2021;771:Article No. 144647.

Sellan G, Thompson J, Majalap N, Brearley FQ. Soil characteristics influence species composition and forest structure differentially among tree size classes in a Bornean heath forest. Plant and Soil 2019;438(1):173-85.

Shannon CE, Weaver W. The Mathematical Theory of Communication. Illinois, United States of America: University of Illinois Press; 1949.

Shumi G, Dorresteijn I, Schultner J, Hylander K, Senbeta F, Hanspach J, et al. Woody plant use and management in relation to property rights: A social-ecological case study from southwestern Ethiopia. Ecosystems and People 2019; 15(1):303-16.

Smitinand T. Thai Plant Names. Bangkok, Thailand: Department of National Parks, Wildlife and Plant Conservation; 2014 (in Thai).

Soil Science Division Staff. Soil Survey Manual: United States Department of Agriculture Handbook No. 18. USA: United States Department of Agriculture; 2017.

Staelens J, Nachtergale L, Schrijver DA, Vanhellemont M, Wuyts K, Verheyen K. Spatio-temporal litterfall dynamics in a 60-year-old mixed deciduous forest. Annals of Forest Science 2011;68:89-98.

Suksawang S. Site Overview: Thong Pha Phoom Study Site. Bangkok, Thailand: Royal Forest Department; 1993.

Sullivan MJ, Talbot J, Lewis SL, Phillips OL, Qie L, Begne SK, et al. Diversity and carbon storage across the tropical forest biome. Scientific Reports 2017;7(1):Article No. 39102.

Swinfield T, Afriandi R, Antoni F, Harrison RD. Accelerating tropical forest restoration through the selective removal of pioneer species. Forest Ecology and Management 2016; 381:209-16.

Takahashi M, Kutintara U, Eaidthong W, Kobayashi S. Changes of the vegetation pattern in different successional stages. Proceedings of the International Workshop on the Changes of Tropical Forest Ecosystems by El Niño and Others; 1995 Feb 7-10; Kanchanaburi: Thailand; 1995.

Takahashi M, Marod D, Panuthai S, Hirai K. Carbon cycling in teak plantations in comparison with seasonally dry tropical forests in Thailand. In: Blanco JA, Lo YH, editors. Forest Ecosystems More Than Just Trees. Rijeka: InTech; 2012. p. 209-30.

Thein HM, Kanzaki M, Fukushima M. Structure and composition of a teak-bearing forest under the Myanmar Selection System: impacts of logging and bamboo flowering. Southeast Asian Studies 2007;45(3):303-16.

Van Hall RL, Cammeraat LH, Keesstra SD, Zorn M. Impact of secondary vegetation succession on soil quality in a humid Mediterranean landscape. Catena 2017;149:836-43.

Wang J, Wang H, Cao Y, Bai Z, Qin Q. Effects of soil and topographic factors on vegetation restoration in opencast coal mine dumps located in a loess area. Scientific Reports 2016;6(1):1-11.

Wang XY, Ling HB, Xu HL, De Pan C, Yuan KY. Relationships between plant communities and environmental factors in an extremely arid area: A case study in China. Polish Journal of Environmental Studies 2019;28(1):359-70.

Wright SJ. Tropical forests in a changing environment. Trends in Ecology and Evolution 2005;20(10):553-60.

Yarwudhi C, Tanaka N, Kobayashi S, Marod D, Kutintara U, Tabaka H, et al. Regeneration dynamics of tree after the simultaneous flowering and death of undergrowing bamboo in a mixed deciduous forest, western Thailand. Proceedings of the International Workshop on the Responses of Tropical Forest Ecosystem to Long Term Cyclic Climate Changes; 2000 Jan 24-27; Kanchanaburi: Thailand; 2000.

Zhang ZH, Hu G, Ni J. Effects of topographical and edaphic factors on the distribution of plant communities in two subtropical karst forests, Southwestern China. Journal of Mountain Science 2013;10(1):95-104.

Zhao H, Wang QR, Fan W, Song GH. The relationship between secondary forest and environmental factors in the southern Taihang Mountains. Scientific Reports 2017;7(1):Article No. 16431.

Characterization and Adsorption Mechanism of Methylene Blue Dye by Mesoporous Activated Carbon Prepared from Rice Husks

Suchada Sawasdee* and Prachart Watcharabundit

Faculty of Science and Technology, Thepsatri Rajabhat University, Lop Buri 15000, Thailand

ARTICLE INFO

Received: 2 Mar 2023
Received in revised: 7 Jul 2023
Accepted: 14 Jul 2023
Published online: 21 Sep 2023
DOI: 10.32526/ennrj/21/20230074

Keywords:
Adsorption/ Activated carbon/ Rice husks/ Methylene blue/ Mesopore

*** Corresponding author:**
E-mail: ps_neng@hotmail.com

ABSTRACT

Environmental contamination due to synthetic dyes is a severe problem due to their adverse eco-toxicological effects. This study prepared activated carbon from H_3PO_4-activated rice husks (AC-RH) to adsorb methylene blue (MB) and predicted the adsorption mechanism. The AC-RH was characterized for N_2 adsorption, surface functional groups, chemical compositions, and surface morphology. The activated carbon was classified to be a mesoporous material because 87% of its pore volume diameters are 3-50 nm. MB adsorption was studied under different conditions. Optimal MB adsorption occurred at pH 8, and the ideal equilibrium time was 360 min. The equilibrium adsorption was evaluated at concentrations of MB between 25 and 200 mg/L at 30°C. The Freundlich isotherm model matched the equilibrium data, and the greatest adsorption capacity of the Langmuir isotherm was 26.31 mg/g. The kinetic analysis revealed that the adsorption was pseudo-second-order, and its rate constant (k_2) was higher at higher temperatures. For the thermodynamic adsorption study at 20 to 40°C, the Gibbs free energy (ΔG) values were -6.291 to -9.197 kJ/mol, and the activation energy (E_a) was 26.248 kJ/mol: therefore, the methylene blue adsorption was spontaneous and physical. This study also revealed that the adsorption mechanisms were H-bonding, pore-filling, Yoshida H-bonding, n-π interactions, electrostatic, and cation exchange.

1. INTRODUCTION

Synthetic dyes are employed in the textile industry, including pulp mills, paper, printing, plastics, foods, and leather, and dye molecules degrade poorly in response to light, heat, and chemicals (Han et al., 2012). Most dyes are toxic and cause serious difficulties for the ecological system; water contaminated with dye harms aquatic life. Methylene blue (MB), a cationic dye, is often used for coloring and dyeing and is found in high concentrations in industrial effluent (Patawat et al., 2020). MB is a stable molecule that is not readily biodegradable (Hu et al., 2017), and it can cause health problems, including increased heart rate, vomiting, shock, cyanosis, mental confusion, eye burns, tissue necrosis, headache, nausea, and chest discomfort (Uner et al., 2016). Various treatment methods have been utilized for dye removal in effluents, and adsorption is widely used to treat dyes from wastewater since it is a low-cost process with excellent efficiency (Uner et al., 2016).

An activated carbon (AC) adsorbent can be utilized in water treatment because its surface area is large, and the functional groups that exist on its surfaces lead to a significant interaction in the adsorptive capacities of activated carbons (Kumar and Jena, 2016; Jawad et al., 2017). Commercial activated carbon is expensive and hard to reuse; hence, AC should be produced from cheap, readily available materials. Several investigations (Zazouli et al., 2016; Patawat et al., 2020; Han et al., 2020) have been conducted to search for activated carbons prepared from agricultural by-products or waste.

Rice husks are agricultural waste, and their residues are abundant in Thailand, ~7.5×10^9 kg per year (Wantaneeyakul et al., 2021). The main components of rice husks are organic matter (70-85%) and mineral components (20-30%), such as silica,

Citation: Sawasdee S, Watcharabundit P. Characterization and adsorption mechanism of methylene blue dye by mesoporous activated carbon prepared from rice husks. Environ. Nat. Resour. J. 2023;21(5):458-470. (https://doi.org/10.32526/ennrj/21/20230074)

alkalis, and trace elements (Hossain et al., 2018). Shrestha et al. (2019) have used NaOH, $ZnCl_2$, and KOH to create nanoporous carbon material from rice husks, whereas Sharma and Uma (2010) have carbonized rice husks for 2 h at 650°C with a nitrogen flow of 150 mL/min to adsorb MB dye. Phosphoric acid (H_3PO_4) treatment, according to Al-Asadi et al. (2023), might increase the ability of activated carbon produced from fig leaves to adsorb MB from aqueous solutions, when compared to other activating agents, such as NaOH and H_2SO_4. No study has discussed the adsorption mechanism of rice husk-activated carbon and MB. This work generated activated carbon from rice husks (AC-RH) using H_3PO_4 as an activator, which was subsequently used to adsorb MB, and the adsorption mechanism was explained. The AC was characterized using N_2 adsorption, surface functional groups, chemical compositions, and surface morphology. The adsorption variables were investigated for the highest adsorption, and the data obtained were analyzed using the isotherm and kinetic models. Also, thermodynamic adsorption was evaluated in order to calculate the Gibbs free energy (ΔG), enthalpy (ΔH), and entropy (ΔS). The overall results were used to confirm the adsorption mechanism.

2. METHODOLOGY

2.1 Material preparations

The rice husks employed in this investigation originated at a rice mill in Lopburi, Thailand. The rice husks were oven-dried at 80°C after being cleaned with distilled water. The dried rice husks were soaked in 1.0 mol/L H_3PO_4 at a ratio of 1/20 (g/mL) for a day. They were then oven-dried at 100°C. At 500°C for 1 h, the dried char was carbonized. It was then rinsed thoroughly with water that had been distilled until its pH value was neutral. The AC was dried and ground into powder. Then, it was sieved to 150-300 µm particle size. It was dried and kept in a desiccator for use as the adsorbent.

MB (CI 52015, $C_{16}H_{18}N_3SCl$, Merck, Germany, M.W. 319.98 g/mol) was used as the adsorbate. By diluting a 1,000 mg/L stock solution with distilled water, working solutions of MB (25-200 mg/L) were obtained. The MB solution was adjusted to the required pH (OHAUS Starter 5000, USA.) by adding hydrochloric acid (0.1 M) or sodium hydroxide (0.1 M). The analytical-grade phosphoric acid (H_3PO_4), sodium hydroxide (NaOH), and hydrochloric acid (HCl) were purchased from Merck and Co.

2.2 Characterization of adsorbent

The N_2 adsorption of the adsorbent was determined using a gas sorption analyzer (Autosorb 1 MP, Quantachrome Instruments, USA), and the adsorption data was used to determine the Brunauer-Emmett-Teller (BET) surface area and Barrett-Joyner-Halenda (BJH) pore size distribution. The surface functional groups, chemical compositions, and surface morphology were analyzed using Fourier transform infrared (FTIR) spectroscopy (Model two, Perkin Elmer, USA), X-ray fluorescence (XRF) spectrometry (MESA-500W, HORIBA, Japan), X-ray diffraction (XRD) spectrometry (Smartlab2, Rigaku Japan), and scanning electron microscopy (SEM, 1450 VP LEO, Leo, UK).

The pH at the point of zero charges, pH_{pzc}, was determined using the pH drift method. A series of 0.1 M KNO_3 solutions were prepared with pH values between 2 and 12. The solution pH was adjusted by adding 0.1 M HCl and 0.1 M NaOH and measured using a pH meter. Then, 0.1 g of adsorbent was added for every 100 mL of 0.1 M KNO_3 solution, and the mixtures were shaken at 150 rpm for 48 h. Each mixture was filtered, and its pH was measured. The pH_{pzc} was calculated by plotting the curve of each ΔpH (pH_{final}-$pH_{initial}$) against $pH_{initial}$. The pH_{pzc} is when the curve (ΔpH vs. $pH_{initial}$) meets the line ΔpH=0.

2.3 Adsorption studies

During the batch adsorption test, the suspended combination of 100 mL of dye solution and 0.6 g of adsorbent was placed into a series of 250-mL Erlenmeyer flasks. The adsorption experiments were conducted at pH 2-10, contact time of 1-540 min, initial dye concentrations of 25-200 mg/L, and temperatures between 20-40°C. The suspended sample in each flask was shaken at 200 rpm. After the sample was filtered at the appointed time, the amount of dye still present in the solution was measured using an UV-visible spectrophotometer (Specord 210 plus, Analytik Jena, Germany) operating at a wavelength of 665 nm. The adsorption capacity (q_t) was determined as follows:

$$q_t = (C_o - C_t)\ V/M \quad (1)$$

Where; C_o (mg/L) and C_t (mg/L) are the concentration of MB dye at initial and any time, respectively; V (L) is the volume of MB dye solution; q_t (mg/g) is the adsorption capacity at any time; and W (g) is the mass of the adsorbent. All the adsorption

experiments were performed in triplicate, and the average adsorption capacity values were used for data analysis.

The adsorption data were analyzed using the linear forms of the pseudo-first-order, pseudo-second-order kinetic, and intraparticle diffusion kinetic models, which are Equations. (2), (3), and (4), respectively.

$$\log(q_e - q_t) = \log q_e - k_1 t/2.303 \quad (2)$$

$$t/q_t = (1/k_2 q_e^2) + t/q_e \quad (3)$$

$$q_e = K_{id}(t)^{1/2} + C \quad (4)$$

Where; k_1 (1/min) and k_2 (g/mg/min) are the rate constant of the pseudo-first-order and pseudo-second-order models, respectively, K_{id} (mg/g/min$^{1/2}$) is the intraparticle diffusion constant, and C (mg/g) is the intercept representing the thickness of the external diffusion layer. Also, q_e (mg/g) is the adsorption capacity at equilibrium.

The adsorption data at equilibrium were analyzed using the non-linear forms of the Langmuir, Freundlich, and Redlich-Peterson isotherm models, which are presented in Equations (5), (6), and (7), respectively:

$$q_e = q_{max} K_L C_e/(1 + C_e K_L) \quad (5)$$

$$q_e = K_F C_e^{1/n} \quad (6)$$

$$q_e = A C_e/(1 + B C_e^g) \quad (7)$$

Where; q_e (mg/g) is the equilibrium adsorption capacity; C_e (mg/L) is the equilibrium concentration of adsorbate; K_L (L/mg) is the Langmuir constant; and q_{max} (mg/g) is the maximum adsorption capacity. For the Freundlich isotherm, K_F (L/g) is the adsorption capacity and 1/n is the adsorption intensity. A (L/g) and B (L/mg) are the Redlich-Peterson isotherm constants, and g is an exponent between 0 and 1. As stated in Equation (8), we calculated the non-linear coefficient of determination (R^2) to assess the fit of an isotherm model to the experimental data (Islam et al., 2015).

$$R^2 = 1 - \frac{\sum_{N=1}^{N}(q_{e.exp} - q_{e.mod})^2}{\sum_{N=1}^{N}(q_{e.exp} - \overline{q_{e.exp}})^2} \quad (8)$$

Where; N is the number of experimental data, $q_{e.exp}$ and $q_{e.mod}$ are the experimental and isotherm model-predicted adsorption capacities at equilibrium, respectively. Further, $q_{\overline{e.exp}}$ is the average of $q_{e.exp}$.

2.4 Adsorption thermodynamics

The adsorption thermodynamics explains the energy change and the mechanism involved in the adsorption process. According to Equation (9), the Gibbs free energy (ΔG) is related to the equilibrium constant, K_c(K_c=q_e/C_e). The linear curve is given by the plot of ln K_c versus 1/T in Equation (10). The enthalpy (ΔH) and entropy (ΔS) can be calculated using the slope and intercept of the plot, respectively.

$$\Delta G = -RT \ln K_c \quad (9)$$

$$\ln K_c = (\Delta S/R) - \Delta H/RT \quad (10)$$

Where; R (8.314 J/mol/K) is the gas constant and T (K) is the absolute temperature.

3. RESULTS AND DISCUSSION

3.1 Characterization of adsorbent

3.1.1 Brunauer-Emmett-Teller (BET) and Barrett-Joyner-Halenda (BJH) analysis

Following the IUPAC classification, the AC-RH N_2 adsorption-desorption isotherm in this study was Type IV(a) (Cychosz and Thommes, 2018). The isotherm showed hysteresis caused by capillary condensation in the mesopores. A Type IV isotherm indicates the existence of mesopores in the adsorbent and the formation of a multilayer structure at low pressure (Jawad et al., 2017). The N_2 adsorption isotherm data were used to determine BET surface area and BJH pore size distribution. The parameters of the BET and BJH analyses are provided in Table 1.

Table 1. Surface area and pore size distribution of AC-RH

Parameters	Values
BET surface area (m^2/g)	244.479
BET total pore volume (cm^3/g)	0.142
BET average pore diameter (nm)	2.324
BET average pore radius (nm)	1.165
BJH pore volume (cm^3/g)	0.025
BJH average pore diameter (nm)	3.701
BJH average pore radius (nm)	1.805

The BET-specific surface area of the adsorbent was 244.479 m^2/g, with a total pore volume of 0.142 cm^3/g and an average pore diameter of 2.324 nm. The

BJH pore size distributions shown in Figure 1 indicated that the average pore diameter was 3.701 nm; the adsorbent was mesoporous. Moreover, the pore diameter distribution was between 3.11 and 136.28 nm, indicating that the AC-RH consisted of mesopores (2-50 nm) and a few macropores (>50 nm). About 87% of the pore volume had pore diameters between 3 and 50 nm, and the pores with a diameter >50 nm comprised about 13% of the total. Because the MB size (0.59-1.38 nm) (Thang et al., 2021) is smaller than the pore size, it can enter and adsorb in the pores of the AC-RH.

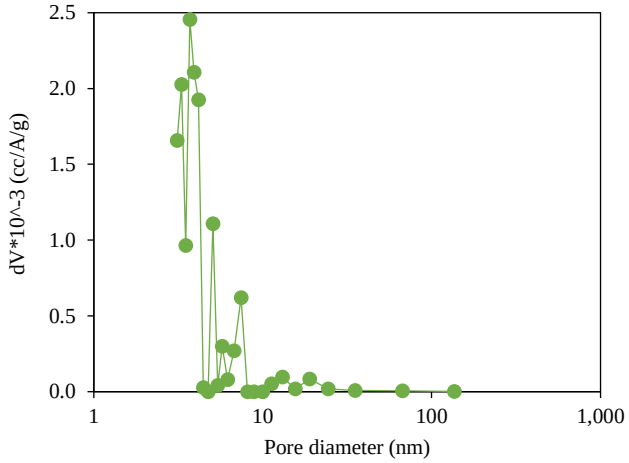

Figure 1. Pore size distribution of activated carbon from H_3PO_4-activated rice husks (AC-RH)

3.1.2 X-ray fluorescence (XRF) analysis

The chemical compositions of the AC-RH adsorbent before and after dye adsorption were investigated by XRF. The main elements present in the adsorbent were Si (45.71%), K (28.85%), Fe (11.97%), and Ca (9.515%). After dye adsorption, the amounts of Si and K were reduced to 41.90% and 27.80%, respectively. The decreased amount of K indicated that cationic exchange plays a role in MB adsorption on the AC-RH surface (Zhu et al., 2018).

3.1.3 X-ray diffraction (XRD) analysis

The XRD patterns of AC-RH before and after dye adsorption are shown in Figure 2. Figure 2(a) shows the XRD patterns of the AC before the adsorption between 2θ of 10° and 60°. The broad diffraction peaks at around 15°-30° indicated that the AC was amorphous (Ziezio et al., 2020), whereas sharp peaks indicate crystalline material (El-Bindary et al., 2021). Diffraction peaks were observed at 27.7°, 28.0°, 30.0°, 31.2°, 42.8°, and 51.3°, with an estimated average crystallite size of 76.8 nm determined by using the Scherrer equation. Also, the broad band at around 22° was attributed to amorphous silica (Wazir et al., 2020). The low intensity of the peak at around 43° showed the graphite structure and disorder formed by the activated carbon (Serafin et al., 2023). Moreover, these peaks at around 43° are associated with the honeycomb structure of sp^2 hybridized carbon, indicating that the sample was formed of turbostratic carbon (Banuprabha et al., 2021). The diffraction peaks after adsorption (Figure 2(b)) appeared at 21.9°, 23.7°, 27.6°, 28.0°, 29.6°, 30.2°, 33.6°, 35.4°, 51.3°, 62.4°, 67.7°, and 69.5°. Figure 2(b) shows that the peak intensity changed, with some peaks disappearing and others reappearing, suggesting that the AC had become saturated with MB (Unugul and Nigiz, 2020).

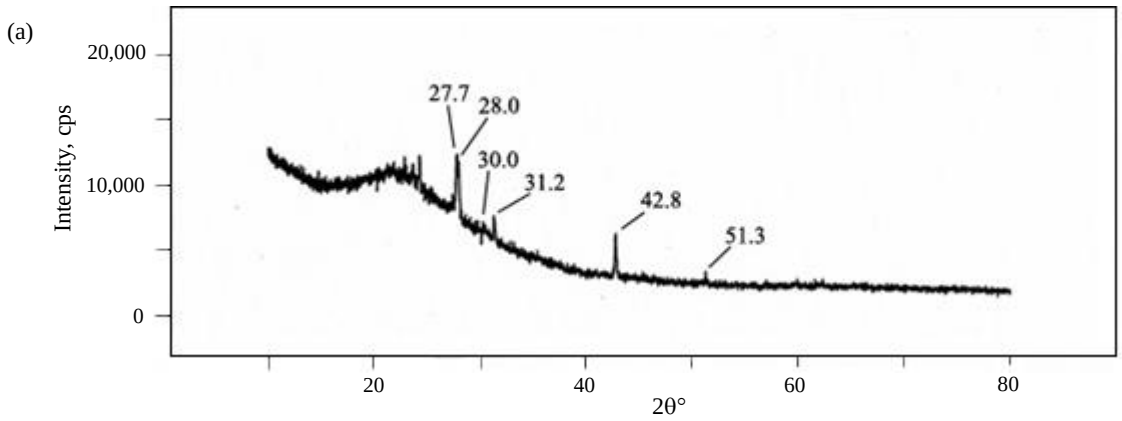

Figure 2. X-ray diffraction (XRD) patterns of AC-RH (a) before and (b) after adsorption

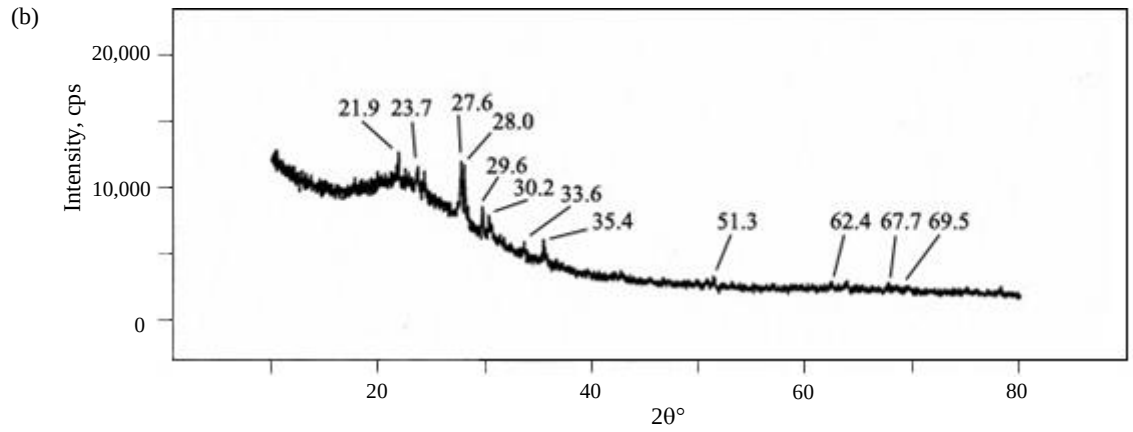

Figure 2. X-ray diffraction (XRD) patterns of AC-RH (a) before and (b) after adsorption (cont.)

3.1.4 Determination of pH at point of zero charges (pH_{pzc})

The pH_{pzc} of the AC-RH was analyzed by the pH drift method, as shown in Figure 3, and the pH_{pzc} was 5.2. When the pH is lower than pH_{pzc}, the surface charge of the adsorbent is positively charged ($\Delta pH>0$). When the pH is higher than pH_{pzc}, the surface charge of the adsorbent is negatively charged ($\Delta pH<0$), and an electrostatic attraction might form between the negatively charged surface and the cationic MB dye molecules. This suggests that MB adsorption on AC is more efficient at a pH higher than 5.2.

3.1.5 Scanning electron microscopy (SEM) analysis

The SEM images of the adsorbent are shown in Figure 4(a, b, and c). The raw rice husks showed a roughly structured fibrous material without pores. In contrast, the SEM image of AC-RH (Figure 4(b)) shows a porous structure. The acid broke down the glycosidic bonds in the cellulose and the aryl bonds in the lignin (Yakout and El-Deen, 2016), forming pores in the adsorbent. At the same time, the silica remained in the rice husk (Ahiduzzaman and Sadrul Islam, 2016). Figure 4(c) shows the surface of AC-RH after MB adsorption coated with MB dye, with no pores visible.

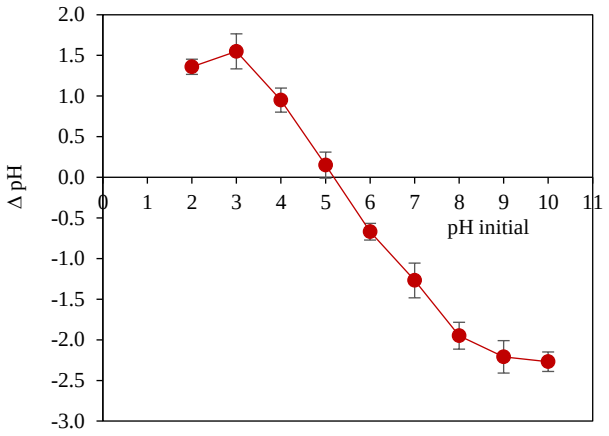

Figure 3. pH_{pzc} of adsorbent

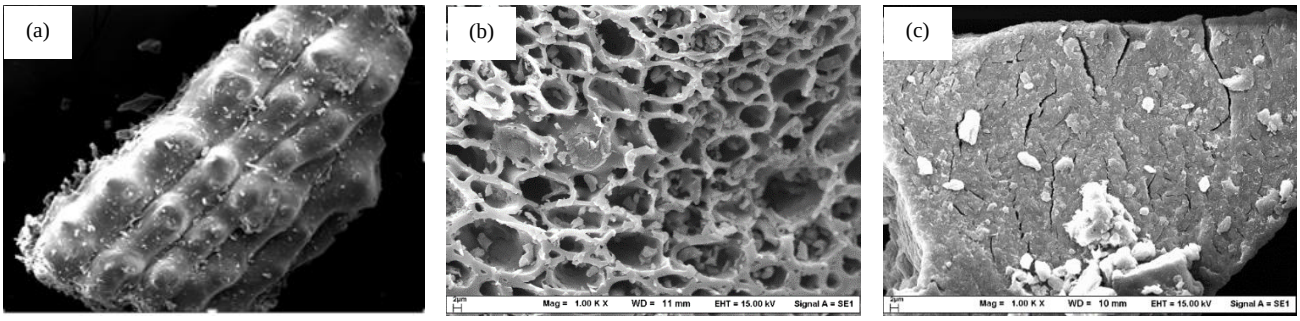

Figure 4. SEM images of AC-RH (a) raw rice husk, (b) before adsorption, and (c) after adsorption

3.1.6 Fourier transform infrared (FTIR) spectroscopy analysis

Figure 5(a, b) shows the FTIR spectra of the AC-RH surface. The broad absorption peak observed prior to adsorption between 3,300 and 3,600 cm^{-1}, peaking at 3,452 cm^{-1}, was ascribed to the OH stretching vibration (Figure 5(a)) (Jawad et al., 2017). According to Al-Ghouti and Al-Absi (2020), the peak

at 1,750 cm^{-1} can be attributed to the stretching vibration of the C=O functional group. According to Liu et al. (2020), the aromatic ring C=C stretching vibration in the AC appeared at 1,596 cm^{-1}. The band at 1,217 cm^{-1} was attributed to the Si-O-Si vibration in amorphous SiO_2 (Hongo et al., 2021). According to Puziy et al. (2002) and İzgi et al. (2018), the peaks between 1,000 and 1,200 cm^{-1} correspond to the O-C bond in carboxylic acids, alcohols, phenols, and esters. The bands at 500-800 cm^{-1} were attributed to the C-H bending mode of out-of-plane aromatic ring deformation (Alau et al., 2015). According to Bakdash et al. (2020), the peak at 789 cm^{-1} is linked to the Si-O-C stretching vibration. Therefore, the AC-RH used in this study contained OH, COOH, C=O, C=C, and Si-O-Si functional groups.

After adsorption, the peaks shifted (Figure 5(b)), and their intensities differed from the original spectrum. For example, the peak at 1,596 cm^{-1} shifted to 1,595 cm^{-1} with an increased intensity due to dye adsorption. Also, the intensities of the Si-O-C and Si-O-Si peaks at 789 and 1,217 cm^{-1} weakened during adsorption due to n-π interactions between the lone pair of O (Si-O) and π-electrons in the MB molecule (Zhu et al., 2018). Moreover, new peaks appeared at 3,359 and 3,237 (stretching vibration of OH group), 2,815 ($-N(CH_3)_3$), 1,656 ($=N^+$ immonium band), 1,357 and 1,342 (C-N), 1,038 (heterocycle skeleton), and 876 cm^{-1} (C-H bending in heterocyclic) (Amin et al., 2017), showing the adsorption of the MB onto the AC-RH.

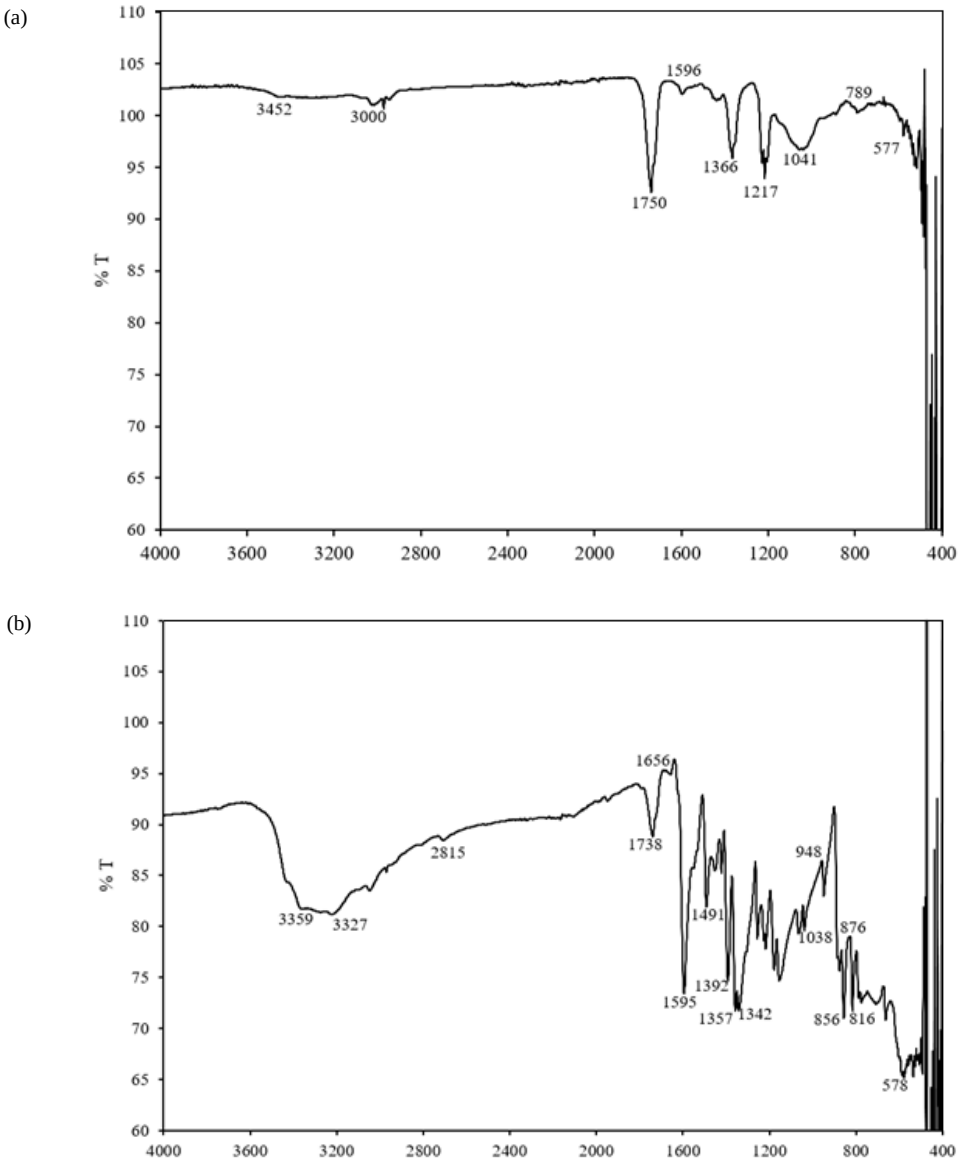

Figure 5. FTIR spectra of adsorbent (a) before and (b) after adsorption

3.2 Effect of pH on adsorption

Figure 6 shows the effects of pH (2-10) on the adsorption. As seen in Figure 6, the adsorption capacity was enhanced when the pH was increased from 2 to 8, and the optimal removal was determined at pH 8. At a pH greater than 8, the adsorption capacity did not change significantly. When the pH of the dye solution was low, the surface charge of the adsorbent became positive, repelling the positive dye molecules.

At a pH greater than 5.2 (pH_{pzc}), the surface of the adsorbent was negative (Equation 11), driving an electrostatic attraction between the cationic dye (MB^+) and the negative surface of the adsorbent ($R\text{-}O^-$), as seen in Equation (12). This observation was consistent with other reports (Zazouli et al., 2016; Pathania et al., 2017) of MB adsorption onto AC from different sources.

$$R - OH + HO^- \rightarrow R - O^- + H_2O \quad (11)$$

$$R - O^- + MB^+ \rightarrow R - O^-MB^+ \quad (12)$$

3.3 Effect of contact time and temperature

Figure 7 shows the contact time-dependent adsorption at 1-540 min. Due to the empty adsorption sites of the adsorbent and the high dye concentration, adsorption occurred quickly during the first 15 min. After that, the adsorption rate slowly decreased until the equilibrium adsorption was reached at 360 min. This is because while the adsorption process occurred, the number of empty sites on the adsorbent and the dye concentration decreased. Mansour et al. (2021) have confirmed that the dye molecules were adsorbed on the exterior surface of the AC via boundary adsorption during the first rapid adsorption stage. A comparable report has been presented for MB adsorption by AC developed from eucalyptus residue (Han et al., 2020).

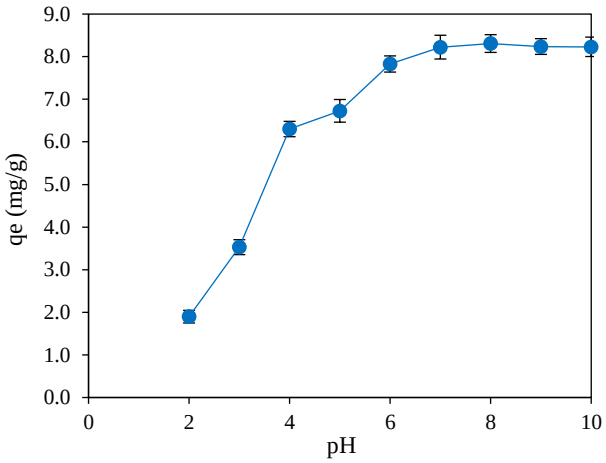

Figure 6. Effect of pH on adsorption (adsorbent dose 0.6 g, initial dye concentration 50 mg/L, contact time 360 min, and temperature 30°C)

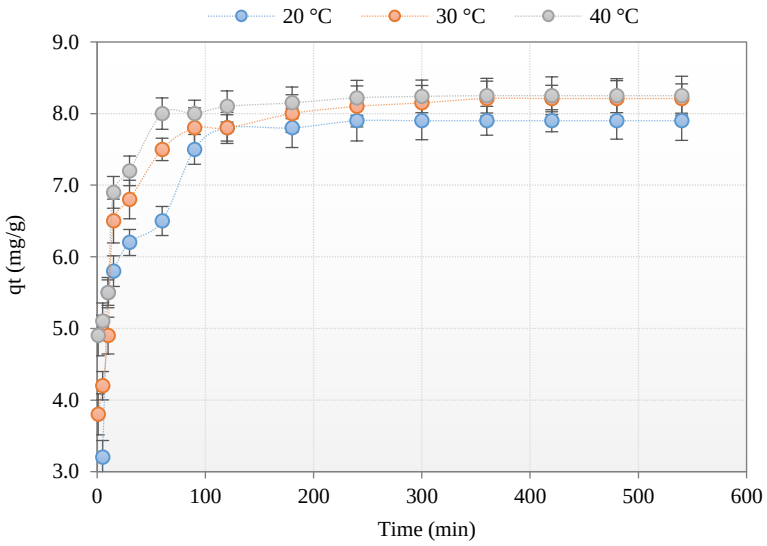

Figure 7. Effect of contact time (1, 5, 10, 15, 30, 60, 90, 120, 180, 240, 300, 360, 420, 480, and 540 min) on adsorption (adsorbent dose 0.6 g, initial dye concentration 50 mg/L, pH 8, and temperature 20-40°C)

Figure 7 also indicates that the endothermic adsorption process improved adsorption capacity as the process temperature rose from 20 to 40°C. The rise in temperature increased pore size and sorbent surface activation, boosting adsorption. In addition, increased temperature enhanced dye ion mobility and decreased swelling, allowing the dye molecules to permeate deeper into the adsorbent pores (Pathania et al., 2017). MB adsorption on activated carbons derived from *Citrullus lanatus* rinds (Uner et al., 2016) and coconut

leaves (Jawad et al., 2017) increased with temperature. However, in this study, the adsorption capacity did not change significantly at higher temperatures because of the reduced attractive force, which favored physisorption (Horsfall Jnr and Spliff, 2005). Also, Zhu et al. (2018) have studied the influence of temperature at 5, 15, 25, and 35°C and discovered that the effects of temperature on the adsorption capacities of MB on cow manure-derived biochar were reduced at temperatures between 25 and 35°C.

3.4 Adsorption kinetics

Kinetic models were employed to analyze the data from the contact time-dependent experiments. Figure 8 shows the linear graphs of the kinetic model. Table 2 shows the calculated kinetic parameters. The pseudo-second-order model exhibited higher R^2 values than the pseudo-first-order and intraparticle diffusion models. The pseudo-second-order model capacities (q_e, cal) were also closer to the experimental values (q_e, exp). The pseudo-second-order model fit the data better, showing that the adsorption of MB onto the AC-RH included the diffusion of an external liquid membrane, surface adsorption, and intraparticle diffusion (Zhu et al., 2018).

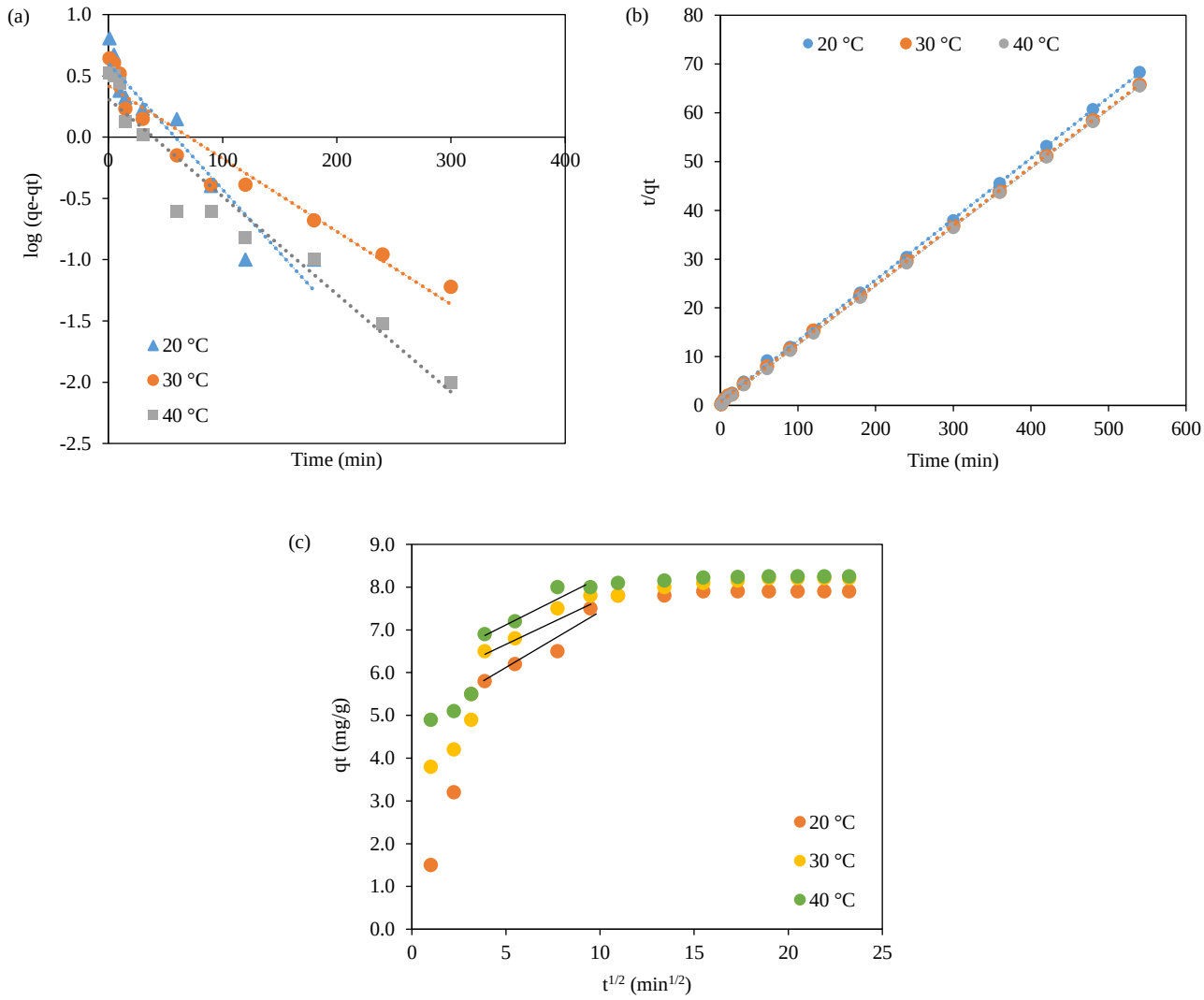

Figure 8. Kinetic models of MB adsorption: (a) pseudo-first-order, (b) pseudo-second-order, and (c) intraparticle diffusion

As seen in Figure 8(c), the plots of q_t versus $t^{1/2}$ show three stages of adsorption. In the first stage, diffusion of the boundary layer rapidly adsorbed MB molecules on the surfaces of the adsorbent. Intraparticle diffusion, the second stage, began at 15 min and lasted until 60 min. At this stage, the adsorbate was transferred from the outer surface of the adsorbent to its pores. The MB molecules were

adsorbed on the active sites of the surfaces of the adsorbent during the third step, known as the equilibrium stage (Ma et al., 2012). The second linear plot for the three temperatures had R^2 values ranging from 0.909 to 0.987. Because the line did not pass through the origin, intraparticle diffusion was not the only rate-determining step. As a result, intraparticle diffusion and external film diffusion were active during adsorption (Patawat et al., 2020). A similar observation has been reported for the adsorption of MB onto AC derived from *Citrullus lanatus* rind (Uner et al., 2016).

The activation energy (E_a) of MB adsorption onto AC-RH was determined from a plot (not shown) of ln k, the pseudo-second-order rate constant, and 1/T. The E_a value calculated from the slope of the graph was 26.248 kJ/mol. Because the E_a value was lower than 40 kJ/mol, the adsorption process of MB on AC-RH was physisorption (Inglezakis and Zorpas, 2012).

Table 2. Kinetic parameters of MB adsorption by AC-RH

Kinetic parameters	Values		
	20°C	30°C	40°C
q_e (exp) (mg/g)	7.90	8.21	8.25
Pseudo-first-order			
q_e (mg/g)	4.00	2.63	2.06
k_1 (1/min)	0.024	0.014	0.018
R^2	0.909	0.928	0.939
Pseudo-second-order			
q_e (mg/g)	8.01	8.30	8.31
k_2 (g/mg·min)	0.019	0.022	0.039
R^2	0.999	0.999	1.000
Intraparticle diffusion			
C (mg/g)	4.64	5.54	6.08
K_{id} (mg/g/min$^{1/2}$)	0.279	0.242	0.217
R^2	0.909	0.987	0.914

3.5 Adsorption isotherm

From the study of the effect of initial dye concentrations of 25-200 mg/L, the results (Figure 9) were plotted as a non-linear function between the adsorption capacity (q_e) and the equilibrium concentration of MB (C_e). Table 3 shows the adsorption isotherm parameters obtained using a non-linear solver (Excel, Microsoft). Based on the R^2, the Freundlich model, as opposed to the Redlich-Peterson and Langmuir models, provided a better description of the adsorption isotherm of MB onto AC-RH. Because the obtained 1/n value (1/n=0.231) was between 0 and 1, adsorption was favorable (Patawat et al., 2020). In addition, the Langmuir monolayer coverage (q_{max}) of MB on AC-RH was 26.31 mg/g. According to Wu et al. (2010), because the g-value for the Redlich-Peterson model was less than 1, it indicated that the adsorption was not comparable to the Langmuir isotherm model. In Table 4, the present work was compared to various research papers on MB adsorption by different ACs.

Table 3. Adsorption isotherm parameters

Isotherms	Values
Langmuir isotherm	
q_{max} (mg/g)	26.31
K_L(L/mg)	0.88
R_L	0.046-0.005
R^2	0.974
Freundlich isotherm	
K_F (L/g)	12.53
1/n	0.231
R^2	0.990
Redlich-Peterson isotherm	
A (L/g)	903.26
B (L/mg)	66.87
g	0.795
R^2	0.983

Table 4. The maximum adsorption capacity of MB on different activated carbons

Activated carbons	Optimal adsorption conditions	q_{max}(mg/g)	References
Coconut leaves	pH=5.6, 303-323°K	357.1-370.4	Jawad et al. (2017)
Bamboo	pH=6, 298°K	183.3	Liu et al. (2010)
Fig leaves	pH=7, 298°K	41.7	Al-Asadi et al. (2023)
Corn cobs	pH=8, 298°K	28.6	El-Sayed et al. (2014)
Sugarcane bagasse	pH=7, 293°K	6.7	Hazzaa and Hussein (2015)
Coconut shells	pH=8, 298°K	15.2	Khuluk et al. (2019)
Rice husks	pH=7, 303-323°K	9.8-14.3	Sharma and Uma (2010)
Rice husks	pH=8, 303°K	26.3	This study

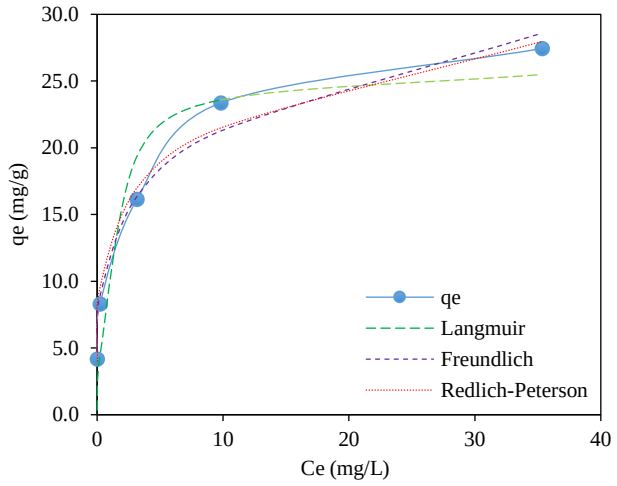

Figure 9. The equilibrium adsorption experiments and the non-linear isotherm prediction plots (initial dye concentration 25-200 mg/L, pH 8, contact time 360 min, and temperature 30°C)

3.6 Thermodynamic study

Thermodynamic equilibrium tests were conducted at 20-40°C, and the adsorption increased from 8.230 to 8.294 mg/g. Using Equation (9), the ΔG values for 20, 30, and 40°C were estimated as -6.291, -8.463, and -9.197 kJ/mol, respectively. Therefore, the adsorption was spontaneous and favorable at higher temperatures. In general, physisorption is suggested by ΔG values between -20 and 0 kJ/mol (Xu et al., 2021). Therefore, physisorption was the main mechanism involved in MB adsorption onto AC-RH.

The slope and intercept seen in Figure 10 were used to calculate ΔH and ΔS, respectively, using Equation (10). As shown by the ΔH, which was 39.565 kJ/mol, adsorption was an endothermic process. Because the ΔH value was less than 84 kJ/mol, the adsorption suggested physical sorption (Hasani et al., 2022). Because ΔS was 0.156 kJ/mol·K, it is possible that there was more randomization at the interface of the dye solution and the active sites of the adsorbent. Several other reports have also concluded that the MB adsorption on activated carbon is endothermic (Ahiduzzaman and Sadrul Islam, 2016; Pathania et al., 2017; Zazouli et al., 2016).

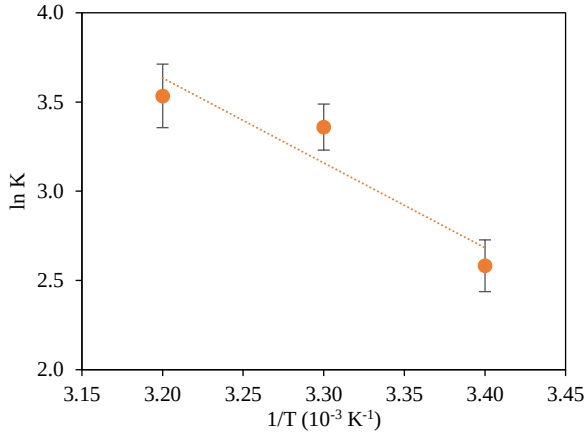

Figure 10. Thermodynamics of MB adsorption on AC-RH (initial dye concentration 50 mg/L, pH 8, and equilibrium time 360 min)

3.7 Adsorption mechanism

AC-RH surfaces contain functional groups containing oxygen atoms, called oxygen groups. These groups are important for adsorption. Additionally, the electrons (n) of the oxygen-free Lewis primary sites (electron donors) on the surfaces of AC-RH and the π-electrons of the conjugated bonds in the aromatic rings of dye molecules contributed to the adsorption interaction (Faria et al., 2004). As seen in Figure 5, the intensity of the Si-O-Si and Si-O peaks decreased after adsorption. The presence of the n-π interaction in the adsorption between the oxygen groups and dye molecules was further confirmed by the C=O peak, which lost some of its intensity and shifted from 1,750 to 1,738 cm^{-1}. The C=C peak center, on the other hand, did not shift noticeably, suggesting there were no π-π interactions (Tran et al., 2017). In addition, the C=C peak increased in intensity because of pore filling. Due to the effect of pH, an electrostatic interaction should exist between the AC-RH and the MB molecules. Therefore, the

possible mechanisms (Figure 11) of MB adsorption on AC-RH are (a) H-bonding interactions between the hydrogen on the adsorbent surface and the nitrogen in the amine group of the dye molecule; (b) pore filling in AC-RH; (c) Yoshida H-bonding interactions between the hydrogen on the OH groups in the adsorbent surface and the aromatic rings of the dye molecule; (d) n-π interactions between the oxygen functional groups of AC-RH and the aromatic rings of the dye molecule; (e) electrostatic interactions between the negatively charged AC-RH and the positively charged dye molecules (MB^+); and (f) cation exchange of MB^+ to K^+.

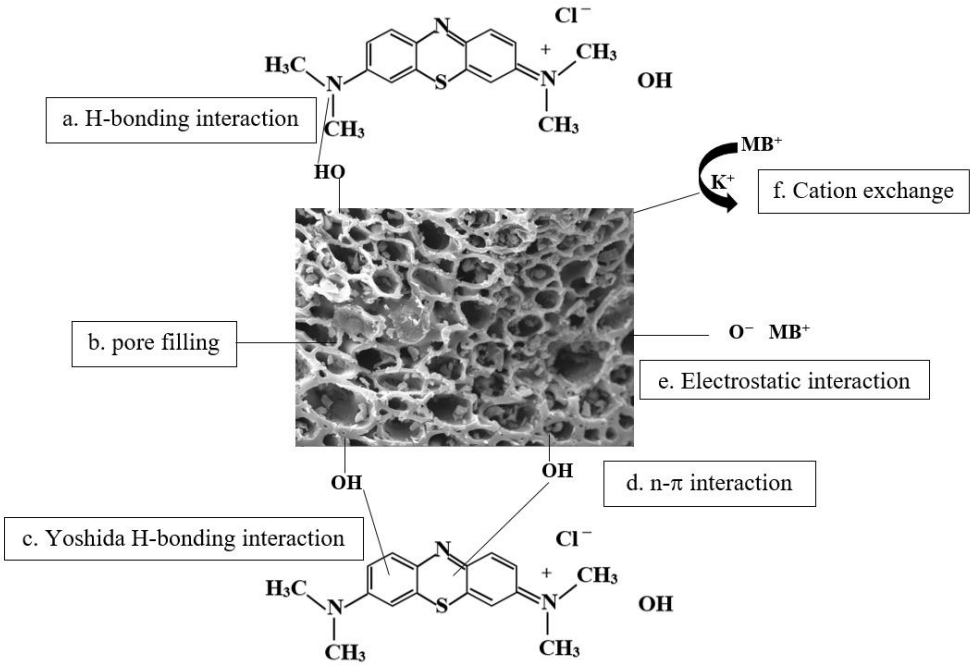

Figure 11. Possible mechanisms of MB dye adsorption on AC-RH

4. CONCLUSION

The N_2 adsorption-desorption isotherm, XRF spectroscopy, XRD, SEM, and FTIR spectroscopy were used to evaluate the pores and surfaces of AC-RH. The nitrogen adsorption-desorption isotherm was Type IV and primarily mesoporous. The BET surface area was 244.479 m^2/g. The BJH-determined pore diameter distribution ranged between 3.11 and 136.28 nm, with 87% in the 3-50 nm range. MB adsorption onto AC-RH was studied at different pH, contact times, initial dye concentrations, and temperatures. The equilibrium time was 360 min, and the highest MB adsorption occurred at pH 8. The adsorption kinetic data corresponded to the pseudo-second-order model, and the equilibrium data fit the Freundlich isotherm. According to thermodynamics models and the activation energy, the process was spontaneous, endothermic, and physisorption. The MB adsorption on AC-RH was also attributed to H-bonding, Yoshida H-bonding, pore filling, n-π interactions, cation exchange, and electrostatic attraction.

ACKNOWLEDGEMENTS

The authors would like to express their gratitude to Thepsatri Rajabhat University for the support of the research.

REFERENCES

Ahiduzzaman Md, Sadrul Islam AKM. Preparation of porous biochar and activated carbon from rice husk by leaching ash and chemical activation. Springerplus 2016;5(1):Article No. 1248.

Al-Asadi ST, Al-Qaim FF, Al-Saedi, HFS, Deyab IF, Kamyab H, Chelliapan S. Adsorption of methylene blue dye from aqueous solution using low-cost adsorbent: Kinetic, isotherm adsorption, and thermodynamic studies. Environmental Monitoring and Assessment 2023;195:Article No. 676

Al-Ghouti MA, Al-Absi RS. Mechanistic understanding of adsorption and thermodynamic aspects of cationic methylene blue dye onto cellulosic olive stones biomass from wastewater. Scientific Reports 2020;10:Article No. 15928.

Alau KK, Gimba CE, Agbaji BE, Abeche SE. Structural and microstructural properties of Neem husk and seed carbon activated with zinc chloride and phosphoric acid. Journal of Chemical and Pharmaceutical Research 2015;7(3):2470-9.

Amin MT, Alazba AA, Shafiq M. Effective adsorption of methylene blue dye using activated carbon developed from

rosemary plant: Isotherm and kinetic studies. Desalination and Water Treatment 2017;74:336-45.

Bakdash RS, Aljundi IH, Basheer C, Abdulazeez I. Rice husk derived Aminated Silica for the efficient adsorption of different gases. Scientific Reports 2020;10:Article No. 19526.

Banuprabha TR, Karthikeyan A, Kalyani P. Evaluation and application of phytomass derived activated carbons as electrodes for coin cell supercapacitors. International Journal of Electrochemical Science 2021;16:Article No. 211251.

Cychosz KA, Thommes M. Progress in the physisorption characterization of nanoporous gas storage materials. Engineering 2018;4:559-65.

El-Bindary MA, El-Desouky MG, El-Bindary AA. Adsorption of industrial dye from aqueous solutions onto thermally treated green adsorbent: A complete batch system evaluation. Journal of Molecular Liquids 2021;346:Article No. 117082.

El-Sayed GO, Yehia MM, Asaad AA. Assessment of activated carbon prepared from corncob by chemical activation with phosphoric acid. Water Resources and Industry 2014;7-8:66-75.

Faria PCC, Orfao JJM, Pereira MFR. Adsorption of anionic and cationic dyes on activated carbons with different surface chemistries. Water Research 2004;38(8):2043-52.

Han Q, Wang J, Goodman BA. High adsorption of methylene blue by activated carbon prepared from phosphoric acid treated eucalyptus residue. Powder Technology 2020;366:239-48.

Han X, Niu X, Ma X. Adsorption characteristics of methylene blue on poplar leaf in batch mode: Equilibrium, kinetics and thermodynamics. Korean Journal of Chemical Engineering 2012;107(3):494-502.

Hasani N, Selimi T, Mele A, Thaçi V, Halili J, Berisha A, et al. Theoretical, equilibrium, kinetics and thermodynamic investigations of methylene blue adsorption onto lignite coal. Molecules 2022;27(6):Article No. 1856.

Hazzaa R, Hussein M. Cationic dye removal by sugarcane bagasse activated carbon from aqueous solution. Global NEST Journal 2015;17(4):784-95.

Hongo T, Moriura M, Hatada Y, Abiko H. Simultaneous methylene blue adsorption and pH neutralization of contaminated water by rice husk ash. ACS Omega 2021;6:21604-12.

Horsfall Jnr M, Spiff AI. Effects o temperature on the sorption of $Pb^{2+}$and Cd^{2+} from aqueous solution by Caladium biochar (Wild Cocoyam) biomass. Electronic Journal of Biotechnology 2005;8(2):43-50.

Hossain SK S, Mathur L, Roy PK. Rice husk/rice husk ash as an alternative source of silica in ceramics: A review. Journal of Asian Ceramic Societies 2018;6(4):299-313.

Hu L, Yang Z, Wang Y, Li Y, Fan D, Wu D, et al. Facile preparation of water soluble hyperbranched polyamine functionalized multiwalled carbon nanotubes for high-efficiency organic dye removal room aqueous solution. Scientific Reports 2017;7(1):Article No. 3611.

Inglezakis VJ, Zorpas AA. Heat of adsorption, adsorption energy and activation energy in adsorption and ion exchange systems. Desalination and Water Treatment 2012;39:149-57.

Islam MA, Tan IAW, Benhouria A, Asif M, Hameed BH. Mesoporous and adsorptive properties of palm date seed activated carbon prepared via sequential hydrothermal carbonization and sodium hydroxide activation. Chemical Engineering Journal 2015;270:187-95.

İzgi MS, Saka C, Baytar O, Saraçoğlu G, Şahin Ö. Preparation and characterization of activated Carbon from microwave and conventional heated almond shells using phosphoric acid activation. Analytical Letters 2018;52(5):772-89.

Jawad AH, Rashid RM, Ismail K, Sabar S. High surface area mesoporous activated carbon developed from coconut leaf by chemical activation with H_3PO_4 for adsorption of methylene blue. Desalination and Water Treatment 2017;74:326-35.

Khuluk RH, Rahmat A, Buhani B, Suharso S. Removal of methylene blue by adsorption onto activated carbon from coconut shell (*Cocous Nucifera* L.). Indonesian Journal of Science and Technology 2019;4(2):229-40.

Kumar A, Jena HM. Preparation and characterization of high surface area activated carbon from *Fox nut* (Euryale ferox) shell by chemical activation with H_3PO_4. Results in Physics 2016;6:651-8.

Liu L, Deng G, Shi X. Adsorption characteristics and mechanism of p-nitrophenol by pine sawdust biochar samples produced at different pyrolysis temperatures. Scientific Reports 2020; 10:Article No. 5149.

Liu QS, Zheng T, Li N, Wang P, Abulikemu G. Modification of bamboo-based activated carbon using microwave radiation and its effects on the adsorption of methylene blue. Applied Surface Science 2010;256(10):3309-15.

Ma J, Yu F, Zhou L, Jin L, Yang M, Luan J, et al. Enhanced adsorptive removal of methyl orange and methylene blue from aqueous solution by alkali-activated multiwalled carbon nanotubes. ACS Applied Materials and Interfaces 2012; 4:5749-90.

Mansour RAE, Simeda MG, Zaatout AA. Removal of brilliant green dye from synthetic wastewater under batch mode using chemically activated date pit carbon. RSC Advances 2021;11:7851-61.

Patawat C, Silakate K, Chuan-Udom S, Supanchaiyamat N, Hunt AJ, Ngernyen Y. Preparation of activated carbon from *Dipterocarpus alatus* fruit and its application for methylene blue adsorption. RSC Advances 2020;10*:*21082-91.

Pathania D, Sharma S, Singh P. Removal of methylene blue by adsorption onto activated carbon developed from *Ficus carica* bast. Arabian Journal of Chemistry 2017;10(1):1445-51.

Puziy AM, Poddubnaya OI, Martınez-Alonso A, Suarez-Garcıa F, Tascon JMD. Synthetic carbons activated with phosphoric acid: I. Surface chemistry and ion binding properties. Carbon 2002;40(9):1493-505.

Serafin J, Dziejarski B, Junior OFC, Srenscek-Nazzal J. Design of highly microporous activated carbons based on walnut shell biomass for H_2 and CO_2 storage. Carbon 2023;201:633-47.

Sharma YC, Uma. Optimization of parameters for adsorption of methylene blue on a low-cost activated carbon. Journal of Chemical and Engineering Data 2010;55,435-9.

Shrestha LK, Thapa M, Shrestha RG, Maji S, Pradhananga RR, Ariga K. Rice husk-derived high surface area nanoporous carbon materials with excellent iodine and methylene blue adsorption properties. Journal of Carbon Research 2019;5(1):Article No. 10.

Thang NH, Khang DS, Hai TD, Nga DT, Tuan PD. Methylene blue adsorption mechanism of activated carbon synthesized from cashew nut shells. RSC Advances 2021;11:26563-70.

Tran HN, You S-J, Chao HP. Insight into adsorption mechanism of cationic dye onto agricultural residues-derived hydrochars: Negligible role of π-π interaction. Korean Journal of Chemical Engineering 2017;34(6):1708-20.

Uner O, Geçgl Ü, Bayrak Y. Adsorption of methylene blue by an efficient activated carbon prepared from *Citrullus lanatus*

rind: Kinetic, isotherm, thermodynamic, and mechanism analysis. Water, Air, and Soil Pollution 2016;227:Article No. 247.

Unugul T, Nigiz FU. Preparation and characterization an active carbon adsorbent from waste mandarin peel and determination of adsorption behavior on removal of synthetic dye solutions. Water, Air, and Soil Pollution 2020;231:Article No. 538.

Wantaneeyakul N, Kositkanawuth K, Turn SQ, Fu J. Investigation of biochar production from copyrolysis of rice husk and plastic. ACS Omega 2021;6(43):28890-902.

Wazir AH, Wazir IU, Wazir AM. Preparation and characterization of rice husk based physical activated carbon. Energy Sources, Part A: Recovery, Utilization, and Environmental Effects 2020;11:Article No. 1715512.

Wu FC, Liu BL, Wu KT, Tseng RL. A new linear form analysis of Redlich-Peterson isotherm equation for the adsorption of dyes. Chemical Engineering Journal 2010;162:21-7.

Xu L, Pan C, Li S, Yin C, Zhu J, Pan Y, et al. Electrostatic self-assembly synthesis of three-dimensional mesoporous lepidocrocite-type layered sodium titanate as a superior adsorbent for selective removal of cationic dyes via an ion-exchange mechanism. Langmuir 2021;37(19):6080-95.

Yakout SM, Sharaf El-Deen G. Characterization of activated carbon prepared by phosphoric acid activation of olive stones. Arabian Journal of Chemistry 2016;9(2):1155-62.

Zazouli MA, Azari A, Dehghan S, Salmani Malekkolae R. Adsorption of methylene blue from aqueous solution onto activated carbons developed from eucalyptus bark and *Crataegus oxyacantha* core. Water Science and Technology 2016;74(9):2021-35.

Zhu Y, Yi B, Yuan Q, Wu Y, Wang M, Yan S. Removal of methylene blue from aqueous solution by cattle manure derived low-temperature biochar. RSC Advances 2018; 8:19917-29.

Ziezio M, Charmas B, Jedynak K, Hawryluk M, Kucio K. Preparation and characterization of activated carbons obtained from the waste materials impregnated with phosphoric acid(V). Applied Nanoscience 2020;10:4703-16.

Estimating Land Use Change Effects on Groundwater Recharge in Nadi and Kabinburi, Thailand

Patchares Chacuttrikul* and Supattra Thueksathit

Department of Conservation, Faculty of Forestry, Kasetsart University, Bangkok, Thailand

ARTICLE INFO

Received: 10 May 2023
Received in revised: 3 Aug 2023
Accepted: 10 Aug 2023
Published online: 12 Sep 2023
DOI: 10.32526/ennrj/21/20230111

Keywords:
CLUE model/ H08 model/ Groundwater recharge/ Land use change

*** Corresponding author:**
E-mail: fforprc@ku.ac.th

ABSTRACT

The effect of land use change on groundwater recharge in Nadi and Kabinburi Districts, Prachinburi Province, Thailand was studied by forecasting land use change using the CLUE model and estimating groundwater recharge using the H08 model. The results suggested that compared to the current average groundwater recharge, the groundwater recharge estimates from scenario 1 (changing the miscellaneous areas of mostly wasteland to mixed perennial areas) and scenario 2 (predicting the land use scenario for the next 10 years based on trends of land use change from the past to the present) were greater by 1.46 and 2.25%, respectively. In scenario 1, the increase in forest and mixed perennial areas increased the groundwater recharge by helping to slow down the surface runoff and, thus, increased the chances of water seepage into the soil. However, increasing the perennial area or turning wasteland into mixed perennial area (scenario 1), resulted in an increase in the groundwater recharge that was similar to the results from simulating future land use scenarios in the next 10 years (scenario 2). Therefore, to increase the efficiency of groundwater management and drought relief, the relevant agencies should adopt appropriate land use planning, be encouraged to plant perennials or support mixed farming on wasteland, restore degraded forest areas, and improve the management of water use concurrently.

1. INTRODUCTION

At present, water shortage is a major global issue, with many countries facing this problem (Miyan, 2015; Zhong et al., 2020), especially in developing countries (Sharafi et al., 2021). This problem is influenced by both natural factors and human activities. Human activities, such as land use change that acts as an important catalyst to droughting problems, are worsening rapidly (Owuor et al., 2016). Water resources are extremely important for the survival of all living things (people, animals, and plants). Thailand is one country facing drought problems annually, where the water shortage problem has a profound effect on people's livelihoods (United Nations, 2022). In addition, Thailand is an agricultural country where the main occupation of the people is agriculture. Drought affects agricultural productivity, including the food security of the country (Keshavarz and Karami, 2018; He et al., 2019). One of the major problems that causes a drought to intensify rapidly is land use change without planning or proper management. Unused area greatly affects water resources because there is nothing to cover the soil surface and no plants protecting the soil. Thus, rain affects the soil surface directly, increase the likelihood of surface runoff and reduce the chance of water seepage into the soil (Kumar et al., 2017). These affect both groundwater recharge and the amount of groundwater.

Groundwater is an important water source that helps to add water to surface water sources during the dry season (Niyom, 1992). Most of the rain that falls on the surface will return to the atmosphere due to evapotranspiration, with only 14% becoming groundwater recharge (Fornes and Pirarai, 2014). Thailand has widely used groundwater, from the past to the present, to alleviate the problem of water shortage and to respond to the increasing water demand of the people (Department of Groundwater Resources, 2018). However, factors affecting groundwater recharge have not been studied much in Thailand. Most studies have examined the relationship between streamflow and land use change, for example, Chacuttrikul et al. (2018) projected the streamflow in the land use change situation at Lam Chi Sub-

Citation: Chacuttrikul P, Thueksathit S. Estimating land use change effects on groundwater recharge in Nadi and Kabinburi, Thailand. Environ. Nat. Resour. J. 2023;21(5):471-478. (https://doi.org/10.32526/ennrj/21/20230111)

watershed, Northeast Thailand, using H08 model, Faksomboon et al. (2019) investigated the land use change of head water area on streamflow, suspended sediment, and water quality in Khlong Lan Watershed, Kamphaeng Phet Province using SWAT model, and Borrabut et al. (2022) studied the effect of land use change on streamflow of Mae Nam Khuan and Nam Pi Sub-watersheds in Nan and Phayao Provinces, Thailand. Therefore, it is not yet clear what factors affect groundwater recharge. Furthermore, there is limited quantitative evidence on how changes in land use affect groundwater recharge.

The selected areas for the current research were the Nadi and Kabinburi Districts, Prachinburi Province, eastern Thailand. The Nadi and Kabinburi Districts are recurring drought-affected and drought-prone areas, respectively. The recurring drought-affected area was the area that experienced drought in agriculture regularly or frequently. It is an area that lacks water for use in agriculture and consumption, affecting the livelihood of the people (Research Institute Developed for Desertification Prevention and Early Warning, 2005). In addition, water demand by the people in this area is continuously increasing. As a result, the amount of surface water and groundwater is insufficient to meet demand. Thus, the drought response plan for the year 2019-2020 was established by the Office for Prevention and Mitigation in Prachinburi Province and one of the drought relief plans was to survey the area that could supply groundwater to help alleviate this problem. Therefore, the Nadi and Kabinburi Districts, Prachinburi Province are very suitable as a relevant study area. The drought problem of the study area may be due to the land use changes that have resulted in an increase in abandoned areas and to increasing people's water demand (Department of Groundwater Resources, 2015), make the water from both surface sources and groundwater not sufficient to meet the demand of the total population.

Therefore, this research simulated the land use change scenario using the Conversion of land use and its effects (CLUE) modelling framework, which is a land use change model (Verburg et al., 1999; Verburg and Overmars, 2009). Afterward, the H08 model, which is an open-source global hydrological model that can consider the interactions between natural hydrological processes and human activities (Mateo et al., 2014; Hanasaki et al., 2018; Hanasaki, 2022), was applied to estimate the impacts of land use changes on groundwater recharge in Nadi and Kabinburi Districts, Prachinburi Province, Thailand.

2. METHODOLOGY

2.1 Study area

The Nadi and Kabinburi Districts (2,611 km^2) in Eastern Thailand, Prachinburi Province, were selected as the study site (Figure 1). To the north, it connects with Nakhon Ratchasima Province, to the east with Sa Kaeo Province, to the south with Chachoengsao Province, and to the west with Nakhon Nayok Province. The Nadi and Kabinburi Districts are constantly experiencing drought.

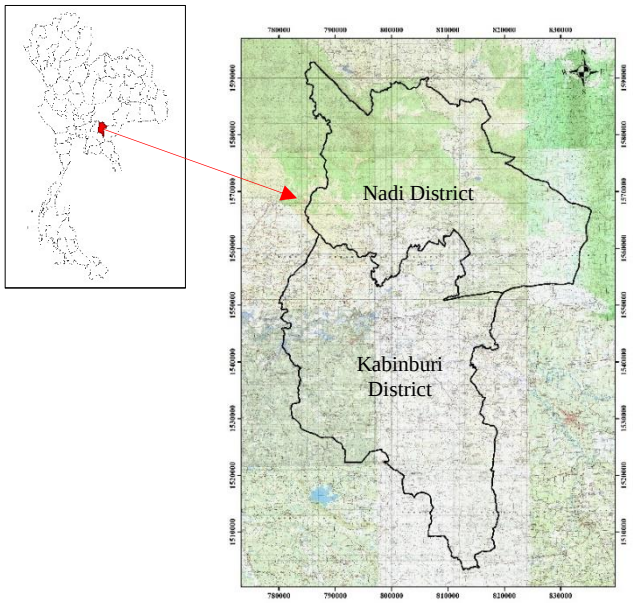

Figure 1. Location of study areas in Nadi and Kabinburi Districts, Prachinburi Province

The research procedures and methods are shown in Figure 2 and detailed as follows:

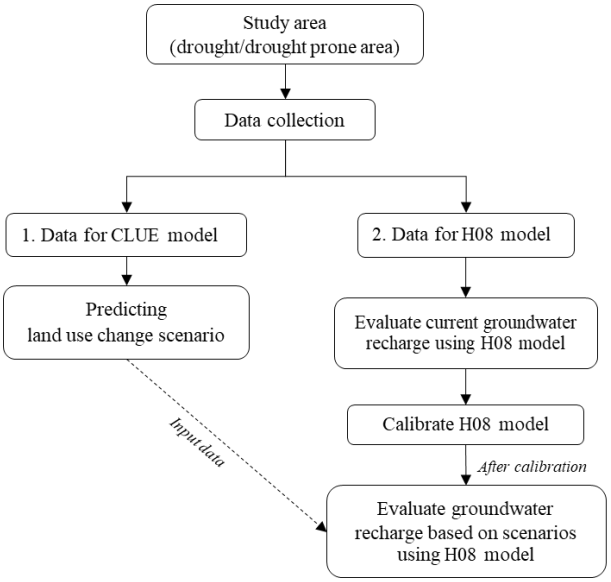

Figure 2. Methodology

2.2 Data preparation for the model

2.2.1 CLUE model

The conversion of land use and its effects modelling framework (the CLUE model) was used to develop the future land use scenario by the boundary of the study area, land use data in 2020 from Land Development Department, elevation and slope data from topographic map, and roads and main streams from topographic map (Verburg, 2015).

Chacuttrikul's findings regarding the impact of land use and climate change on future soil erosion and sediment yield in Northern Thailand indicate that the CLUE model has high performance for simulated land use change scenarios. The results from the CLUE model closely corroborate the land use change data from the actual measurement for over 82% of the total area. However, there are some errors in simulating small areas such as water and urban areas (Chacuttrikul, 2018).

2.2.2 H08 model

H08 model (Hanasaki, 2022) estimating land use change impact on groundwater recharge during 5 years by the Meteorological data (rainfall, air temperature, and relative humidity) were collected from the weather monitoring station of the Thai Meteorological Department and the Royal Irrigation Department for 2016-2020, in daily time scale, boundary from topographic map, land use data in 2020 from Land Development Department, elevation and slope from topographic map, and data regarding artesian wells or groundwater such as well depth and water level in the well from field data collection by the Department of Groundwater Resources. Soil moisture, soil texture, soil depth, and water holding capacity of soil from field data collection. For field data collection, the soil sampling points were chosen based on different land use and soil groups. The soil samples were collected at a depth of 0-30 cm at 11 points, with 3 replications at each sample collection points (total of 33 samples).

In addition, a geographic information system (GIS) was used to prepare the data for the H08 model, including boundary, elevation, slope, and land use data. Data were prepared at 1 arc-minute spatial resolution, or approximately 2 × 2 kilometers. In addition, some soil hydrological data from the field collection were also included in the GIS after analysis in the laboratory.

2.3 Simulation of land use situation based on CLUE model

After preparing the input data, land use situation was created using the CLUE model, which is an integrated land use change model (Verburg et al., 2002; Verburg, 2007; Verburg, 2015). The relationships were analyzed among land use types and factors that affect land use change, such as elevation, slope of the area, slope direction, and distances from communities to rivers and roads.

There were two land use scenarios: scenario 1 changed other agricultural areas (such as floricultural, animal husbandry, and pasture) and miscellaneous areas (such as bare areas and wasteland) to an area for mixed perennial plants to be consistent with the daily life and well-being of the people in the area; and scenario 2 simulated the next 10 years of land use change from the trends in land use change from the past to the present, to forecast the groundwater recharge rate in the near future and plans for water use. As basic data for simulation, both land use scenarios used the GIS, the CLUE model (Dyna version) and land use data in 2020 from the Land Development Department. The CLUE model is an integrated land use change model (Verburg et al., 1999) that can be used to simulated land use change scenarios from land use data in the past along with the data that are related to land use change, including slope data, elevation, distances from roads, and distances from water sources.

2.4 Forecasting effect of land use change on groundwater recharge based on H08 model

Step 1: Assessment of groundwater recharge was based on current land use (in 2020) and climatic data (2016-2020).

Step 2: Calibration of the H08 model was done using the groundwater level data that had been measured by the Department of Groundwater Resources. The model was calibrated by changing the values of the parameters that related to the amount of groundwater and groundwater recharge. In addition, the coefficient of determination (R^2) and standard error of the estimate (SSE) were used to measure the accuracy of the values obtained from the models.

Step 3: Evaluation of the effects of land use change on groundwater recharge using land use data from the CLUE model along with current climatic data.

3. RESULTS AND DISCUSSION

3.1 Land use and land use change

The land use data for the research site between 2008 and 2020 from the Land Development Department showed that the major land uses were forest, perennial, field crop, and paddy field, with areas of 26.45, 16.73, 15.77, and 15.47%, respectively, in 2008 and 29.32, 18.81, 17.91, and 12.42% in 2020, respectively. These figures suggested that land use for the study site had slightly changed. In 2020, the forest area, field crops, perennial, water, and miscellaneous areas increased by approximately 2.79, 2.15, 2.08, 1.47, and 1.18%, respectively. In contrast, paddy field, other agricultural, urban, and degraded forest area decreased by approximately 3.05, 2.43, 1.61, and 1.61%, respectively. The areas with little change were forest plantations and orchards that decreased and increased by only 0.99 and 0.02%, respectively, of the total area (Table 1).

3.2 Forecasting land use change under the two scenarios

Scenario 1 (changing the land use area of other agricultural and miscellaneous areas to mixed perennial) involved approximately 219.6 km^2 or 8.4% of the total area. The relevant maps and land use data are shown in Table 2 and Figure 3(a).

Scenario 2 (trends in land use change from 2008 to 2020) showed that the forest, field crops, fruit trees, perennial plants, water, and miscellaneous areas tended to increase, while degraded forest, forest plantations, paddy fields, other agricultural, and urban areas tended to decrease. This affected land use in scenario 2. The future land use areas under the two scenarios are shown in Table 2 and Figure 3.

Table 1. Changes in land use (2008-2020)

Land use type	Land use in 2008		Land use in 2020		% Change
	km^2	%	km^2	%	
Forest	690.70	26.45	763.52	29.23	2.79
Degraded forest	81.18	3.11	39.15	1.50	1.61
Paddy field	404.05	15.47	324.40	12.42	3.05
Field crops	411.79	15.77	467.88	17.91	2.15
Orchard	42.83	1.64	43.34	1.66	0.02
Perennial	436.89	16.73	491.28	18.81	2.08
Other agricultural areas	231.50	8.86	168.08	6.44	2.43
Forest plantations	32.35	1.24	6.45	0.25	0.99
Urban area	218.33	8.36	176.35	6.75	1.61
Water area	41.41	1.59	79.79	3.05	1.47
Miscellaneous area	20.79	0.80	51.57	1.97	1.18

Table 2. Original land use and future land use under scenarios 1 and 2

Land use type	Land use in 2008		Land use in 2020		Scenario 1		Scenario 2	
	km^2	%	km^2	%	km^2	%	km^2	%
Forest	690.7	26.4	763.5	29.2	763.5	29.2	823.0	31.5
Degraded forest	81.2	3.1	39.2	1.5	39.2	1.5	0.0	0.0
Paddy field	404.0	15.5	324.4	12.4	324.4	12.4	251.3	9.6
Field crops	411.8	15.8	467.9	17.9	467.9	17.9	517.1	19.8
Orchard	42.8	1.6	43.3	1.7	43.3	1.7	53.1	2.0
Perennial	436.9	16.7	491.3	18.8	491.3	18.8	567.3	21.7
Other agricultural areas	231.5	8.9	168.1	6.4	0.0	0.0	75.7	2.9
Mixed perennial tree	0.0	0.0	0.0	0.0	219.6	8.4	0.0	0.0
Forestry plantations	32.3	1.2	6.5	0.2	6.5	0.2	0.0	0.0
Urban area	218.3	8.4	176.3	6.8	176.3	6.8	127.9	4.9
Water area	41.4	1.6	79.8	3.1	79.8	3.1	109.6	4.2
Miscellaneous area	20.8	0.8	51.6	2.0	0.0	0.0	86.8	3.3
Total	2,611.8	100.0	2,611.8	100.0	2,611.8	100.0	2,611.8	100.0

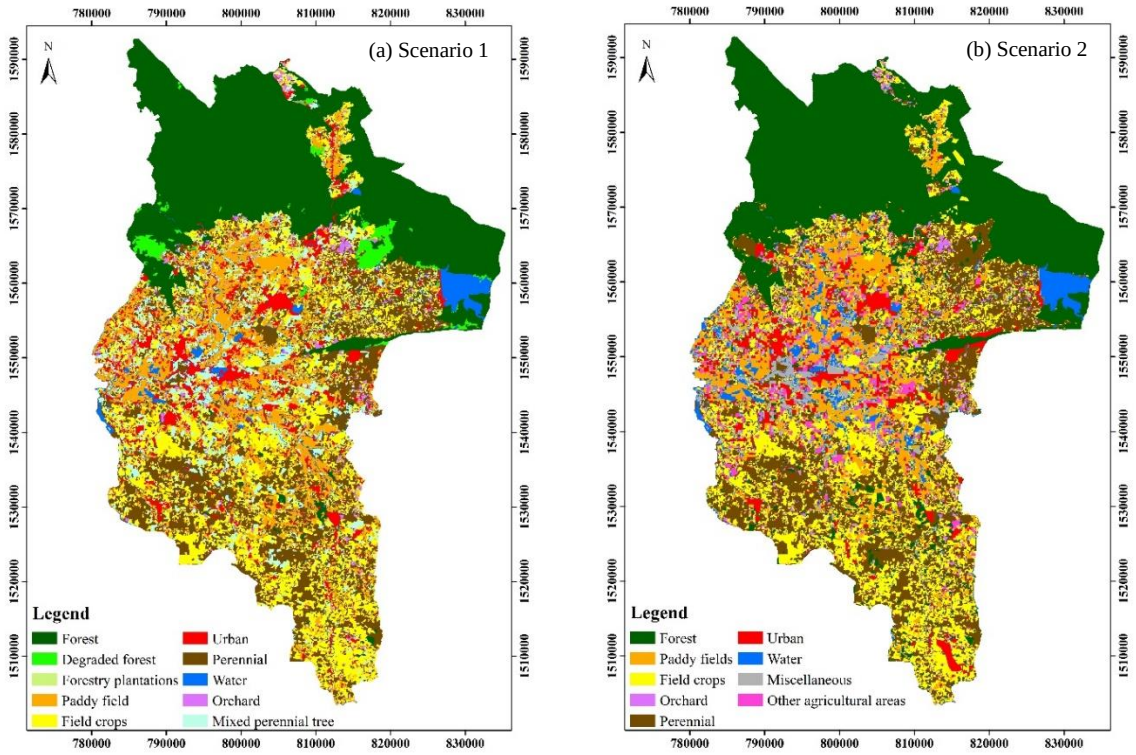

Figure 3. Land use maps: (a) scenario 1 and (b) scenario 2

3.3 Predicting the effect of land use change on groundwater recharge using H08 model

3.3.1 Calibration of H08 model

To calibrate the H08 model, the groundwater data obtained from the actual measurements was compared with the results from the model and used to modify the relevant parameters such as groundwater depth, groundwater yield (Gwyield), the maximum time constant for groundwater runoff per day (Tau), and parameters related to groundwater flow (Gamma). In this study, the Gwyield, Tau, and Gamma parameters were adjusted according to land use in 2020 in the Nadi and Kabinburi districts, with the groundwater depth data of the Department of Groundwater Resources being used as a baseline. The actual measurement groundwater data were recorded during 2018-2020 from two groundwater wells of the Department of Groundwater Resources. The coefficient of determination (R^2) and standard error of the estimate (SSE) were used to measure the accuracy of the values obtained from the model. However, due to the lack of continuity of the measurement groundwater data, only 5 data values per well were available for calibration. The results of the model calibration are shown in Table 3.

For model calibration, the groundwater data from the Kabinburi and Ladtakian wells were compared with the data output from the model. It was found that the R^2 value for the Kabinburi well was 0.97 and the SEE was 0.017, while for the Ladtakian well, the R^2 value was 0.76 and the SEE was 0.012.

Table 3. Results of H08 model calibration

Statistic	Groundwater well	
	Kabinburi	Ladtakian
R^2	0.97	0.76
SEE	0.017	0.012

3.3.2 Effect of land use change on groundwater recharge

The simulations for both land use scenarios using the GIS and the CLUE model indicated that land use change clearly affected the groundwater recharge. The results of the assessment of groundwater recharge for both scenarios (scenario 1 that changed other agricultural areas and miscellaneous areas, such as mixed perennial area, and scenario 2 that predicted the next 10 years of land use based on land use change trends from the past to the present) showed that the average monthly groundwater recharge for the current situation and all scenarios were the highest in October and the lowest in May (Table 4 and Figure 4) and that the groundwater recharge amounts from scenarios 1 and 2 were higher than the groundwater recharge from the current situation. The average groundwater

recharge for 5 years of the current situation, scenario 1, and scenario 2 were 7.33×10^{-4}, 7.44×10^{-4}, and 7.49×10^{-4} m^3/s, respectively. The average groundwater recharge amounts of scenario 1 and scenario 2 were greater than the current situation by 1.46 and 2.25%, respectively, due to the decrease in miscellaneous areas (mostly wasteland), the increase in forest area in scenario 2, and the increase in mixed perennial areas in scenario 1. These all helped to cover the surface soil leading to reduced surface runoff, reduced soil erosion, an increased chance of greater penetration of water into the soil, which affected the groundwater recharge and the amount of groundwater (Winter et al., 2003; Graf and Przybylek, 2018). The results of the current study were consistent with the research of Zomlot et al. (2015) that assessed the control factors regarding the spatial distribution of groundwater recharge and found that land use had a profound effect on the rate of groundwater recharge, especially an increase in forest area, because the forest helped to slow down surface runoff and increased the chance of water seepage into the soil. On the other hand, groundwater recharge tends to decrease when the built-up area increases (Ghimire et al., 2021; Ashraf et al., 2022; Salem et al., 2023) or the vegetated land cover decreases (Sajjad et al., 2022; Siddik et al., 2022). The groundwater recharge rate was dependent on land cover, soil properties, surface runoff, and infiltration, which were influenced by land use change (Sajikumar and Remya, 2015; Owuor et al., 2016; Abdelaziz et al., 2020).

Moreover, this research showed the benefits of land use management. If the wasteland were converted into mixed perennial, there is a tendency of increasing groundwater recharge and may help to relieve the drought problem in this study area. The average groundwater recharge is shown in Table 4.

Table 4. Average groundwater recharge

Groundwater recharge ($\times10^{-4}$ m^3/s)						
	Current situation		Scenario 1		Scenario 2	
	Min-max	Average	Min-max	Average	Min-max	Average
January	2.20-12.76	7.30	2.20-13.17	7.40	2.27-14.44	7.46
February	2.07-12.83	7.29	2.07-13.25	7.39	2.13-14.55	7.45
March	1.93-12.90	7.28	1.93-13.33	7.38	1.99-14.66	7.44
April	1.85-12.96	7.28	1.85-13.39	7.37	1.89-14.75	7.44
May	1.79-13.01	7.27	1.79-13.45	7.37	1.81-14.84	7.43
June	1.95-13.06	7.29	1.95-13.50	7.38	1.95-14.92	7.45
July	2.24-13.10	7.33	2.24-13.55	7.43	2.30-14.99	7.49
August	2.53-3.13	7.38	2.59-15.06	7.54	2.59-15.06	7.54
September	2.69-13.16	7.41	2.69-13.62	7.51	2.76-15.11	7.57
October	2.75-13.19	7.43	2.75-13.66	7.53	2.83-15.16	7.59
November	2.53-13.03	7.39	2.56-13.68	7.52	2.64-15.20	7.58
December	2.27-12.62	7.31	2.29-13.19	7.43	2.36-14.48	7.49
Average		7.33		7.44		7.49

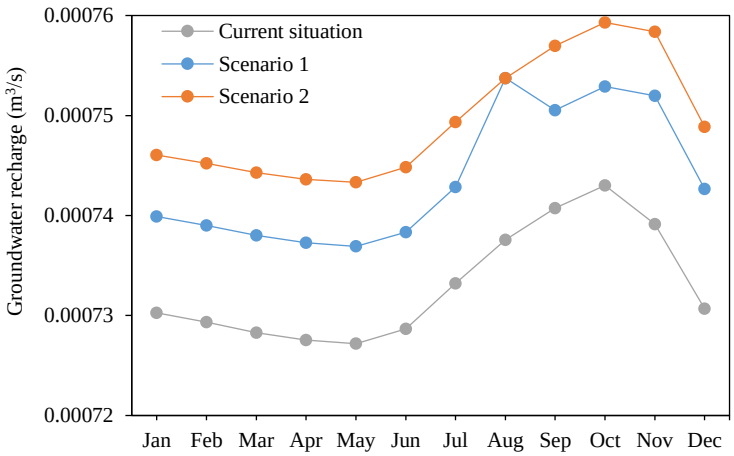

Figure 4. Monthly groundwater recharge for current situation, scenario 1, and scenario 2

4. CONCLUSION

Land use changes between 2008 and 2020 in the Nadi and Kabinburi Districts, Prachinburi Province, showed that the increased areas of forest, field crops, perennials, water, and miscellaneous and decreased areas of paddy fields, other agricultural, urban, and degraded forest areas. In addition, the areas with very little change were forest plantations and fruit tree areas. The major focus of this research was evaluating the impact of land use change on groundwater recharge. The simulation showed that the average monthly groundwater recharge amounts in scenario 1 that changed other agricultural areas and miscellaneous areas, and scenario 2 that predicted the future land use based on land use change trends from the past to the present, were more than the current situation. Changes in land use in the study area, such as increasing land cover or turning wasteland into mixed perennial areas (scenario 1), affected the groundwater recharge in the Nadi and Kabinburi Districts and produced recharge values, close to the results from the simulating future land use scenarios in the next 10 years (scenario 2), which was based on the trends of land use change from the past to present. Therefore, planting more and protecting the forest area, establishing a forest care policy, creating water use plans for both surface water and groundwater, and following the principles of soil and water conservation to prevent the occurrence of surface runoff are increasing the opportunity to replenish the groundwater in Nadi and Kabinburi Districts, Prachinburi Province.

ACKNOWLEDGEMENTS

This research was supported by the Research and Development Institute of Kasetsart University, Bangkok, Thailand and the Faculty of Forestry, Kasetsart University (project code R-M 7.63). The Department of Groundwater Resources and the Department of Land Development provided the groundwater data and land use data, respectively.

REFERENCES

Abdelaziz K, Nicaise Y, Seguis L, Ouattara I, Moussa O, Auguste K, et al. Influence of land use land cover change on groundwater recharge in continental terminal area of Abidjan, Ivory Coast. Journal of Water Resource and Protection 2020;12(5):431-53.

Ashraf S, Ali M, Shrestha S, Hafeez M, Moiz A, Sheikh Z. Impacts of climate and land-use change on groundwater recharge in the semi-arid lower Ravi River Basin, Pakistan. Groundwater for Sustainable Development 2022;17:Article No. 100743.

Borrabut A, Pukngam S, Kheereemangkla Y. Effect of land use change on streamflow of Mae Nam Khuan and Nam Pi Sub-watersheds in Nan and Phayao Provinces. Thai Journal Forest 2022;41(1):127-38 (in Thai).

Chacuttrikul P. Study of Future Soil Erosion and Sediment Yield Considering Land Use and Climate Changes in Northern Thailand [dissertation]. Tokyo, University of Tokyo; 2018.

Chacuttrikul P, Kiguchi M, Oki T. Impacts of climate and land use changes on river discharge in a small watershed: A case study of the Lam Chi Sub-watershed, Northeast Thailand. Hydrological Research Letters 2018;12(2):7-13.

Department of Groundwater Resources. Report of Groundwater Situation in Thailand: Project to Establish an Observation Network to Monitor the Situation of Groundwater, the Fiscal Year 2015. Bangkok, Thailand: Bureau of Groundwater Conservation and Restoration; 2015.

Department of Groundwater Resources. The benefits of groundwater recharge [Internet]. 2018 [cited 2022 Jul 27]. Available from: http://www.dgr.go.th/bgr9/th/newsAll/305/5155.

Faksomboon B, Suanmali W, Chaivino N, Khamcharoen N, Buasruang S. Land use changes of head watershed area on streamflow, suspended sediment and water quality in Khlong Lan Watershed, Kamphaeng Phet Province. Burapha Science Journal 2019;24(2):532-49 (in Thai).

Fornes J, Pirarai K. Groundwater in Thailand. Journal of Environmental Science and Engineering 2014;3:304-15.

Ghimire U, Shrestha S, Nuepane S, Mohanasundaram S, Lorphensri O. Climate and land-use change impacts on spatiotemporal variations in groundwater recharge: A case study of the Bangkok Area, Thailand. Science of the Total Environment 2021;792:Article No. 148370.

Graf R, Przybytek J. Application of the WetSpass simulation model for determining conditions governing the recharge of shallow groundwater in the Poznan Upland, Poland. Geologos 2018;24(3):189-205.

Hanasaki N. H08 Manual User's Edition Second Edition. Tsukuba, Japan: National Institute for Environmental Studies; 2022.

Hanasaki N, Yoshikawa S, Pokhrel Y, Kanae S. A global hydrological simulation to specify the sources of water used by humans. Hydrology and Earth System Sciences 2018; 22(1):789-817.

He X, Estes L, Konar M, Tian D, Anghileri D, Baylis K, et al. Integrated approaches to understanding and reducing drought impact on food security across scales. Environmental Sustainability 2019;40:43-54.

Keshavarz M, Karami E. Drought and agricultural ecosystem services in developing countries. In: Gaba S, Smith B, Lichtfouse E, editors. Sustainable Agriculture Reviews 28. New York: Springer International Publishing; 2018. p. 309-59.

Kumar N, Tischbein B, Kusche J, Beg K, Bogardi J. Impact of land-use change on the water resources of the Upper Kharun catchment, Chhattisgarh, India. Regional Environmental Change 2017;17:2373-85.

Mateo C, Hanasaki N, Komori D, Tanaka K, Yoshimura K, Kiguchi M, et al. Assessing the impacts of reservoir operation to floodplain inundation by combining hydrological, reservoir management, and hydrodynamic models. Water Resources Research 2014;50(9):7245-66.

Miyan M. Droughts in Asian least developed countries: Vulnerability and sustainability. Weather and Climate Extremes 2015;7:8-23.

Niyom W. Forest Hydrology. Bangkok, Thailand: Department of Conservation, Faculty of Forestry, Kasetsart University; 1992 (in Thai).

Owuor S, Bahi K, Guzha A, Rufino M, Pelster D, Pines E, et al. Groundwater recharge rates and surface runoff response to land use and land cover changes in semi-arid environments. Ecological Processes 2016;5:Article No. 16.

Research Institute Developed for Desertification Prevention and Early Warning. Guidelines for the Development of Repetitive Drought Areas for Agriculture. Bangkok, Thailand: Department of Land Development; 2005.

Sajjad M, Wang J, Abbas H, Ullah I, Khan R, Ali F. Impact of climate and land-use change on groundwater resources, study of Faisalabad District, Pakistan. Atmosphere 2022;13(7):1-15.

Sajikumar N, Remya R. Impact of land cover and land use change on runoff characteristics. Journal of Environmental Management 2015;161:460-8.

Salem A, Abduljaleel Y, Dezso J, Loczy D. Integrated assessment of the impact of land use changes on groundwater recharge and groundwater level in the Drava floodplain, Hungary. Scientific Reports 2023;13:Article No. 5061.

Sharafi L, Zarafshani K, Keshavarz M, Azadi H, Passel S. Farmers' decision to use drought early warning system in developing countries. Science of the Total Environment 2021;758:Article No. 142761.

Siddik M, Tulip S, Rahman A, Islam M, Haghighi A, Mustafa S. The impact of land use and land cover change on groundwater recharge in northwestern Bangladesh. Journal of Environmental Management 2022;315:Article No. 115130.

United Nations. World 'at a crossroads' as droughts increase nearly a third in a generation [internet]. 2022 [cited 2022 Jul 10]. Available from: https://news.un.org/en/story/2022/05/1118142.

Verburg P. The CLUE-S Model, Tutorial CLUE-s (Version 2.4) and DYNA-CLUE (Version 2). Netherlands: University Amsterdam; 2007.

Verburg P. The CLUMondo land use change model: Manual and exercises. Netherlands: Institute for Environmental Studies, University Amsterdam; 2015.

Verburg P. Overmars K. Combining top-down and bottom-up dynamics in land use modeling: Exploring the future of abandoned farmlands in Europe with the Dyna-CLUE model. Landscape Ecology 2009;24:1167-81.

Verburg P, Soepboer W, Veldkamp A, Limpiada R, Espaldon V. Modeling the spatial dynamics of regional land use: The CLUE-S model. Environmental Management 2002;30:391-405.

Verburg P, Veldkamp A, de Koning J, Kok K, Bouma J. A spatial explicit allocation procedure for modelling the pattern of land use change based upon actual land use. Ecological Modelling 1999;116(1):45-61.

Winter C, Rosenberry O, LaBaugh W. Where does the ground water in small watersheds come from? Ground Water 2003;41(7):989-1000.

Zhong L, Hua L, Yan Z. Datasets of meteorological drought events and risks for the developing countries in Eurasia. Big Earth Data 2020;4(2):191-223.

Zomlot Z, Verbeiren B, Huysmans M, Batelaan O. Spatial distribution of groundwater recharge and base flow: Assessment of controlling factors. Journal of Hydrology: Regional Studies 2015;4:349-68.

INSTRUCTION FOR AUTHORS

Publication and Peer-reviewing processes of Environment and Natural Resources Journal

Environment and Natural Resources Journal is a peer reviewed and open access journal that is published in six issues per year. Manuscripts should be submitted online at https://ph02.tci-thaijo.org/index.php/ennrj/about/submissions by registering and logging into this website. Submitted manuscripts should not have been published previously, nor be under consideration for publication elsewhere (except conference proceedings papers). A guide for authors and relevant information for the submission of manuscripts are provided in this section and also online at: https://ph02.tci-thaijo.org/index.php/ennrj/author. All manuscripts are refereed through a **single-blind peer-review** process.

Submitted manuscripts are reviewed by outside experts or editorial board members of **Environment and Natural Resources Journal**. This journal uses double-blind review, which means that both the reviewer and author identities are concealed from the reviewers, and vice versa, throughout the review process. Steps in the process are as follows:

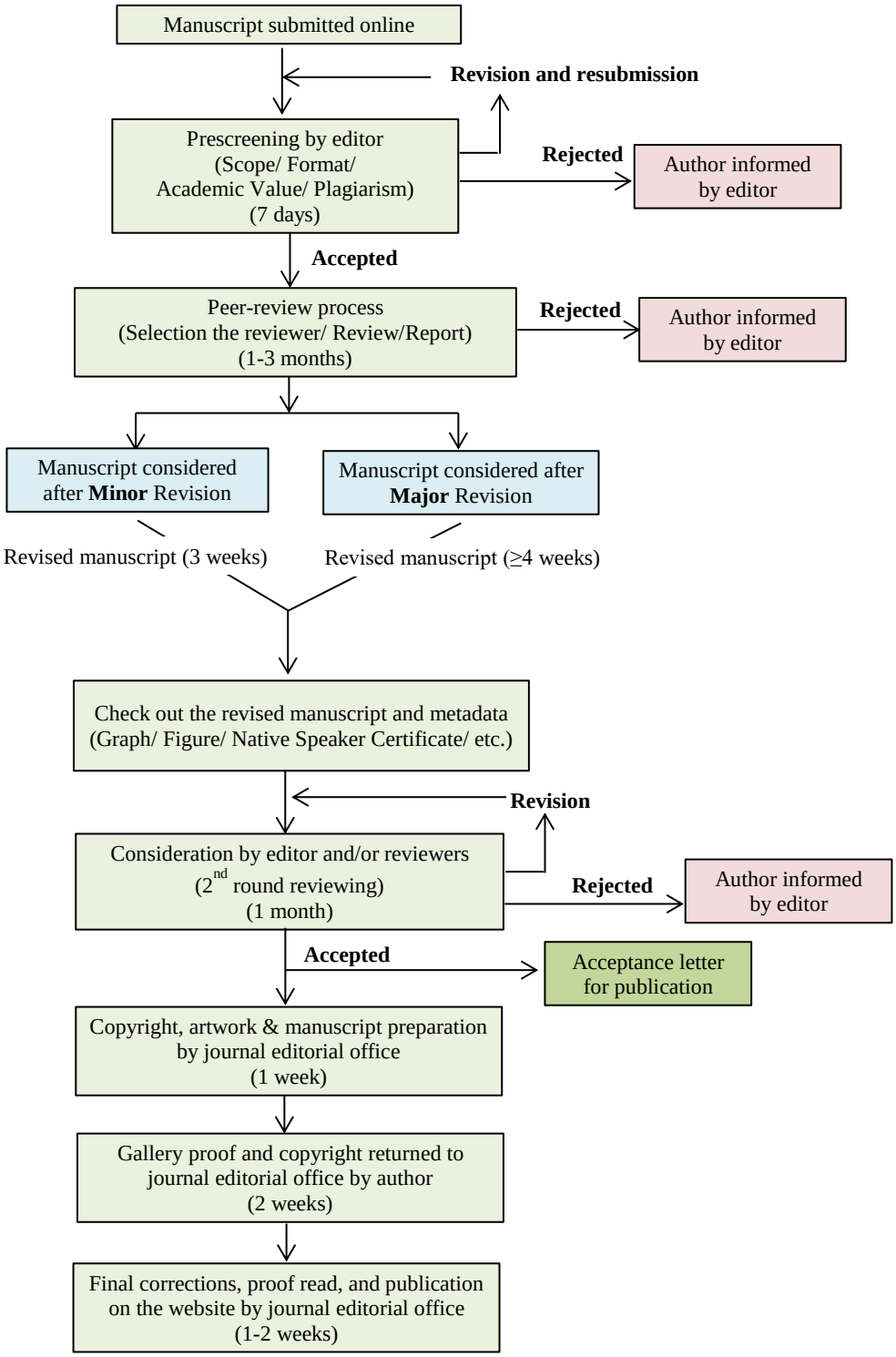

The Environment and Natural Resources Journal (EnNRJ) accepts 2 types of articles for consideration of publication as follows:

- *Original Research Article:* Manuscripts should not exceed 3,500 words (excluding references).
- *Review Article (by invitation):* This type of article focuses on the in-depth critical review of a special aspect in the environment and also provides a synthesis and critical evaluation of the state of the knowledge of the subject. Manuscripts should not exceed 6,000 words (excluding references).

Submission of Manuscript

Cover letter: Key points to include:

- Statement that your paper has not been previously published and is not currently under consideration by another journal
- Brief description of the research you are reporting in your paper, why it is important, and why you think the readers of the journal would be interested in it
- Contact information for you and any co-authors
- Confirmation that you have no competing interests to disclose

Manuscript-full: Manuscript (A4) must be submitted in Microsoft Word Files (.doc or .docx). Please make any identifying information of name(s) of the author(s), affiliation(s) of the author(s). Each affiliation should be indicated with superscripted Arabic numerals immediately after an author's name and before the appropriate address. Specify the Department/School/Faculty, University, Province/State, and Country of each affiliation.

Manuscript-anonymized: Manuscript (A4) must be submitted in Microsoft Word Files (.doc or .docx). Please remove any identifying information, such as authors' names or affiliations, from your manuscript before submission and give all information about authors at title page section.

Reviewers suggestion *(mandatory)*: Please provide the names of 3 potential reviewers with the information about their affiliations and email addresses. *The recommended reviewers should not have any conflict of interest with the authors. Each of the reviewers must come from a different affiliation and must not have the same nationality as the authors.* Please note that the editorial board retains the sole right to decide whether or not the recommended potential reviewers will be selected.

Preparation of Manuscript

Manuscript should be prepared strictly as per guidelines given below. The manuscript (A4 size page) must be submitted in Microsoft Word (.doc or .docx) with Times New Roman 12 point font and a line spacing of 1.5. *The manuscript that is not in the correct format will be returned and the corresponding author may have to resubmit*. The submitted manuscript must have the following parts:

Title should be concise and no longer than necessary. Capitalize first letters of all important words, in Times New Roman 12 point bold.

Author(s) name and affiliation must be given, especially the first and last names of all authors, in Times New Roman 11 point bold.

Affiliation of all author(s) must be given in Times New Roman 11 point italic.

Abstract should indicate the significant findings with data. A good abstract should have only one paragraph and be limited to 250 words. Do not include a table, figure or reference.

Keywords should adequately index the subject matter and up to six keywords are allowed.

Text body normally includes the following sections: 1. Introduction 2. Methodology 3. Results and Discussion 4. Conclusions 5. Acknowledgements 6. References

Reference style must be given in Vancouver style. Please follow the format of the sample references and citations as shown in this Guide below.

Unit: The use of abbreviation must be in accordance with the SI Unit.

Format and Style

Paper Margins must be 2.54 cm on the left and the right. The bottom and the top margin of each page must be 1.9 cm.

Introduction is critically important. It should include precisely the aims of the study. It should be as concise as possible with no sub headings. The significance of problem and the essential background should be given.

Methodology should be sufficiently detailed to enable the experiments to be reproduced. The techniques and methodology adopted should be supported with standard references.

Headings in Methodology section and Results and Discussion section, no more than three levels of headings should be used. Main headings should be typed (in bold letters) and secondary headings (in bold and italic letters). Third level headings should be typed in normal and no bold, for example;

2. Methodology
2.1 Sub-heading
2.1.1 Sub-sub-heading

Results and Discussion can be either combined or separated. This section is simply to present the key points of your findings in figures and tables, and explain additional findings in the text; no interpretation of findings is required. The results section is purely descriptive.
Tables Tables look best if all the cells are not bordered; place horizontal borders only under the legend, the column headings and the bottom.
Figures should be submitted in color; make sure that they are clear and understandable. Please adjust the font size to 9-10, no bold letters needed, and the border width of the graphs must be 0.75 pt. *(Do not directly cut and paste them from MS Excel.)* Regardless of the application used, when your electronic artwork is finalized, please 'save as' or convert the images to TIFF (or JPG) and separately send them to EnNRJ. The images require a resolution of at least 300 dpi (dots per inch). If a label needed in a figure, its font must be "Times New Roman" and its size needs to be adjusted to fit the figure without borderlines.

All Figure(s) and Table(s) should be embedded in the text file.

Conclusions should include the summary of the key findings, and key take-home message. This should not be too long or repetitive, but is worth having so that your argument is not left unfinished. Importantly, don't start any new thoughts in your conclusion.

Acknowledgements should include the names of those who contributed substantially to the work described in the manuscript but do not fulfill the requirements for authorship. It should also include any sponsor or funding agency that supported the work.

References should be cited in the text by the surname of the author(s), and the year. This journal uses the author-date method of citation: the last name of the author and date of publication are inserted in the text in the appropriate place. If there are more than two authors, "et al." after the first author' name must be added. Examples: (Frits, 1976; Pandey and Shukla, 2003; Kungsuwas et al., 1996). If the author's name is part of the sentence, only the date is placed in parentheses: "Frits (1976) argued that . . ."

Please be ensured that every reference cited in the text is also present in the reference list (and vice versa).

In the list of references at the end of the manuscript, full and complete references must be given in the following style and punctuation, arranged alphabetically by first author's surname. Examples of references as listed in the References section are given below.

Book
Tyree MT, Zimmermann MH. Xylem Structure and the Ascent of Sap. Heidelberg, Germany: Springer; 2002.

Chapter in a book
Kungsuwan A, Ittipong B, Chandrkrachang S. Preservative effect of chitosan on fish products. In: Steven WF, Rao MS, Chandrkachang S, editors. Chitin and Chitosan: Environmental and Friendly and Versatile Biomaterials. Bangkok: Asian Institute of Technology; 1996. p. 193-9.

Journal article
Muenmee S, Chiemchaisri W, Chiemchaisri C. Microbial consortium involving biological methane oxidation in relation to the biodegradation of waste plastics in a solid waste disposal open dump site. International Biodeterioration and Biodegradation 2015;102:172-81.

Published in conference proceedings
Wiwattanakantang P, To-im J. Tourist satisfaction on sustainable tourism development, amphawa floating marketSamut songkhram, Thailand. Proceedings of the 1st Environment and Natural Resources International Conference; 2014 Nov 6-7; The Sukosol hotel, Bangkok: Thailand; 2014.

Ph.D./Master thesis

Shrestha MK. Relative Ungulate Abundance in a Fragmented Landscape: Implications for Tiger Conservation [dissertation]. Saint Paul, University of Minnesota; 2004.

Website

Orzel C. Wind and temperature: why doesn't windy equal hot? [Internet]. 2010 [cited 2016 Jun 20]. Available from: http://scienceblogs.com/principles/2010/08/17/wind-and-temperature-why-doesn/.

Report organization:

Intergovernmental Panel on Climate Change (IPCC). IPCC Guidelines for National Greenhouse Gas Inventories: Volume 1-5. Hayama, Japan: Institute for Global Environmental Strategies; 2006.

Remark

** Please be note that manuscripts should usually contain at least 15 references and some of them must be up-to-date research articles.*

** Please strictly check all references cited in text, they should be added in the list of references. Our Journal does not publish papers with incomplete citations.*

Changes to Authorship

This policy of journal concerns the addition, removal, or rearrangement of author names in the authorship of accepted manuscripts:

Before the accepted manuscript

For all submissions, that request of authorship change during review process should be made to the form below and sent to the Editorial Office of EnNRJ. Approval of the change during revision is at the discretion of the Editor-in-Chief. The form that the corresponding author must fill out includes: (a) the reason for the change in author list and (b) written confirmation from all authors who have been added, removed, or reordered need to confirm that they agree to the change by signing the form. Requests form submitted must be consented by corresponding author only.

After the accepted manuscript

The journal does not accept the change request in all of the addition, removal, or rearrangement of author names in the authorship. Only in exceptional circumstances will the Editor consider the addition, deletion or rearrangement of authors after the manuscript has been accepted.

Copyright transfer

The copyright to the published article is transferred to Environment and Natural Resources Journal (EnNRJ) which is organized by Faculty of Environment and Resource Studies, Mahidol University. The accepted article cannot be published until the Journal Editorial Officer has received the appropriate signed copyright transfer.

Online First Articles

The article will be published online after receipt of the corrected proofs. This is the official first publication citable with the Digital Object Identifier (DOI). After release of the printed version, the paper can also be cited by issue and page numbers. DOI may be used to cite and link to electronic documents. The DOI consists of a unique alpha-numeric character string which is assigned to a document by the publisher upon the initial electronic publication. The assigned DOI never changes.

Mahidol University

Wisdom of the Land

Research and Academic Service Section, Faculty of Environment and Resource Studies, Mahidol University
999 Phutthamonthon 4 Rd, Salaya, Nakhon Pathom 73170, Phone +662 441-5000 ext. 2108 Fax. +662 441 9509-10
E-mail: ennrjournal@gmail.com Website: https://www.tci-thaijo.org/index.php/ennrj